ANGLIA RUSKIN UNIVERSITY

FACULTY OF HEALTH, EDUCATION, MEDICINE AND SOCIAL CARE

CHARACTERISATION OF THE EXPRESSION OF ADENOSINE AND ESTROGEN RECEPTORS IN MYOFIBROBLAST DIFFERENTIATION IN PEYRONIE'S DISEASE

Marta Isabel Rosa Mateus

First Supervisor: Prof Selim Cellek
Second Supervisor: Prof Richard Aspinall
External Supervisor: Prof David Ralph

A thesis in partial fulfilment of the requirements of Anglia Ruskin University for the degree of Doctor of Philosophy.

December 2018

ANGLIA RUSKIN UNIVERSITY

ABSTRACT

FACULTY OF HEALTH, EDUCATION, MEDICINE AND SOCIAL CARE

DOCTOR OF PHILOSOPHY

CHARACTERISATION OF THE EXPRESSION OF ADENOSINE AND ESTROGEN RECEPTORS IN MYOFIBROBLAST DIFFERENTIATION IN PEYRONIE'S DISEASE

MARTA MATEUS

December 2018

Introduction: Peyronie's disease (PD) is a fibroproliferative disease of the penis in which myofibroblast differentiation has a central role. Adenosine and estrogen signalling mediate their effect via interaction with their respective receptors which have been associated with the pathophysiology of a variety of fibroproliferative diseases, but this has yet to be studied in PD.

Hypothesis: Adenosine and/or estrogen receptor expression is involved in myofibroblast differentiation in PD and may, therefore, be novel potential targets for anti-fibrotic therapies in this disease.

Aim: The aim of this project was to characterise the myofibroblast differentiation process in human tunica albuginea-derived fibroblasts and to investigate the role of adenosine and estrogen receptors in this process.

Methods: Tissue samples from non-PD TA tissue and PD plaque tissue were obtained and fibroblast cell lines were established from each sample. Cells were exposed to transforming growth factor (TGF)-β1. The mRNA levels and the protein levels of several targets of interest, alpha-smooth muscle actin (α-SMA), four adenosine receptors and two estrogen receptors (ERs), were evaluated using real-time RT-PCR (RT-qPCR), immunocytochemistry (ICC), immunohistochemistry (IHC), Western blot and In-Cell Western (ICW). The effect of compound modulators of two of the receptors on TGF-β1-induced myofibroblast transformation was assessed.

Results: Both RT-qPCR and ICW methods were successfully developed and/or validated. The α-SMA mRNA and protein levels increased in cells isolated from non-PD TA tissue and PD plaque tissue when exposed to TGF-β1. The two cell groups expressed ADORA1 and ADORA2B and there was a differential effect to TGF-β1 in these two receptors. An ADORA2B agonist (BAY 60-6583) significantly inhibited TGF-β1-induced myofibroblast differentiation in the two cell types investigated. The two cell groups expressed ERβ but did not express ERα. Two selective estrogen receptor modulators (SERMs), tamoxifen and raloxifene, significantly inhibited TGF-β1-induced myofibroblast differentiation, suggesting that these SERMs interact with ERβ.

Conclusions: Cells isolated from non-PD TA tissue and PD plaque tissue expressed ADORA1, ADORA2B and ERβ. TGF-β1 had differential effects on the receptors investigated depending on the cell type. An adenosine receptor agonist and two SERMs significantly inhibited TGF-β1-induced myofibroblast differentiation in a concentration-dependent manner suggesting that these receptors and consequently the adenosine and estrogen pathways may be involved in the differentiation of myofibroblasts and may be potential novel therapeutic targets in PD.

Key words: Peyronie's disease, myofibroblast differentiation, adenosine receptors, estrogen receptors, transforming growth factor, anti-fibrotic therapies.

ACKNOWLEDGEMENTS

Firstly, I would like to thank my supervisor Prof Selim Cellek for this opportunity and for his constant support and advice. Thank you for providing the right balance of freedom and guidance, which made this a very enjoyable experience. I could not have imagined having a better mentor for my PhD thesis.

To Prof David Ralph for his support and advice throughout this project. Thanks to all his team for providing tissue samples, which made this project possible.

To all my friends back home and in the UK for their understanding, motivation and friendship.

To my parents and sister for their love, motivation and support. I appreciate all your hard work, so I could have this opportunity. I hope that I made you proud of me.

Finally, to Will for his infinite support and patience during this project and for putting up with me all these years. Without you I would not be submitting this thesis.

TABLE OF CONTENTS

LIST OF FIGURES

LIST OF TABLES

LIST OF EQUATIONS

LIST OF ABBREVIATIONS

18S	18S ribosomal RNA
5-PL	5-parameter logistic
ACTB	Beta-actin
ADA	Adenosine deaminase
ADORA1	Adenosine receptor A_1
ADORA2A	Adenosine receptor A_{2A}
ADORA2B	Adenosine receptor A_{2B}
ADORA3	Adenosine receptor A_3
ADP	Adenosine diphosphate
AF-1	N-terminal transactivation domain
ALK	Activin receptor-like kinase
AMP	Adenosine monophosphate
APS	Ammonium persulfate
ARU	Anglia Ruskin University
ASH	Alcoholic steatohepatitis
ATP	Adenosine triphosphate
ATP5B	ATP synthase
AUA	American Urological Association
B2M	Beta-2-microglobulin
BPH	Benign prostatic hyperplasia
BSA	Bovine serum albumin
cAMP	Cyclic adenosine monophosphate
CCFCs	Corpus cavernosal fibroblast cells
CCl4	Carbon tetrachloride
CD39	Nucleoside triphosphate phosphohydrolase
CD73	Ecto-5’-nucleotisade
cDNA	Complementary DNA
cGMP	Cyclic guanosine monophosphate
CKD	Chronic kidney disease
CLD	Chronic liver disease
COPD	Chronic obstructive pulmonary disease
CPA	N^6-Cyclopentyladenosine

Cq	Quantification cycle
CRCs	Concentration response curves
CTGF	Connective tissue growth factor
CYC1	Cytochrome C-1
DES	Diethylstibesterol
DM	Diabetes mellitus
DMEM/F-12	Dulbecco's Modified Eagle Medium/Nutrient Mixture F-12
DMSO	Dimethyl sulfoxide
DNA	Deoxyribonucleic acid
dsDNA	Double-stranded DNA
DTT	DL-dithiothreitol
E	Efficiency
E2	17 β-oestradiol
EAU	European Association of Urology
EC_{50}	Half maximal effective concentration
ECM	Extracellular matrix
ED	Erectile dysfunction
EDTA	Ethylenediaminetetraacetic acid
EGTA	Ethylene glycol-bis(2-aminoethylether)-N,N,N′,N′-tetraacetic acid
EIF4A2	Eukaryotic translation initiator factor 4A2
EMT	Epithelial to mesenchymal transition
ERs	Estrogen receptors
ERα	Estrogen receptor alpha
ERβ	Estrogen receptor beta
ET	Endothelin
FAP	Fibroblast activation protein
FasL	Fas ligand
FBS	Foetal bovine serum
FDA	Food and Drug Administration
FITC	Fluorescein isothiocyanate
GAPDH	Glyceraldehyde 3-phosphate dehydrogenase
GDF8	Growth differentiation factor 8
gDNA	Genomic DNA

GM-CSF	Granulocyte-macrophage colony-stimulating factor
HLA	Human leukocyte antigen
HSC	Hepatic stellate cells
HSP	Heat-shock protein
HTS	High-throughput screening
IC_{50}	Half maximal inhibitory concentration
ICC	Immunocytochemistry
ICW	In-Cell Western
IHC	Immunohistochemistry
IIEF	International Index of Erectile Function
IL	Interleukin
iNOS	Inducible nitric oxide synthase
IPF	Idiopathic pulmonary fibrosis
LBD	Ligand-binding domain
LUT	Low urinary tract
LUTS	Lower urinary tract symptoms
MCP	Monocyte chemoattractant protein
MEC	Minimum effective concentration
MIQE	Minimum information for publication of quantitative real-time PCR experiments
MMPs	Matrix metalloproteinases
mRNA	Messenger RNA
Na_3VO_4	Sodium orthovanadate
$Na_4P_2O_7$	Sodium pyrophosphate tetrabasic
NaCl	Sodium chloride
NaF	Sodium fluoride
NAFLD	Non-alcoholic fatty liver disease
NECA	5'-(*N*-ethylcarboxamido)-adenosine
NFDM	Non-fat dried milk
NF-κB	Nuclear factor kappa B
NO	Nitric oxide
NRT	No reverse transcriptase enzyme control
NTC	No template control
OCT	Optimal cutting temperature compound

OSF	Osteoblast specific factor
PAI	Plasminogen activator inhibitor
PB	Phosphate buffer
PBS	Phosphate-buffered saline
PBST	0.1% (v/v) tween 20 in phosphate-buffered saline
PCR	Polymerase chain reaction
PD	Peyronie's disease
PDE5i	Phosphodiesterase type 5 inhibitors
PDEs	Phosphodiesterases
PDGF	Platelet-derived growth factor
PDI	Peyronie's Disease Index
PFA	Paraformaldehyde
PI	Propidium iodide
PMSF	Phenylmethylsulfonyl fluoride
PVDF	Polyvinylidene fluoride
qPCR	Real-time PCR
RIN	RNA integrity number
RIPA	Radioimmunoprecipitation assay
RNA	Ribonucleic acid
ROS	Reactive oxygen species
RPL13A	Ribosomal protein L13A
rRNA	Ribosomal RNA
RT	Reverse transcription
RT-qPCR	Real-time reverse-transcription PCR
SAR	Structure-activity relationship
SDHA	Homo sapiens succinate dehydrogenase
SDS	Sodium dodecyl sulfate
SDS-PAGE	Sodium dodecyl sulfate polyacrylamide gel electrophoresis
SEM	Standard error of the mean
SERMs	Selective estrogen receptor modulators
sFAs	Soluble Fas
SMC	Smooth muscle cells
TA	Tunica albuginea

TAA	Thioacetamide
TAC	Normal TA from patients with penile cancer
TAN	Normal TA from patients without PD
TBS	Tris-buffered saline
TBST	0.1% (v/v) tween 20 in tris-buffered saline
TE	Trypsin/EDTA
TEMED	N,N,N′,N′-Tetramethylethylenediamine
TGF	Transforming growth factor
TIMP	Tissue inhibitors of metalloproteinase
TNF	Tumour necrosis factor
TNF-R1	TNF-receptor 1
TOP1	DNA topoisomerase I
TRAIL	TNF-related apoptosis-inducing ligand receptor
UBC	Ubiquitin C
UCLH	University College London Hospital
WT	Wild-type
YWHAZ	Phospholipase A2
Z’	Z-factor
α-SMA	alpha-smooth muscle actin
β-ME	β-mercaptoethanol

1 Introduction

1.1 Fibrosis

Fibrogenesis is becoming increasingly recognised as the main cause of morbidity and mortality in most chronic inflammatory diseases[1]. Fibrotic diseases account for up to 45% of deaths in the developed world, representing an unmet medical need for the identification of novel antifibrotic therapies.

Fibrosis is defined as improper wound healing, characterised by the excessive accumulation of fibroblasts and persistent synthesis and deposition of extracellular matrix (ECM) in and around the damaged tissue, potentially leading to disrupted tissue architecture, organ failure and, eventually, death[1,2]. It is a complex, progressive and multi-stage process, which can be initiated by several factors either alone or in combination, such as inflammatory response; connective tissue repair; persistent infections; inherited genetic disorders and poorly controlled diabetes, triggering the physiological repair mechanism of the body[1,3]. This scarring process can affect various tissues, including the lung, skin, kidney, heart and liver. Although fibrotic disorders have different aetiologies and clinical manifestations, the cellular and biochemical mechanisms are thought to be similar[4].

The process that leads to fibrotic diseases is analogous to the process of normal wound healing, where a series of events take place once the primary tissue injury occurred. Those events include damage to the epithelial/endothelial barrier; acute inflammation where inflammatory cells are recruited; release of several cytokines, such as transforming growth factor (TGF)-β1, monocyte chemoattractant protein (MCP)-1 and plasminogen activator inhibitor (PAI)-1; induction of reactive oxygen species (ROS); synthesis of non-collagenous and collagenous ECM components; myofibroblasts differentiation and accumulation and tissue remodelling[5,6]. During normal wound healing, the remodelling of ECM and the regeneration of organised parenchyma occurs; however, in a fibrotic process, excessive production and improper remodelling of ECM results in the

formation of fibrotic tissue, which can lead to organ malfunction and death[3,7] (Figure 1-1).

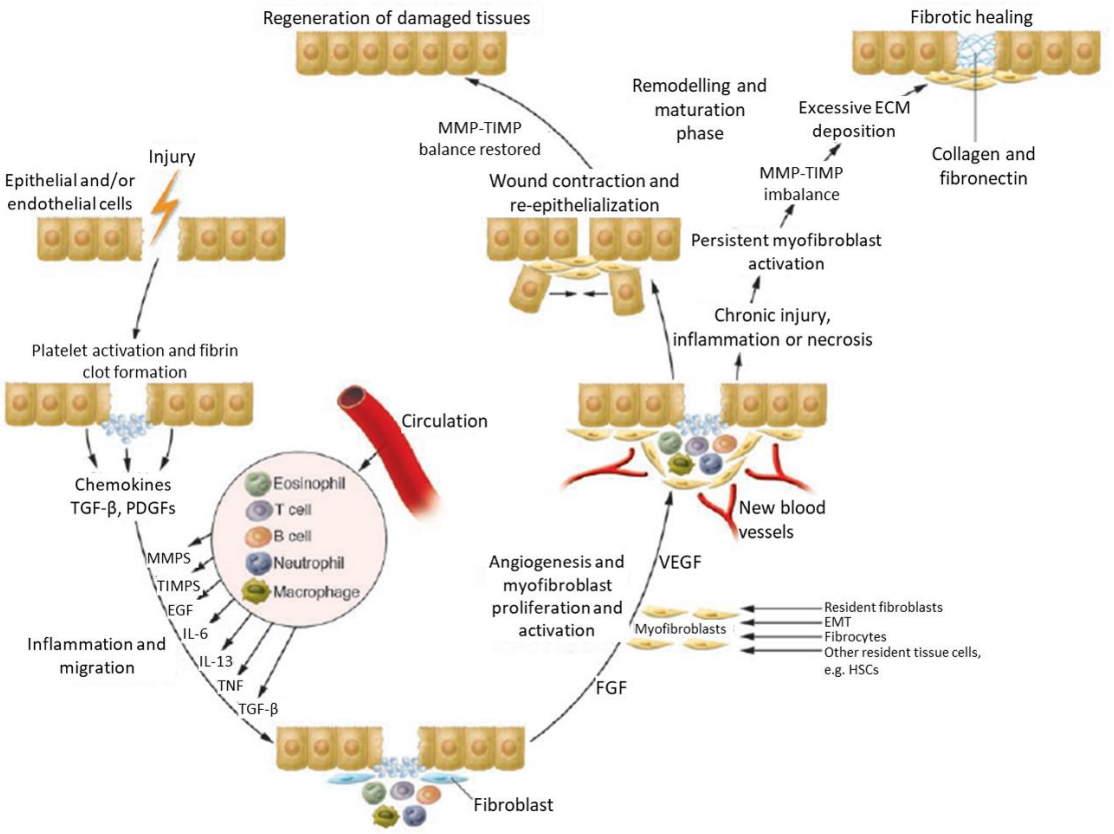

Figure 1-1: Process leading to normal wound healing or fibrosis. After tissue damage, inflammatory mediators are released from epithelial and/or endothelial cells, which will initiate an inflammation response. This initial inflammation phase is followed by the differentiation of fibroblasts to myofibroblasts, which are responsible for producing ECM components and stimulating wound contraction. In the remodelling and maturation phase, collagen fibres become organised, scar tissue is eliminated, and the tissue is regenerated. Nevertheless, in a fibrotic disorder, the normal healing process is disrupted, by persistent inflammation, myofibroblast activation and excessive deposition of ECM components, leading to the formation of a permanent fibrotic scar. Adapted from Wynn (2007)[7].

Furthermore, there are numerous cytokines involved in the pathogenesis of fibrosis, such as TGF-β1[8,9]; granulocyte-macrophage colony-stimulating factor (GM-CSF)[10]; tumour necrosis factor (TNF)-α[11]; interleukin (IL)-6[12]; IL-1β[13]; IL-10[14]; IL-13[15]; connective tissue growth factor (CTGF)[16,17]; endothelin (ET)[18]; oncostatin M[19]; platelet-derived growth factor (PDGF)[12] and fibroblast activation protein (FAP)-α[20], which can result in the activation and differentiation of mesenchymal cells. These factors can also lead to the remodelling and

destruction of normal tissue architecture and deposition of connective tissue, which again leads to organ malfunction.

Fibroblasts are cells of mesenchymal origin, which are responsible for producing a diversity of biochemical mediators (such as growth factors and proteases), deposition of ECM as part of the wound healing process, regulation of inflammation, regulation of epithelial differentiation and maintenance of tissue homoeostasis by regulating the turnover of ECM[2,21]. Fibroblasts are identified by their spindle-shaped morphology and are widely distributed in numerous types of tissues, especially in the connective tissue[21,22]. These cells have been reported to be vimentin-positive as well as desmin-negative and α-smooth muscle actin (α-SMA)-negative[23]. After tissue injury, fibroblasts are activated, leading to increased production of ECM and differentiation to myofibroblasts.

Myofibroblasts are a specialised cell type heavily involved in the fibrotic process. These cells are morphologically between fibroblasts and smooth muscle cells (SMC), since they combine the cytoskeletal and contractile properties of SMC and the ECM-producing characteristics of fibroblasts[24]. The general lack of smooth muscle markers (e.g. desmin and smooth muscle myosin) by myofibroblast is how they are distinguished from smooth muscle cells[25]. Myofibroblasts are defined by their *de novo* expression of α-SMA in large bundles of actin filaments (also known as stress fibres), by secreting abundant ECM proteins and by their contractile force, which is responsible for wound contraction and closure, reducing the size of the wound[24].

The differentiation of fibroblasts to myofibroblasts is a key event in connective tissue wound healing. This differentiation is caused by a series of events that are described in Figure 1-2.

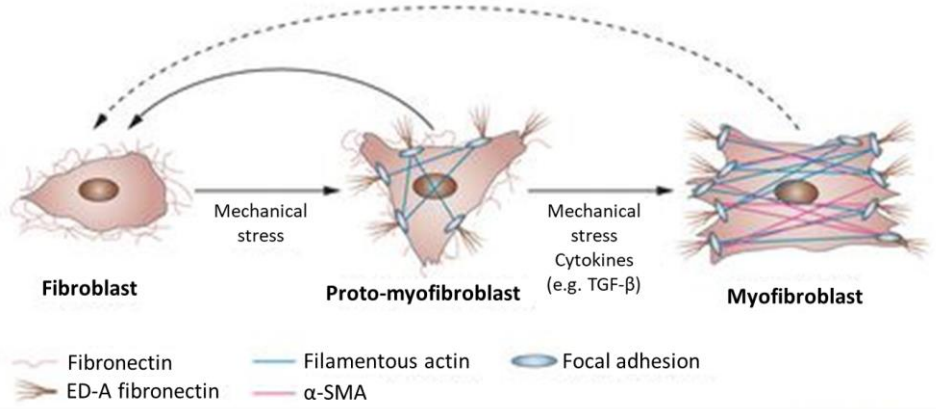

Figure 1-2: Differentiation of fibroblasts to myofibroblasts. Upon injury, fibroblasts differentiate into proto-myofibroblasts in response to mechanical stress created by the remodelling of ECM of damaged tissue, leading to the appearance of contractile stress fibres. The proto-myofibroblasts will further differentiate to myofibroblasts due to the expression of TGF-β and ED-A fibronectin, as well as the presence of mechanic tension. The differentiated myofibroblasts are characterised by the expression of α-SMA and by their capacity to generate more contractile forces than the proto-myofibroblasts. These contractile forces are responsible for contracting the edges of the wound, reducing its size. The conversion of proto-myofibroblasts to fibroblasts is reversible (solid line); however, it is not known whether the dedifferentiation from myofibroblast to fibroblast can occur (dotted line). Adapted from Falke *et al.* (2015)[26].

First, the quiescent fibroblasts acquire a migratory phenotype, migrating to the centre of the injured tissue, inducing the appearance of contractile bundles (stress fibres). This phenotypic change is due to the changes in the composition, mechanical tension and organisation of the ECM. These fibroblasts with a migratory phenotype are known as proto-myofibroblasts. The proto-myofibroblasts further develop to myofibroblasts, which express α-SMA[22,27,28]. This differentiation is further induced by continued exposure to mechanical tension and also by exposure to TGF-β and ED-A splice variant of cellular fibronectin[28,29].

Several studies have reported that myofibroblasts can originate from a variety of precursor cells, depending on the type of tissue to be repaired. Locally residing fibroblasts are the most frequent source of myofibroblasts[26]. However, other cells, such as pericytes, mesenchymal stem cells, bone marrow-derived cells (fibrocytes) and cells circulating in the cardiovascular system have also been suggested to be the sources of myofibroblasts[22,30]. Endothelial to mesenchymal

transition and epithelial to mesenchymal transition (EMT) have also been described as a potential source of myofibroblast differentiation[30,31].

Both fibroblasts and myofibroblasts are metabolically highly active cells; both are capable of synthesising numerous ECM components, such as fibronectin, collagens, proteoglycans, laminin and tenascin[25]. Furthermore, numerous studies have demonstrated that myofibroblasts are responsible for producing several cytokines in different organs, such as PAI-1 in breast tissue as well as TGF-β1, MCP-1 and collagen in lung tissue[25,28]. Matrix metalloproteinases (MMPs) are also produced by fibroblasts and are part of a family of 25 zinc ion-dependent proteolytic enzymes capable of degrading and rearranging ECM components[32]. The MMPs are regulated by a group of inhibitors known as tissue inhibitors of metalloproteinase (TIMP). The balance between MMPs and TIMP have been shown to be linked to several biological processes where the disruption of ECM components occurs such as in the wound healing process[32,33]. Furthermore, specific MMPs have been shown to have anti-fibrotic properties, whereas other MMPs are able to promote fibrosis. Both MMP-12 and MMP-19, for instance, have been shown to be anti-fibrotic in the lung; however, they present profibrotic activity in the liver[34]. In addition, Iwanami and colleagues (2009)[35] have reported that myofibroblasts express mRNA and protein levels of MMP-12. The reduction of MMP-2 has also been shown after treatment with TGF-β1[36].

Following normal wound repair, the expression of α-SMA decreases and the myofibroblasts undergo apoptosis. However, in a fibrotic process, it is thought that the activity of these cells persists, leading to the expansion of ECM and tissue deformation[1].

1.1.1 Apoptosis in fibrosis

Apoptosis is a process that leads to a programmed and controlled type of cell death differing from necrosis which is a form of unprogrammed cell death. Apoptosis can occur during development and ageing, as a defence mechanism and for tissue homeostasis. Apoptosis can be induced by a diversity of extracellular and intracellular stimuli leading to two major apoptotic signalling

pathways: the death receptor or extrinsic pathway and the mitochondrial or intrinsic pathway. These two pathways have been suggested to be connected and the molecules from one pathway can affect the other[37]. The death receptor or extrinsic pathway involves the activation of receptors that belong to the TNF receptor family, which include Fas receptor (CD95 or Apo-1), TNF-receptor 1 (TNF-R1) and TNF-related apoptosis-inducing ligand receptors 1 and 2 (TRAIL-R1 or DR4 and TRAIL-R2 or DR5). These receptors are located on the cell membrane and are stimulated by extracellular ligands (Fas ligand – FasL - binds to Fas, TNF-α binds to TNF-R1 and TRAIL binds to TRAIL-R1 and TRAIL-R2)[38]. The mitochondrial or intrinsic pathway can also lead to the activation of caspases by releasing pro-apoptotic proteins in response to an apoptotic stimulus (e.g. DNA damage, radiation, ROS, drugs and infectious agents)[37,39].

There are several mechanisms that during the resolution of a wound healing event lead to fibroblast apoptosis, including reduced growth factor expression, nitric oxide (NO) generation and increased ECM turn-over[40]. However, the acquisition of an apoptosis-resistant phenotype by myofibroblasts has been associated with TGF-β1-induced myofibroblasts due to the release of endothelin-1 triggering the Pi3K-AKT pathway[41]. Furthermore, IL-1β was reported to selectively induce apoptosis in myofibroblasts through the induction of inducible nitric oxide synthase (iNOS), whereas TGF-β1 was reported to stimulate myofibroblast differentiation and impede iNOS production. It has been demonstrated that TGF-β1 was capable of impeding apoptosis induced by IL-1β, suggesting that this cytokine enhances the myofibroblasts' survival by inhibiting IL-1β-induced apoptosis[42,43].

However, there are several studies that have shown that when fibroblasts are stimulated with extracellular ligands, these can trigger apoptosis in fibroblasts. A study by Huang *et al.* (2013)[44] demonstrated that Fas-mediated apoptosis was induced *in vitro* by the addition of anti-Fas antibody and the response could be increased with the addition of cycloheximide, a suppressor of protein synthesis. Another study also showed that lung fibroblasts and myofibroblasts are resistant to FasL-induced apoptosis and this could be overcome with TNF-α sensitisation,

suggesting that by increasing the expression of this cytokine it may decrease fibroblast and myofibroblast accumulation being beneficial in treating lung fibrosis[45].

A study by Moodley *et al.* (2004)[46] compared the morphological and biochemical changes in FasL-induced apoptosis between fibroblasts isolated from lungs of patients with idiopathic pulmonary fibrosis (IPF) and normal human lung fibroblasts. These authors demonstrated that fibroblasts derived from fibrotic lungs were more resistant to induction of apoptosis through FasL/Fas than fibroblasts isolated from normal lung. According to Bühling *et al*. (2005)[47], this decreased vulnerability to FasL-induced apoptosis may be due to high levels of apoptosis-inhibiting soluble Fas (sFas) and a lower expression of cell surface Fas by these cells. Moreover, another study showed that IL-6 increases expression of pro-apoptotic protein Bax and increases FasL-induced apoptosis in normal fibroblasts. However, in fibroblasts isolated from patients with IPF, IL-6 induces the expression of the anti-apoptotic protein Bcl-2 and inhibits apoptosis, suggesting that altered IL-6 signalling in IPF may increase apoptosis resistance of these cells leading to the progression of fibrosis[48].

Loreto and co-workers showed overexpression of DR5 and TRAIL in fibroblasts and myofibroblasts derived from patients with Peyronie's disease (PD)[49]. These authors also investigated the involvement of the intrinsic pathway. They showed that fibroblasts isolated from PD patients expressed Bax (a pro-apoptotic protein); however, Bcl-2 protein (an anti-apoptotic protein) was not detected in fibrotic and control samples. The executioner caspase-3 was intensely detected in fibrous tissue and TUNEL staining was also used to detect apoptosis in fibroblasts and myofibroblasts suggesting that apoptosis in PD plaque could be induced by the intrinsic pathway[50].

In addition, a study that characterised the pattern of mRNA expression of apoptotic genes in both healthy tunica albuginea (TA) and PD plaque demonstrated that the mRNA levels of plaque tissues were not significantly different from normal tissues samples. Moreover, apoptotic gene expression was reduced in comparison to the reference genes in half of the healthy TA samples

and two-thirds of the plaque samples, suggesting that PD plaque samples are more resistant to apoptosis than healthy TA samples[51].

1.1.2 Adenosine receptors in fibrosis

Adenosine is a ubiquitous purine nucleoside generated by the dephosphorylation of adenine nucleotides released from cells and tissues under conditions of stress or injury[52,53]. Adenosine can be found in the extracellular compartment due to several biological processes, such as adenosine transport, extracellular adenosine production, adenosine metabolism to inosine or adenosine monophosphate (AMP) and adenosine production from intracellular adenosine sources. Extracellular adenosine can either result from the breakdown of extracellular nucleotides such as adenosine triphosphate (ATP) and adenosine diphosphate (ADP) or from the external transport of intracellularly generated adenosine. Upon conditions of stress and injury, including leakage from cells undergoing cell death and inflammatory response, ATP is released and converted to ADP or AMP through nucleoside triphosphate phosphohydrolase (CD39) and then to adenosine by ecto-5'-nucleotidase (CD73)[54].

Adenosine regulates its effects on tissue regeneration and repair via interaction with a family of G-protein coupled receptors: A_1 (ADORA1), A_{2A} (ADORA2A), A_{2B} (ADORA2B) and A_3 (ADORA3)[53].

Several studies have shown that adenosine receptors play different roles in acute and chronic injuries. In acute tissue injury, adenosine has been shown to be beneficial, as it is responsible for tissue protection and anti-inflammatory responses[55] (e.g. promotion of barrier function and wound healing) in several organs, including kidney[56], lung[57,58], heart[59] and liver[60]. These responses are regulated by ADORA2A and ADORA2B signalling[55].

Conversely to acute states, a sustained increase in adenosine levels has been associated with the progression of chronic tissue injuries. In these settings, adenosine has been suggested to promote fibrosis in several organs, such as heart[61], skin[52,62], liver[63], lung[64,65], penis[66,67] and kidney[68], which is mainly regulated again by ADORA2A and ADORA2B[55] (Figure 1-3).

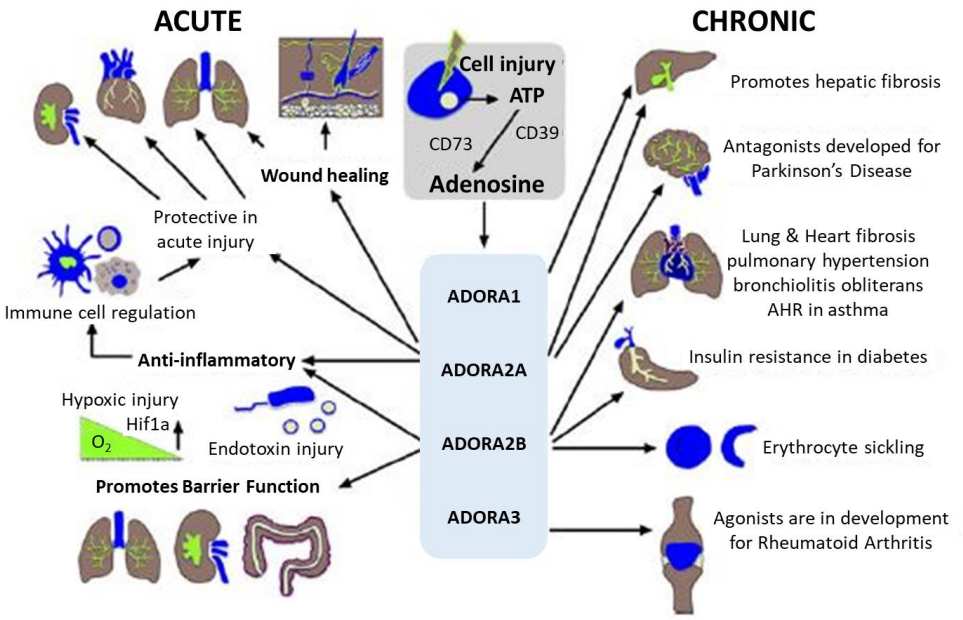

Figure 1-3: Adenosine production and signalling. Adenosine is generated intracellularly and extracellularly from adenine nucleotides, which are then dephosphorylated to adenosine. CD39 and CD73 are two cell surface molecules responsible for catalysing the dephosphorylation of adenine nucleotides to adenosine in the extracellular space. In acute states, adenosine is responsible for tissue protection; whereas, in chronic states, it can be responsible for promoting aberrant wound healing. Adapted from Karmouty-Quintana, Xia & Balckburn (2013)[55].

Several studies suggest that differential effects on the cyclic adenosine monophosphate (cAMP) synthesis can occur depending on the adenosine receptor. Both ADORA1 and ADORA3 bind to the G-inhibitory subunit, resulting in a decrease in intracellular cAMP, whereas ADORA2A and ADORA2B will couple with the G-stimulatory subunit leading to the increment of intracellular cAMP[69].

Furthermore, the adenosine receptors appear to play different roles in the pathogenesis of fibrosis depending on the tissue involved, i.e. the same receptor may cause an agonistic or antagonistic effect in different tissues.

Wakeno *et al*. (2006)[70] demonstrated a decrease in the progression of fibrosis and remodelling of the myocardium after infarction when ADORA2B was stimulated. Furthermore, ADORA2B agonism has also been shown to impede collagen synthesis by cardiac fibroblasts and promotes cardiac remodelling, which suggests that this receptor has a protective effect in myocardial fibrosis[71].

Nevertheless, the activation of ADORA2B has been shown to engage with adenosine to induce differentiation of pulmonary fibroblasts into myofibroblasts, suggesting that adenosine may promote profibrotic activities in the lung[65]. A further study performed by Zhong *et al.* (2005)[72] reported that 5'-(*N*-ethylcarboxamido)-adenosine (NECA), an adenosine receptor agonist, possessed the capability to induce the transformation of pulmonary fibroblasts to myofibroblasts, which was mediated by the release of IL-6. In addition, Sun *et al.* (2006)[64] used an ADORA2B antagonist to demonstrate the decrease of α-SMA staining and myofibroblasts in adenosine deaminase-deficient mice and the reduction of expression of several chemokines and cytokines, such as TGF-β. Furthermore, Sun and co-workers showed that ADORA1 might have anti-inflammatory activity in the lung[73].

ADORA2B agonism has also been reported to increase the levels of adenosine in adenosine deaminase-deficient mice in the penis, leading to the development of priapism and it was also associated with fibrosis in the corpus cavernosum and corpus spongiosum[66].

Adenosine has an essential role in the development of dermal fibrosis. A study by Fernández *et al.* (2008)[62] showed that administration of an ADORA2A antagonist in adenosine deaminase-deficient mice led to the decrease of the development of dermal fibrosis and to the decrease in the production of numerous growth factors and profibrotic cytokines. In addition, it was also demonstrated that in liver fibrosis, agonism of ADORA2A triggered the decrease of actin stress fibres in hepatic cells[74].

Current literature presents very limited plausible explanation for the evolution of the different roles and physiologic responses by the four receptors in different tissues. The cellular context may play a role, as different types of tissue will have different signalling pathways present/absent that may be affected by adenosine receptor modulation. Different types of tissues may have different wound healing responses, which is modulated by, amongst other factors, the number and types of immune cells present, the amount of connective tissue present, blood flow and physical constraints. Additionally, this difference may also probably be dependent

on the stimuli that induces adenosine release and modulate receptor expression and function. For example, as lung and heart are organs which are constantly exposed to several antigens, these may respond differently to adenosine than liver or skin[75], which may explain the different effects of adenosine receptors in different tissues.

The table below shows a summary of the effects caused by adenosine receptor agonists and antagonists in the fibrotic disorders described in this chapter.

Table 1-1: Summary table of the effects caused by adenosine receptor agonists and antagonists. The effect of the agonist or antagonist on adenosine receptors in the fibrotic disorders described in this chapter has been summarised. Legend - green: impedes fibrosis, red: promotes fibrosis, black: anti-inflammatory and blank: unknown.

Tissue	Effect caused	Adenosine receptors			
		ADORA1	ADORA2A	ADORA2B	ADORA3
Lung	Agonist	Adenosine[73]	CGS21680[76]	NECA[72]	
	Antagonist			CVT-6883[64]	
Kidney	Agonist		CGS21680[77]	NECA[68]	
	Antagonist		ZM241385[77]	PSB1115[68] MRS1754[68]	
Liver	Agonist		NECA[74] CGS-21680[63]		
	Antagonist		ZM241385[63,74]		
Heart	Agonist			NECA[78]	
	Antagonist			MRS1754[70]	
Skin	Agonist		CGS21680[79]		
	Antagonist		ZM241385[62]		
Penis (corpus cavernosum)	Agonist			NECA[66]	
	Antagonist			MRS1754[66]	

1.1.3 Estrogen receptors in fibrosis

Estrogen is a steroid hormone, which plays an important role in the growth, development and maintenance of several tissues. 17 β-estradiol (E2), an intracellular estrogen has been conventionally connected with the female reproductive system; however, this hormone has also been reported in the male reproductive system and in other organ systems, such as the central nervous system, the cardiovascular system, bone tissue and the breast[80].

Estrogen mediates its physiological effects through ligand-activated transcription factors, known as estrogen receptors (ERs). These receptors belong to a superfamily of intracellular nuclear receptors, which consist of a highly conserved DNA-binding domain; a variable N-terminal transactivation (AF-1) domain and a C-terminal ligand-binding domain (LBD)[81].

Two ERs have been identified in humans, estrogen receptor-alpha (ERα) and estrogen receptor-beta (ERβ)[82], which are encoded by distinct genes located on different chromosomes. The ERα is found on chromosome 6 (6q25.1 locus) while the ERβ is located on chromosome 14 (the boundary between 14q11.1 and 14q11.2)[82]. Both ERs bind to estrogen with practically equivalent affinity and show an analogous binding profile for an abundant number of natural and synthetic ligands.

Estrogen action may induce cellular changes, activating target genes through various mechanisms. In the traditional mechanism, estrogen crosses the cell membrane and binds to the ERs in the nucleus. This estrogen-ER complex binds directly or indirectly to estrogen response element sequences, leading to the recruitment of coregulatory proteins, decreasing or increasing the synthesis of target genes. A quick mechanism of action can also take place within minutes by non-genomic pathways, either through the ERs situated in or surrounding the plasma membrane or through another non-ERs plasma membrane-associated estrogen-binding proteins. This process leads to cellular responses, including activation of kinases and increased levels of NO[83] (Figure 1-4).

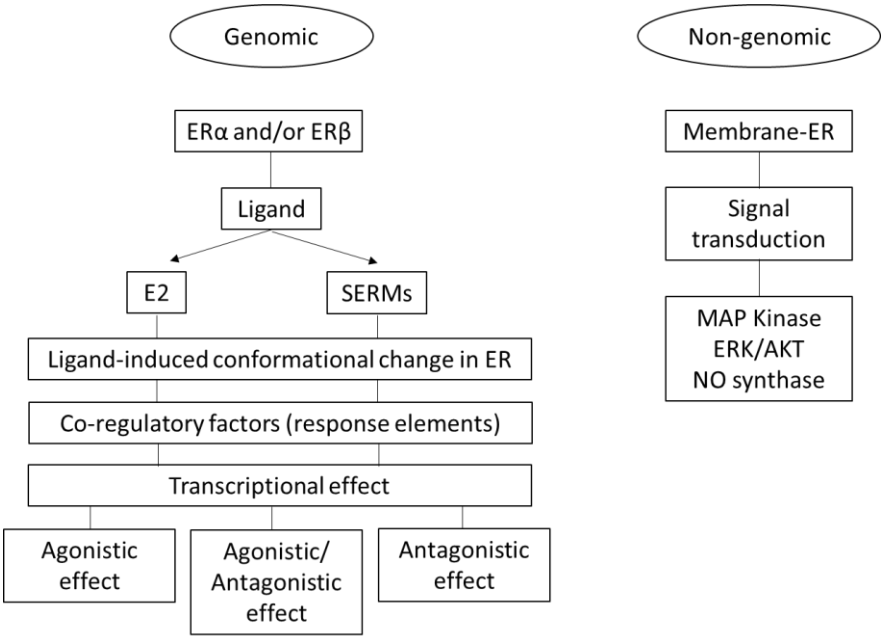

Figure 1-4: Mode of action of estrogen. Estrogen receptors undergo a conformational change upon binding to E2 and/or selective estrogen receptor modulators (SERMs), which facilitates the interaction of the receptor with estrogen response elements (ERE) located within the target gene. Different effects on the ER's structure can be due to different ligands. The interaction with ERE can act as co-regulatory factors, which will lead to different transcriptional effects inducing an agonistic, an antagonistic or a mixture of agonistic/antagonistic effects. Adapted from Deroo & Korach (2006)[83].

Several studies have reported that the expression of the two ERs varies between the tissue type and on the location. ERα is expressed in female reproductive organs (e.g. uterus, ovary, mammary gland); whereas ERβ is more broadly expressed and has been reported to be present in female reproductive organs, as well as lung, heart, bladder, kidney, thymus and skin[84,85]. The difference in expression of the two ERs suggests that these receptors have cell-specific roles, which may regulate the expression of other genes.

Selective estrogen receptor modulators (SERMs) are a class of non-steroidal compounds, which act as ligands for ERs. In contrast to estrogen that acts as ER agonist, the SERMs possess the capability to selectively function as antagonists or agonists in a target gene and in a tissue[86,87]. This tissue-selective pharmacology is an advantage for SERMs, as they can mimic the beneficial actions of estrogen in target tissues (e.g. liver, bone and the cardiovascular system) and avoid harmful off-target effects (e.g. breast and brain)[86,88].

This tissue-selective pharmacology depends on a diversity of factors, such as estrogen concentration in the environment, the cellular and promoter context and the SERM chemical structure. When a SERM binds to the ER, it causes a conformational change in the receptor. This structural change controls which corepressors and/or coactivators engage with the promoter, resulting in either an agonist or antagonist activity by the SERM. Furthermore, the ratio between the expression of ERα and ERβ in the tissue also affects the SERM agonist or antagonist activity[83].

SERMs are used in the prevention and treatment of breast cancer, maintenance of beneficial serum lipid profiles and prevention of osteoporosis in postmenopausal women. Nevertheless, it has been reported that SERMs can promote side effects, including thromboembolic events and occasionally carcinogenesis[86].

The most well-known SERMs include tamoxifen, raloxifene and toremifene. Tamoxifen was the first clinically relevant SERM, which is an ER antagonist in the breast and an ER agonist in liver, uterus and bone[83]. This SERM was the first drug to be approved by the Food and Drug Administration (FDA) and used in high-risk premenopausal and postmenopausal women to attenuate breast cancer incidence[89]. Raloxifene is also a SERM that has been reported to preserve bone density and is being used to prevent and treat osteoporosis in postmenopausal women, as it exhibits greater agonist activity in bone than tamoxifen[90]. Toremifene is a new SERM with similar properties and side effects to tamoxifen; however, FDA has restricted its use in postmenopausal women with metastatic breast cancer[88].

Several studies have found that estrogen impedes fibrogenesis and the activation of fibroblasts in various organs, such as heart[91], kidneys[92], lung[93] and liver[94].

A study performed by Ashcroft *et al.* (1999)[95] reported that after topical application of estrogen, skin wound healing improved. Their study showed significantly decreased wound size, increased wound stiffness and increment of collagen amount. Furthermore, Merlo and colleagues (2009)[96] reported in an *in vitro* study that ER plays distinct roles in wound healing on human keratinocytes. This study

also presented increased cell proliferation associated with an increase in TGF-β1 production by ERα agonist. In contrast, ERβ agonism increased cell proliferation independently of TGF-β1.

However, estrogen has also been reported to increase the secretion of fibronectin and TGF-β1[80,97], leading to myofibroblast differentiation, contraction and collagen production in dermal fibroblasts. Furthermore, Novotny and colleagues (2011)[98] showed that ERs agonists induced myofibroblast differentiation and excessive ECM deposition in ovariectomised rats. In contrast to the above studies, Pedram *et al*. (2010)[91], has reported that E2 acting at ERβ prevented myofibroblast differentiation and production of fibrosis-inducing proteins including collagen, TGF-β1 and fibronectin. Several studies have demonstrated that tamoxifen has anti-myofibroblast activity. The expression of α-SMA was reduced in healing pig biliary tract tissue after bile duct reconstruction and treatment with tamoxifen[99]. Moreover, previous reports have shown the efficacy of tamoxifen in reversing the fibrotic process, by preventing the deposition of ECM, leading to the inhibition of collagen production[100].

Estrogen has been known to play an important role in the development of penis. For example, male offspring of humans and animals that are exposed to estrogen-like endocrine disruptors [e.g. diethylstibesterol (DES)] or phytoestrogens during development exhibit abnormal reproductive organs including stunted penises[101–103]. Furthermore, exposure of neonatal rats to tamoxifen has been reported to disrupt the development of os penis and glans penis[104,105]. These developmental effects of estrogen has been proposed to be mediated mainly by ERα[106].

The role of estrogen in the adult penis is relatively less understood than in the neonatal penis or the penile development. Estrogen has been shown to be produced in the adrenal gland and in the testis in quantities overall far less than in the female[107]. The two ERs have been shown to be expressed in urethral epithelia and vascular and neuronal structures of adult rat penis[108]. Dietrich, *et al.* (2004)[109] observed that both receptors are expressed in human corpus cavernosum smooth muscle cells, endothelial cells and urethral epithelial cells in

adult penis. It is thought that through these two receptors, estrogen plays a role in regulation of blood flow and epithelial function in the adult penis[109], but functional studies in this topic to support these assertions have been missing.

Despite the cellular effect of estrogen on fibrosis signalling being unclear, the effect of estrogen receptor agonism by either estrogen or tamoxifen has consistently shown an anti-fibrotic effect in different tissues. The table below shows a summary of the effects caused by the ligands of the estrogen receptors in the fibrotic disorders described in this chapter.

Table 1-2: Summary table of the effects caused by estrogen receptor ligands. The effect of ligands on estrogen receptors in the fibroproliferative disorders described in this chapter has been summarised. Legend - green: impedes fibrosis, red: promotes fibrosis, black: anti-inflammatory and blank: unknown.

Tissue	Estrogen receptors ligands
Lung	Estrogen[110]
Kidney	Estrogen[92] Tamoxifen[100]
Liver	Estrogen[111] Idoxifene[112]
Heart	Estrogen[91]
Skin	Estrogen[80]
Penis	Estrogen[113]

Several tissues can be affected by fibrosis and examples of fibrotic disorders will be described including pulmonary fibrosis, renal fibrosis, liver fibrosis and a more detailed overview of Peyronie's disease. The role of adenosine and estrogen receptors in each fibrotic disease will also be discussed in further detail.

1.2 Pulmonary fibrosis

Pulmonary fibrosis is a complex fibroproliferative disease secondary to other interstitial lung diseases, including autoimmune disorders and viral infections to the lung[114]. This fibrotic disorder is characterised by the excessive accumulation

of ECM components within the pulmonary interstitium, resulting in the destruction of the air sacs (alveoli) around capillaries and lung tissues. The resulting fibrotic mass causes loss of elasticity and the development of rigid lung as well as permanent loss of function (Figure 1-5)[114]. TGF-β1 has been shown to induce myofibroblast differentiation in human lung fibroblasts, leading to increasing α-SMA mRNA expression in a concentration-dependent manner[115].This fibrotic disorder can be initiated by a diversity of factors, such as drugs (bleomycin, gentamicin, cisplatin and cyclosporine) and exposure to radiation, toxic vapours or inorganic dust.

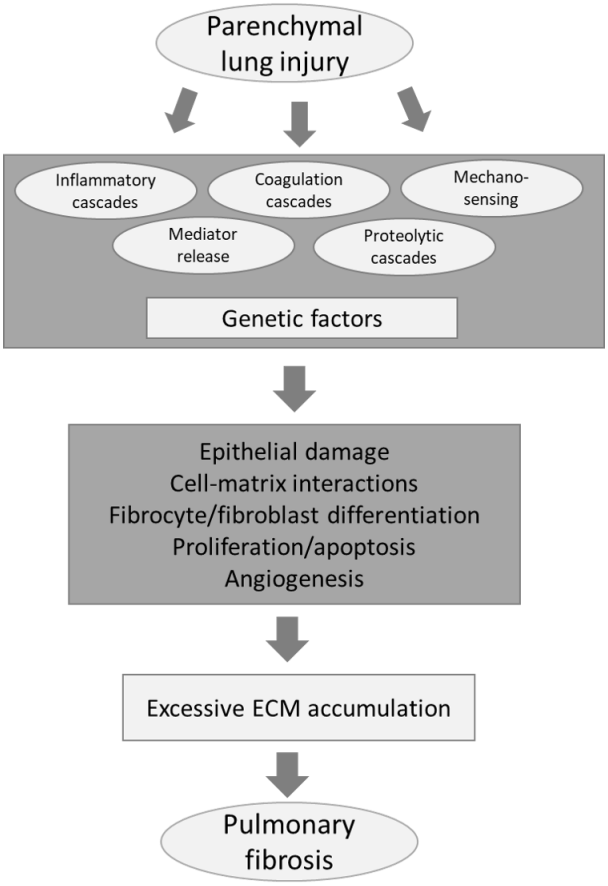

Figure 1-5: Pulmonary fibrosis process. Upon lung injury, a series of events occur, which will lead to excessive ECM accumulation and consequently to pulmonary fibrosis. Adapted from Chua *et al*. (2005)[116].

Idiopathic pulmonary fibrosis is one of the most frequent and most fatal among the interstitial lung diseases with an average survival time of 2-3 years following diagnosis[117]. IPF is defined by cell injury and stimulation of alveolar epithelial, fibroblast/myofibroblast foci development and exaggerated deposition of ECM in

the lung parenchyma, leading to the loss of pulmonary function[14], with no known cause. In the USA alone, this disease affects between 150,000 and 200,000 people and approximately 40,000 patients die per year[118]. Similar prevalence, incidence and mortality rates have been reported in Europe[119].

The treatment of IPF has been based on the current evidence-based guidelines published by Raghu *et al*. (2011)[120], which includes lung transplantation, oxygen therapy and pulmonary rehabilitation. Medical treatment options are limited to pirfenidone and nintedanib which have been shown to reduce disease progression and functional decline in patients with mild to moderate functional impairment[118].

Adenosine receptors in pulmonary fibrosis

All four adenosine receptors have been shown to be expressed in mice and human lungs with different roles. The activation of ADORA1 and ADORA3 by adenosine or an agonist results in pulmonary protection and have a pro-inflammatory role. Whereas the activation of ADORA2B has been suggested to lead to the release of several inflammatory cytokines promoting the transformation of lung fibroblasts into myofibroblasts[121].

The transcript levels of the four adenosine receptors were investigated in human lung fibroblasts and it was observed that among the four receptors, ADORA2B had the highest mRNA levels, followed by ADORA1, ADORA2A and ADORA3, where lower transcript levels were detected. The mRNA levels of the adenosine receptors were confirmed by immunofluorescence staining. Human lung fibroblasts were stained with an anti-human ADORA2B antibody, showing the protein levels of this receptor in these cells[72,122]. In addition, a study characterised the expression of adenosine receptors in subjects with preserved lung function and patients with severe IPF and stage 4 chronic obstructive pulmonary disease (COPD) and showed that all four adenosine receptors were observed in preserved lung samples; whereas, only the ADORA2B transcript levels were significantly increased in stage 4 COPD and severe IPF patients[123].

In the lungs of mice exposed to bleomycin (fibrosis-inducing agent), adenosine levels have been reported to be elevated leading to alterations of the adenosine metabolism and signalling with up-regulation of CD73 (responsible for adenosine production)[124]. Furthermore, in adenosine deaminase (ADA)-deficient mice, chronic adenosine levels have been documented and has been suggested to be correlated with lung fibrosis, indicating that adenosine has a profibrotic activity in the lung[65].

Inhibition of ADORA2B activity using a specific and selective antagonist in the lungs of ADA-deficient mice has been shown to interfere with the progression of the inflammatory and fibrotic processes[121]. In addition, topical application of an ADORA2A agonist (CGS-21680) has been reported to significantly increase excisional wound closure and healing in both normal and diabetic rats[125].

Estrogen receptors in pulmonary fibrosis

The mRNA levels of ERα and ERβ were investigated in normal human lung fibroblast cell lines and in human lung tumour cell lines and it was demonstrated that both receptors were expressed in these cells. The protein levels were also examined for both receptors in normal lung fibroblasts and in lung tumour fibroblasts. Western blot analyses showed the protein expression of both ERs in these cells. Moreover, the ERα was localised in the cytoplasm, whereas the ERβ expression was mainly localised in the nucleus of human lung fibroblasts[126,127].

Morani and colleagues (2006)[93] demonstrated that ERβ knockout mice have increased levels of collagen and abnormal clusters of collagen fibres in the alveolar septa of these mice, suggesting that ERβ is essential for the maintenance of ECM composition in the lung.

Card and Zeldin (2009)[128] showed that E2 increased the expression of TGF-β1 and procollagen mRNA levels in fibroblasts isolated from rat fibrotic lung. A similar study also demonstrated that fibroblasts from bleomycin-treated rats showed an enhanced response to E2 treatment caused by increased procollagen 1 and TGF-β1 transcript levels compared to untreated controls[129]. Conversely, a study by Voltz *et al*. (2008)[110] reported that E2 played a role in decreasing lung

fibrosis in bleomycin-induced pulmonary fibrosis in C57BL/6 mice after bleomycin administration.

The development of lung fibrosis is significantly higher in patients treated with tamoxifen and radiotherapy than in patients only treated with radiotherapy[130]. In addition, Bese and colleagues (2006)[131] assessed the effects of tamoxifen on lung fibrosis in Wistar albino rats and reported that the use of tamoxifen concurrently with irradiation led to the progression of lung fibrosis.

1.3 Renal fibrosis

A common pathological feature of progressive chronic kidney disease (CKD) is renal fibrosis, leading to end-stage renal failure. This fibrotic disorder is characterised by myofibroblast accumulation and excessive scarring, progressing to the destruction of renal tubules[132]. This condition can also be characterised by loss of renal parenchyma, tubulointerstitial fibrosis, inflammatory cell infiltration and glomerulosclerosis[133]. All these pathological features originate from a series of events typical of the fibrotic process, including excessive synthesis and deposition of ECM components; myofibroblast differentiation and accumulation and activation of profibrotic cytokines[133] (Figure 1-6). TGF-β1 induces its profibrotic effects on the kidney by producing ECM, transforming fibroblasts into myofibroblasts and acting on numerous renal resident cells, which can result in the deterioration of renal injury[134].

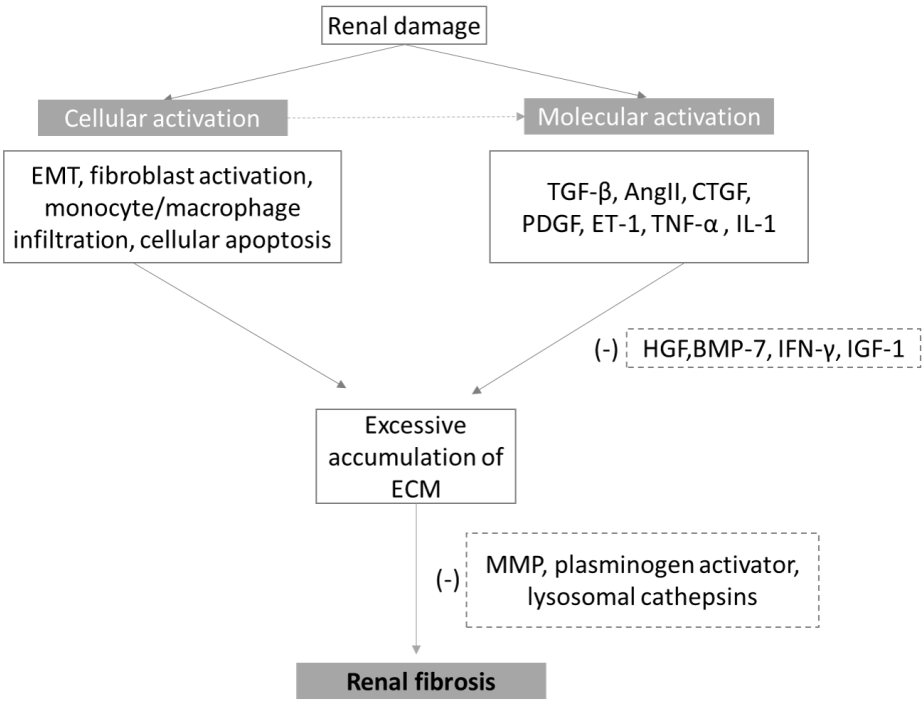

Figure 1-6: Renal fibrosis process. Upon renal damage, cellular and molecular activation occurs, where inflammatory cells are recruited and several profibrotic cytokines are released, resulting in excessive accumulation of ECM. Renal fibrosis is the outcome of this process. Adapted from Cho (2010)[133].

CKD incidence appears to have been increasing over the past decade with an annual incidence of end-stage renal disease of approximately 100 patients per 1,000,000 population[135]. In England, studies have reported 6 - 8.5% of adults present late-stage CKD and 6,000 new cases are diagnosed annually[136]. In the USA alone, chronic kidney disease affects 12% of all adults and these patients require renal replacement therapies, including transplantation and dialysis. The annual incidence of dialysis has doubled in the past decade, in developed countries, being highest in the USA[23,133].

Adenosine receptors in renal fibrosis

The distribution of the four adenosine receptors in the normal kidney is not fully defined; however, these receptors have been detected in this organ[137,138]. Adenosine has been shown to be increased in patients with CKD[68]. A study performed by Zhang *et al.* (2013)[139] showed that renal biopsy samples from CKD patients had increased levels of ADORA2B mRNA expression compared to patients without CKD, suggesting that ADORA2B signalling may have a role in

the development of renal fibrosis. The protein levels of ADORA2B showed that the expression of this receptor was elevated in both tubules and glomeruli of kidney biopsies collected from CKD patients compared to control samples. Furthermore, Xiao and colleagues (2013)[140] observed that ADORA2A mRNA and protein levels were present in kidney tissue samples from mice.

Several studies have shown that inhibition of ADORA2B attenuated the development of renal fibrosis in ADA-deficient mice where the mice showed chronically elevated levels of adenosine[68]. A rat model with CKD and treated with an ADORA2A agonist (CGS21680) was reported to attenuate the progression of renal fibrosis, where the reduction of TGF-β, α-SMA and collagen expression was observed in agonist-treated rats[77].

Estrogen receptors in renal fibrosis

The transcript levels of both ERs have been demonstrated in human and mouse mesangial cells of the glomerulus, where ERα is the main receptor expressed. The protein levels of these two receptors were investigated in both human and mouse mesangial cells using Western blot analyses. The respective band for each receptor at the correct molecular weight was observed in both human and mouse mesangial cells[100,141].

A study by Dixon *et al*. (2007)[92] showed that E2 diminished the development of renal fibrosis by regulating TGF-β1 and ECM expression. In addition, a rat model with hypertensive nephrosclerosis was treated with tamoxifen and it was reported that tamoxifen impeded the accumulation of ECM proteins by reducing the mRNA and protein expression of collagen and fibronectin. Tamoxifen also significantly decreased the expression of α-SMA positive cells and inhibited TGF-β1 and PAI-1 in the renal interstitium[100].

1.4 Liver fibrosis

Liver fibrosis is a frequent pathological characteristic of chronic liver disease (CLD) that occurs in response to liver damage. Similar to other fibrotic disorders, this results in an inflammatory response leading to hepatic stellate cell (HSC) activation, myofibroblast differentiation and excessive production and deposition

of ECM components[142]. Disruption of the hepatic architecture occurs, as well as, reduction of blood flow to hepatocytes and alteration of liver function, progressing to cirrhosis[143,144] (Figure 1-7). Liver damage can be triggered by several factors, including hepatitis B virus, hepatitis C virus, alcoholism, fatty liver, metabolic disease, ischemia-reperfusion, alcoholic steatohepatitis (ASH) and toxins[143,145].

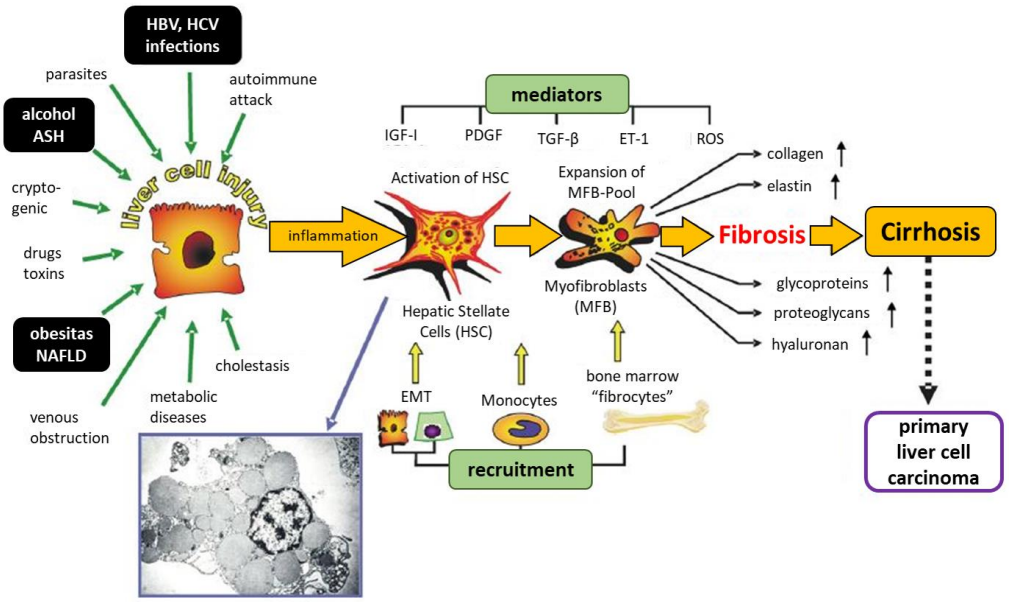

Figure 1-7: Pathogenesis of liver fibrosis. Liver fibrosis is a complex process, which is predisposed by a diversity of factors, including viral infections, alcohol consumption, non-alcoholic fatty liver disease (NAFLD) among others. This has been suggested to result in the activation and differentiation of hepatic stellate cells to myofibroblasts, leading to fibrosis. Adapted from Gressner *et al.* (2007)[146].

Chronic liver diseases are among the leading causes of morbidity and mortality worldwide. The incidence of chronic liver disease is rising in the UK and worldwide, where alcohol abuse and viral infections are the main causes. In the USA, approximately 150,000 people are diagnosed with chronic liver disease each year[144,147].

Currently, liver transplantation is the gold standard treatment for cirrhosis, which has a number of disadvantages, such as limited organ donors and the complexity of the procedure[145]. Several studies using *in vivo* and *in vitro* models have shown potential new approaches, targeting the underlying disease processes (e.g. viral infections); however, no drug has yet emerged as an anti-fibrotic treatment option in this disease.

Adenosine receptors in liver fibrosis

A study by Hashmi *et al*. (2007)[148] showed that an immortalised human HSCs expressed ADORA2A, ADORA2B and ADORA3 mRNA levels, but not ADORA1 transcript levels. Furthermore, another study demonstrated that the ADORA2A mRNA expression was increased in fibrotic murine liver compared with normal liver, suggesting that this receptor plays a main role in liver fibrosis, as the central profibrotic actions of adenosine are mediated through this receptor[63]. In addition, these authors also treated mice liver sections with carbon tetrachloride (CCl4) and thioacetamide (TAA) to induce liver fibrosis. They reported that the *ex vivo* mice samples treated with CCI4 and TAA released more adenosine than the untreated samples.

ADORA2A-deficient mice, when treated with ADORA2A antagonists, have been reported to halt the development of liver fibrosis, suggesting that this receptor play a role in the pathophysiology of this fibrotic disorder[75]. In addition, C57BL/6 control [wild-type (WT)] mice and CD73 knockout mice were treated with CCl4 or TAA to induce hepatic fibrosis. The authors showed that WT mice released more adenosine than CD73 knockdown mice and there was less collagen content than in WT mice after treatment. Furthermore, the expression of all four adenosine receptors was increased after CCI4 treatment in both WT and CD73 knockout mice[149]. All these studies indicate that treatment with ADORA2A antagonist could in principle protect the liver from liver fibrosis[150].

Estrogen receptors in liver fibrosis

Various studies performed in female and male rat HSCs demonstrated expression of mRNA and protein levels of ERα[111,151]. Xu *et al*. (2004)[111] showed that E2 prevented the accumulation of ECM proteins in rats subjected to CCI4. The authors also observed that the hepatic mRNA levels of ERα were enhanced after treatment with E2. Furthermore, idoxifene (a tissue-specific SERM) effects were evaluated on liver fibrosis in rats. This SERM showed protection against hepatic fibrosis in rats by decreasing the protein expression of collagen in HSC cells[112].

One of the studies also showed that ERβ protein was mainly found to be localised in the nucleus in both hepatocytes and HSCs; however, some ERβ was also localised in the cytoplasm of the cells[151].

1.5 Peyronie's disease

Peyronie's disease was first reported in 1743 by Francois Gigot de la Peyronie, who was the personal physician of King Louis XV of France[152]. PD is a localised connective tissue disorder, which is characterised by the formation of fibrotic plaques in the TA and surrounding vascular tissue in the corpus cavernosum of the penis[153] (Figure 1-8). The fibrotic plaque results in penile pain; penile deformities, such as narrowing, bending and shortening during erection and erectile dysfunction (ED)[154].

Even though, there are many similarities between PD and other fibrotic disorders, such as abnormal wound healing, excessive production of ECM proteins and cytokines and myofibroblast differentiation process, PD is self-limiting and very unlikely to cause death as observed in other fibroproliferative diseases of vital organs (such as pulmonary fibrosis, renal fibrosis, liver fibrosis).

The precise cause of this is unclear but it is possible due to the anatomical uniqueness of the location, as, contrary to other tissues, there only a thin layer of fibrous tissue in the TA that has physical barriers on either side (deep fascia and corpus cavernosum), whereas in other tissues the capacity for growth of the fibrous tissue is much greater. It may also suggest that the initiating cause of the fibrosis in PD is a single event as opposed to continuous micro-traumas, that would continually lead to the transformation of new myofibroblasts and subsequent ECM deposition.

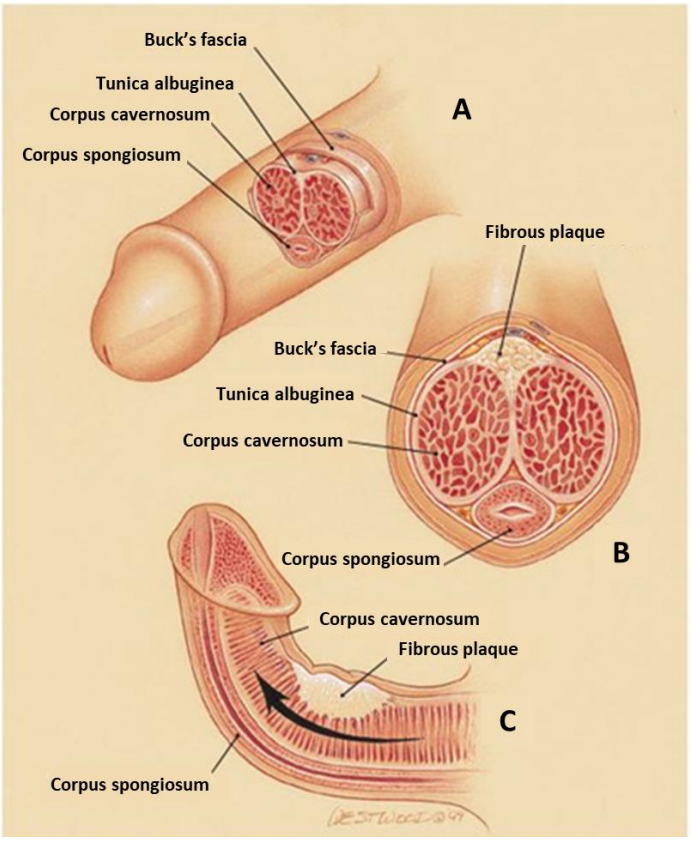

Figure 1-8: Penile bending related to Peyronie's disease. (A) Anatomy of a normal erection. (B) Cross-section of a penis presenting a fibrous plaque. (C) Penile curvature. The fibrous plaque impedes a normal erection, leading to the bending of the penis. Adapted from Fitkin & Ho (1999)[155].

1.5.1 Epidemiology & aetiology

Peyronie's disease principally affects males between 45 and 65 years of age, with several reports of cases in younger males. The prevalence of PD is usually underestimated and ranges from 0.39% to 8.9%. According to Lindsay *et al.* (1991)[156], the prevalence rate of PD was 388.8 per 100,000 men (0.39%) in Rochester, Minnesota. However, a study performed by Sommer *et al.* (2002)[157] found that the prevalence of PD was 3.2%, through a validated questionnaire survey involving 8,000 men in the greater Cologne area, Germany. A study involving 534 men who presented to a prostate cancer screening centre to provide a physical examination and their medical history reported that 8.9% of those men had a palpable penile plaque[158]. Moreover, a study performed by Arafa *et al.* (2007)[159] reported the highest prevalence of PD (20.3%) in a subsection of patients that also presented ED and diabetes mellitus (DM).

Even though studies on PD prevalence are quite inconsistent and limited, the disease prevalence has been suggested to increase consistently over the last 30 years and it may be higher than the reported occurrence, due to patients' hesitancy to report to their physician for diagnosis and treatment. The under-diagnosis of PD by physicians may also contribute to this under-estimation, due to limited understanding of this fibrotic disorder[160].

The pathogenesis of PD is still unclear; however, its aetiology is thought to be multifactorial and several theories suggest that a diversity of factors may be involved, including ED, trauma, genetic predisposition or uncontrolled fibrosis. Although its aetiology is thought to be multifactorial, trauma has been postulated as the initiating factor, which is then followed by aberrant wound healing and scar formation[157,160].

ED is known to occur in 20-40% of patients with PD[161,162] and is one of the risk factors related to the development of PD. A recent study performed by Kadioglu *et al.* (2011)[163] involving 1,001 patients reported that 58.1% of patients with PD also presented ED. Several factors may contribute to the development of ED, such as penile deformity preventing intercourse; penile pain during erection; psychological effects or performance anxiety due to the appearance of the penis and impaired veno-occlusive mechanism due to extensive fibrosis[164,165]. Furthermore, a study performed by Lopez and Jarow (1993)[166] using ultrasonography stated that 59% of 76 men with PD had veno-occlusive dysfunction and 36% had an arterial disease which caused ED. The presence and the severity of ED should be considered when weighing surgical options, as it remains a complication for reconstructive surgeries.

PD has also been associated with several other conditions, including DM[167], hypertension[158], Ledderhose's disease[168], use of β-blockers[157] and Knuckle pads[168].

Although PD has not been genetically linked to a predisposed population; several reports have associated PD with Dupuytren's contracture[169], Paget's disease of the bone[170] and specific human leukocyte antigen (HLA) subtypes[171]. Both Dupuytren's contracture and Paget's disease of the bone are genetic disorders,

which are transmitted in an autosomal dominant pattern. A study comparing the gene expression variations in PD and Dupuytren's contracture patients reported that the pattern of variations in the gene expression is similar to both disorders, proposing that these two diseases share common pathophysiologic features[172]. In addition, a study involving 61 men with Paget's disease reported that 31.4% had developed a deformity or bend in their erect penis, suggesting that PD may be associated with Paget's disease of the bone[170,173].

According to Nachtsheim & Rearden (1996)[171], there is an association between PD and the HLA class II antigen HLA-DQ5, suggesting HLA-DQ5 as a risk factor for the development of PD and also inferring an autoimmune aetiology for PD.

An immunological component has also been proposed as one of the aetiological factors of PD. A study involving 66 patients investigated the immune response pattern of the disease and reported alterations in cell-mediated immunity in 48.5% of the patients, modifications of humoral immunity in 31.8% of the patients and changes in markers of autoimmune diseases in 37.9% of the patients[174]. Patients with PD showed higher levels of anti-tropoelastin (responsible for elastin synthesis) and anti-α-elastin (responsible for elastin destruction) than healthy patients. These findings suggest the presence of autoimmune mechanisms in the pathogenesis of PD[175].

1.5.2 Pathophysiology of Peyronie's disease

In the TA of the penis, the elastic fibres form an irregularly latticed framework upon which the collagen rests, which is crucial to maintaining the structure of the collagen bundles. Both structural components are crucial to penile erection, as these structures allow an increment in length and girth during tumescence[176]. In the case of any flaw of the tunica collagen or elastic fibre network, it can result in major modifications in the hemodynamics of erection[175,177].

The histopathology of PD reveals an inflammatory process, which is characterised by the presence of a diversity of inflammatory cells, such as mast cells, neutrophils, leukocytes and macrophages in the TA and in the surrounding erectile tissues[176,178]. The cause of the initial inflammatory process that results in

fibrosis, calcification and plaque formation is still unclear and poorly understood, but it has been suggested that trauma or repetitive microtrauma might be an initiating factor[178,179].

Trauma might cause excessive physical forces inflicted on the penis during intercourse, resulting in bleeding into the subtunical spaces or tunical delamination[178]. A study involving 732 patients showed a link between penile trauma and both PD and ED[180]. Trauma is then followed by aberrant wound healing and formation of scar tissue in the TA. As a consequence of repetitive injury, fibrin deposition occurs (a normal component of wound healing), activating fibroblast proliferation and ECM accumulation[164,181]. It is suggested that the balance between scar tissue formation and ECM exceeds that of degradation of both ECM and collagen due to abnormal fibroblast activity[175].

Fibrin further stimulates an increase in collagen deposition, acting as a profibrotic protein due to the presence of TGF-β and PAI-1 within the TA[165]. PAI-1 is a protease responsible for inhibiting fibrin degradation[182]; whereas TGF-β is involved in several crucial processes (e.g. normal wound healing, inflammation and stimulation of ECM)[165]. Fibrin deposition has been demonstrated in PD plaques, but not in normal or scarred TA of control patients[183]. Furthermore, several reports showed that type III collagen is present in PD plaques, which contains dense collagenous connective tissue with fragmented and reduced elastin fibres[164,175].

In addition to trauma and inflammatory response in the TA, overexpression of growth factors and cytokines (e.g. TGF-β and PAI-1) by leucocytes also occurs, leading to the recruitment of more inflammatory cells and release of profibrotic factors and ROS[165]. El-Sakka and colleagues (1997)[184] reported that TGF-β was upregulated in the TA of patients with PD when compared to the TA of men without PD.

El-Sakka and colleagues have also proposed an animal model for PD, where the authors investigated histological and ultrastructural modifications in the penis of rats after inducing a PD-like condition by injecting a TGF-β-like substance (cytomodulin) and by inducing trauma of the TA[185,186]. The histological alterations

observed included diffuse and focal degeneration of elastic tissue; chronic inflammation, infiltration and disorganisation, thickening and clumping of the TA. On the other hand, the ultrastructural alterations involved separation of neuronal fibres by clumps of packed collagen and dense collagen bundles.

Another animal model by Bivalacqua and colleagues was proposed to demonstrate the role of nuclear factor kappa B (NF-κB), which is a transcription factor responsible for regulating the expression of numerous genes that encode adhesion molecules (reviewed in Hellstrom & Bivalacqua, 2000[175]). The authors showed the immunohistochemical presence of NF-κB in rats with Peyronie's-like condition after TGF-β injection and injury to the rat penis. These rat studies also demonstrated that TGF-β injection and surgical injury can induce symptoms analogous to those found in men with PD.

Molecular basis of Peyronie's disease

TGF-β1 has been associated with a variety of soft tissue fibrotic disorders and it has a pleiotropic effect on fibroblast function. This protein induces ECM production; stimulates myofibroblast differentiation; increases transcription and synthesis of collagen, fibronectin and proteoglycans and inhibits collagenase, preventing connective tissue breakdown as well as increasing fibroblast proliferation and inducing chemotaxis[178,187].

Moreover, TGF-β1 can also induce ROS formation and inhibit NO production by repressing iNOS, lowering the NO/ROS ratio[164,187]. In normal tissues, fibrosis is inhibited by the expression of iNOS, which produces NO. NO can inhibit TGF-β1, due to its anti-fibrotic role, neutralising ROS, promoting collagen breakdown and decreasing myofibroblast differentiation. A rat model was used to show the role of NO in rats with Peyronie's disease-like condition and cells isolated from human non-PD TA tissue and PD plaque tissue. The authors reported that NO appears to reduce myofibroblast differentiation and collagen I synthesis, suggesting that NO has an anti-fibrotic role[188].

In PD, the balance between anti-fibrotic and profibrotic factors is altered, due to the ability of TGF-β1 to induce its own production in a positive feedback loop,

leading to excessive scarring and unimpeded fibrosis[187]. Protein and mRNA levels of TGF-β1 have been shown to be up-regulated in several fibrotic disorders including PD. Several other growth factors and cytokines, such as MCP-1[189] and PAI-1[190] have also been reported to be altered in PD plaques as well as skin, lung, liver and kidney fibrosis. Furthermore, patients with PD have also been demonstrated to express PDGF-α, PDGF-β, PDGF-AA, and PDGF-BB receptors in the TA, which are growth factors released by platelets after trauma and capable of exacerbating fibroblast proliferation[191].

Gonzalez-Cadavid *et al.* (2002)[179] applied DNA microarray technology to describe the gene expression profile in PD, by comparing the mRNA levels of the plaque and of the TA. The results obtained showed that the genes associated with collagen metabolism (e.g. collagen I or TGF-β1) in the plaque were up-regulated; whereas the genes involved in pathways inhibiting TGF-β1 (e.g. decorin) or related to the pathways contrasting collagen synthesis (e.g. pro-collagenase IV) were down-regulated. Moreover, the up-regulation of osteoblast-specific factor (OSF)-1, MCP-1, heat-shock protein (HSP) 28 and α-SMA were also observed, suggesting fibrosis, ossification, inflammation and myofibroblast accumulation.

Myofibroblasts in Peyronie's disease

Myofibroblasts are involved in numerous fibroproliferative diseases, including PD. Myofibroblast differentiation is an essential step in the wound healing process, as these cells are responsible for contracting the edges of the wound and synthesising ECM proteins to temporarily cover the wound and cytokines to recruit other cell types needed for normal wound resolution. The contractile property has been proposed to cause the contracture in the PD plaque (reviewed in Gonzalez-Cadavid, 2002[179]).

Several gene expression studies have shown that increased myofibroblast accumulation in the injury is associated with collagen deposition[179]. As stated above, α-SMA is increased in the fibrotic wound when comparing with normal TA. The inhibition of iNOS activity can lead to an increase in α-SMA/vimentin ratio, suggesting either a decrease in myofibroblasts apoptosis rate and/or further

myofibroblast differentiation[188]. It has also been shown that myofibroblasts constitute approximately 20% of cells cultured from PD plaques[192].

Furthermore, a study reported that myostatin (also known as growth differentiation factor 8; GDF8) is overexpressed in the PD plaque and absent in normal TA, especially due to myofibroblast accumulation during tissue damage and repair. Myostatin is another member of the TGF-β family and the results of this study suggested that both TGF-β1 and myostatin act concurrently[193].

1.5.3 Clinical Presentations and Evaluation

PD can be divided into an active phase and a stable or mature phase. In the early stages of PD, patients complain of penile pain and/or penile deformity during erection as well as the presence of penile nodules or palpable plaques. Penile pain during erections generally resolves within 6 months, whereas the penile curvature stabilises by 12 months. In later stages of PD, the clinical presentations include stable penile deformity or curvature during erection, harder plaque and development of ED[153,194].

The rigid plaque present in PD patients is generally located on the dorsal aspect of the penis, which causes an upward deviation during erection[161]. Plaques located on the ventral and lateral surface of the penis are less common, causing a downward and lateral curvature, respectively, which becomes more difficult during intercourse, as the deviation is greater than the natural coital angle[161,164].

For the evaluation of the disease, detailed medical, sexual and family history and physical examination should be performed. The detailed history and symptoms of patients should include the presence or absence of pain; duration of the disease; an estimation of the degree of the penile deformity; the orientation of the bend and the presence of penile shortening and hourglass constriction. All these clinical presentations can affect treatment options[164,194]. However, there are several questions that do not bear upon treatment of PD, these questions are still important, such as the psychological impact of PD on the lives of the patient and his partner and the patient's expectations of therapy[195]. The medical and sexual history as well as the follow-up to measure treatment efficacy, can be obtained

through standardised questionnaires, such as the Peyronie's Disease Index (PDI; used as an objective assessment of treatment and a subjective evaluation of PD) and the International Index of Erectile Function (IIEF; to assess the quality erections)[152].

In regards to the physical examination, it should include an evaluation of the pubis-to-glans length, due to the shortening of the penis; an assessment of the location and the number of plaques; the degree of plaque calcification and the observation for the presence of associated conditions (Dupuytren's disease, hypertension, diabetes, hyperlipidaemia)[152,194]. To identify the degree of plaque calcification and the location and the number of plaques, as well as venous leakage, penile vascular flow, and erectile response, the use of duplex ultrasonography can be very useful in this regard. Furthermore, to measure the curvature severity, an intracavernosal injection-induced penile erection is still the gold standard method[165]. Although blood tests are unreliable in the diagnosis, determination of several factors such as testosterone; prostate-specific antigen; glucose and lipid profile can be performed according to the clinical presentation[152,165].

1.5.4 Treatment of Peyronie's Disease

A definitive treatment course for PD has not been established yet; however, in the early stages of PD (6 - 12 months), non-surgical treatments are attempted. On the other hand, in the later stages of PD, where patients present a stable PD plaque (>12 months), surgical treatment is recommended.

Non-surgical treatments

Non-surgical treatments are minimally invasive treatments that are considered for patients to relieve the pain as well as to reduce PD deformity or progression. Although several of these non-surgical treatment options appear to have some benefit when applied in the early phase of PD, the majority of these therapies have not undergone accurate evaluation in suitably designed studies (i.e. double-blind, placebo-controlled clinical trials)[196]. These treatments include oral therapy,

intralesional injection therapy, topical treatments, iontophoresis, extracorporeal shock wave therapy and penile traction devices.

Oral therapy, such as vitamin E[197], potassium para-aminobenzoate[198], tamoxifen[199,200], acetyl-L-carnitine[199], colchicine[197,201] and phosphodiesterase type 5 inhibitors (PDE5i)[202] have been trialled and it has been shown that these compounds have limited efficacy in preventing PD progression or reversing the fibrosis.

Intralesional injection therapy has several advantages over oral therapy, as it provides a higher concentration of the drug and the pharmacologically active agent is injected directly into penile plaques. It has less adverse effects and it is a less invasive therapy than surgery. It has been demonstrated to have different degrees of efficacy in reducing penile pain and improving plaque size and penile curvature. This treatment includes steroids[203], verapamil[204,205] and interferons[206,207].

Purified clostridial collagenase is the only non-surgical treatment that is approved for PD. The drug works by altering collagen content of the penile plaque, showing important benefits when administrated in the early phase of PD. A phase III clinical trial has been performed, showing significant improvement in penile curvature in patients treated with collagenase when compared with the placebo group[208,209].

Furthermore, PDE5i[202,210,211] have shown anti-myofibroblast activity in animal models. It has been suggested that the administration of these compounds inhibit myofibroblast transformation through the increase in NO and/or cGMP/cAMP (cyclic guanosine and adenosine monophosphate) levels.

Other non-surgical treatments, such as topical treatments[212], iontophoresis[213], extracorporeal shock wave therapy[214] and penile traction devices[215] have shown some beneficial effects; however, long-term and controlled studies should be carried out.

Surgical treatments

Surgical treatment is reserved for PD patients who have failed non-surgical treatment and present severe curvature or narrowing that impedes sexual intercourse. The aim of surgical treatment is to make the two sides of the penis equal in size, either by shortening the longer side (plication) or lengthening the shorter side (grafting). Penile implant is one option when ED is present in patients with PD. These surgical procedures should be performed when the disease has stabilised (>12 months after onset). Regardless of the treatment, the patient should be aware of the expected outcomes and possible side effects, such as failure to completely straighten the penis, decreased penile sensation and shortening of the penis[194]. There are three types of surgical treatment: tunical shortening procedure (plication); tunical lengthening procedure (grafting) and penile prosthesis implantation.

The tunical shortening procedures are executed on the convex side of the penis, opposite the penile deformity[194]. Nesbit first described the correction of congenital penile deformities by excising an ellipse of TA, shortening the long side of the penis[164]. This type of procedure is ideal for men who have a good erectile function, adequate penile length and no narrowing or hourglass type of deformity[194].

Tunical lengthening procedure includes the use of reconstructive techniques to lengthen the concave side of the penis, which involves incision or excision of the plaque on the short side of the penis and restoring the defect with graft material[164]. This type of procedure should be considered for patients with hourglass or narrowing and severe curvature[165]. The ideal graft material should be flexible, readily available, resistant to infection, able to preserve erectile capacity and inexpensive. There are several autologous grafts (tunica vaginalis, temporalis fascia, saphenous vein and penile skin); cadaveric tissues (dermis, pericardium, fascia and porcine small intestine submucosa) and synthetic materials (polyester and polytetrafluoroethylene) that have been used with variable results[164].

The use of penile prosthesis implantation is reserved for patients with severe ED and vascular impairment that do not respond to non-surgical treatments. The penile length can be restored by excising or incising the plaque during prosthesis placement[216]. In cases where modelling is ineffective or the penile defect is severe, the use of plaque incision with or without grafting in addition to prosthesis placement might be necessary[175].

The clinical presentations and evaluation should be considered when managing and treating PD. The following scheme presents an overview of the management of this disease.

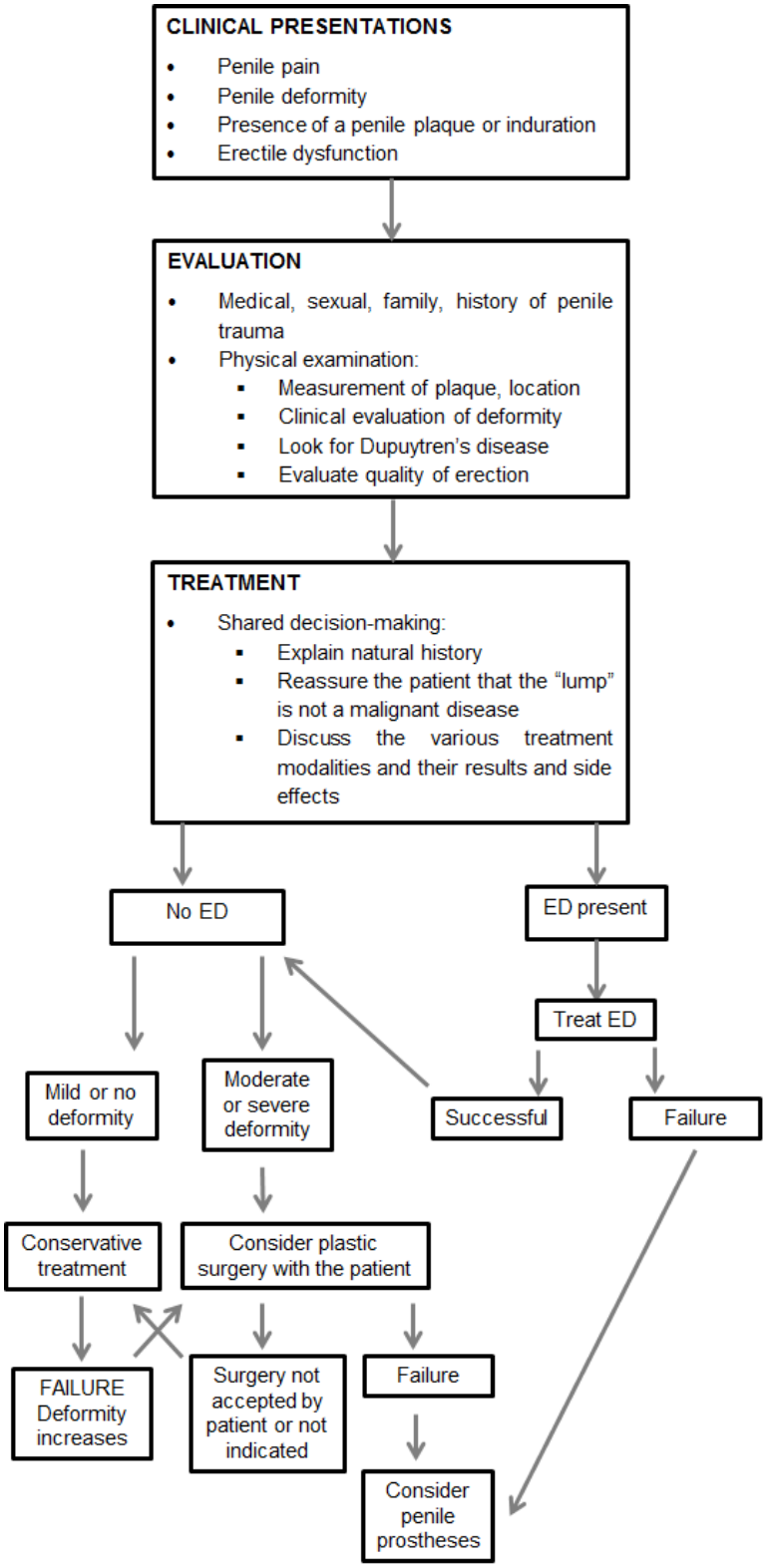

Figure 1-9: Peyronie's disease management. The clinical presentations and the evaluation of the disease should be considered when choosing the ideal treatment for the patient. Adapted from Pryor *et al.* (2004)[217].

The benefits of non-surgical treatment are inconsistent and further controlled studies are required before recommending any therapy. The successful results of surgical treatment have been well documented; however, this treatment is expensive, carries adverse effects and is invasive. A better understanding of the mechanisms by which fibrosis occurs in the tunica albuginea and the myofibroblast differentiation process will offer new possibilities for future medical interventions in PD.

Adenosine receptors in Peyronie's disease

A study performed by Mi *et al.* (2008)[67] showed that corpus cavernosal smooth muscle cells expressed transcript levels of ADORA2B supporting that this receptor is important for adenosine-induced cAMP synthesis and vascular smooth muscle relaxation. A similar study observed mRNA levels of ADORA2B in primary corpus cavernosal fibroblast cells (CCFCs)[66]. Wen *et al.* (2010)[66] reported that primary CCFCs derived from ADA-deficient mice treated with and without NECA (adenosine receptor agonist) showed that NECA-treated samples presented enhanced transcript levels of procollagen and TGF-β1. Furthermore, the increase of the mRNA levels of these cytokines was attenuated when CCFCs were exposed to MRS1754, an ADORA2B specific antagonist.

However, despite the above studies showing the presence and effect of adenosine receptor modulation in the penis, this has not been specifically determined in the tunica albuginea of the penis and consequently has also not been directly associated with Peyronie's disease.

Estrogen receptors in Peyronie's disease

Several studies have shown the expression of both ERα and ERβ in the penis[109,218,219]. The mRNA levels of ERα were mainly found in regions within and close to the glans penis. On the other hand, the mRNA levels of ERβ were found in the corpus cavernosum, corpus spongiosum, cells near to the glans penis and stroma of the glans penis. In regard to the protein levels, ERα protein was essentially localised in the corpus cavernosum, corpus spongiosum and glans penis; on the other hand, the protein levels of ERβ were localised in the dorsal

nerve of the corpus spongiosum, corpus cavernosum, blood vessels and urethral glands[108]. In addition, Jesmin *et al*. (2002)[108] showed that the transcript levels and protein levels of both ERs were present and expressed in male rat penis and their distribution was age dependent.

Jiang *et al.* (2015)[220] demonstrated the effects of estrogen on TA-derived fibroblasts from male rats *in vitro* and observed that estrogen partially impeded myofibroblast transformation. Estrogen also reduced TGF-β1-induced collagen secretion as well as the contraction of myofibroblasts.

To be best of the author's knowledge, there are no studies investigating the effect of SERMs in animal models in PD. However, there are studies reporting that the administration of tamoxifen in the penis of male rats led to the abnormal development of the penis[104,105]. Although an early clinical study suggested some benefit (pain, deformity and plaque shrinkage) from tamoxifen[221], a subsequent randomised placebo-controlled trial in patients with PD, tamoxifen did not significantly improve penile pain, plaque size or curvature compared to the placebo group[222].

1.6 Summary of adenosine and estrogen receptors in fibrosis

The expression of adenosine and estrogen receptors differs according to the tissue investigated as described in this chapter. The table below summarises the expression of adenosine receptors in each tissue.

Table 1-3: Summary table of the expression of adenosine receptors in different tissues. Qualitative expression of adenosine receptors in the different tissues mentioned in this chapter. The relative mRNA expression of each receptor in each tissue is reported as a relative scale to the other receptors, according to *in vivo*, *in vitro* or human studies with +++ indicating the highest expression and + indicating the lowest expression of the receptors found to be present (Blank indicates no reports of expression).

Tissues	Adenosine receptors			
	ADORA1	ADORA2A	ADORA2B	ADORA3
Lung	+[72]	++[72]	+++[72]	
Kidney		+[138]	+++[68]	
Liver		+++[63]		
Heart	+[78]	++[78]	+++[78]	
Skin		+++[62]		
Penis (corpus cavernosum)			+++[66]	

The table below summarises the expression of estrogen receptors in each tissue.

Table 1-4: Summary table of the expression of estrogen receptors in different tissues. Qualitative expression of estrogen receptors in the different tissues mentioned in this chapter. The relative mRNA expression of each receptor in each tissue is reported as a relative scale to the other receptors, according to *in vivo*, *in vitro* or human studies with +++ indicating the highest expression and + indicating the lowest expression of the receptors found to be present (Blank indicates no reports of expression).

Tissues	Estrogen receptors	
	ERα	ERβ
Lung	+[126,127]	+++[126,127]
Kidney	+++[141]	+[141]
Liver	+++[111]	+[151]
Heart	+[91]	+++[91]
Skin	+++[223]	+[223]
Penis (corpus cavernosum)	+[109,219]	+++[109,219]

1.7 Rationale, aim and objectives

Clinical relevance and fit into the larger research programme

In Peyronie's disease clinical management, there is not much that can be offered to those patients who present penile pain and nodule(s) in early stages of the disease. The nodule usually grows into a plaque which eventually can cause deformity. The starting point of this research aims to develop novel medicines that will help those patients in the early stages of PD. The overall aim of the research programme, therefore, is to gain insights into the cellular and molecular basis of PD and other fibrotic disorders and attempt to identify novel potential therapeutics for these diseases by focusing on myofibroblast differentiation. The idea being that by inhibiting myofibroblast transformation, it may be able to prevent the growth of a nodule into a plaque.

My part of the project was to specifically characterise the expression of adenosine and estrogen receptors in myofibroblast differentiation and to assess the effect of agonism and antagonism of these pathways on myofibroblast differentiation.

Rationale

Briefly, this chapter has summarised the current literature in the field with the following main points for emphasis:

- Fibrosis is a chronic and incurable disease with substantial morbidity and mortality, particularly in the Western world.
- Adenosine and estrogen receptor signalling have been suggested to be involved in fibroproliferative disorders through mRNA and protein expression studies as well as some *in vitro* and *in vivo* studies, showing fibrosis modifying effects of agonists/antagonists.
- Peyronie's disease is a fibrotic disease affecting the tunica albuginea of the penis with a similar pathophysiology to other fibroproliferative disorders and with no viable treatment options other than intralesional collagenase injection or surgery.
- Myofibroblast differentiation is known to play a key role in the pathophysiology of fibrosis in several tissues, including in PD.

- No characterisation of adenosine and estrogen receptors has been performed in Peyronie's disease, despite the similarities with other fibrotic diseases in which these receptors are present.
- Investigating the expression of adenosine and estrogen receptors in Peyronie's disease and in myofibroblast differentiation, in particular, may yield novel insights into this disease and even reveal novel therapeutic targets.

Hypothesis: Adenosine and/or estrogen receptor expression is involved in myofibroblast differentiation in PD and may, therefore, be a novel potential target for anti-fibrotic therapies in this disease.

Therefore, the aim of this project was to characterise the myofibroblast differentiation process in human tunica albuginea-derived fibroblasts and to investigate the role of adenosine and estrogen receptors in this process to identify potential, novel targets for anti-fibrotic therapies, through the following objectives:

1. Developing a method to investigate mRNA levels of myofibroblasts based on real-time RT-PCR in cells derived from non-PD TA tissue and PD plaque tissue;
2. Validating a method to investigate protein expression of myofibroblasts based on the In-Cell Western method in cells derived from non-PD TA tissue and PD plaque tissue as well as to assess the effect of specific receptor agonist and antagonist compounds on myofibroblast differentiation;
3. Investigating the expression of adenosine receptors and the effect of modulation of these receptors on myofibroblast transformation;
4. Investigating the expression of estrogen receptors and the effect of modulation of these receptors on myofibroblast transformation.

2 Materials and Methods

2.1 Search criteria

To summarise the current understanding in the field, a thorough literature review was performed (Figure 2-1). Briefly, the search terms “fibrosis”, “myofibroblasts”, “adenosine receptors”, “estrogen/estrogen receptors” and “Peyronie’s disease” were used, which yielded 62420 total papers. After removal of the duplicates, 846 papers were relevant and had the full text available. Of these, 162 papers were included in this thesis since they had the highest relevance to this study. The remainder of the references were acquired by revision from these primary sources.

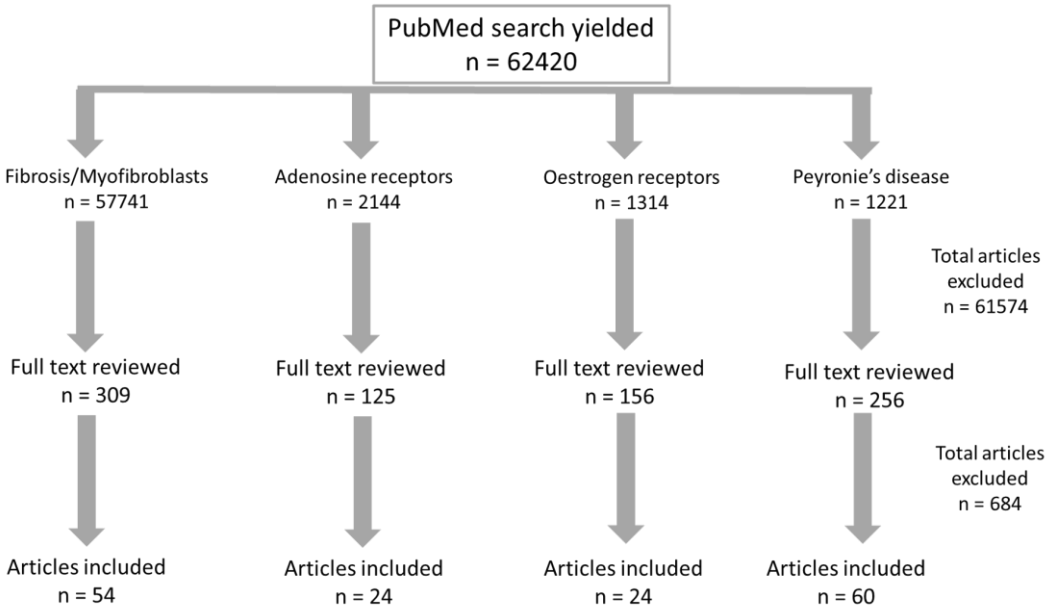

Figure 2-1: Brief flowchart of the search criteria used to produce the literature review. Several keywords were used to write the introduction below. During this search, various articles were excluded for numerous reasons, such as duplication or were not relevant for this study after review of the title and abstract.

2.2 Cell biology techniques

2.2.1 Cell culture conditions and basic cell culture techniques

2.2.1.1 Cell culture conditions

Cells were cultured in Dulbecco’s Modified Eagle Medium/Nutrient Mixture F-12, GlutaMAX™ (DMEM/F-12; GIBCO, Invitrogen, UK) supplemented with 10%

foetal bovine serum (FBS; GIBCO, Invitrogen, UK) and 1% of 5,000 units/ml of penicillin and 5,000 µg/ml of streptomycin (GIBCO, Invitrogen, UK).

Aseptic techniques were employed by using a class II biological safety cabinet (NuAire; Triple Red, UK) when manipulating cell populations. Cells were cultured in T75 flasks (NUNC; Thermo Scientific, UK) and grown at 37°C, 5% CO_2 in a humidified atmosphere until cultures reached approximately 90% confluence, being fed every two to three days with fresh and warm medium.

2.2.1.2 Cell passage and maintenance

Once the cells reached approximately 90% confluence, the cell populations were split in a 1:4 ratio by removing the medium from the T75 flask and washing the cells with sterile and warm phosphate-buffered saline (PBS; GIBCO, Invitrogen, UK). To detach cells from the flask, 2 ml of warm 0.25% trypsin/EDTA (TE; GIBCO, Invitrogen, UK) was used and cells were incubated at 37°C for 2 minutes, after which, cells were examined under the microscope to confirm their detachment. Once detached, 6 ml of warm medium was added to neutralise TE and cell suspension was split into T75 flasks containing fresh and warm medium. Cells were then observed under the microscope and placed in the incubator at 37°C, 5% CO_2.

2.2.1.3 Cell freezing/storage

For long-term storage of cells, these must be detached from the T75 surface, as described previously in section 2.2.1.2 (Cell passage and maintenance). The cell suspension was transferred to a 15 ml falcon tube (Fisher Scientific, UK) and centrifuged for 5 minutes at 400 g at 4°C. The supernatant was discarded and the cell pellet was resuspended in 1 ml of freezing medium, which contained 90% FBS and 10% dimethyl sulfoxide (DMSO; Fisher Scientific, UK). The contents of the falcon tube were transferred to a sterile 1.8 ml cryotube vial (NUNC cryotube vial; Thermo Scientific, UK) and placed immediately in the -80°C or in liquid nitrogen.

2.2.1.4 Cell thawing

To prevent the DMSO present in the freezing medium from affecting cell viability, the thawing procedure should be performed quickly to minimise the time cells are at room temperature.

The cryotube containing frozen cells was transferred from the -80°C freezer or from liquid nitrogen to the water bath (Fisher Scientific, UK) at 37°C. As soon as the last portion of ice thawed, the content of the cryotube was transferred to a 15 ml falcon tube containing warm media. Cells were centrifuged at 400 g for 5 minutes at 4°C and then transferred to a T75 flask containing 11 ml of warm, fresh medium. Cells were observed under the microscope and placed in the incubator at 37°C, 5% CO_2.

2.2.2 Sample acquisition and establishment of primary cell cultures

Tunica albuginea samples were acquired from patients undergoing surgery for PD or invasive penile cancer (control samples) at University College London Hospital (UCLH). Patients aged between 18 and 75, listed for surgical treatment of PD or penile cancer, able to understand the patient information sheet and to give consent were included in the study. Patients were excluded from the study if unable to understand the patient information sheet, to give consent or below 18 years of age or above 75 years of age. Ethical approval was obtained and all patients included in this study signed a written informed consent (Appendix I).

As aforementioned, tissues were obtained from patients undergoing surgery at UCLH, which included Lue, Nesbit, penile prosthesis implant surgery and penectomy. From these surgeries, three groups of tissue samples were acquired: PD plaque tissue (henceforth termed “PD”), normal TA from patients with penile cancer (hereafter termed “TAC”) and normal TA from patients without PD (hereafter termed “TAN”).

Tissues samples were removed from the patient and placed in a 50 ml falcon tube containing culture media (as mentioned in section 2.2.1.1: Cell culture conditions). Tubes were labelled and placed in a thermos containing ice and

wrapped with absorbent pads to transport from UCLH to the university laboratories.

Upon arrival, tissue samples were removed from the thermos and placed on a sterile surface, where the tissue was cut into two equal pieces. One of the pieces was placed in a 50 ml falcon tube containing 4% paraformaldehyde (PFA) in phosphate buffer (PB; recipes can be found in Appendix II) and wrapped in foil. Tubes were stored at room temperature and these tissues were used for immunohistochemistry (IHC).

The other piece of tissue was transferred to a sterile 6 well plate (Fisher Scientific, UK), cut into smaller fragments and split into approximately 3 wells containing sufficient media to submerge the entire tissue. In each well, the tissues were rubbed into the surface of the 6 well plate until it was anchored. Plates were then incubated at 37°C, 5% CO_2 in a humidified atmosphere for 5-7 days without being disturbed to obtain fibroblast cultures.

Tissue was removed from the 6 well plate, once cells were observed growing out of the tissue, dried and stored at -80°C. Cells were washed three times with sterile, warm PBS and fresh, warm medium was added to each well. Cells were then incubated at 37°C, 5% CO_2 in a humidified atmosphere until reached 50-70% confluence.

Once fibroblast cultures reached 50-70% confluence, old medium was removed and cells were washed with 2 ml of warm PBS. The cells were detached from the 6 well plate surface by adding 1 ml of TE and incubating the plate at 37°C for 2 minutes. TE was then neutralised by adding 2 ml of warm medium and the cell suspension was transferred to T75 flasks containing fresh, warm medium. Cells were maintained until they reached passage number 5 as previously described in sections 2.2.1.1 to 2.2.1.4. Throughout the study, primary cell lines were used between passages 3 and 9.

2.3 Real-time RT-PCR

The mRNA levels of several genes of interest in fibroblasts exposed to control conditions and TGF-β1 (Sigma-Aldrich, UK) were assessed using real-time RT-

PCR (RT-qPCR). Initially, RNA was extracted from cultured cells and then converted to complementary DNA (cDNA). The gene expression was evaluated using real-time PCR (qPCR). An example of a detailed protocol used for real-time RT-PCR can be found in Appendix II.

2.3.1 RNA extraction

RNA extraction from cultured cells

To obtain cell pellet for RNA extraction, cells were detached from 6 well plate surfaces as previously described in section 2.2.1.2 (Cell passage and maintenance). Once detached, the cell suspension was transferred to an RNase-free eppendorf and cell counting was determined using the Scepter™ automated cell counter (hereafter termed “Scepter”; Millipore, UK). Cells were centrifuged at 300 g for 5 minutes and the supernatant was discarded.

Total RNA was extracted from the cell pellet using RNeasy Mini Kit (QIAGEN, UK) according to the manufacturer’s guidelines. Briefly, the cell pellet was lysed using 350 µl of lysis buffer (buffer RLT with 14.3 M β-mercaptoethanol; β-ME, Sigma-Aldrich, UK) and then transferred to a QIAshredder spin column (QIAGEN, UK) for homogenisation. The cell lysate was centrifuged for 2 minutes at 13,000 rpm at room temperature. To provide suitable binding conditions, 350 µl of 100% ethanol (Fisher Scientific, UK) was added to the homogenised lysate and the sample was then transferred to a RNeasy spin column where the contaminants were washed away using different washing buffers. First, 350 µl of buffer RW1 was added twice and centrifuged for 15 seconds at 11,000 rpm at room temperature. Subsequently, 500 µl of buffer RPE was added twice and centrifuged for 15 seconds and 2 minutes at 11,000 rpm at room temperature. A DNAse digestion step was also included in the RNA extraction using the RNase-free DNAse set (QIAGEN, UK) by adding 80 µl of DNAse I incubation mix (70 µl of buffer RDD to 10 µl of DNAse I) per sample for 15 minutes at room temperature. RNA was then eluted in 50 µl of RNase-free water.

RNA extraction from tissue samples

RNA extraction from tissue samples was attempted using the RNeasy Mini Kit. However, the lysis and the homogenisation steps were performed using a different technique to the one described above for cultured cells.

Briefly, the frozen tissue (maximum amount of starting material per tube of 30 mg) was transferred from the -80°C freezer to a cold tube containing 2.8 mm ceramic beads (Precellys, UK) and 600 µl of lysis buffer (buffer RLT with β-ME) in dry ice. The disruption and homogenisation of the tissue were performed using the Precellys® 24-Dual (hereafter termed "Precellys", Precellys, UK) at 6,000 rpm for 2 x 30 seconds (program number 2). After homogenisation, the lysate was centrifuged at full speed for 3 minutes and the supernatant was then transferred to a new RNase-free eppendorf. Ethanol was added to the cleared lysate and the subsequent steps were performed as described in RNA extraction from cultured cells section. Several optimisations were performed to the lysis and homogenisation steps including using two types of beads (ceramic vs glass beads), use of fresh tissue instead of frozen tissue, stabilisation of harvested tissues in RNA*later* RNA Stabilization Reagent (hereafter termed "RNA*later*"; QIAGEN, UK), use of a different homogenisation protocol (6,500 rpm for 2 x 25 seconds) and use of liquid nitrogen instead of dry ice to keep the tissue frozen.

2.3.2 RNA Quality Control

To ensure high-quality, free of contaminants RNA, it is essential to assess the quantity, purity and integrity of the RNA.

The concentration and purity of the RNA were assessed using NanoDrop 2000c spectrophotometer (Thermo Scientific, UK). The concentration was determined by measuring the absorbance at 260 nm (A_{260}), where 44 µg/ml of RNA corresponds to an absorbance of 1 unit at 260 nm. On the other hand, the purity was determined by the ratio of the readings at 260 nm and 280 nm (A_{260}/A_{280}), where at 260 nm corresponds to the absorbance of RNA and at 280 nm corresponds to the absorbance of proteins. Therefore, an A_{260}/A_{280} ratio greater than 1.8 (acceptable cut-off value[224]) indicated that the extracted RNA was free

of proteins. In addition to the A_{260}/A_{280} ratio, the peak produced by the sample could also provide information about the presence of impurities, such as chaotropic salts and residual phenol, which absorb at 230 nm; hence, a single peak at 260 nm indicated that the RNA was pure.

To evaluate the RNA integrity, either the Agilent 2100 Bioanalyzer (hereafter termed “Bioanalyzer”; Agilent Technologies, UK) or the Experion™ Automated Electrophoresis System (hereafter termed “Experion system”; Bio-Rad, UK) were utilised according to the manufacturer’s instructions. Both systems use a microfluidic technology to automate electrophoresis for RNA analysis, generating ribosomal RNA (rRNA) ratios, visual electropherogram data, a virtual gel image and an RNA integrity number (RIN). This RIN indicates the RNA quality by assigning a number ranging from 1 (degraded RNA) to 10 (intact RNA), overcoming the main disadvantage of the traditional agarose gel electrophoresis, where the interpretation of the data is subjective. According to Fleige & Pfaffl (2006)[225], a RIN higher than 5 indicated a good total RNA quality, whereas a RIN higher than 8 indicates a perfect RNA sample for downstream applications. In addition to the RIN, the rRNA ratio (28S:18S) could also provide a good indication that the RNA was intact, where the 28S rRNA band should be approximately twice as intense as the 18S rRNA band. For RNA quality analysis, either the Agilent RNA 6000 Nano Kit (Agilent Technologies, UK) or the Experion™ RNA StdSens Analysis kit (Bio-Rad, UK) were used to assess the RNA integrity. Briefly, the electrodes of the Bioanalyzer and the Experion system were decontaminated using RNAseZAP (Fisher Scientific, UK) followed by RNase-free water. The Gel-Dye mix was prepared by adding 65 µl of filtered gel to 1 µl of RNA dye concentrate and added to the RNA Nano chip. Before loading 1 µl of RNA samples and RNA ladder to each well of the RNA Nanochip, these were denatured at 70°C for 2 minutes. RNA Nano chip was placed in the adapter of the IKA vortex mixer and vortexed for 60 seconds at 2,400 rpm. Subsequently, the chip was inserted in the Bioanalyzer or Experion system to start the RNA quality analysis. At the end of every run, the electrodes were cleaned with RNase-free water.

2.3.3 cDNA synthesis by reverse transcription

Extracted RNA was converted to cDNA by reverse transcription (RT) using the High Capacity cDNA Reverse Transcription Kit (Applied Biosystems, UK) according to the manufacturer's instructions. Briefly, a master mix (Table 2-1) was prepared on ice, where 10 µl of RNA sample at 50 ng/µl was added.

Table 2-1: Components used for the reverse transcription reactions.

Components	Volume/reaction (µl)	Final concentration
10X RT buffer	2.0	2X
25X dNTP Mix (100 mM)	0.8	2X
10X RT random primers	2.0	2X
MultiScribe™ Reverse Transcriptase (50 U/µl)	1.0	5 U/µl
Nuclease-free H_2O	4.2	-
TOTAL	10.0	-

PCR tubes containing the reaction mix (master mix and RNA sample) were placed in the G-STORM thermal cycler (G-STORM, UK) and incubated at the following conditions (Table 2-2).

Table 2-2: Conditions used for the reverse transcription reactions.

	Step 1	Step 2	Step 3	Step 4
Temperature (°C)	25	37	85	4
Time (min)	10	120	5	∞

The produced cDNA was stored for short-term storage at 4°C (up to 24 hours) or for long-term storage at -25°C.

2.3.4 Real-time PCR

Real-time PCR was performed using QuantiTect® SYBR® Green PCR kit (QIAGEN, UK), according to the manufacturer's guidelines. Briefly, a PCR

cocktail was prepared according to Table 2-3 and then cDNA template was added to the cocktail.

Table 2-3: Components used for real-time PCR reactions.

Component	Volume/reaction (µl)	Final concentration
2X QuantiTect SYBR Green PCR master mix	2.5	1X
10X Primer mix	0.5	1X
RNase-free water	0.6	-
cDNA template	1.4	≤ 500 ng/reaction
TOTAL	5.0	-

Both PCR cocktail and cDNA template were added either to individual 0.1 ml PCR tubes (QIAGEN, UK) or to Hard-Shell® Low-Profile Thin-Wall 96-well skirted PCR plate (hereafter termed “PCR plate”; Bio-Rad, UK), which was sealed with an optically clear heat seal (Bio-Rad, UK) using PX1™ PCR Plate Sealer (Bio-Rad, UK). Two negative controls: no template control (NTC; RNAse-free water instead of cDNA template) and no reverse transcriptase enzyme control (NRT) were included in every PCR run. The PCR tubes or the PCR plates were placed in a real-time cycler, either the Rotor-Gene Q (QIAGEN, UK) or the CFX Connect Real-time PCR detection system (hereafter termed “CFX cycler”; Bio-Rad, UK), where the PCR reactions were carried out by performing an initial activation step for 15 minutes at 95°C, followed by 40 cycles at 94°C for 15 seconds, 55°C for 30 seconds and then 72°C for 30 seconds. A melting curve analysis between 60°C and 95°C of the PCR products was also performed in every PCR run. All samples and negative controls were run in triplicate.

The target genes that were investigated included α-SMA, ADORA1, ADORA2A, ADORA2B, ADORA3, ERα and ERβ; whereas β-actin (ACTB), 18S ribosomal RNA (18S), eukaryotic translation initiator factor 4A2 (EIF4A2) and DNA topoisomerase I (TOP1) were used as reference genes.

Gene-specific primer pairs for genes encoding α-SMA, β-actin and 18S were purchased from Sigma-Aldrich; whereas ADORA1, ADORA2A, ADORA2B and ADORA3 were purchased from Primerdesign. However, ERα, ERβ, EIF4A2 and TOP1 primer pairs were purchased from QIAGEN (Table 2-4).

Table 2-4: Primers pair details for both target and reference genes. Information about the accession number from NCBI Reference Sequence (NM or NR), primer sequence and amplicon length are included. Legend: F – forward primer; R – reverse primer.

Genes	Detected transcript	Primer Sequence	Amplicon length
α-SMA[226]	NM_001613	F: 5'GACCGAATGCAGAAGGAGAT3' R: 5'CCACCGATCCAGACAGAGTA3'	98 bp
β-actin[226]	NM_001101	F: 5'TGCTATCCAGGCTGTGCTAT3' R: 5'AGTCCATCACGATGCCAGT3'	62 bp
18S[227]	NR_003286.2	F: 5'CTACCACATCCAAGGAAGGCA3' R: 5'TTTTTCGTCACTACCTCCCCG3'	71 bp
ADORA1	NM_000674.2	F: 5'TGATGGAGAGGAGAACACTAGA3' R: 5'CAACACTGAGTCCTTACAGACA3'	96 bp
ADORA2A	NM_000675.5	F: 5'TCCTACTTTGGACTGAGAGAAG3' R: 5'CATGAAACATCTGCTTCCTCAG3'	93 bp
ADORA2B	NM_000676.2	F: 5'ACGGCTGGTTTTCATTGTGAA3' R: 5'GCCTACTACTGACACATACATATTAG3'	117 bp
ADORA3	NM_000677.3	F: 5'GGCCAATGTTACCTACATCAC3' R: 5'CAGGGCTAGAGAGACAATGAA3'	139 bp
ERα	NM_000125	Information not available	73 bp
ERβ	NM_001040275	Information not available	97 bp
EIF4A2	NM_001967	Information not available	87 bp
TOP1	NM_003286	Information not available	89 bp

Several optimisations were performed to obtain efficiencies close to 100%, which included the use of QIAgility (QIAGEN, UK), a benchtop apparatus, which can

set up PCR reactions automatically and PCR reactions were performed in different conditions.

Selection of reference genes

The selection of suitable reference genes was also performed as part of the optimisation process, where the geNorm™ Reference Gene Selection Kit (Primerdesign, UK) was used according to the manufacturer's guidelines. This kit included a panel of 12 candidate reference genes (Table 2-5) that were tested in samples exposed to different experimental conditions.

Table 2-5: List of the 12 candidate reference genes included in the geNorm™ reference gene selection kit.

Candidate reference genes
Glyceraldehyde phosphate dehydrogenase (GAPDH)
Eukaryotic translation initiator factor 4A2 (EIF4A2)
18S Ribosomal RNA (18S)
DNA topoisomerase I (TOP1)
Phospholipase A2 (YWHAZ)
Beta-actin (ACTB)
Homo sapiens succinate dehydrogenase (SDHA)
Ubiquitin C (UBC)
Beta-2-microglobulin (B2M)
Ribosomal protein L13a (RPL13A)
Cytochrome c-1 (CYC1)
ATP synthase (ATP5B)

Briefly, each primer mix was resuspended in 220 µl RNAse/DNAse-free water and a PCR cocktail was prepared according to Table 2-6. Both PCR cocktail and cDNA template were added to the PCR tubes and placed in the Rotor-Gene Q. The PCR reactions were carried out by performing an initial activation step for 15 minutes at 95°C, followed by 50 cycles at 95°C for 15 seconds and 60°C for 1

minute. A melting curve analysis between 60°C and 95°C of the PCR products was also performed. All samples and negative controls were run in triplicate. Data were analysed using the geNorm software: qbase^{PLUS}, which ranks the candidate reference genes according to their expression stability.

Table 2-6: Components used for real-time PCR reactions.

Component	Volume/reaction (µl)	Final concentration
2X QuantiTect SYBR Green PCR master mix	10.0	1X
Primer mix	1.0	300 nM
RNase-free water	6.6	-
cDNA template	2.4	≤ 500 ng/reaction
TOTAL	20.0	-

2.4 Immunocytochemistry

An example of a detailed protocol used for immunocytochemistry (ICC) can be found in Appendix II.

Briefly, in a sterile 6 well plate, 2 ml of 100% ethanol was added and coverslips (Fisher Scientific, UK) were placed in the wells for 1 minute to sterilise them. Using sterile forceps (Fisher Scientific, UK), coverslips were placed vertically in empty wells and left to dry for approximately 10 minutes. Once dried, these coverslips were transferred to a new 6 well plate and set horizontally in each well. Approximately 2 ml of medium was added to each well and the bubbles underneath the coverslips were removed by gently pressing with a sterile pipette. Plates were then incubated at 37°C, 5% CO_2 for 2 hours.

Cells were detached from T75 flasks as described in section 2.2.1.2 (Cell passage and maintenance), and the cell suspension was transferred to a 15 ml falcon tube, where the number of cells was determined using the Scepter. Plates were removed from the incubator and any bubbles formed were removed by pressing the coverslip against the 6 well plate surface. The medium was discarded, and the cell suspension was added directly to each coverslip at 2.5 x

10^4 cells/well. Cells were observed under the light microscope and plates were incubated overnight at 37°C, 5% CO_2. The next day, some of the cells were exposed to TGF-β1, by replacing the old medium with warm medium with or without TGF-β1 at 5 or 10 ng/ml. Plates were then incubated at 37°C, 5% CO_2 for 72 hours.

Coverslips were removed from the 6 well plate, submerged in PBS and transferred to ice-cold methanol (at -25°C; Fisher Scientific, UK) for 10 seconds. Cells were washed twice in two beakers containing PBS and coverslips were placed on a glass slide (Fisher Scientific, UK) with cells facing up and left to dry. A contour was made around each coverslip using a hydrophobic pen (Mini Pan Pen; Invitrogen, UK) and block solution was added for 1 hour at room temperature in a humidified chamber by spreading evenly 50 µl of 10% donkey serum (Millipore, UK) in PBS over each coverslip. Block solution was replaced by 50 µl of primary antibody solution (Table 2-7) diluted in PBS and incubated at room temperature for 2 hours in a humidified chamber. The primary antibody solution was then removed by washing coverslips three times with PBS, after which, the secondary antibody solution (Table 2-7) diluted in PBS was added to the contoured area and incubated for 2 hours at room temperature in a humidified chamber in the dark. After the incubation period, the secondary antibody solution was washed three times with PBS and coverslips were mounted in a new glass slide (cells facing down) with VECTASHIELD® mounting medium with propidium iodide (PI; Vector Laboratories, UK). Cells were observed using the Zeiss confocal microscope (LSM 510; Carl Zeiss, UK). The fluorescence images were taken at three random areas in each coverslip at 200x or 400x magnification utilising the laser scanning microscope 510 v3.2 software (Carl Zeiss, UK). The number of myofibroblasts was determined by counting the number of α-SMA positive cells in the three areas per sample. The total number of cells was also determined by counting the number of nuclei stained.

Table 2-7: Primary and secondary antibody dilutions used in immunocytochemistry. All antibodies were diluted in PBS.

Antibody		Dilution
Primary antibody	Anti-ASMA antibody raised in mouse (Sigma-Aldrich, UK; A5228)	1:1,000
	Anti-Estrogen receptor alpha antibody (abcam, UK; ab32063)	1:200
	Anti-Estrogen receptor beta antibody (abcam, UK; ab3576)	1:100
Secondary antibody	Donkey anti-mouse IgG antibody, FITC conjugate (Millipore, UK; AP192F)	1:250
	Donkey anti-rabbit IgG antibody, FITC conjugate (Millipore, UK; AP182F)	1:250

2.5 Immunohistochemistry

An example of a detailed protocol used for immunohistochemistry can be found in Appendix II.

Tissue samples from non-PD TA tissue and PD plaque tissue were fixed in 4% PFA for 24 hours, after which, these specimens were dehydrated for 48 hours at 4°C in a 30% sucrose solution. Specimens were then stored and frozen at -80°C in optimal cutting temperature compound (OCT; VWR, UK).

Initially, the frozen tissues were sectioned in 18 µm thick slices using a cryostat (Model OTF, Bright Instruments Co Ltd, UK) at -20°C and placed on Superfrost Plus Gold slides (Fisher Scientific, UK). Tissues samples were left to dry for 3 hours and a contour was made around each tissue sample using a hydrophobic pen. To each glass slide, 200 µl of blocking buffer (10% donkey serum in 0.1% Triton X-100 in PBS) was added ensuring that the tissues were covered and were not dislodged. The tissues were incubated for 90 minutes at room temperature in a humidified chamber, followed by application of 150 µl of primary antibody solution (1:100 diluted in PBS for both ADORA1 and ADORA2B) and incubated overnight at 4°C. On the next day, slides were washed three times with PBS and

150 µl of secondary antibody solution (1:250 diluted in PBS, donkey anti-rabbit conjugated with fluorescein dye) was added to each slide and incubated for 2 hours at room temperature in a humidified chamber in the dark. The secondary antibody solution was removed and slides were washed with PBS three times and VECTASHIELD® mounting medium with PI was added. The coverslip was placed on top and cells were observed using the Zeiss confocal microscope (LSM 510; Carl Zeiss, UK). The fluorescence images were taken at three random areas in each coverslip at 200x magnification utilising the laser scanning microscope 510 v3.2 software (Carl Zeiss, UK). Negative controls sections were obtained by omitting the primary antibody solution.

2.6 In-Cell Western assay

The In-Cell Western (ICW) assay is an immunological technique that uses immunofluorescent staining to measure protein levels in fixed cultured cells. This technique was used to develop a high throughput screening (HTS) assay for anti-myofibroblast activity in Peyronie's disease to yield objective and quantitative data on the number of myofibroblasts in cell populations and to test several potential new anti-myofibroblast compounds. This technique was chosen as the target can be measured *in situ* to obtain quantifiable data, that is robust, sensitive and amenable to the HTS assays. An example of a detailed protocol used for ICW and buffer recipes can be found in Appendix II.

Cell suspension was obtained from cultured cells growing in T75 flasks and 100 µl of cell suspension was added to each well of a 96 well microplate (NUNC® 96 well optical flat bottom black microplates; Fisher Scientific, UK) at 5.0 x 10^3 cells/well and incubated at 37°C, 5% CO_2 overnight. On the next day, cells were exposed to TGF-β1, by replacing the old medium and adding fresh medium with or without TGF-β1 at 5 or 10 ng/ml to the appropriate wells. Plates were then incubated at 37°C, 5% CO_2 for 72 hours.

After the incubation period, old medium was discarded and cells were fixed with 150 µl of 4% PFA for 20 minutes at room temperature. Fixing solution was removed and cells were washed three times with 150 µl of permeabilisation buffer (0.1% Triton X-100 in PBS) for 5 minutes at room temperature on a plate shaker.

After which, 150 µl of blocking buffer (5% donkey serum in permeabilisation buffer) was added to each well and incubated for 90 minutes at room temperature on a plate shaker.

After removing blocking buffer from the wells, 50 µl of primary antibody solution diluted in PBS (Table 2-8) was added and incubated for 2 hours at room temperature on a plate shaker. After incubation, cells were washed three times with 150 µl of 0.1% tween 20 in PBS (0.1% PBST) for 5 minutes on a plate shaker. Secondary antibody solution (Table 2-8) and DRAQ5 (1:1,000; Biostatus, UK) diluted in PBS were then added to each well and incubated for 1 hour at room temperature in the dark on a plate shaker. After which, cells were washed three times with 0.1% PBST and once with PBS for 5 minutes on a plate shaker.

Table 2-8: Primary and secondary antibody dilutions used in In-Cell Western. All antibodies were diluted in PBS.

Antibody		Dilution
Primary antibody	Anti-ASMA antibody (Sigma-Aldrich, UK; A5228)	1:3,000
	Anti-adenosine A1 receptor (abcam, UK; ab124780)	1:500
	Anti-adenosine A2B receptor (abcam, UK; ab135865)	1:500
	Adenosine A2B receptor peptide (abcam, UK; ab45817)	1:100
	Anti-Estrogen receptor alpha antibody (abcam, UK; ab32063)	1:500
	Anti-Estrogen receptor beta antibody (abcam, UK; ab3576)	1:500
	Estrogen receptor beta peptide (abcam, UK; ab5018)	1:100
Secondary antibody	800CW IRDye donkey anti-mouse (Li-COR, UK; 926-32212)	1:500
	680RD IRDye donkey anti-rabbit (Li-COR, UK; 926-68073)	1:500
	800CW IRDye donkey anti-rabbit (Li-COR, UK; 926-32213)	1:500

The ADORA2B peptide was bought from Abcam and the peptide sequence is CQADVKSGNGQ (311 amino acid to 321 amino acid). A molar ratio of 5:1 (5-parts peptide to 1-part antibody) was utilised in the ICW and Western blot experiments. Regarding the ERβ peptide, no peptide sequence was available from the supplier (Abcam) and a molar ratio of 5:1 was also used in the ICW and Western blot experiments.

The plate was scanned using the Odyssey® CLx (Li-COR, UK) at both 700 and 800 nm channels and data were collected and analysed using the Image Studio™ software v5.2.5 (Li-COR, UK).

2.7 Western blot

An example of a detailed protocol used for Western blot and buffer recipes can be found in Appendix II.

2.7.1 Protein extraction and quantification

Cell suspension was obtained and added to each well of a 6 well plate at 1.0 x 10^5 cells/well. Cells were observed under the light microscope and plates were incubated overnight at 37°C, 5% CO_2. The next day, cells were exposed to TGF-β1, by replacing the old medium with warm medium with or without TGF-β1 at 5 ng/ml. Plates were then incubated at 37°C, 5% CO_2 for 72 hours.

After incubation, protein extraction was carried out by removing the cell culture medium and washing the cells with ice-cold PBS. Cells were scraped off from the bottom of the well with a pre-cooled sterile plastic cell scraper (Fisher Scientific, UK) and the cell suspension was transferred to an ice-cold eppendorf tube. The cell suspension was centrifuged at 3,000 rpm for 5 minutes at 4°C. The supernatant was discarded, and the cell pellet was resuspended in 300 µl of either ice-cold RIPA lysis buffer or Tris-Triton lysis buffer with protease inhibitor cocktail. Samples were left on ice for 30 minutes, after which a centrifugation step was performed for 5 minutes at 3,000 rpm at 4°C. The supernatant was then transferred to a new ice-cold eppendorf tube and cell lysate was stored at -80°C after quantification.

Protein quantification was performed in a 96 well plate using the DC Protein Assay Kit II (Bio-Rad, UK) according to the manufacturer's guidelines. Briefly, 25 µl of working reagent (20 µl of reagent S to each millilitre of reagent A) was added to 5 µl of each sample. Reagent B was then added to all wells and the plate was thoroughly mixed on a plate shaker for 15 minutes. The absorbance of each sample was read in a plate reader (iMark™ Microplate Absorbance Reader; Bio-Rad, UK) at 750 nm. For the protein quantification, a standard curve was

constructed using a BSA protein standard (1.5 mg/ml to 0.09 mg/ml; Bio-Rad, UK).

2.7.2 Western blotting

2.7.2.1 Sample preparation and SDS-PAGE

After protein concentrations were determined, the appropriate dilutions of cell lysate were prepared to have the same protein concentration (20 µg of lysate per lane) in all samples. An equal volume of 2X laemmli sample buffer containing 1M DL-Dithiothreitol (DTT; Bio-Rad, UK) was added and samples were denatured by boiling at 95°C for 10 minutes. Samples were kept on ice to prevent protein clumping. In addition to the patient samples, an ADORA2B HEK293T cell transient overexpression lysate (Origene, UK) and an ERβ HEK293T cell transient overexpression lysate (Origene, UK) were also used as a positive control for ADORA2B and ERβ, respectively. As a negative control for both ADORA2B and ERβ, an HEK293 cell lysate (no transient overexpression) was used.

Denatured protein samples were separated according to their molecular weight using SDS-PAGE (Sodium Dodecyl Sulfate PolyAcrylamide Gel Electrophoresis) and Mini-PROTEAN® TGX™ Precast Protein Gels (Bio-Rad, UK). The Hoefer SE300 miniVE Vertical Electrophoresis System (Hoefer, UK) was assembled according to manufacturer's instructions. First, the pre-cast gel was washed with distilled water and the well comb and the green tape at the bottom of the gel were carefully removed to allow the transfer of the current. Once the gel was inserted in the tank, running buffer was added to completely immerse the gel and the wells were washed by pipetting running buffer into them. A molecular weight protein marker (PageRuler^{TM} Prestained Protein Ladder, range: 10 to 180 kDa; Thermo Scientific, UK) and denatured samples were loaded into the gel. Both anode and cathode of the electrophoresis system were connected to EPS 3501 XL Power Supply Unit (GE Healthcare, UK) and gel electrophoresis was run at 120V for 10 minutes and subsequently at 200V for 1 hour.

2.7.2.2 Transferring the protein from the gel to the membrane

To transfer the separated proteins to a polyvinylidene fluoride (PVDF) membrane (Immobilon-FL transfer membrane; Fisher Scientific, UK) for antibody detection, a wet transfer method was employed. The PVDF membrane was cut to the appropriate size and soaked in 100% methanol for 1 minute; after which, the membrane was transferred to transfer buffer. A sandwich of sponge/filter paper/gel/membrane/filter paper/sponge soaked in transfer buffer was positioned between the negative and positive electrodes of the Hoefer SE300 miniVE Vertical Electrophoresis System (Hoefer, UK) containing transfer buffer. The gel was placed closest to the negative electrode and the membrane closest to the positive electrode and air bubbles in the sandwich were removed by rolling them out with a pipette. Electrode connections were attached to the EPS 3501 XL Power Supply Unit and the electrotransfer was carried out for 1 hour at 50V.

2.7.2.3 Antibody incubation

The PVDF membrane was washed once for 5 minutes in PBS and subsequently, the membrane was blocked for 1 hour at room temperature in 10% (w/v) non-fat dried milk (NFDM, Marvel) in PBS.

After blocking incubation, the membrane was incubated with primary antibody solution diluted in 5% (w/v) NFDM at the dilution specified in Table 2-9 overnight at 4°C on a rocker platform. The membrane was washed four times with tris-buffered saline (TBS) containing 0.1% tween 20 (0.1% TBST) for 5 minutes at room temperature on a rocker. Secondary antibody solution (Table 2-9) was then incubated with the membrane for 1 hour at room temperature on a rocker in the dark. Subsequently, the membrane was washed four times with 0.1% TBST for 5 minutes on a rocker. In addition to the use of GAPDH or α-tubulin as a loading control, a lane in which the primary antibody was omitted was also included in all Western blots experiments as a negative control.

Table 2-9: Primary and secondary antibody dilutions used in Western blot. All antibodies were diluted in 5% (w/v) NFDM.

Antibody		Dilution
Primary antibody	Anti-ASMA antibody raised in mouse (Sigma-Aldrich, UK; A5228)	1:3,000
	Anti-adenosine A2B receptor (abcam, UK; ab135865)	1:500
	Adenosine A2B receptor peptide (abcam, UK; ab45817)	1:100
	Anti-Estrogen receptor beta antibody (abcam, UK; ab3576)	1:1,000
	Estrogen receptor beta peptide (abcam, UK; ab5018)	1:200
	Anti-GAPDH antibody raised in rabbit (abcam, UK; ab128915)	1:5,000
	Anti-alpha tubulin antibody raised in rabbit (abcam, UK; ab4074)	1:5,000
Secondary antibody	800CW IRDye donkey anti-mouse (Li-COR, UK; 926-32212)	1:5,000
	680RD IRDye donkey anti-rabbit (Li-COR, UK; 926-68073)	1:5,000
	800CW IRDye donkey anti-rabbit (Li-COR, UK; 926-32213)	1:5,000

To detect and visualise the proteins, the Odyssey® CLx (Li-COR, UK) with infrared technology was utilised by scanning the membrane at both the 700 and 800 nm channels and data were collected and analysed using the Image Studio™ software v5.2.5 (Li-COR, UK).

2.8 Statistical analysis

For this study, cell lines established from at least three PD plaque tissues and cell lines derived from at least three non-PD TA tissues were used in all experiments and performed in triplicate and repeated at least three times (N=3).

Data analyses and graphs were plotted using Microsoft® Excel 2013, where basic descriptive statistics and Student's t-test for unpaired means (two-sided) were performed. P value < 0.05 was considered statistically significant. All the data points were expressed as mean ± standard error of the mean (SEM).

2.8.1 Real-time RT-PCR data analysis

For relative gene expression analysis, the $2^{-\Delta\Delta Cq}$ method[228] was used. This method assumes that both target and reference genes are amplified with efficiencies near 100% and within 10% of each other.

To determine the amplification efficiencies of the target and the reference genes, a 10-fold serial dilution was performed in every PCR run and the quantification cycle (C_q) values obtained were used to generate a standard curve. The amplification efficiency (E) was calculated from the slope of the generated standard curve using the following equation (presented as a percentage).

$$\%\mathrm{E} = \left(10^{-1/\mathrm{slope}} - 1\right) \times 100\% \qquad \textbf{Equation (2-1)}$$

Serial dilutions should produce amplification curves that are evenly spaced, and if the perfect doubling occurs, the spacing of the fluorescence curves can be calculated using the following equation: 2^n = dilution factor (n = number of cycles between curves). Therefore, with a 10-fold dilution, the Cq values of each dilution should be separated by 3.32 cycles, which corresponds to an ideal slope of -3.32. However, slopes ranging from -3.6 (90%) to -3.1 (110%) are usually considered acceptable[224]. The efficiency of a PCR reaction is the rate at which the enzyme *Taq* polymerase converts the reagents to amplicons. The ideal increase of PCR product per cycle is two-fold, corresponding to an amplification efficiency of 100%. The determination of efficiency is essential, as it is indicative of problems with the real-time PCR reactions. Each standard curve was generated using calibrator samples, which corresponded to untreated cells derived from non-PD TA tissue. Whereas, test samples corresponded to cells established from non-PD TA tissue treated with TGF-β1 and PD plaque tissue exposed or not exposed to TGF-β1.

The relative expression of target genes in different samples could be determined by following the steps below.

First, the C_q value of the target gene (of both test samples and calibrator samples) needed to be normalised to the reference (ref) gene using the following equation.

$$\Delta C_q = C_{q\ (target)} - C_{q\ (ref)} \qquad \textbf{Equation (2-2)}$$

After normalisation of the C_q value, the ΔC_q of the test sample needed to be normalised against the ΔC_q of the calibrator sample by using the equation below.

$$\Delta\Delta C_q = \Delta C_{q\ (test)} - \Delta C_{q\ (calibrator)} \qquad \textbf{Equation (2-3)}$$

Finally, the normalised gene expression ratio was calculated utilising the following equation.

$$2^{-\Delta\Delta Cq} = \text{normalised expression ratio} \qquad \textbf{Equation (2-4)}$$

The result obtained corresponded to the fold-change of the target gene in the test sample relative to the calibrator sample and normalised to the expression of the reference genes.

2.8.2 In-Cell Western data analysis

To measure the effect of TGF-β1-induced myofibroblast differentiation, Z' factor (Z') was determined to validate the ICW method in order to investigate protein expression of myofibroblasts and to assess the effect of specific receptor agonist and antagonist compounds on myofibroblast differentiation using the following equation.

$$Z' = 1 - \frac{3(\sigma p + \sigma n)}{|\mu p - \mu n|} \qquad \textbf{Equation (2-5)}$$

Where σn and σp correspond to the standard deviations of the negative and positive controls, respectively and μn and μp correspond to the averages of the negative and positive controls, respectively.

The % activity of TGF-β1 was calculated using the following equation.

$$\% \text{ activity} = 100 \times \frac{(\text{Cmpd} - \text{Min})}{\text{Max} - \text{Min}}$$ **Equation (2-6)**

The concentration response curves (CRCs) of the tested compounds were performed to assess their ability to inhibit TGF-β1-induced myofibroblast differentiation. A custom made Microsoft Excel template based on the method described by Brown (2001)[229], was used to plot the CRCs. This template used the solver add-on to determine the CRC and fitted to a 5-parameter logistic (5-PL) curve, by solving the following formula to produce the highest possible correction coefficient between the CRC and the data values obtained.

$$Y = D + \frac{(A - D)}{\left(1 + \left(\frac{X}{EC50}\right)^{k}\right)^{e}}$$ **Equation (2-7)**

Where y = response; x = concentration of compound; D = estimated response at infinite concentration; half maximal effective concentration (EC_{50}) = mid-range concentration; A = estimated response at zero concentration; e = asymmetry factor and k = slope.

3 Results

3.1 Development of a real-time RT-PCR method

To study the mRNA levels of genes of interest, a real-time RT-PCR method was developed using fibroblasts derived from non-PD TA tissue and PD plaque tissue. Initially, the quality and purity of the extracted RNA were evaluated and standard curves were generated using untreated non-PD TA cells as the calibrator sample to validate both target and reference genes. After extensive optimisations, standard curves of target and reference genes were performed in all non-PD TA cells and PD plaque-derived cells used and subsequently the relative changes of the target genes in different samples were determined.

3.1.1 RNA Quality Control

Before converting the RNA to cDNA, it was necessary to ensure that the extracted RNA was intact and free of contaminants by measuring its concentration, purity and quality. A typical example of the concentration, purity and quality of the extracted RNA from cultured cells can be found in Appendix III (Table 7-10). A wide range of RNA concentrations (52.5 ± 2.88 to 141.1 ± 4.99 ng/µl) was obtained from different cell lines, where the A_{260}/A_{280} ratio (2.01 ± 0.01 to 2.29 ± 0.02) was above 1.8, suggesting that the extracted RNA was pure. In addition to the A_{260}/A_{280} ratio, the peak produced by the samples was also evaluated (data not shown); however, RNA samples that presented impurities (such as residual alcohol, phenol and chaotropic salts, which are components of the reagents used in the RNA extraction protocol) were not used for downstream applications, as these impurities may lead to inhibition of RT and qPCR reactions, yielding biased data.

Both the Experion system and the Bioanalyzer generated rRNA ratios (28S:18S), virtual gel images of the electropherogram data (Appendix III, Figure 7-4) and a RIN for all samples used. RIN values ranging from 9.7 ± 0.03 to 10.0 ± 0.00 and rRNA ratios ranging from 1.68 ± 0.04 to 2.00 ± 0.04 were obtained. These results showed that the extracted RNA was of high integrity and quality; therefore, it was used for downstream applications.

To support 28S:18S ratio data, a representative illustration of a virtual gel displaying the rRNA bands is shown in Figure 3-1.

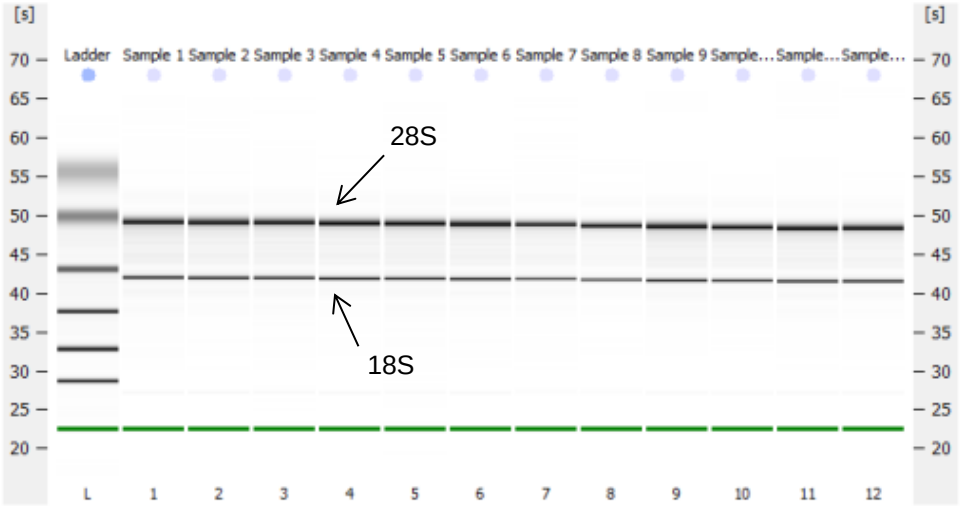

Figure 3-1: Representative illustration of a virtual gel generated from the electropherogram data. The first lane corresponds to the RNA ladder with seven RNA sizes ranging from 6000 nucleotides to 25 nucleotides. The other 12 lanes correspond to the RNA samples exposed and not exposed to TGF-β1 of TAN2A1, TAC1B1, TAC4A2, PD1B1, PD2A2 and PD3A1 cell lines, where the first band represents the 28S rRNA and the second band is the 18S rRNA. The 2:1 ratio (28S:18S) is a good indication that the RNA is intact, where the 28S rRNA band is approximately twice as intense as the 18S rRNA band. The band at 25 nucleotides that appears in both ladder and sample lanes correspond to the lower alignment marker.

The figure above shows a representative gel image generated from the Bioanalyzer of RNA extracted from three non-PD TA cells lines and three PD plaque-derived cells lines exposed and not exposed to TGF-β1, where it can be observed that the 28S band is approximately twice as intense as the 18S band.

RNA extraction from tissue samples

RNA extraction from non-PD TA tissue and PD plaque tissue was also attempted. A typical example of the concentration and purity obtained in the different optimisations performed can be found in Appendix III (Table 7-11).

Briefly, frozen tissues (used to establish cell lines) were used; however, no RNA was obtained from those tissues. Although several optimisations were carried out, RNA was still not obtained from intact tissue. Gene expression analysis of tissue samples was therefore abandoned, and the results shown hereafter are for

samples obtained from cells derived from non-PD TA tissue and PD plaque tissue (further information regarding RNA extraction from tissues samples can be found in Appendix III).

3.1.2 Optimisation of real-time PCR

For each qPCR run, an amplification plot (log scale and linear scale in Appendix III, Figure 7-5) and a melting curve were provided by either the Rotor-Gene Q or the CFX cycler software.

Before any optimisations, a qPCR run was carried out using the cDNA obtained from an untreated cell line derived from non-PD TA tissue (calibrator sample), after which, standard curves were generated for α-SMA, β-actin and 18S (Appendix III, Figure 7-6). From the standard curves, efficiencies were calculated for the genes tested (Table 3-1).

Table 3-1: Representative R^2, slope and efficiencies of α-SMA, β-actin and 18S genes obtained from the standard curves. Standard curves were generated for each gene for one of the untreated cell lines established from non-PD TA tissue (TAC4A2).

Genes	R^2	Slope	Efficiency (%)
α-SMA	0.9909	-3.2847	101.58
β-actin	0.9909	-2.9010	121.16
18S	0.9973	-3.0425	113.15

As can be observed in the table above, in all three genes, the R^2 was above 0.980 (recommended cut-off value) and the replicates did not deviate more than 0.5 Cq values, showing no variability between them. Although the slope for α-SMA (-3.2847) was within the range; for β-actin and 18S, the slope was above the acceptable range (-2.9010 and -3.0425, respectively), corresponding to higher amplification efficiencies than expected. The high reactions efficiencies (>110%) may indicate co-amplification of non-specific products, such as primer-dimers or secondary structures), pipetting errors during reaction set up, error in the serial dilution or presence of PCR inhibitors. Furthermore, both target and reference genes were not within 10% of each other.

The use of suitable reference genes is important, as qPCR data will be normalised to these genes; therefore, reference genes should be stably expressed in all different experimental conditions. A geNorm^{TM} reference gene selection kit was used, which included a panel of 12 candidate reference genes, where the geNorm analysis was carried out on four experimental conditions (Figure 3-2).

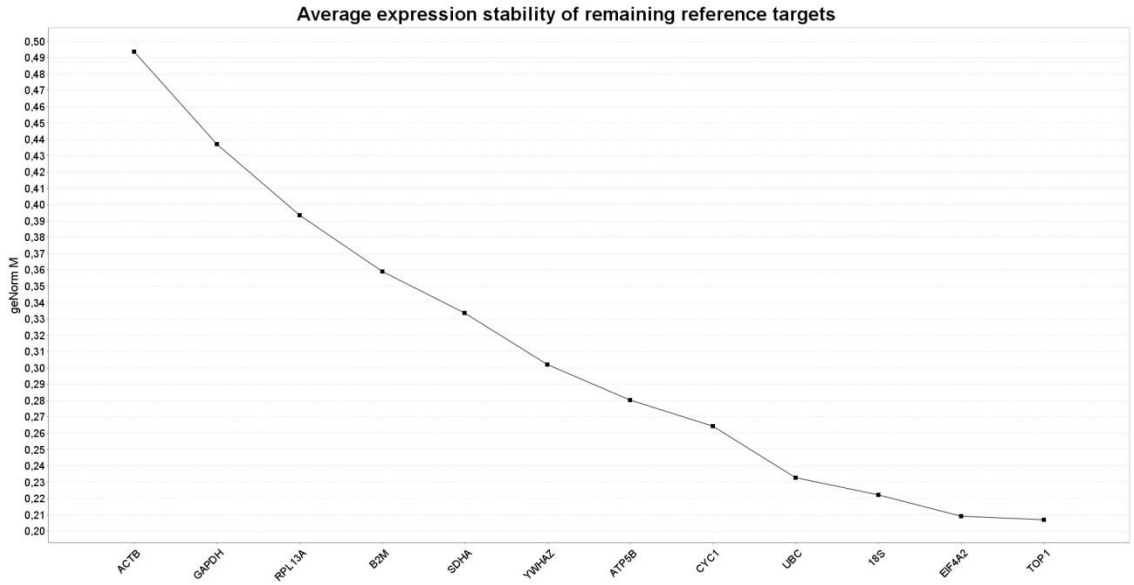

Figure 3-2: Average expression stability of reference genes. Twelve potential reference genes were used to test their stability under 4 experimental conditions. The lower the geNorm M value, the more stable the reference gene is under the tested experimental conditions. Each experimental condition was run in duplicate and negative controls were included.

As shown in Figure 3-2, the four most stable genes were TOP1, EIF4A2, 18S and UBC from the 12 potential reference genes, as these genes showed the lowest geNorm M value.

The optimal number of references genes used to normalise qPCR data can be calculated using the V value (Figure 3-3).

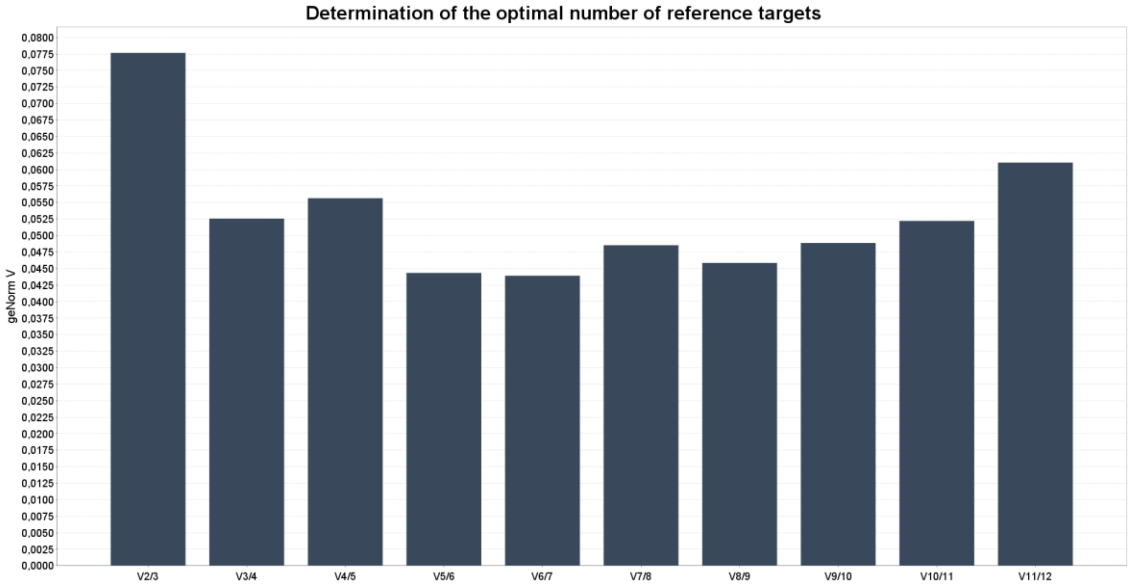

Figure 3-3: Determination of the optimal number of reference genes. The use of the geNorm kit demonstrated the optimal number of reference genes that should be used when using the tested experimental conditions.

A V score of below 0.15 is recommended as the ideal for having good stability on relative quantification. When using the two top genes in this system, a V score of 0.078 was achieved. Therefore, the optimal normalisation factor can be calculated as the geometric mean of EIF4A2 and TOP1 genes.

After performing several optimisations to obtain amplification efficiencies for all genes near 100% and selecting appropriate reference genes, standard curves were constructed for gene validation (Appendix III, Figure 7-7). From the standard curves, efficiencies were calculated for all the genes tested (Table 3-2).

Table 3-2: Representative R^2, slope and efficiencies of all target and reference genes used in this study. Standard curves were generated for each gene for one of the untreated cell lines established from non-PD TA tissue.

Genes	R^2	Slope	Efficiency (%)
α-SMA	0.9983	-3.413	96.33
ADORA1	09993	-3.425	95.87
ADORA2A	0.9959	-3.410	96.45
ADORA2B	0.9996	-3.401	96.80
ADORA3	0.9988	-3.498	93.14
ERα	0.9996	-3.314	100.33
ERβ	0.9978	-3.325	99.87
EIF4A2	0.9993	-3.379	97.67
TOP1	0.9977	-3.351	98.80

As can be observed in Table 3-2, the R^2 was above 0.980 for all genes and no variability was observed between replicates (<0.5 Cq values between replicates). The slope of each standard curve was within the acceptable range (-3.60 to -3.1), corresponding to efficiencies within 90% to 110%. In addition, both target and reference genes were within 10% of each other.

3.1.3 Melting curve analysis

In all qPCR runs, a melting curve analysis was carried out to ensure that the signal acquired from the amplification plot was, in fact, the expected PCR product (Appendix III, Figure 7-8). Each pair of primers used in this study showed no signs of non-specific products of primer-dimers, as only one peak per sample was observed corresponding to the temperature at which the PCR product dissociates. Therefore, the primer pairs used in this project were specific for the genes of interest.

3.2 Validation of ICW assay

To investigate protein expression of myofibroblasts and to assess the effect of specific receptor agonist and antagonist compounds on myofibroblast differentiation, the ICW assay was validated.

To select the most appropriate TGF-β1 concentration to use, a full CRC was performed by exposing the primary fibroblasts to varying concentrations of TGF-β1 (0.001 to 30 ng/ml) for 72 hours on non-PD TA cells (Figure 3-4).

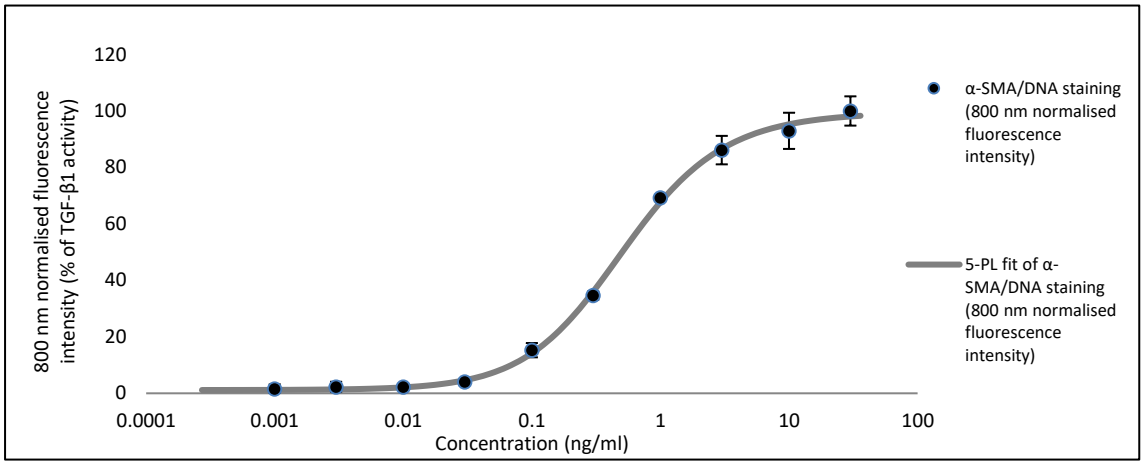

Figure 3-4: Effect of TGF-β1 on non-PD TA cells. Cells were exposed to a range of concentrations of TGF-β1 between 0.001 and 30 ng/ml for 72 hours. Data points were plotted as mean ± SEM of the percentage of activity achieved, N=3.

As can be observed in Figure 3-4, a classical sigmoid curve was obtained, reaching a maximum of 100% with an EC_{50} of 0.4 ng/ml, meaning that at this TGF-β1 concentration, half of the fibroblasts would be differentiated into myofibroblasts. However, for the HTS, an $EC_{90\text{-}100}$ would be ideal as 90-100% of the fibroblasts would differentiate into myofibroblasts. During the study, TGF-β1 was either used at concentrations of 5 or 10 ng/ml, which corresponds to EC91.4% and EC95.3% of activity, respectively.

Non-PD TA cells were treated with TGF-β1 at 5 ng/ml for 72 hours and the data obtained was used to calculate the Z' factor, which is used to report the variability within the assay (Figure 3-5).

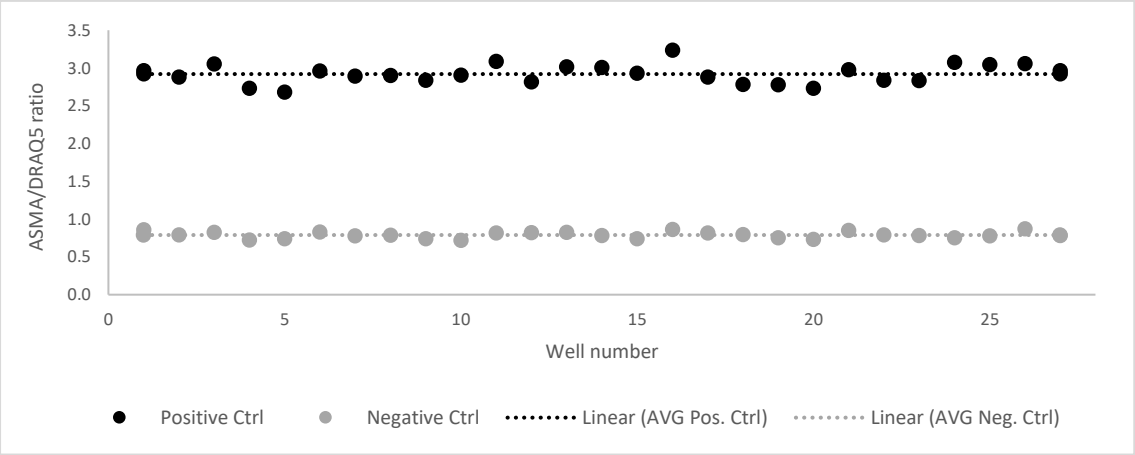

Figure 3-5: Validation of the ICW method by assessing the effect of TGF-β1-induced myofibroblast differentiation in non-PD TA cells. Positive controls correspond to cells treated with 5 ng/ml TGF-β1 for 72 hours and negative controls correspond to untreated cells. Values for 27 positive control wells and 27 negative wells were acquired in the same 96 well plate and were used to analyse the statistical reproducibility of the ICW assay for detection of α-SMA positive cells. Data presented as the fluorescence intensity of α-SMA expression normalised for nuclear dye (DRAQ5) intensity.

As shown in the above figure, a 3-fold change was obtained upon stimulation with TGF-β1. The Z' factor was calculated comparing α-SMA/DNA staining ratio in cells exposed to TGF-β1 (positive control) and in cells not exposed to TGF-β1 (negative control), yielding a Z' value of 0.76 ± 0.05. This Z' value indicated that the assay had low variability and it was appropriate to investigate protein expression of myofibroblasts and to assess the efficacy of compounds at impeding TGF-β1-induced myofibroblast differentiation.

Further control experiments were carried out by performing a full concentration response curve for DMSO (Figure 3-6), which was used as vehicle control to investigate its cytotoxic effect on fibroblasts and its inhibitory effect on TGF-β1-induced myofibroblast differentiation.

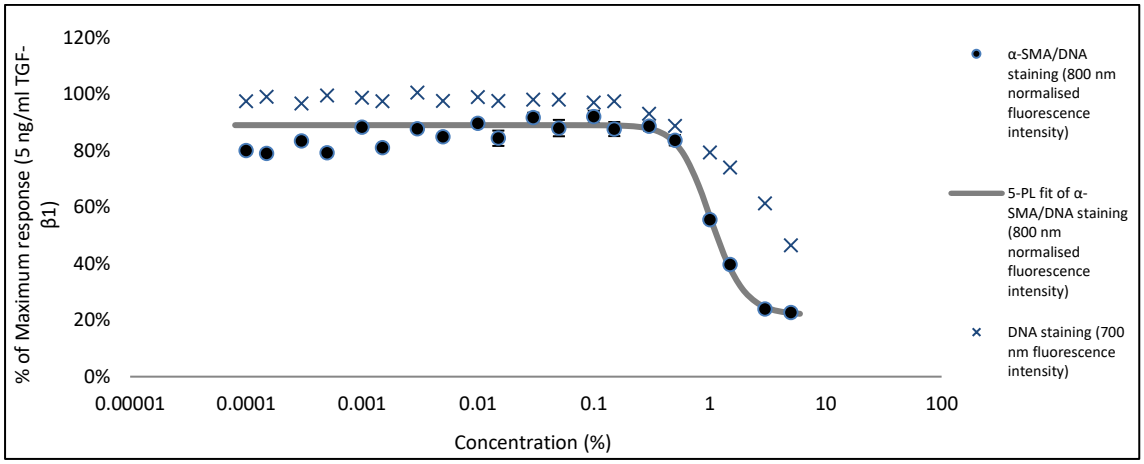

Figure 3-6: Effect of DMSO on TGF-β1-induced myofibroblast differentiation. Cells derived from non-PD TA tissue were exposed to a range of concentrations of DMSO between 0.0001 and 5% and applied in co-incubation with 5 ng/ml TGF-β1 for 72 hours. Data points were plotted as average ± SEM of the percentage of maximum response of either the α-SMA/DNA staining ratio (800 nm normalised fluorescence intensity) or DNA staining (700 nm fluorescence intensity) of N=3. Z' factor was determined using the average and standard deviation of the negative and positive controls to validate the experiment, yielding a Z' factor of 0.91 ± 0.01.

A range of concentrations of DMSO from 0.0001 to 5% was applied in co-incubation with 5 ng/ml of TGF-β1 for 72 hours. As can be observed in Figure 3-6, DMSO significantly decreased α-SMA/DNA staining ratio at concentrations of 1% and above. Regarding the DNA staining, DMSO had a negative effect at concentrations of 0.3% and above, leading to cell death due to DMSO and not because of the effect caused by the tested compounds in the differentiation process. Therefore, in all ICW experiments, the DMSO concentration never exceeded 0.3%.

To further validate the ICW assay and to ensure that it could be used to quantify inhibition of TGF-β1-induced myofibroblast differentiation, SB-505124 was used as a positive control. A full concentration response curve was performed with a range of concentrations of SB-505124 from 0.009 to 300 µM (0.003 to 100 µg/ml) applied in co-incubation with TGF-β1 for 72 hours (Figure 3-7).

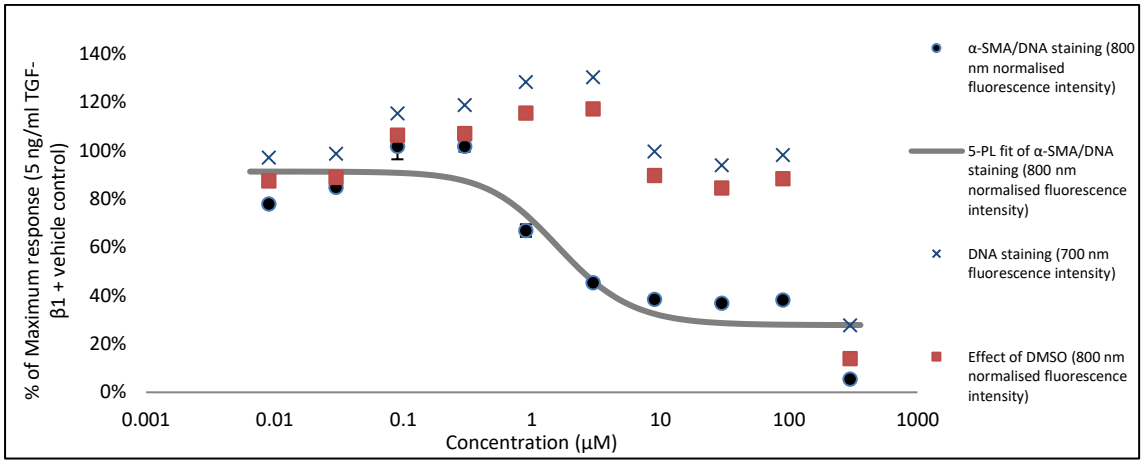

Figure 3-7: Effect of SB-505124 on TGF-β1-induced myofibroblasts transformation. Cells derived from non-PD TA tissue were exposed to a range of concentrations of SB-505124 between 0.009 and 300 µM and applied in co-incubation with 5 ng/ml TGF-β1 for 72 hours. Data points were plotted as average ± SEM of the percentage of maximum response of either the α-SMA/DNA staining ratio (800 nm normalised fluorescence intensity) or DNA staining (700 nm fluorescence intensity) or effect of DMSO, N=3. Z' factor was determined using the average and standard deviation of the negative and positive controls to validate the experiment, yielding a Z' factor of 0.89 ± 0.02.

As shown in Figure 3-7, a classical sigmoid curve was observed, with a minimum effect of approximately 30%. The α-SMA/DNA staining ratio was significantly reduced at the concentration of 0.9 µM and above, with a half maximal inhibitory concentration (IC_{50}) of 1.39 µM and a minimum effective concentration (MEC) of 0.9 µM. The DNA staining was significantly reduced at the highest concentration (300 µM).

The ADORA2B antibody was validated in the ICW assay by co-incubating with a blocking peptide (Figure 3-8). Cells were treated with TGF-β1, after which, the cells were stained with the ADORA2B antibody with or without excess of free full-length ADORA2B (blocking peptide).

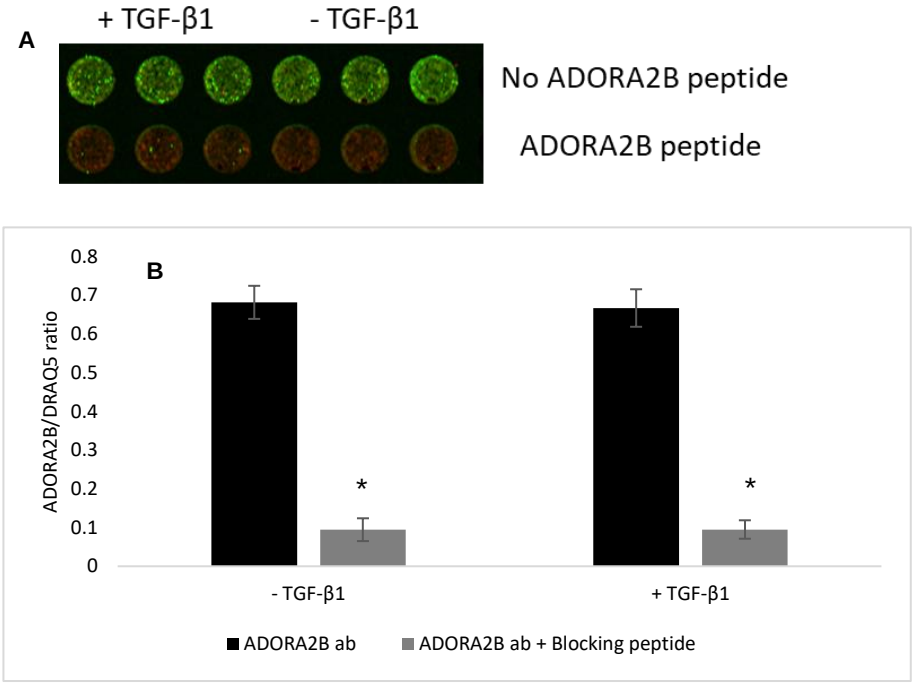

Figure 3-8: ADORA2B antibody in co-incubation with a blocking peptide. (A) Representative raw data output from Odyssey infrared imager and (B) Histographical representation of normalised fluorescence intensity. In-Cell Western was performed to validate the ADORA2B antibody by co-incubating the ADORA2B antibody at 2 µg/ml with or without blocking peptide at 2 µg/ml in non-PD TA cells. Green colour corresponds to ADORA2B protein levels, corresponding to emission at 800 nm wavelength. Red colour corresponds to DRAQ5, which is emitted at 700 nm wavelength. Data points were plotted as mean ± SEM, N=3. Legend: * indicates $P<0.05$ tested by Student's t-test vs ADORA2B antibody.

In both treated and untreated cells, the expression of ADORA2B was observed when treated with the antibody on its own; however, in the presence of ADORA2B peptide, it resulted in the loss of 85% of staining (Figure 3-8), meaning that only approximately 15% of the signal in the ICW was non-specific with the remaining signal being specific for expression of ADORA2B.

The blocking peptide experiment was also attempted by Western blot in combination with ADORA2B HEK293T cells transient overexpression lysate as positive control for ADORA2B and HEK293 cell lysate (no transient overexpression) as negative control for ADORA2B. However, no band was detected at any molecular weight in neither the antibody alone nor the positive control cell lysate used (data not shown).

ERβ antibody was also assessed by co-incubating an excess full length ERβ (blocking peptide) with the primary antibody in both ICW and WB. Cells were treated with TGF-β1 for 72 hours, after which, the cells were stained with the ERβ antibody with or without a blocking peptide (Figure 3-9).

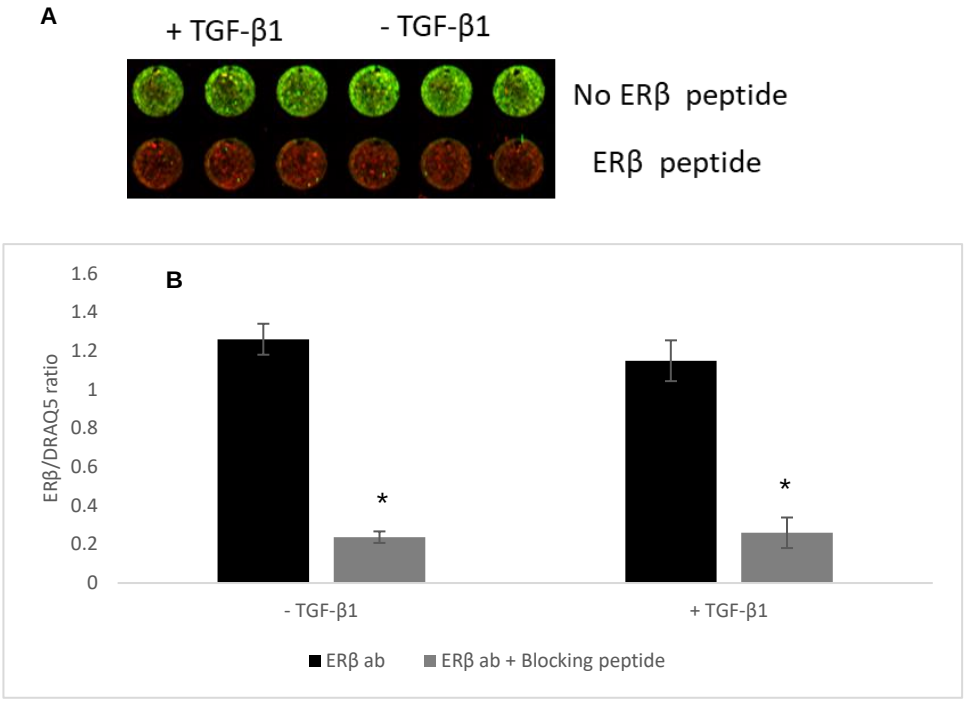

Figure 3-9: ERβ antibody in co-incubation with a blocking peptide. (A) Representative raw data output from Odyssey infrared imager and (B) Histographical representation of normalised fluorescence intensity. In-Cell Western was performed to validate the ERβ antibody by co-incubating the ERβ antibody at 1 µg/ml with or without blocking peptide at 1 µg/ml in non-PD TA cells. Green colour corresponds to ADORA2B protein levels, corresponding to emission at 800 nm wavelength. Red colour corresponds to DRAQ5, which is emitted at 700 nm wavelength. Data points were plotted as mean ± SEM, N=3**.** Legend: * indicates P<0.05 tested by Student's t-test vs ERβ antibody.

In both treated and untreated cells, the expression of ERβ was observed; however, the expression of ERβ was absent in the presence of the ERβ peptide and reduced by 84% in the ICW (Figure 3-9), meaning that only approximately 16% of the signal in the ICW was non-specific with the remaining signal being specific for expression of ERβ.

The ERβ expression was also tested in WB in co-incubation with the blocking peptide (Figure 3-10). In addition, ERβ HEK293T cell transient overexpression lysate was also used as a positive control for ERβ alongside a negative control for ERβ, an HEK293 cell lysate (no transient overexpression).

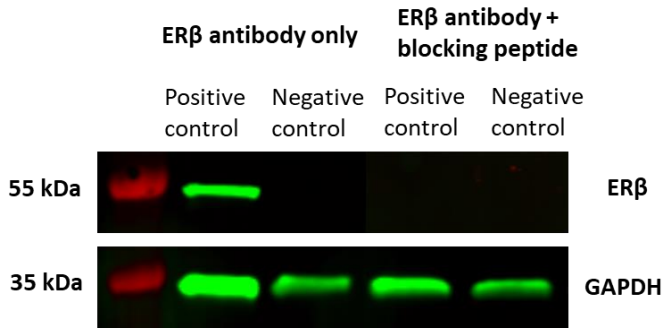

Figure 3-10: Immunoblotting of ERβ in positive and negative control lysates. Western blot was performed to validate the ERβ antibody by co-incubating the ERβ antibody at 1 µg/ml with or without blocking peptide at 1 µg/ml in both positive and negative control lysate. Green colour corresponds to ADORA2B protein levels, corresponding to emission at 800 nm wavelength. Red colour corresponds to DRAQ5, which is emitted at 700 nm wavelength.

Similar to ICW data, the expression of ERβ was observed with a band at the correct molecular weight (55 kDa) in the positive control, which was absent in the negative control. Furthermore, the results obtained for the blocking peptide experiment were in accordance with the ICW data obtained, where no band was observed in the presence of the blocking peptide in both controls (Figure 3-10). It should also be noted that after optimisation of the Western blot, no non-specific bands were noted at different molecular weights with ADORA2B or ERβ antibody, further stating that the antibodies are specific.

3.3 Characterisation of cells derived from non-PD TA tissue and PD plaque tissue

3.3.1 Expression of α-SMA

3.3.1.1 mRNA levels of α-SMA

The mRNA levels of α-SMA were investigated in cells derived from non-PD TA tissue and PD plaque tissue (Figure 3-11).

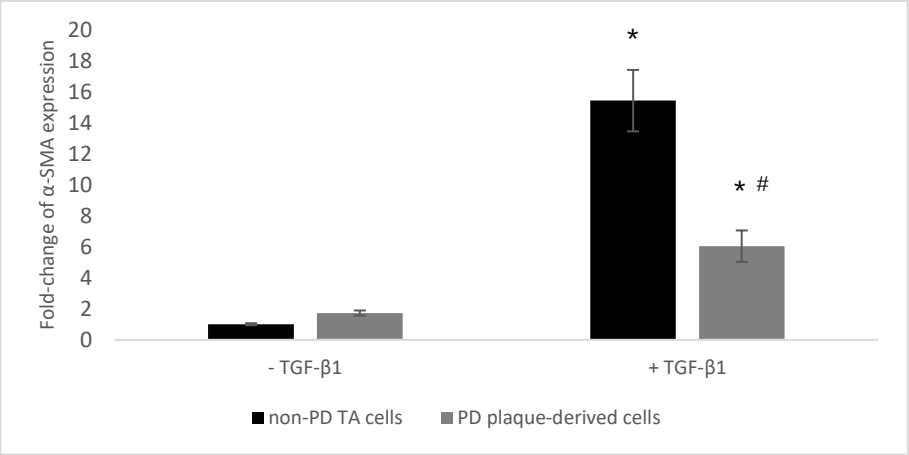

Figure 3-11: α-SMA mRNA levels in cells derived from non-PD TA tissue and PD plaque tissue. Fibroblasts were exposed to 10 ng/ml of TGF-β1 for 72 hours. The expression of α-SMA was determined using the $2^{-\Delta\Delta Cq}$ method, where the result obtained corresponds to the fold-change of α-SMA in the test sample relative to the calibrator sample (untreated cells derived from non-PD TA tissue) and normalised to the expression of EIF4A2 and TOP1. Each sample was run in triplicate. Data points were plotted as mean ± SEM, N=3. Legend: * and # indicates $P<0.05$ tested by Student's t-test vs untreated cells or non-PD TA cells, respectively.

As shown in Figure 3-11, a significant increase in α-SMA expression was observed in both cell populations when exposed to TGF-β1 for 72 hours. In addition, statistically significant difference was observed between non-PD TA cells and PD plaque-derived cells when exposed to TGF-β1 but not in untreated conditions, with PD plaque-derived cells decreased in comparison to non-PD TA cells.

3.3.1.2 Immunostaining of α-SMA

Immunocytochemistry was carried out to investigate the protein levels of α-SMA and ERs and to confirm results obtained in PCR experiments. Table 3-3 shows an overview of all the optimisations performed on the immunocytochemistry protocol.

Table 3-3: Summary of optimisations performed on the ICC protocol.

Optimisations performed	Results obtained
Comparison of different seeding surfaces (microplate vs coverslip)	Well-to-well fluorescence contamination occurred when using both 96 well microplate and 6 well plate (Data not shown).
Comparison of two fixation methods (ice-cold methanol vs 4% paraformaldehyde)	Fixation of cells with ice-cold methanol produced lower background than 4% PFA (Figure 3-12).
Comparison of 5% vs 10% donkey serum in blocking buffer	10% donkey serum yielded lower background levels than 5% donkey serum (Data not shown).
Use of different washing techniques	By inclining the slides and flowing washing buffer over the surface of the slide dislodged part of the cells when compared to the addition of the washing buffer through the corner of coverslip (Data not shown).

By performing these optimisations, it was clear that immunocytochemistry would need to be performed in coverslip, so no crosstalk would occur from well-to-well when using 6 well plates or microplates. The use of 10% donkey serum in the blocking buffer yielded lower background levels compared to 5% donkey serum and the wash steps would need to be carried out by adding washing buffer through the corner of the coverslip. In addition, the fixation method (ice-cold methanol versus 4% PFA) was also assessed (Figure 3-12).

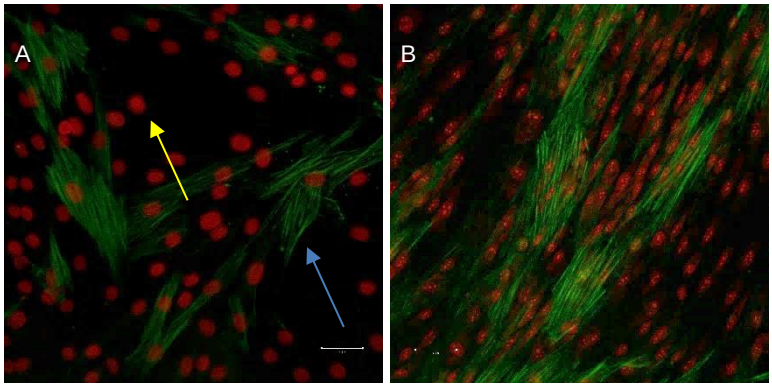

Figure 3-12: Representative illustrations of α-SMA staining using two fixation methods. (A) Non-PD TA cells treated with TGF-β1 fixed with ice-cold methanol and (B) PD plaque-derived cells treated with TGF-β1 fixed with 4% PFA. ICC targeting α-SMA was performed to observe the effect of two fixation methods. The nucleus of cells was stained with PI, a red nuclear counterstain (yellow arrow), whereas the α-SMA positive cells were stained in green, which is conferred by the FITC conjugated secondary antibody (blue arrow). Confocal microscope at 200x magnification. Bar in the corner of each image represents 50 µm.

Figure 3-12 shows that when using 4% PFA, a high background was observed, whereas when cells were fixed with ice-cold methanol, the stain was neater. Therefore, methanol was used for subsequent experiments.

To confirm the mRNA levels of α-SMA and the presence of myofibroblasts in cells derived from non-PD TA tissue and PD plaque tissue, both cell populations were exposed to TGF-β1 for 72 hours, after which, ICC was carried out (Figure 3-13).

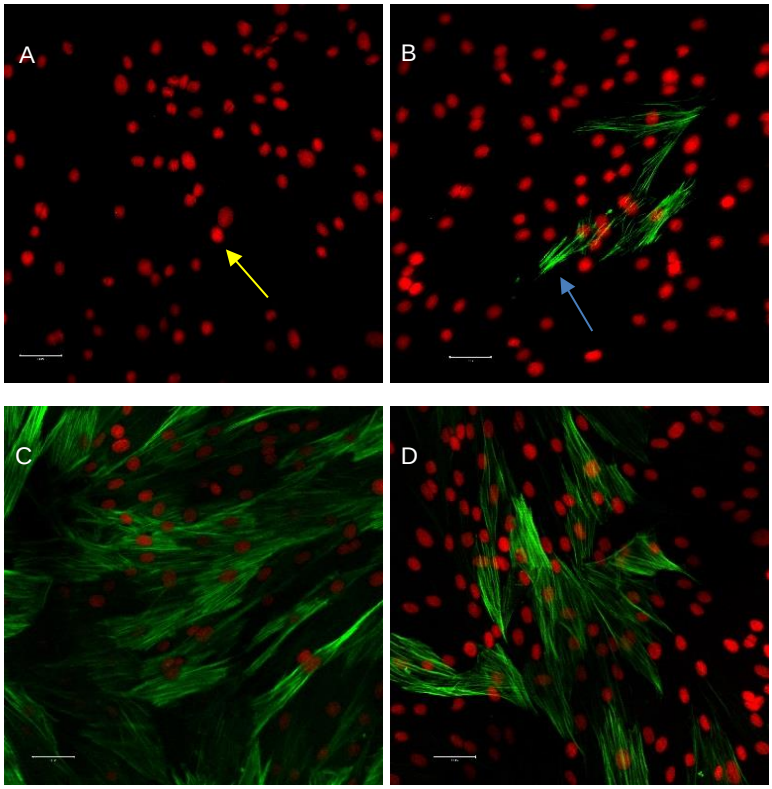

Figure 3-13: Representative illustrations of α-SMA staining in cells established from non-PD TA tissue and PD plaque tissue. (A) untreated non-PD TA cells, (B) untreated PD plaque-derived cells, (C) non-PD TA cells treated with TGF-β1 and (D) PD plaque-derived cells treated with TGF-β1. ICC targeting α-SMA was performed to observe the effect of cells exposed to TGF-β1 at 10 ng/ml for 72 hours. The nucleus of the cells was stained with PI, a red nuclear counterstain (yellow arrow), whereas the α-SMA positive cells were stained in green, which is conferred by the FITC conjugated secondary antibody (blue arrow). Confocal microscope at 200x magnification. Bar in the corner of each image represents 50 µm.

Figure 3-13 demonstrates the ICC results targeting α-SMA with PI nuclear counterstain. In both cell populations, α-SMA positive cells were observed in the presence of TGF-β1. Nevertheless, in the absence of TGF-β1, the presence of α-SMA positive cells was rare or non-existent in both cell populations.

Three random areas of each sample were selected to capture images, after which, the number of myofibroblasts was calculated to estimate the difference in the number of α-SMA positive cells in samples treated and not treated with TGF-β1 (Figure 3-14).

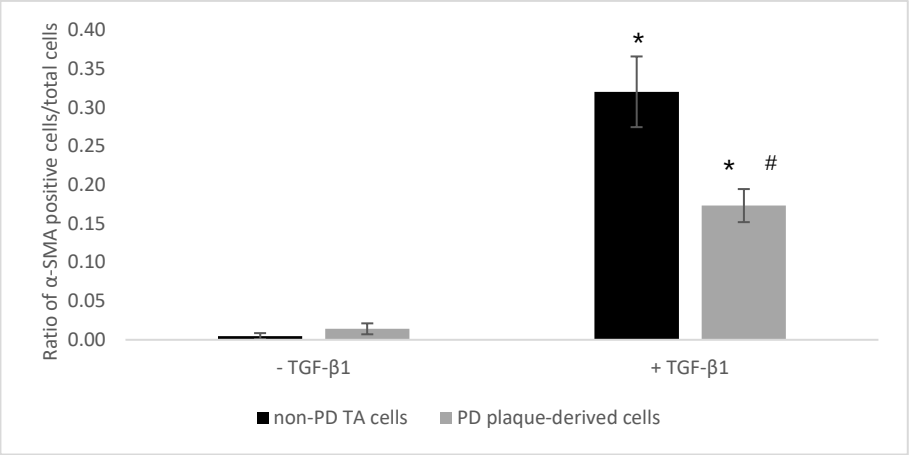

Figure 3-14: Ratio of α-SMA positive cells in cells derived from non-PD TA tissue and PD plaque tissue. Cells were exposed to TGF-β1 at 10 ng/ml for 72 hours, after which, the number of myofibroblasts was calculated by counting the number of α-SMA positive cells in each field and then divided by the number of total cells. Data points were plotted as an average of nine replicates of N=3 ± SEM. Legend: * and # indicates $P<0.05$ tested by Student's t-test vs untreated cells or non-PD TA cells, respectively.

As shown in Figure 3-14, statistically significant difference was found in cells derived from non-PD TA tissue and PD plaque tissue when exposed to TGF-β1 compared to untreated cells. Additionally, the number of myofibroblasts was significantly greater in the non-PD TA cells when compared to the PD plaque-derived cells when both are treated with TGF-β1 but not in untreated conditions.

To quantify the protein levels in an objective and higher throughput manner, the ICW method was used to test the effect of TGF-β1 on non-PD TA cells and PD plaque-derived cells (Figure 3-15).

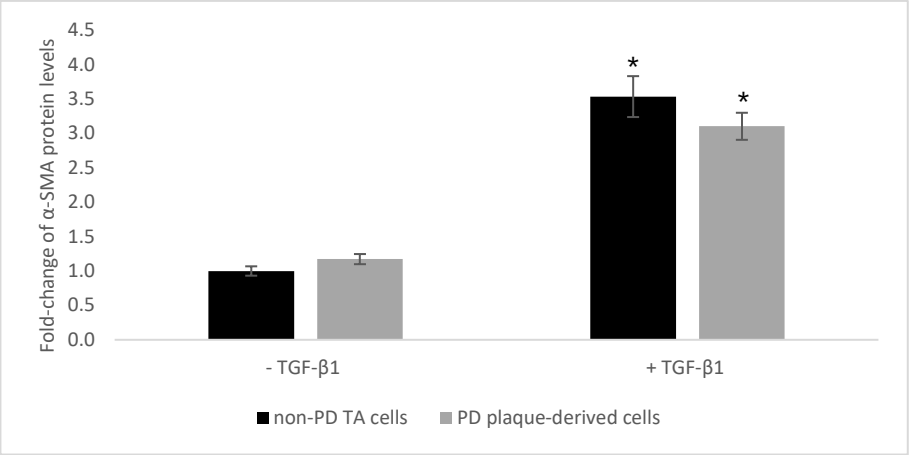

Figure 3-15: α-SMA protein levels in cells derived from non-PD TA tissue and PD plaque tissue. ICW was performed to assess the α-SMA protein levels in fibroblasts exposed to TGF-β1 at 10 ng/ml for 72 hours. Data points were plotted as mean ± SEM, N=3. Legend: * indicates P<0.05 tested by Student's t-test vs untreated cells.

As can be observed in the figure above, TGF-β1 significantly increased α-SMA protein expression in cells established from non-PD TA tissue and PD plaque tissue. However, no statistically significant difference was observed between non-PD TA cells and PD plaque-derived cells.

The amount of α-SMA protein following treatment with TGF-β1 was also quantified by immunoblotting for the 42 kDa protein in both cells derived from non-PD TA tissue and PD plaque tissue (Figure 3-16). GAPDH antibody was used as loading control (35 kDa), to ensure the integrity of the protein.

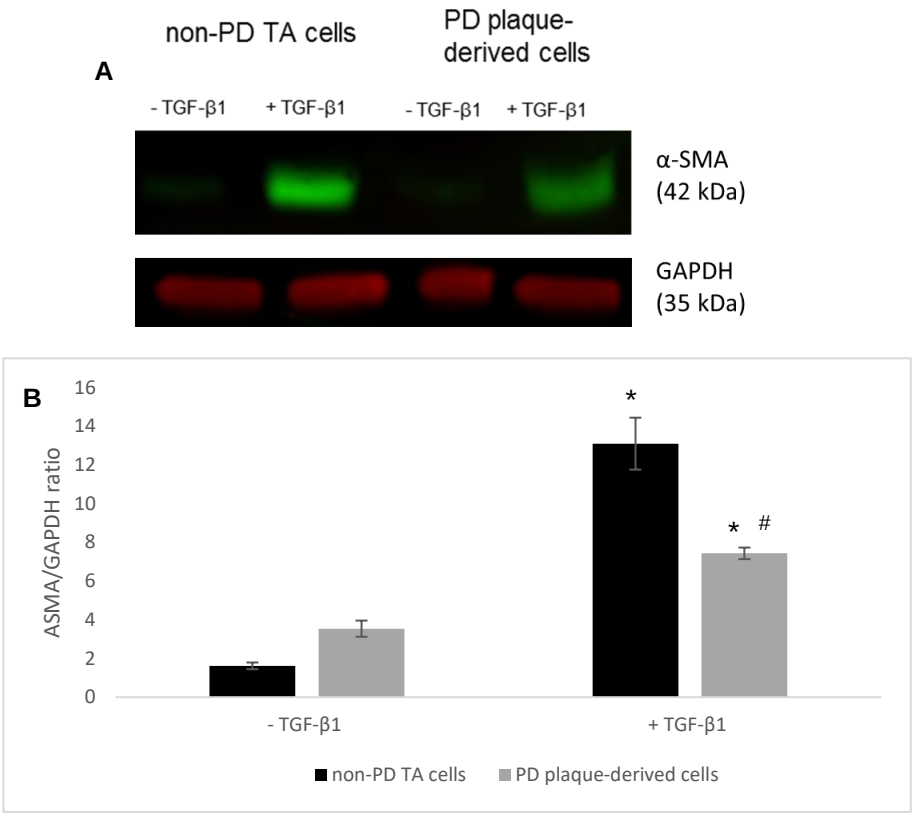

Figure 3-16: Immunoblotting of α-SMA in cells derived from non-PD TA tissue and PD plaque tissue. (A) Representative Western blot bands and (B) Western blot analysis. Cells were exposed to TGF-β1 at 5 ng/ml for 72 hours, after which, the protein was extracted from both cell populations. Green colour corresponds to α-SMA protein levels, corresponding to emission at 800 nm wavelength. Red colour corresponds to GAPDH protein levels, corresponding to emission at 700 nm wavelength. Data points were plotted as mean ± SEM, N=3. Legend: * and # indicates $P<0.05$ tested by Student's t-test vs untreated cells and non-PD TA cells, respectively.

As shown in Figure 3-16, protein bands were observed at the expected molecular weight of 42 and 35 kDa. Similar to mRNA levels and immunostaining data, a significant increase of α-SMA expression was observed in cell lysates treated with TGF-β1 in both cell populations. Furthermore, there was significantly greater value in the non-PD TA derived cells exposed to TGF-β1 compared with the PD plaque-derived cells exposed to TGF-β1.

3.3.2 Expression and modulation of adenosine receptors

3.3.2.1 mRNA levels of adenosine receptors

The expression of four adenosine receptors was investigated in cells isolated from non-PD TA tissue and PD plaque tissue (Figure 3-17).

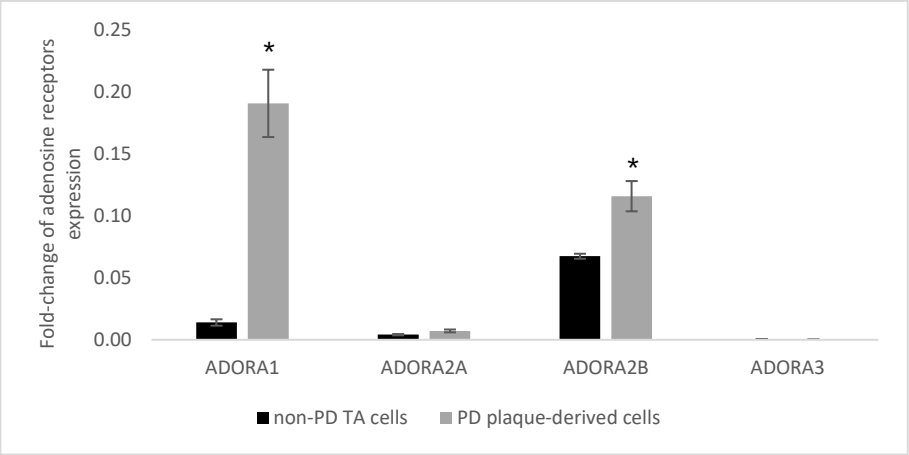

Figure 3-17: Adenosine receptors mRNA levels in cells derived from non-PD TA tissue and PD plaque tissue. The expression of adenosine receptors was determined using the $2^{\Delta Cq}$ method, where the result obtained corresponds to the fold change of each adenosine receptor relative to the expression of reference genes (EIF4A2 and TOP1). Each sample was run in triplicate. Data points were plotted as mean ± SEM, N=3. Legend: * indicates $P<0.05$ tested by Student's t-test vs non-PD TA cells.

As observed in Figure 3-17, ADORA2A and ADORA3 showed low levels of mRNA in both cell populations; whereas, ADORA2B was expressed in cells derived from both healthy and fibrotic tissues and ADORA1 was expressed in cells derived from PD plaque tissue. ADORA1 and ADORA2B were significantly higher in cells derived from PD plaque tissue than from non-PD TA tissue.

ADORA1 mRNA levels were investigated in the presence of TGF-β1 in both cells populations (Figure 3-18).

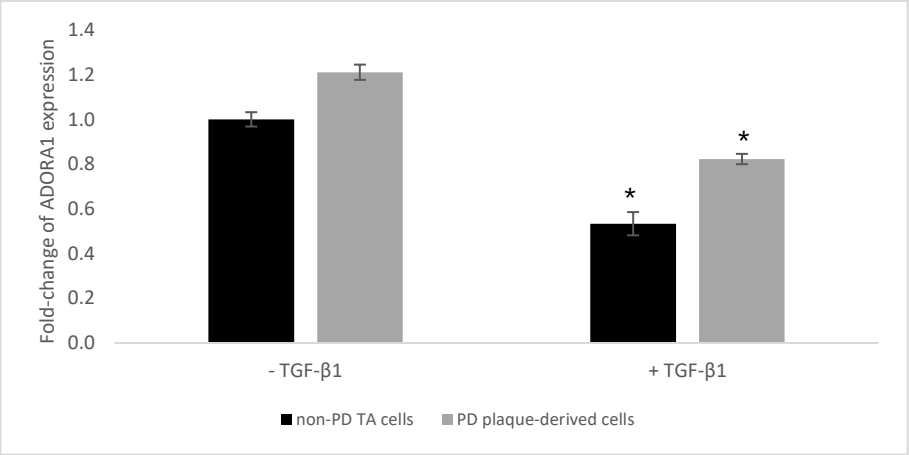

Figure 3-18: ADORA1 mRNA levels in cells derived from non-PD TA tissue and PD plaque tissue. Fibroblasts were treated with TGF-β1 at 10 ng/ml for 72 hours. The expression of ADORA1 was determined using the $2^{-\Delta\Delta Cq}$ method, where the result obtained corresponds to the fold change of ADORA1 in the test sample relative to the calibrator sample (untreated cells derived from non-PD TA tissue) and normalised to the expression of EIF4A2 and TOP1. Each sample was run in triplicate. Data points were plotted as mean ± SEM, N=3. Legend: * indicates $P<0.05$ tested by Student's t-test vs untreated cells.

In the above figure, the mRNA levels of ADORA1 significantly decreased in cells treated with TGF-β1 compared to untreated cells, in cells derived from non-PD TA tissue and PD plaque tissue. However, no statistically significant difference was observed between cell populations. In addition, a discrepancy between the ADORA1 mRNA levels in non-PD TA cells and PD plaque-derived cells not exposed to TGF-β1 in Figure 3-17 and Figure 3-18 was observed. However, this discrepancy was observed because the analysis method employed for each set of data was different. In Figure 3-18, the mRNA levels were relative to the calibrator sample (untreated non-PD TA cells) and normalised to the expression of the reference gene, whereas in Figure 3-17, the mRNA levels were only normalised to the expression of the reference gene.

The expression of ADORA2B in non-PD TA cells and PD plaque-derived cells treated with TGF-β1 was also investigated (Figure 3-19).

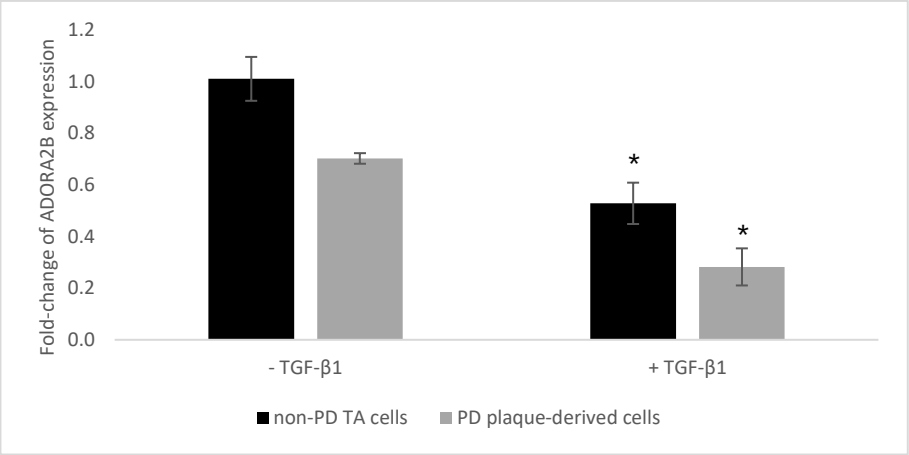

Figure 3-19: ADORA2B mRNA levels in cells derived from non-PD TA tissue and PD plaque tissue. Fibroblasts were exposed to TGF-β1 at 10 ng/ml for 72 hours. The expression of ADORA2B was determined using the $2^{-\Delta\Delta Cq}$ method, where the result obtained corresponds to the fold change of ADORA2B in the test sample relative to the calibrator sample (untreated cells derived from non-PD TA tissue) and normalised to the expression of EIF4A2 and TOP1. Each sample was run in triplicate. Data points were plotted as mean ± SEM, N=3. Legend: * indicates $P<0.05$ tested by Student's t-test vs untreated cells.

As shown in Figure 3-19, a significant decrease of ADORA2B mRNA levels was observed in cells exposed to TGF-β1 when compared to cells not exposed to TGF-β1. However, no statistically significant difference was observed between cell populations.

3.3.2.2 Immunostaining of adenosine receptors

The protein levels of ADORA1 and ADORA2B were investigated in non-PD TA tissue and in PD plaque tissue (Figure 3-20).

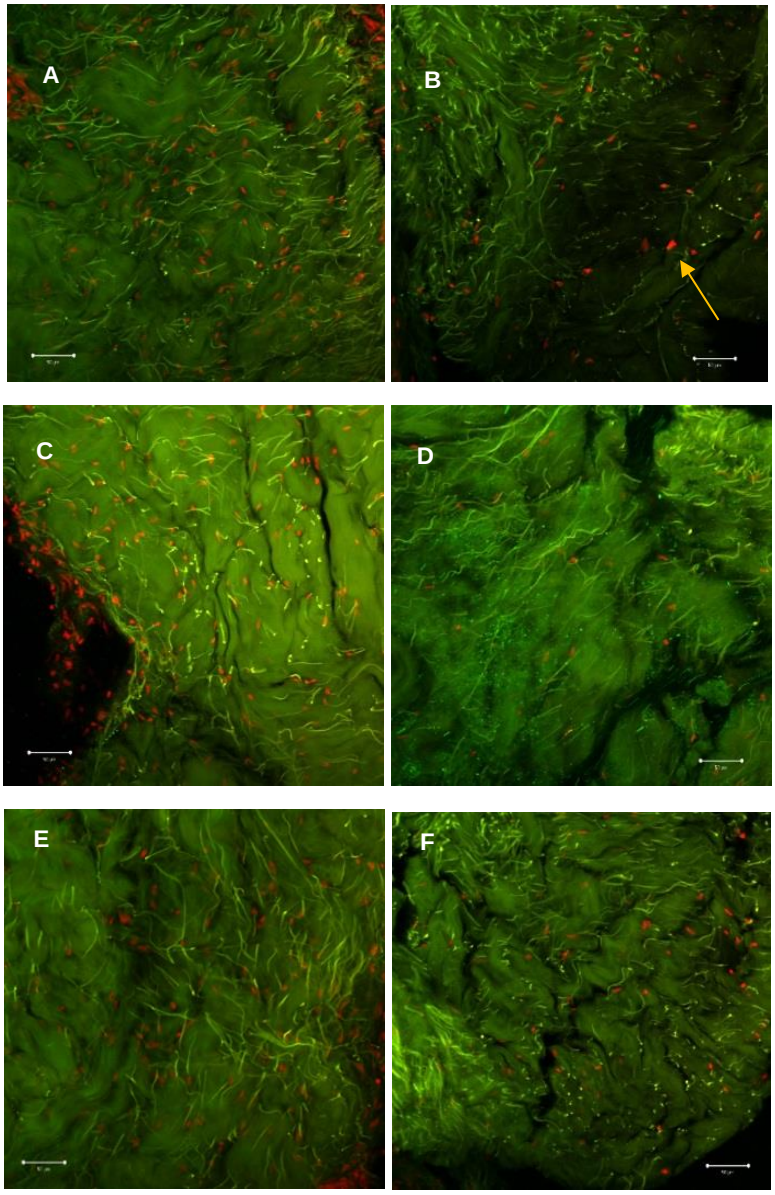

Figure 3-20: Representative illustrations of adenosine receptors' immunostaining in non-PD TA tissue and PD plaque tissue. (A) ADORA1 staining on non-PD TA tissue, (B) ADORA1 staining on PD plaque tissue, (C) ADORA2B staining on non-PD TA tissue, (D) ADORA2B staining on PD plaque tissue, (E) No primary antibody added on non-PD TA tissue and (F) No primary antibody added on PD plaque tissue. IHC targeting ADORA1 and ADORA2B was performed to observe the expression of these receptors in both healthy and fibrotic tissues. The nucleus of the cells was stained with PI, a red nuclear counterstain (yellow arrow), whereas the adenosine receptors were stained in green, which is conferred by the FITC conjugated secondary antibody. Confocal microscope at 200x magnification. Bar in the corner of each image represents 50 µm.

As shown in Figure 3-20, neither ADORA1 expression nor ADORA2B expression was observed in either tissue sample. Even though green fluorescence was observed in the sections, similar levels of fluorescence were also observed in negative controls (Figure 3-20E and F).

Figure 3-21 represents the ADORA1 protein levels in cells established from non-PD TA tissue and PD plaque tissue.

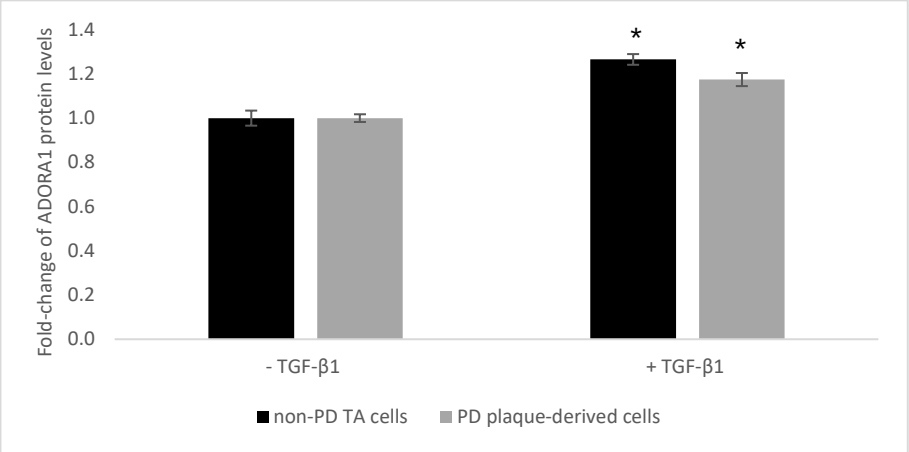

Figure 3-21: ADORA1 protein levels in cells derived from non-PD TA tissue and PD plaque tissue. ICW was performed to assess the ADORA1 protein levels in fibroblasts exposed to TGF-β1 at 10 ng/ml for 72 hours. Data points were plotted as mean ± SEM, N=3. Legend: * indicates P<0.05 tested by Student's t-test vs untreated cells.

In the above figure, a statistically significant difference was found in cells treated with TGF-β1 when compared to untreated cells in both cell populations.

The protein levels of ADORA2B was also carried out in both non-PD TA cells and PD-plaque derived cells (Figure 3-22).

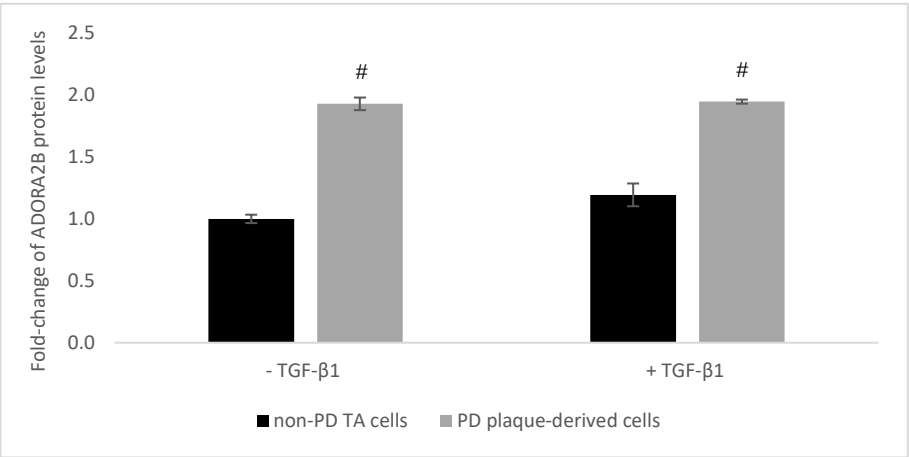

Figure 3-22: ADORA2B protein levels in cells derived from non-PD TA tissue and PD plaque tissue. ICW was performed to assess the ADORA2B protein levels in fibroblasts exposed to TGF-β1 at 10 ng/ml for 72 hours. Data points were plotted as mean ± SEM, N=3. Legend: # indicates P<0.05 tested by Student's t-test vs non-PD TA cells.

Regarding the protein levels of ADORA2B in both non-PD TA cells and PD plaque-derived cells, no statistically significant difference was observed in cells exposed to TGF-β1 compared to cells not exposed to TGF-β1 (Figure 3-22). However, significance was achieved between non-PD TA cells and PD plaque-derived cells.

3.3.2.3 Effect of specific adenosine receptor agonist and antagonist compounds on myofibroblast differentiation

To further investigate the change in expression of ADORA1 and ADORA2B and their ability to inhibit myofibroblast differentiation; specific, commercially available agonists and antagonists were used. N^6-Cyclopentyladenosine (CPA) and BAY 60-6583 were used as ADORA1 and ADORA2B agonists, respectively. On the other hand, SLV 320 and MRS 1754 were used as ADORA1 and ADORA2B antagonists, respectively. Fibroblasts derived from non-PD TA tissue and PD plaque tissue were treated with either agonist or antagonist compounds in co-incubation with TGF-β1 for 72 hours (Figure 3-23).

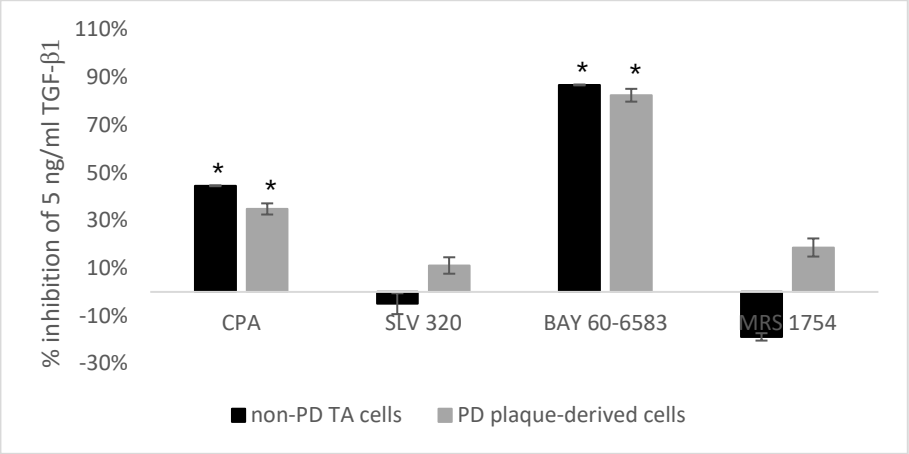

Figure 3-23: Effect of ADORA1 and ADORA2B agonist and antagonist on TGF-β1-induced myofibroblast differentiation. Fibroblasts derived from non-PD TA tissue and PD plaque tissue were incubated with 5 ng/ml TGF-β1 and the respective agonist or antagonist compounds of ADORA1 or ADORA2B for 72 hours (CPA at 100 µM; SLV 320 at 100 µM; BAY 60-6583 at 100 µM and MRS 1754 at 100 nM). Data points were plotted as the average of three replicates ± SEM. Legend: * indicates $P<0.05$ tested by Student's t-test vs 5 ng/ml TGF-β1. Z' factor was determined using the average and standard deviation of the negative and positive controls to validate the experiment, yielding a Z' factor of 0.88 ± 0.01.

As can be observed in Figure 3-23, the ADORA1 and ADORA2B agonists significantly inhibited TGF-β1-induced myofibroblast differentiation at

concentrations of 100 μM in the two cell groups investigated. On the other hand, both ADORA1 and ADORA2B antagonist compounds did not inhibit TGF-β1-induced myofibroblast differentiation at concentrations of 100 μM and 100 nM, respectively.

Further analyses were carried out on the two agonists (CPA and BAY 60-6583) that significantly inhibited α-SMA/DNA staining. Full concentration responses curves of both compounds were performed in non-PD TA cells and PD plaque-derived cells (Figure 3-24). A range of concentrations of each compound was assessed in their ability to impede myofibroblast transformation, from which α-SMA/DNA staining values and the 5-PL curve-fit for those values were obtained. For each CRC, the shape of the 5-PL curve-fit and the effect on cell death were evaluated.

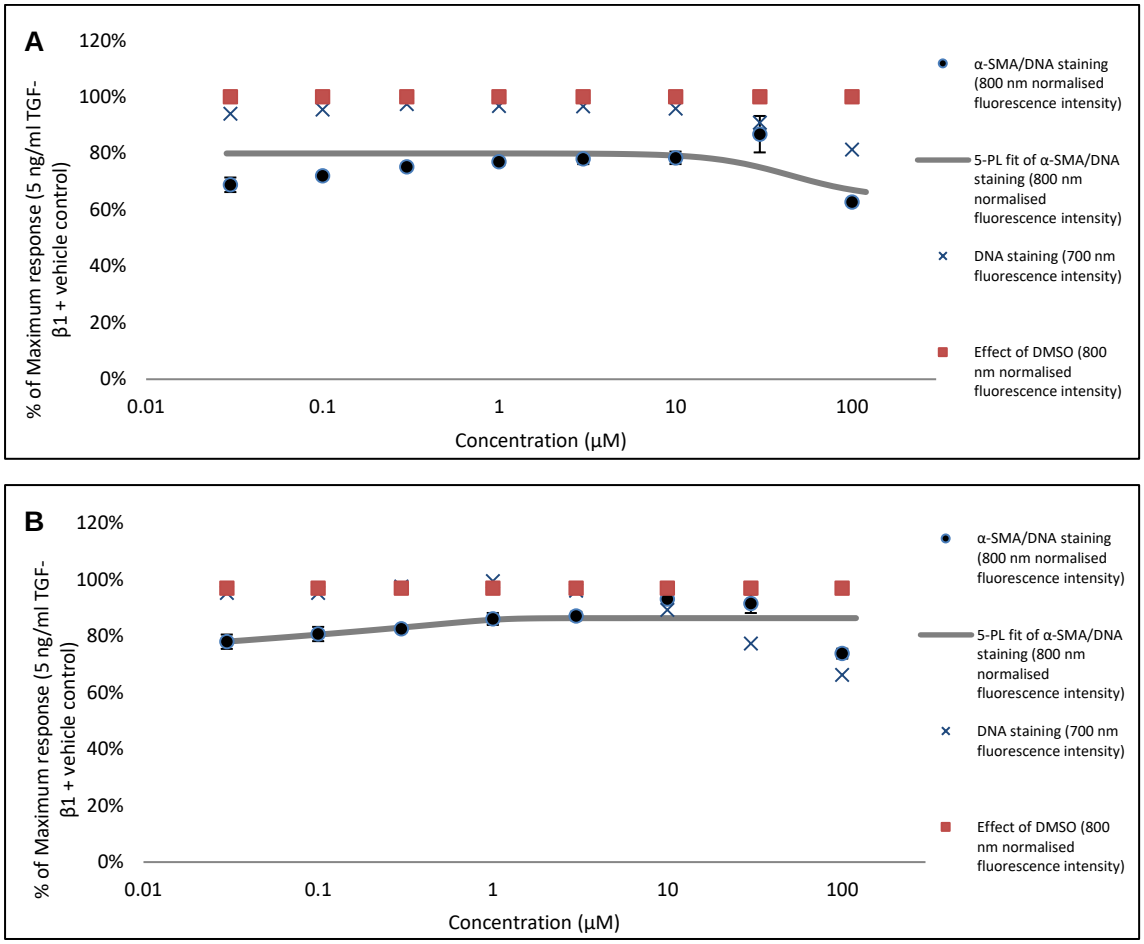

Figure 3-24: Effect of CPA on TGF-β1-induced myofibroblasts transformation. (A) Cells derived from non-PD TA tissue and (B) cells derived from PD plaque tissue were exposed to a range of concentrations of CPA between 0.03 and 100 µM and applied in co-incubation with 5 ng/ml TGF-β1 for 72 hours. Data points were plotted as average ± SEM of the percentage of maximum response of either the α-SMA/DNA staining ratio (800 nm normalised fluorescence intensity) or DNA staining (700 nm fluorescence intensity) or effect of DMSO, N=3. Z' factor was determined using the average and standard deviation of the negative and positive controls to validate the experiment, yielding a Z' factor of 0.82 ± 0.02.

Figure 3-24 illustrates the CRC performed for CPA (ADORA1 agonist) applied in co-incubation with TGF-β1 for 72 hours in non-PD TA cells and PD plaque-derived cells. The range of concentrations used failed to produce a classical sigmoid curve, where no lower plateau was observed in both cell populations.

A full concentration response curve of BAY 60-6583 (ADORA2B agonist) applied in co-incubation with TGF-β1 for 72 hours was also performed in both cell types (Figure 3-25).

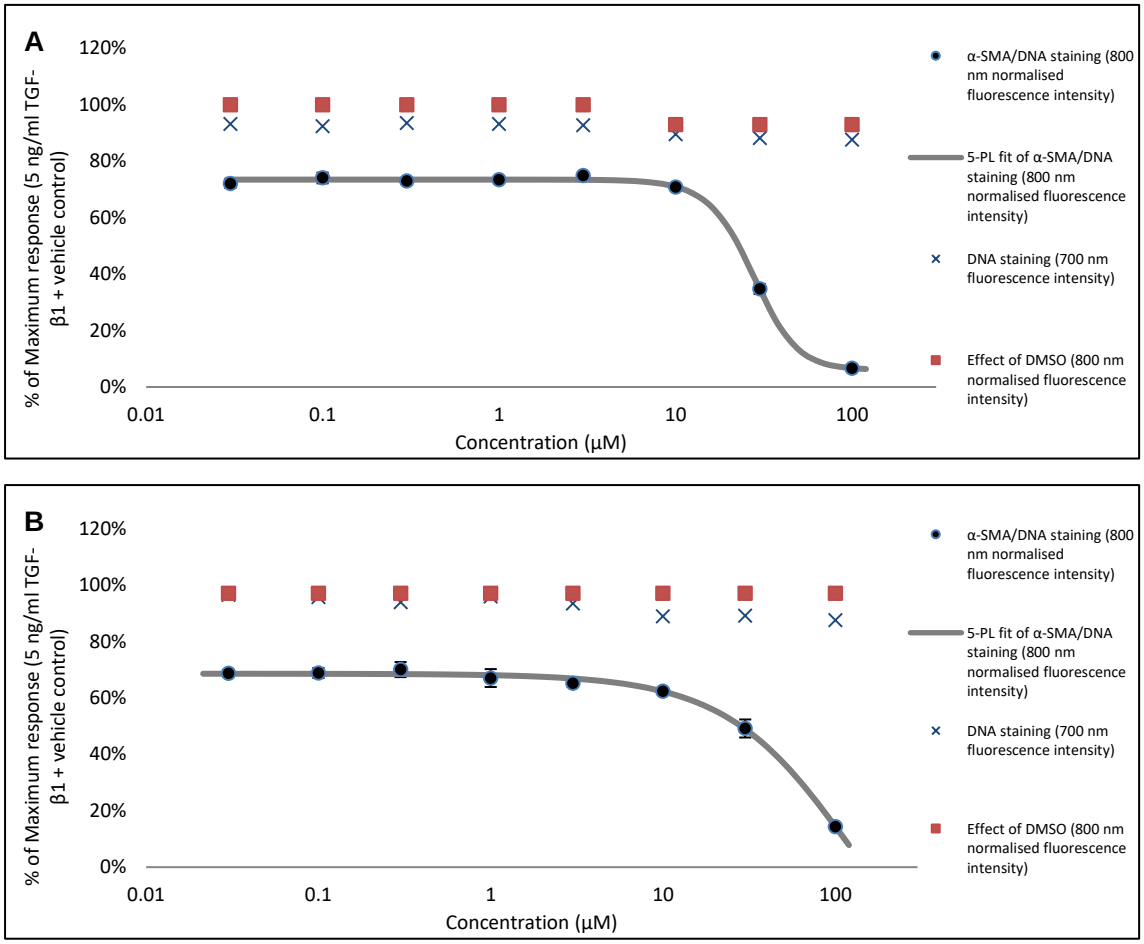

Figure 3-25: Effect of BAY 60-6583 on TGF-β1-induced myofibroblasts transformation. (A) Cells derived from non-PD TA tissue and (B) cells derived from PD plaque tissue were exposed to a range of concentrations of BAY 60-6583 between 0.03 and 100 µM and applied in co-incubation with 5 ng/ml TGF-β1 for 72 hours. Data points were plotted as average ± SEM of the percentage of maximum response of either the α-SMA/DNA staining ratio (800 nm normalised fluorescence intensity) or DNA staining (700 nm fluorescence intensity) or effect of DMSO, N=3. Z' factor was determined using the average and standard deviation of the negative and positive controls to validate the experiment, yielding a Z' factor of 0.87 ± 0.01.

When non-PD TA cells were exposed to a range of concentrations, a classical sigmoid curve was produced, reaching a minimum of approximately 10% with an IC_{50} value of 29.98 µM and a MEC of 30 µM. TGF-β1-induced myofibroblast differentiation was significantly decreased at concentrations of 30 µM and above without affecting cell numbers (Figure 3-25A).

Even though the α-SMA/DNA staining ratio produced by BAY 60-6583 in PD plaque-derived cells did not show a complete sigmoid curve, it did significantly reduce the TGF-β1-induced myofibroblast differentiation at concentrations of 30 µM and above without affecting cell number (Figure 3-25B).

3.3.3 Expression and modulation of estrogen receptors

Both estrogen receptors (ERα and ERβ) were assessed in cells isolated from non-PD TA tissue and PD plaque tissue.

3.3.3.1 mRNA levels of estrogen receptors

Figure 3-26 represents the mRNA levels of ERα in cells derived from healthy and fibrotic TA tissue.

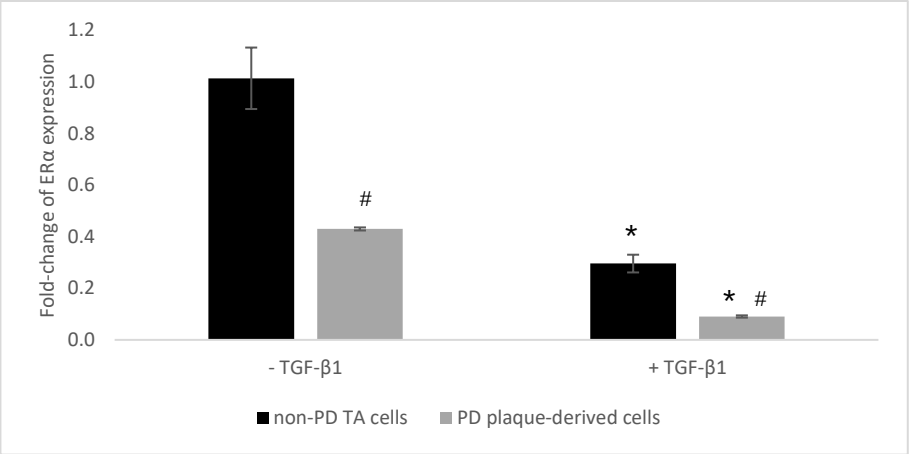

Figure 3-26: ERα mRNA levels in cells derived from non-PD TA tissue and PD plaque tissue. Cells were exposed to 5 ng/ml of TGF-β1 for 72 hours. The expression of ERα was determined using the $2^{-\Delta\Delta Cq}$ method, where the result obtained corresponds to the fold-change of ERα in the test sample relative to the calibrator sample (untreated cells derived from non-PD TA tissue) and normalised to the expression of EIF4A2 and TOP1. Each sample was run in triplicate. Data points were plotted as mean ± SEM, N=4. Legend: * and # indicates $P<0.05$ tested by Student's t-test vs untreated cells and non-PD TA cells, respectively.

As can be observed, a statistically significant difference was found between untreated cells and those exposed to TGF-β1 for 72 hours. Significance was also achieved when comparing PD plaque-derived cells to non-PD TA cells, with PD plaque-derived cells decreased.

The mRNA levels of ERβ were also investigated in non-PD TA cells and in PD plaque-derived cells (Figure 3-27).

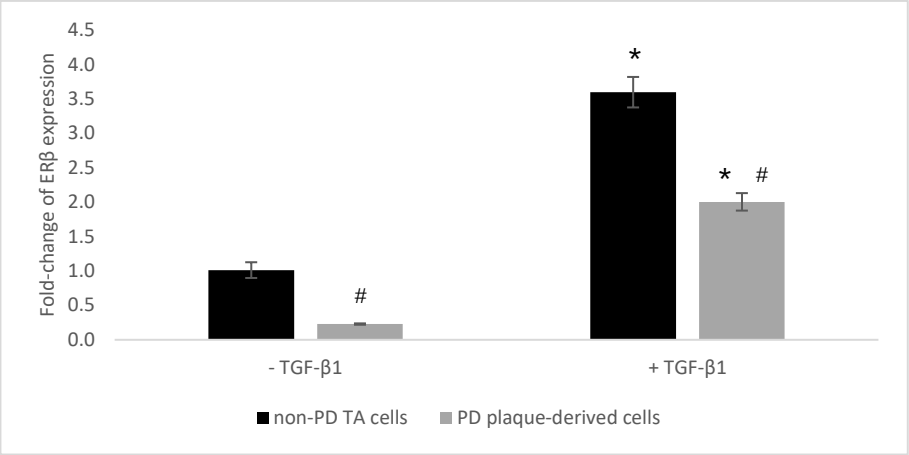

Figure 3-27: ERβ mRNA levels in cells derived from non-PD TA tissue and PD plaque tissue. Cells were treated with 5 ng/ml of TGF-β1 for 72 hours. The expression of ERβ was determined using the $2^{-\Delta\Delta Cq}$ method, where the result obtained corresponds to the fold-change of ERβ in the test sample relative to the calibrator sample (untreated cells derived from non-PD TA tissue) and normalised to the expression of EIF4A2 and TOP1. Each sample was run in triplicate. Data points were plotted as mean ± SEM, N=4. Legend: * and # indicates $P<0.05$ tested by Student's t-test vs untreated cells and non-PD TA cells, respectively.

The transcript levels of this receptor were significantly increased in non-PD TA cells and in PD plaque-derived cells exposed to TGF-β1 when compared to cells not exposed to TGF-β1 (Figure 3-27). Conversely, a statistically significant decrease was observed in PD plaque-derived cells when compared to non-PD TA cells with or without TGF-β1.

3.3.3.2 Immunostaining of estrogen receptors

To confirm the mRNA levels of both ERs in cells established from non-PD TA tissue and PD plaque tissue, immunocytochemistry was carried out. First, ICC targeting both ERα and ERβ was performed in MCF-7 cell line (human breast adenocarcinoma cell line; Figure 3-28), as these cells have been shown to express both ERs and was therefore used as a positive control[230].

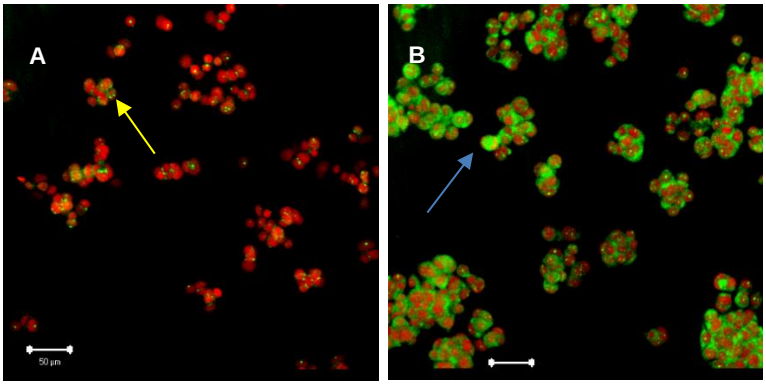

Figure 3-28: Representative illustrations of both ERs in MCF-7 cell line. (A) ERα and (B) ERβ. The nucleus of the cells was stained with PI, a red nuclear counterstain (yellow arrow), whereas the ERs were stained in green (blue arrow), which is conferred by the FITC conjugated secondary antibody. Confocal microscope at 200x magnification. Bar in the corner of each image represents 50 µm.

Figure 3-28 shows both ERs staining in MCF-7 cells. Although the expression of ERβ is stronger than ERα, the antibody and methods used successfully detected both ERs in MCF-7 cells and therefore can be used to investigate the protein levels in cells derived from human TA tissue.

ICC was carried out in cells derived from non-PD TA tissue and PD plaque tissue that were treated with TGF-β1 at 5 ng/ml for 72 hours (Figure 3-29).

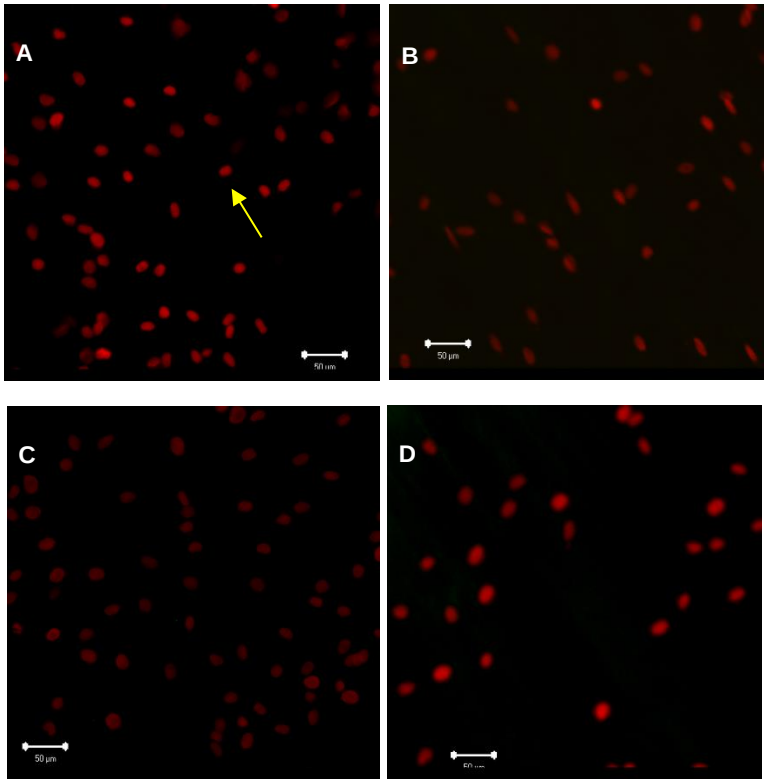

Figure 3-29: Representative illustrations of ERα in cells derived from non-PD TA tissue and PD plaque tissue. (A) untreated non-PD TA cells, (B) untreated PD plaque-derived cells, (C) non-PD TA cells treated with TGF-β1 and (D) PD plaque-derived cells treated with TGF-β1. ICC targeting ERα was performed to observe ERα expression in cells exposed to TGF-β1 at 5 ng/ml for 72 hours. The nucleus of the cells was stained with PI, a red nuclear counterstain (yellow arrow), whereas the ERα was stained in green, which is conferred by the FITC conjugated secondary antibody. Confocal microscope at 200x magnification. Bar in the corner of each image represents 50 µm.

Figure 3-29 demonstrates the ICC results targeting ERα with PI nuclear counterstain. In both cell populations, no ERα staining was observed either in cells not exposed to TGF-β1 or in cells exposed to TGF-β1.

Immunocytochemistry was also performed to target ERβ in both non-PD TA cells and PD plaque-derived cells (Figure 3-30).

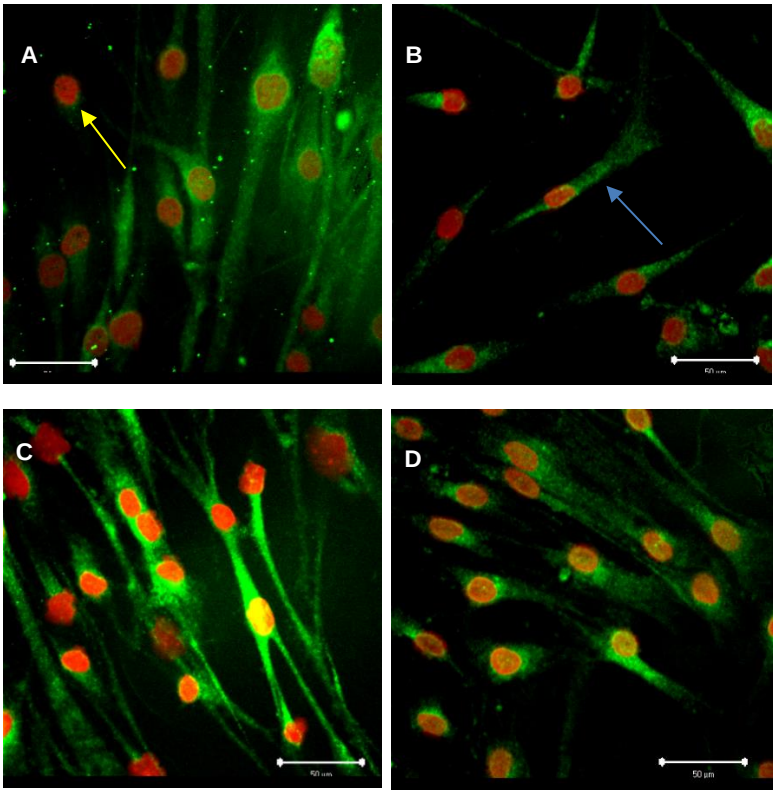

Figure 3-30: Representative illustrations of ERβ in cells derived from non-PD TA tissue and PD plaque tissue. (A) untreated non-PD TA cells, (B) untreated PD plaque-derived cells, (C) non-PD TA cells treated with TGF-β1 and (D) PD plaque-derived cells treated with TGF-β1. ICC targeting ERβ was performed to observe ERβ expression in cells exposed to TGF-β1 at 5 ng/ml for 72 hours. The nucleus of the cells was stained with PI, a red nuclear counterstain (yellow arrow), whereas the ERβ was stained in green (blue arrow), which is conferred by the FITC conjugated secondary antibody. Confocal microscope at 400x magnification. Bar in the corner of each image represents 50 µm.

Regarding ERβ, Figure 3-30 shows the ICC results with PI nuclear counterstain. In both cell populations, ERβ staining in cells exposed and not exposed to TGF-β1 was observed.

To further investigate the protein levels of both ERs in both cell populations, ICW was performed (Figure 3-31).

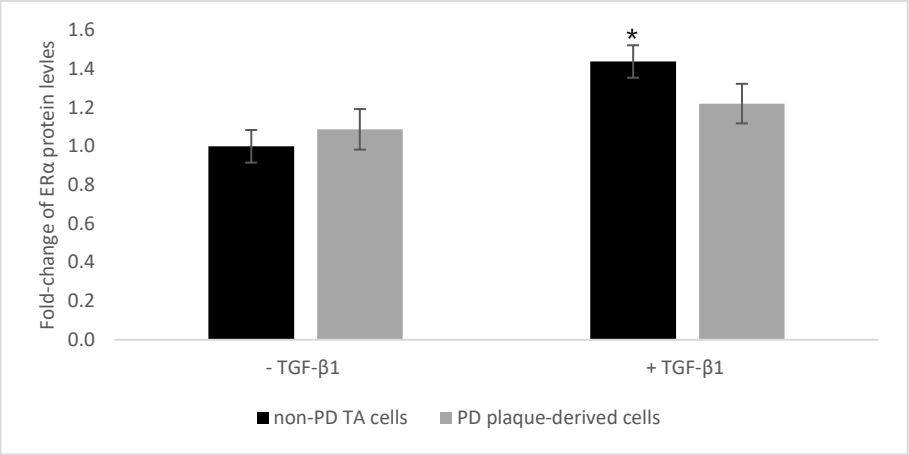

Figure 3-31: ERα protein levels in cells derived from non-PD TA tissue and PD plaque tissue. ICW was performed to assess the ERα protein levels in fibroblasts exposed to TGF-β1 at 5 ng/ml for 72 hours. Data points were plotted as mean ± SEM, N=4. Legend: * indicates P<0.05 tested by Student's t-test vs untreated cells.

Figure 3-31 represents the expression of ERα in non-PD TA cells and PD plaque-derived cells treated with TGF-β1 for 72 hours. As can be observed, only non-PD TA cells show a statistically significant increase in ERα when exposed to TGF-β1, with no difference between the two populations noted.

Figure 3-32 denotes the expression of ERβ in both cell populations when exposed to TGF-β1 for 72 hours.

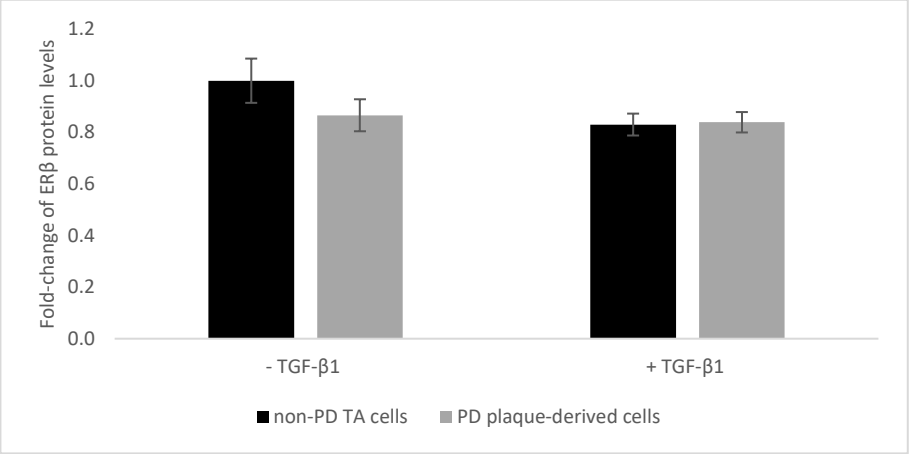

Figure 3-32: ERβ protein levels in cells derived from non-PD TA tissue and PD plaque tissue. ICW was performed to assess the ERβ protein levels in cells treated with TGF-β1 at 5 ng/ml for 72 hours. Data points were plotted as mean ± SEM, N=4.

As shown in the figure above, no significance was found between cells treated with TGF-β1 and not treated with TGF-β1 nor between the two cell groups investigated.

3.3.3.3 Effect of SERMs on myofibroblast differentiation

To study the effect of SERMs on myofibroblast transformation, both tamoxifen and raloxifene were tested. Figure 3-33 represents the effect of a range of concentrations from 0.018 to 53 µM (0.01 to 30 µg/ml) of tamoxifen applied in co-incubation with 5 ng/ml TGF-β1 for 72 hours.

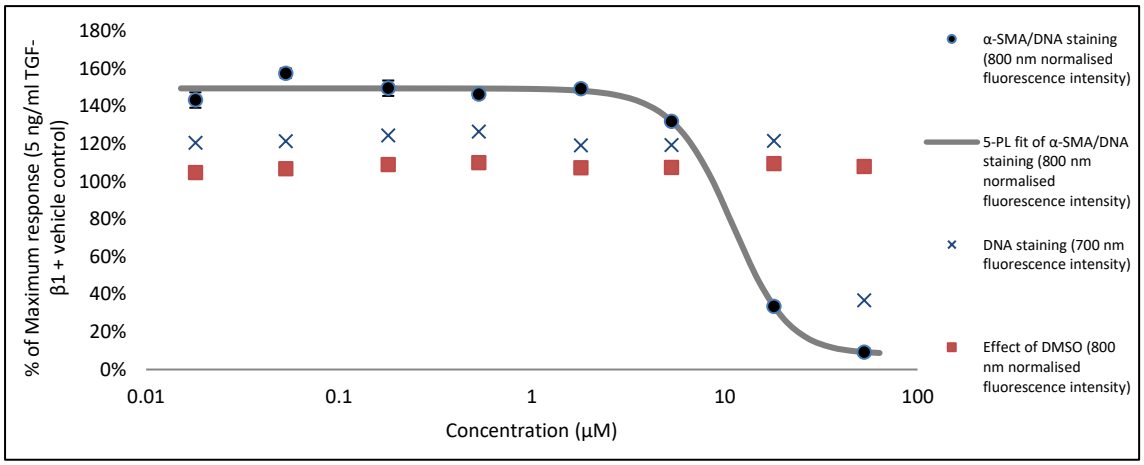

Figure 3-33: Effect of tamoxifen on TGF-β1-induced myofibroblasts transformation. Cells derived from non-PD TA tissue were exposed to a range of concentrations of tamoxifen between 0.018 and 53 µM in co-incubation with 5 ng/ml TGF-β1 for 72 hours. Data points were plotted as average ± SEM of the percentage of maximum response of either the α-SMA/DNA staining ratio (800 nm normalised fluorescence intensity) or DNA staining (700 nm fluorescence intensity) or effect of DMSO, N=3. Z' factor was determined using the average and standard deviation of the negative and positive controls to validate the experiment, yielding a Z' factor of 0.82 ± 0.05.

As can be observed, a sigmoid curve was produced, reaching a minimum of 10% with an IC_{50} value of 11.98 µM and a MEC of 18 µM. Tamoxifen significantly inhibited TGF-β1-induced myofibroblast differentiation at concentrations of 18 µM and above and only significantly decreased cell numbers at 53 µM.

As shown in the figure below, a full concentration response curve with a range of concentrations from 0.059 to 196 µM (0.03 to 100 µg/ml) of raloxifene applied in co-incubation with 5 ng/ml TGF-β1 for 72 hours was also performed.

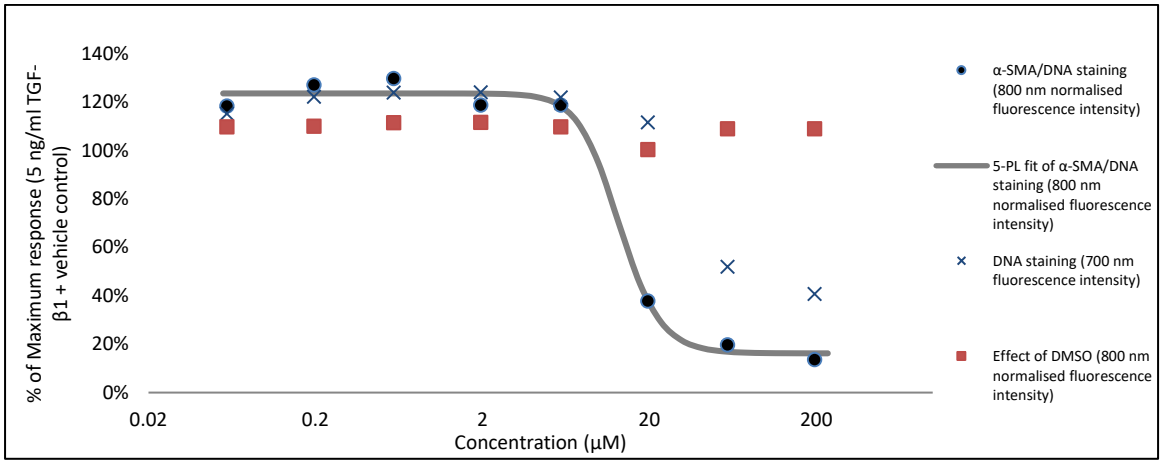

Figure 3-34: Effect of raloxifene on TGF-β1-induced myofibroblasts transformation. Cells derived from non-PD TA tissue were exposed to a range of concentrations of raloxifene between 0.059 and 196 µM in co-incubation with 5 ng/ml TGF-β1 for 72 hours. Data points were plotted as average ± SEM of the percentage of maximum response of either the α-SMA/DNA staining ratio (800 nm normalised fluorescence intensity) or DNA staining (700 nm fluorescence intensity) or effect of DMSO, N=3. Z' factor was determined using the average and standard deviation of the negative and positive controls to validate the experiment, yielding a Z' factor of 0.89 ± 0.01.

A classical sigmoid curve was produced by the range of concentrations used, reaching a minimum of approximately 20% with an IC_{50} value of 12.23 µM and a MEC of 19.6 µM. TGF-β1-induced myofibroblast differentiation was significantly reduced at concentrations of 19.6 µM and above. Nevertheless, a cytotoxic effect was detected only at concentrations of 59 µM and above, where a significant decrease of DNA staining was observed.

4 Discussion

4.1 Development of a real-time RT-PCR method

Real-time RT-PCR is a powerful technique used to quantify gene expression levels between different samples (healthy versus diseased tissue-derived samples). RT-qPCR allows the accumulation of PCR products to be detected and measured by a fluorescence molecule that reports an increment in the quantity of DNA with a proportional increase in fluorescence signal as the reaction progresses. This technique enables the determination of the starting copy number of the template with high sensitivity and accuracy over a wide range of quantities; however, several technical deficiencies can affect the assay performance (e.g. poor quality of RNA samples, poor choice of primers for both reverse transcription and qPCR reactions, improper or lack of validation of reference genes and unsuitable methods for data analyses).

In order to generate high quality and consistent data, the minimum information for publication of quantitative real-time PCR experiments (MIQE) guidelines have been published, which consist of a checklist with all the essential and desired information when submitting real-time PCR data to guarantee scientific literature integrity and to promote consistency between laboratories[231]. These guidelines were followed during this project, where all the essential and desired information was reported if available by the manufacturers.

Further information can be found in Appendix III about the methods employed in this project and why they were used.

To investigate the mRNA levels of genes of interest (α-SMA, adenosine receptors and estrogen receptors), RNA was extracted from cultured cells, converted to cDNA, which was then used as a template for qPCR.

To ensure high-quality RNA samples, the RNA extraction and purification process were performed in an RNase-free environment, small batches of samples were processed at the same time and the RNA samples were stored in suitable conditions (frozen at -80°C straight after the extraction procedure and until use).

Another potential risk for data quality resulting from PCR is the selection of suitable reference genes for data normalisation. According to several authors[231,232], two or more reference genes should be used to have an accurate normalisation. The geNorm M value was also used, which is the average pairwise variation of a specific gene compared to all the other reference genes. The genes with the lowest geNorm M value are the most stably expressed in the tested experimental conditions[233,234]. This data also enables the calculation of the optimal number of reference genes that should be used to achieve the best normalisation strategy[235]. This methodology indicated that the use of the two most stably expressed reference genes would be adequate to accomplish the best normalisation strategy in the tested experimental conditions.

For all qPCR runs, two negative controls (NTC and NRT, corresponding to no template control and no RT control, respectively) were included to ensure the efficiency of the method and the absence of PCR contaminants and gDNA. When amplification was observed in the negative controls, these samples were excluded and considered outliers only if the difference in the Cq value between the sample with the highest Cq value and the negative control was large enough (a Cq value difference above 5, which corresponds to a fold increase of about 32)[233].

SYBR Green was used as the detection reagent in this experiment and the main drawback of this reagent is the lack of specificity; therefore, it was essential to perform a melting curve analysis in each qPCR run to check the specificity of PCR products. By performing this quick test at the end of the qPCR run, it enabled to confirm that the PCR products observed were indeed the target of interest.

In summary, the mRNA levels of myofibroblasts could be assessed using the real-time RT-PCR methods developed herein in cells isolated from non-PD TA tissue and PD plaque tissue. All the MIQE guidelines were followed and all controls were performed to ensure proper evaluation of the targets of interest.

4.2 Validation of the ICW assay

A high-throughput cell-based assay was developed for the identification of compounds with potential anti-myofibroblast activity in cells derived from non-PD TA tissue and PD plaque tissue.

In regards to the ICW protocol itself, no optimisations were performed as it was already put through a process of extensive optimisations that included the establishment of the optimum concentrations of the primary and secondary antibody, the primary antibody incubation times (overnight vs two hours' incubation), comparison of three different antibodies targeting α-SMA (information of antibody validation in Appendix IV), percentage of donkey serum in blocking buffer, optimum concentration of surfactants in wash buffers and comparison of transparent 96 well plates vs bottom black 96 well plates[236]. Nevertheless, several control experiments were carried out to validate the use of the ICW assay for this project.

TGF-β is a cytokine implicated in the tissue differentiation and morphogenesis in fibrosis through enhancing inflammation, ECM deposition, cell differentiation and growth. There are three known isoforms of TGF-β: TGF-β1, TGF-β2 and TGF-β3, all of which function through the same receptor pathways. However, in *in vitro* investigations, TGF-β1 is the most commonly used isoform, due to its increased pro-fibrotic effects[237]. This cytokine binds to type II TGF-β receptor, which will recruit and activate the type I TGF-β receptor. This receptor is then responsible for recruiting and phosphorylating Smad 2 and 3 (intracellular mediators of TGF-β1), resulting in a complex with Smad 4, which is translocated to the nucleus to regulate the TGF-β1 target genes[238]. The regulation of TGF-β1 target genes can also occur through Smad-independent pathways, such as MAPK, RhoA, Wnt, Notch, Ras and PI3 kinase signalling pathways[239].

TGF-β1 was therefore selected as the inducer of myofibroblast differentiation process *in vitro*, as this cytokine is well documented in the literature as being profibrotic and an activator of myofibroblast transformation in PD and fibrosis in general[178,240–243].

In the experiments carried out in this study, TGF-β1 was applied in co-incubation with the compounds to reveal if the compound could prevent the myofibroblast differentiation process from occurring if present at the time when the cells were exposed to TGF-β1. In a clinical setting, if a compound with potential anti-myofibroblast activity is administrated in the moment when fibroblasts are stimulated to differentiate, that is, when TGF-β1 is present in the environment, then this compound might be effective in impeding this differentiation process from occurring.

To validate the assay for use in assessing the effect of compounds on myofibroblast differentiation in a medium to high throughput format, the Z' factor was used. A Z' factor below 0.5 is considered to be highly variable therefore not suitable for HTS, whereas a Z' factor between 0.5 and 1 is considered to have low variability and amenable to the assessment of novel potential compounds through HTS[244,245]. When comparing the negative controls (cells not exposed to TGF-β1) to the positive controls (cells exposed to TGF-β1), Z' factors above 0.5 were obtained using the ICW assay.

The objective of the DMSO concentration response curve was to assess its cytotoxic effect on fibroblasts and its inhibitory effect on TGF-β1-induced myofibroblast differentiation. Similar to the results described herein, a study by Xu *et al.* (2013)[246] demonstrated that DMSO had an effect on ear skin fibroblasts, leading to apoptosis of those cells. These data lead to a maximum DMSO concentration to be used of 0.3%.

SB-505124 was used as a positive control for the assay as it is a selective inhibitor of type I TGF-β receptors that has been reported to inhibit TGF-β1-induced myofibroblast differentiation. SB-505124 works by inhibiting the ATP binding site of activin receptor-like kinase (ALK) 5, which is also known as TGF-β type I receptor that when activated is capable of phosphorylating Smad2 and Smad3. Byfield and colleagues (2004)[247] showed that SB-505124 is a highly potent and selective inhibitor of TGF-β1. SB-505124 has been shown to reduce levels of α-SMA of rabbit subconjunctival fibroblasts that have been exposed to 2 ng/ml TGF-β for 48 hours[248]. In addition, SB-505124 has been reported to

decrease the α-SMA immunostaining in wounds topically treated with SB-505124 compared to control wounds[249].

The positive results observed for SB-505124 in the myofibroblasts inhibition assay validated this assay for use in the assessment of the effect of compounds on TGF-β1-induced myofibroblast differentiation.

With regards to the ADORA2B and ERβ antibodies used in the ICW assay, these were validated by co-incubating with or without excess of the full-length receptor. As these two antibodies are both polyclonal antibodies, non-specific binding to proteins other than the antigen of interest may occur; therefore, this is a good method to detect whether the staining is specific. When the antibody is neutralised by incubating with an excess of peptide that is recognised as the epitope by the antibody, the antibody will no longer be available to bind to the epitope present in the cells[250].

For the ADORA2B antibody, no bands were observed in the Western blot neither in the antibody alone nor in the positive control cell lysate used. Antibodies may not work well when a protein is fully denatured which is the case of the protein lysates used when running SDS WB. Nevertheless, the antibody may work well for proteins in their native conformation with intact 3-D structure, but not when denatured. Therefore, when the primary protein assay (in this case, ICW) used contains the antigen in its native conformation, WB should not be an absolute standardisation for antibody validation, instead antibody validation should be performed in the main protein assay used[250]. However, the WB is suitable as a first validation step and is still extensively used to assess antibody's specificity if the antibody recognises the denatured antigen. Further validation from the manufacturer for both proteins in question can be found in Appendix IV.

Taken together, the data discussed above shows that the ICW assay was deemed valid to be used to assess the protein levels of α-SMA, adenosine receptors and estrogen receptors as well as the effect of adenosine receptor modulators and SERMs on TGF-β1-induced myofibroblast differentiation.

4.3 Characterisation of cells derived from non-PD TA tissue and PD plaque tissue

Cells from non-PD TA tissue and PD plaque tissue were established and the expression of several targets, including adenosine and estrogen receptors, was assessed to understand their involvement in myofibroblast differentiation in PD.

Establishment of primary cell cultures was carried out throughout the study. Tissue samples acquired from patients undergoing surgery for either treatment of PD or invasive penile cancer were obtained, and fibroblasts were isolated from these tissue samples.

Primary cell cultures were established using the explant technique, which is a technique where the tissue fragments were forcefully rubbed onto the surface of a well of a 6-well plate. Cells migrated out of the tissue onto the surface of each well, after being left in culture medium for a few days at 37°C, 5% CO_2. Even though there are other techniques available to isolate a specific cell type, this method successfully established fibroblasts derived from non-PD TA tissue and PD plaque tissue.

Fibroblasts were identified by their spindle-shaped morphology as well as by the presence or absence of various markers, as no specific marker is expressed only by fibroblasts. The primary cell cultures established from non-PD TA tissue and PD plaque tissue were characterised by the analysis of the expression of vimentin, desmin and α-SMA. It was observed that these fibroblasts were vimentin-positive, desmin-negative and α-SMA-negative using immunostaining[251], which according to several authors define the fibroblast phenotype[192].

Furthermore, tissue fragments were carefully excised by the surgeon and during the *in vitro* cutting procedure, caution was taken to avoid contamination of other cell types, mainly smooth muscle cells present in the corpus cavernosum, which could have led to the increment of the number of myofibroblasts in the primary cell cultures due to the differentiation of the smooth muscle cells[28]. Nevertheless, this was not detected, as the cells observed growing out of the tissue did not

present the morphology of the smooth muscle cells, and subsequent α-SMA staining of cells from control tissues in the absence of TGF-β1 stimulation showed <1% myofibroblasts.

To investigate and characterise the myofibroblast transformation process, the expression of α-SMA was assessed, followed by the study of adenosine receptors and estrogen receptors expression in cells isolated from non-PD TA tissue and PD plaque tissue exposed and not exposed to TGF-β1.

4.3.1 Expression of α-SMA

After tissue injury, fibroblasts are activated and, under stress, differentiate into myofibroblasts. Myofibroblasts have a crucial role not only in normal wound healing but also in fibrosis. These cells are responsible for contracting the edges of a wound together and for producing several cytokines and abundant ECM proteins. Myofibroblast differentiation was selected as the target as it is well established in the literature as being a crucial contributor in the pathophysiology of several fibrotic disorders including PD[188,252,253] and it is also extensively used as a marker in this field. A key feature of myofibroblasts is their α-SMA expression; therefore, by targeting α-SMA, it is possible to investigate the myofibroblast transformation process. In addition, this marker is also well-studied protein and there are several specific and validated monoclonal antibodies.

The increase in α-SMA mRNA and protein levels induced by TGF-β1 observed in cells derived from non-PD TA tissue and PD plaque tissue presented herein is supported by previously published reports that have shown that both α-SMA mRNA and protein levels increase in the presence of TGF-β1 in fibroblasts isolated from PD tissue[188,192]. A differential response to TGF-β1 was observed between non-PD TA cells and PD plaque-derived cells, suggesting that these group of cells have different phenotypes, which might have been carried over from the tissue. The prior exposure to TGF-β1 in PD plaque tissue might have led the cells to partially resist TGF-β1; therefore, presenting a lower response to TGF-β1 in cells isolated from PD plaque tissues.

4.3.2 Expression and modulation of adenosine receptors

Various studies have shown that adenosine receptors play different roles in acute and chronic injuries. In acute injuries, it has been shown to be beneficial; however, when adenosine levels are increased, it has been associated with the progression of chronic tissue injuries, suggesting that adenosine may promote fibrosis[55]. This is not surprising given that fibrosis can be effectively thought of as persistent wound healing, therefore, a stimulus for wound healing can be both beneficial in acute states and detrimental when present for prolonged periods of time.

The objective of the results reported in section 3.3.2 (Expression and modulation of adenosine receptors) was to investigate the expression of four adenosine receptors in cells derived from non-PD TA tissue and PD plaque tissue. The mRNA levels were assessed in all four receptors and subsequently the effect of TGF-β1 on mRNA levels and protein levels was only investigated in two of the four receptors (ADORA1 and ADORA2B) that presented detectable levels of mRNA. Even though the mRNA levels were significantly decreased (fold-change of approximately 1.6) in the presence of TGF-β1 in both receptors, it may not represent a biological change in the transcript levels, as according to MIQE guidelines to show biological changes a 2-fold (recommended cut-off value) increase or decrease should be observed. It was therefore considered that the cells expressed ADORA1 and ADORA2B mRNA, but this expression was not affected by TGF-β1.

The expression levels of ADORA1 and ADORA2B was investigated in non-PD TA tissue and in PD plaque tissue; however, similar levels of fluorescence for ADORA1 and ADORA2B were observed in the negative control and in the tissue samples, which suggested that the fluorescence observed was autofluorescence. Various optimisations were attempted; however, the detection of low-level expression in human tissue using fluorescent techniques is a well-known and stubborn problem due to the phenomenon of autofluorescence[254].

The expression of these two receptors were also investigated in cells derived from non-PD TA tissue and PD plaque tissue. A differential response to TGF-β1 was observed for the protein levels of these two receptors.

Nevertheless, the expression of these receptors has been assessed in fibroblasts derived from other fibrotic tissues, with contrasting results depending on the tissue in question. A study performed by Zhong *et al.* (2005)[72] found that primary human lung fibroblasts expressed high mRNA levels of ADORA2B and the expression of this receptor at protein level was confirmed by immunofluorescence. These authors also showed that the activation of ADORA2B by adenosine promoted myofibroblast differentiation.

A further study by Wen *et al*. (2010)[66] showed that primary corpus cavernosal fibroblasts from mice expressed ADORA2B, which was suggested to be responsible for adenosine-mediated penile fibrosis. Furthermore, two other studies have also shown that deaminase-deficient mice had an increment of adenosine levels and ADORA2B activation in the penis, suggesting an essential mechanism for the progression of priapism in these mice[66,67].

These two studies are in accordance with the data presented in this report, as increased presence of both mRNA and protein in PD tissues indicates that ADORA2B is involved in this fibroproliferative disorder.

Even though the ADORA2B antagonist (MRS 1754) did not inhibit TGF-β1-induced myofibroblast transformation in this report, several authors reported that MRS 1754 lowered the mRNA levels of TGF-β1 and procollagen I, suggesting an anti-fibrotic role for this antagonist[66].The ADORA1 antagonist (SLV 320) also failed to inhibit TGF-β1-induced myofibroblast differentiation; however, SLV 320 has been reported to suppress cardiac fibrosis and reduce the amount of collagen in nephrectomised rats[255]. Taken together, these data may suggest that the antifibrotic role of adenosine receptor antagonists may be through an upstream process to TGF-β1, decreasing mRNA and potentially, protein levels of this profibrotic factor. Any compound working through such a mechanism may not be identified in the developed ICW assay. It is also worth noting that as agonism of these receptors had an inhibitory effect, it is unlikely that antagonism of these

same receptors would have the same effect. The results for the antagonists are, therefore, consistent with the data achieved for the agonists.

As both ADORA1 and ADORA2B agonists (CPA and BAY 60-6583, respectively) inhibited TGF-β1-induced myofibroblast transformation, further analyses were performed to evaluate their ability to inhibit TGF-β1-induced myofibroblast differentiation in a concentration-dependent manner. These two compounds were co-incubated with TGF-β1 to reveal whether they could prevent myofibroblast transformation from occurring if present in the moment at the cells were exposed to TGF-β1. Even though, the ADORA1 agonist CPA failed to show inhibition of TGF-β1-induced myofibroblast differentiation at any concentration; BAY 60-6583 (ADORA2B agonist) significantly inhibited TGF-β1-induced myofibroblast differentiation in non-PD TA cells in a concentration-dependent manner, while in PD plaque-derived cells an incomplete sigmoid curve was observed.

Both CPA[256,257] and BAY 60-6583[56,258] have been used by several authors as ADORA1 and ADORA2B agonists, respectively, to study the involvement of these adenosine receptors in different diseases.

It has been reported that CPA improved wound healing when applied topically, leading to increased proliferation of both BALB/3T3 fibroblasts (mouse embryonic fibroblast cell line) and endothelial cells in diabetic and normal mice[259]. Although on the surface this may appear to contradict the data in this report, as CPA improved wound healing in the literature but did not show a CRC in this report, the mechanism by which this occurred is in effect fibroproliferative by increasing the growth rate of fibroblasts. This is not a mechanism of interest for the prevention/treatment of fibrotic disorders nor is it a mechanism that would be identified in the developed ICW assay.

The ADORA2B agonist, BAY 60-6583, has been reported to improve renal function[56] and attenuating infarct sizes after ischemia[59]. These data are consistent with those of this thesis as an inhibition of TGF-β1-induced myofibroblast differentiation would also decrease the level of scarring, leading potentially to both attenuated infarct sizes and improved renal function in the respective studies.

To the best of the author's knowledge, this is the first time that the expression of the adenosine receptors has been investigated in cells derived from non-PD TA tissue and PD plaque tissue, showing expression of ADORA1 and ADORA2B. This is also the first time that an ADORA2B agonist have been shown to significantly inhibit TGF-β1-induced myofibroblast differentiation in a concentration-dependent manner in cells derived from human TA tissue.

Summary of results:

The table below is a collation of the tables shown in the Introduction section (pages 11 and 40) corresponding to adenosine receptor expression and effect of adenosine receptor modulation, with the addition of the data acquired in this report in order to contextualise the results.

Table 4-1: Summary table of the expression of adenosine receptors and the effect of agonists and antagonist in different tissues. Qualitative expression of adenosine receptors in different tissues. Highlighted in grey is the new data obtained in this study from cells established from tunica albuginea tissues. The relative mRNA expression of each receptor in each tissue is reported as a relative scale to the other receptors, according to *in vivo*, *in vitro* or human studies with +++ indicating the highest expression and + indicating the lowest expression of the receptors found to be present. Legend: red - promote fibrosis; green - impede fibrosis, black – anti-inflammatory and black – not detected/unknown.

Tissues		**Adenosine receptors**			
		ADORA1	**ADORA2A**	**ADORA2B**	**ADORA3**
Lung	**Expression**	+[72]	++[72]	+++[72]	
	Agonist	Adenosine[73]	CGS21680[76]	NECA[72]	
	Antagonist			CVT-6883[64]	
Kidney	**Expression**		+[138]	+++[68]	
	Agonist		CGS21680[77]	NECA[68]	
	Antagonist		ZM241385[77]	PSB1115[68] MRS1754[68]	

Tissues		Adenosine receptors			
		ADORA1	ADORA2A	ADORA2B	ADORA3
Liver	Expression		+++[63]		
	Agonist		NECA[74] CGS-21680[63]		
	Antagonist		ZM241385[63,74]		
Heart	Expression	+[78]	++[78]	+++[78]	
	Agonist			NECA[78]	
	Antagonist			MRS1754[260]	
Skin	Expression		+++[62]		
	Agonist		CGS21680[79]		
	Antagonist		ZM241385[62]		
Penis (corpus cavernosum)	Expression			+++[66]	
	Agonist			NECA[66]	
	Antagonist			MRS1754[66]	
Penis (tunica albuginea)	Expression	+		+++	
	Agonist			BAY 60-6583	
	Antagonist				

Taken together, the data discussed above show that adenosine receptors, specifically ADORA1 and ADORA2B appear to be involved in PD with ADORA2B, in particular, being a potential novel target for inhibition of myofibroblast differentiation in PD due to the increased expression over ADORA1 and the effect of the specific ADORA2B receptor agonist BAY 60-6583. It is interesting to note that Peyronie's disease and other fibroproliferative disorders have contradictory data, as ADORA2B agonism has been shown in this report to have an anti-fibrotic effect in PD, but not in the corpus cavernosum, kidney, and lung. This is not unexpected as adenosine receptors appear to play different roles in fibrosis depending on the tissue involved.

4.3.3 Expression and modulation of estrogen receptors

Estrogen mediates its physiological effects through two ERs, which have been suggested to be involved in the pathophysiology of several fibroproliferative diseases.

The objective of the results presented in section 3.3.3 (Expression and modulation of estrogen receptors) was to investigate the expression of ERα and ERβ in cells established from non-PD TA tissue and PD plaque tissue and to assess the effect of modulation of these receptors on myofibroblast transformation.

The expression of ERβ was observed in both cell populations and its localisation in non-PD TA cells and PD plaque-derived cells was principally in the cytoplasm, which it is in agreement with the findings reported by Pedram *et al.* (2010)[91]. The authors found that ERβ was predominantly in the extranuclear locations such as cytoplasm and plasma membrane fractions in cardiac fibroblasts. Conversely to the results reported herein and the study above, ERβ has also been observed mainly in the nucleus of human lung fibroblasts[126,127] as well as in the nucleus of HSCs and hepatocytes with a small percentage of ERβ localised in the cytoplasm of these cells[151]. The location of these receptors in fibroblasts derived from different tissues is not unexpected, as there is a differential expression of these receptors in the tissues and such specific localisation of the receptors may be related to the varying effects observed by E2 in each tissue. In addition, the ability of a specific cell derived from a specific tissue to respond to estrogen depends on the presence of each estrogen receptor in that tissue[261].

Even though there was a difference between ERα and ERβ mRNA and protein levels, it should be noted that the detection of mRNA levels does not provide information on whether that mRNA will be translated into a functional protein[262] as mRNA do not directly indicate bioactivity of the protein and post-transcriptional events can modulate the amount of protein[263,264].

In contrast to the data presented herein, Hattori *et al.* (2011)[265] reported that TGF-β1 upregulated both mRNA and protein levels of ERα. This discrepancy could be

attributed to the fact that the authors used human dermal fibroblasts and only exposed the cells to TGF-β1 for 24 hours at 2 ng/ml. According to Haczynski *et al.* (2002)[266], human skin fibroblasts express both ERα and ERβ. However, these authors reported that ERβ was weakly detected in these cells and it was found predominantly in the nuclear compartment, compared to ERα. Similar to the data reported herein, a study by Palmieri *et al*. (2004)[267] showed that human mammary fibroblasts expressed ERβ, but did not express ERα.

These data attest to the fact that the expression of ERs is highly varied in different fibroblast populations originating from different tissues. This would likely translate to different levels of involvement of these receptors in fibroproliferative diseases in different tissues, as described in the introduction chapter of this thesis.

To further probe the involvement of ERs in PD, two SERMs: tamoxifen and raloxifene were assessed for their effect on TGF-β1-induced myofibroblast differentiation.

Tamoxifen is a SERM that has been used in the treatment of breast cancer; however, it has been reported to be useful in *in vitro* models of PD, by facilitating the release of TGF-β1 from fibroblasts, inhibiting the inflammatory response and reducing fibroblasts secretion and/or angiogenesis[152]. According to the presented results, tamoxifen significantly inhibited TGF-β1-induced myofibroblast differentiation in a concentration-dependent manner. Moreover, tamoxifen has also been shown to reduce the synthesis of TGF-β1 and TGF-β2 as well as fibroblast contraction and proliferation in *in vitro* studies[268–271].

Despite these *in vitro* data, the reports on the clinical efficacy of tamoxifen have been conflicting. One of the first studies using tamoxifen as a potential treatment for PD involved 36 patients with PD, which were treated with this drug over 3 months period. This study reported an improvement in penile pain (80%), reduction in plaque size (34%) and reduced penile deformity (35%), especially in patients presenting at early stages of the disease (duration <4 months)[221]. A further placebo-controlled study involving 25 patients showed no statistically significant differences between tamoxifen and placebo group in regards to the reduction of penile deformity, decrease penile pain and decrease in plaque

size[222]. Although the authors selected patients with no calcified plaques, the mean duration of PD was 20 months which may explain the discrepancy between the results reported by these authors and the previous study where the patients were in the early phase of PD.

Biagiotti & Cavallini (2001)[199] compared tamoxifen and acetyl-L-carnitine in randomised groups of PD patients in acute (15 patients, mean duration 5 weeks) and in initial chronic (33 patients, mean duration 6.5 months) phase of PD. It was reported that acetyl-L-carnitine significantly reduced pain, plaque size and penile curvature compared to tamoxifen in acute and early chronic PD, as well as less adverse effects than tamoxifen.

In addition, Kim *et al*. (2012)[200] compared the progression of tamoxifen treatment in patients with acute and chronic PD and reported that tamoxifen did not show any benefit in slowing the progression of PD. However, the authors did not specify the duration of the PD at the start of study.

A study by Park *et al.* (2016)[272] involving 109 patients who presented PD were treated with either potassium para-aminobenzoate daily or a combination therapy: tamoxifen and acetyl-L-carnitine twice daily in addition to tadalafil (PDE5i, once daily). The authors showed that penile pain, penile curvature and plaque size were improved; however, no statistical difference was observed between the two groups. Even though, statistically significant difference was not observed between groups, a better response rate was reported in patients treated with the combination therapy, and the number of patients who underwent surgical treatment was significantly higher in patients treated with potassium para-aminobenzoate daily only. Again, the authors did not specify the duration of the disease at the start of the study; but one can speculate that most of their patients were at the late stages since they had fibrotic plaques.

Overall, the evidence to support the efficacy of tamoxifen has been limited; therefore, the European Association of Urology (EAU) guidelines (2012)[273] and the American Urological Association (AUA) guidelines (2015)[274] do not recommend the use of tamoxifen clinically for PD.

Apart from the first study[221], all other clinical studies on tamoxifen utilised patients who were in late stages of the disease (i.e. duration longer than 12 months and/or with fibrotic plaque). The only clinical benefit with tamoxifen was observed in the first study and the authors commented "*patients with early disease (duration less than 4 months) responded better than patients with a longer history*"[221]. The data presented in this report, which assessed the effect of co-incubation of tamoxifen with TGF-β1 supports the notion that this compound may be beneficial only in the early, non-stable phase of PD, as inhibition of myofibroblast differentiation may halt the progression of fibrosis but may not necessarily reverse the already formed fibrosis. Further clinical studies would be required to test tamoxifen alone or in combination with PDE5 inhibitors[275] in patients who present with PD at early stages. Further clinical studies would also be required to test other SERMs such as raloxifene and idoxifene in PD as explained below.

Tamoxifen was used in this report as it is the prototypical SERM, well characterised and widely commercially available. The data generated in this thesis can be used in support of the use of other SERMs, with better efficacy and safety pharmacology profiles.

Raloxifene, for instance, acts by binding to the ERs, causing a change in their conformation which can lead to the activation or blocking of estrogen responsive genes[276]. This SERM significantly reduced α-SMA/DNA staining showing cytotoxicity only at higher concentrations in this report. This data is supported by the literature, as raloxifene has been shown to improve liver fibrosis in ovariectomised mice[277], as well as ameliorate diabetes-associated tubulointerstitial fibrosis in diabetic rats[90,278]. In addition, raloxifene reduced abnormal ECM protein turnover by pelvic fibroblasts by increasing TIMPs expression[279]. Furthermore, in skin fibroblasts, raloxifene inhibited the expression of MMP-9 suggesting a reduction in collagen degradation[280]. Another SERM, idoxifene has been shown to improve liver fibrosis in a rat model[112].

To the best of the author's knowledge, this is the first report to show expression of ERβ in cells isolated from non-PD TA tissue and PD plaque tissue. This is also the first time that raloxifene has been shown to significantly inhibit TGF-β1-

induced myofibroblast differentiation in a concentration-dependent manner in cells derived from human TA tissue. These data suggest that these SERMs may produce an anti-fibrotic effect in PD through interaction with ERβ and subsequent inhibition of myofibroblast differentiation.

Summary of Results:

The table below is a collation of the tables shown in the Introduction section (pages 16 and 40) corresponding to estrogen receptor expression and effect of estrogen receptor modulation, with the addition of the data acquired in this report in order to contextualise the results.

Table 4-2: Summary table of the expression of estrogen receptors and the effect of ligands in different tissues. Qualitative expression of estrogen receptors in different tissues. Highlighted in grey is the new data obtained in this study from cells established from tunica albuginea tissues. The relative mRNA expression of each receptor in each tissue is reported as a relative scale to the other receptors, according to *in vivo*, *in vitro* or human studies with +++ indicating the highest expression and + indicating the lowest expression of the receptors found to be present. Legend: red - promote fibrosis; green - impede fibrosis and black – anti-inflammatory.

Tissues		Estrogen receptors	
		ERα	ERβ
Lung	Expression	+[126,127]	+++[126,127]
	Effect of ligands	Estrogen[110]	
Kidney	Expression	+++[141]	+[141]
	Effect of ligands	Estrogen[92], tamoxifen[100]	
Liver	Expression	+++[111]	+[151]
	Effect of ligands	Estrogen[111], idoxifene[112]	
Heart	Expression	+[91]	+++[91]
	Effect of ligands	Estrogen[91]	
Skin	Expression	+++[223]	+[223]
	Effect of ligands	Estrogen[80]	
Penis	Expression	+[109,219]	+++[109,219]
	Effect of ligands	Estrogen[113]	
Penis (tunica albuginea)	Expression		+++
	Effect of ligands	Tamoxifen, raloxifene	

The data discussed above show that ERβ appears to be involved in PD, being a potential novel target for inhibition of myofibroblast differentiation in PD. It is interesting to note that the effect of estrogen and/or SERMs have an anti-fibrotic effect, not only in other fibroproliferative disorders, but also in PD.

4.4 Limitations of the study

Contradiction between mRNA and protein expression

As can be observed in the summary table below, there are some contradictory data within this report in terms of the mRNA and protein expression levels noted in non-PD TA samples and PD plaque samples with and without exposure to TGF-β1. α-SMA is the exception to the rule, as the effect of TGF-β1 on both populations is consistent in both mRNA and protein and there is a difference between non-PD TA cells and PD plaque-derived cells. This is to be expected as α-SMA is a hallmark of myofibroblast transformation and increased mRNA and protein levels are expected after TGF-β1 treatment. The differential response to TGF-β1 between the populations is likely due to the prior exposure to TGF-β1 in the PD plaque tissue, which may lead to partial resistance to TGF-β1.

In terms of the remaining targets, there are substantive differences between the protein and mRNA levels but mRNA levels often do not translate to protein expression levels[263] and inconsistencies between these two datasets are not unexpected.

Additionally, it could also be supposed that TGF-β1 treatment would have the effect of transforming the non-PD TA cells to PD plaque-derived like cells. However, there are differences between untreated and TGF-β1 treated samples and between non-PD TA derived and PD plaque-derived cells. This is likely because TGF-β1 treatment will not account for the numerous other differences between these two cell populations and that TGF-β1 treatment changes virtually all fibroblasts into myofibroblasts, and it has been shown that myofibroblasts constitute only approximately 20% of cells cultured from PD plaques[192].

Table 4-3: Summary table of mRNA and protein expression data. Protein data corresponds to ICW data. Legend: + present; - absent; ↓↑*different from matched untreated; ↓↑# significantly different from non-PD TA cells; ND Not determined.

	mRNA				Protein			
	TA	**PD**	**TA+ TGF**	**PD+TGF**	**TA**	**PD**	**TA+TGF**	**PD+TGF**
α-SMA	+	+	↑*	↑*	+	+	↑*	↑*
ADORA1	+	↑#	↓*	↓*	+	+	↑*	↑*
ADORA2A	-	-	ND	ND	ND	ND	ND	ND
ADORA2B	+	+	↓*	↓*	+	↑#	+	↑#
ADORA3	-	-	ND	ND	ND	ND	ND	ND
ERα	+	↓#	↓*	↓* ↓#	-	-	-	-
ERβ	+	↓#	↑*	↑* ↓#	+	+	+	+

Furthermore, it should also be noted that changes in expression both at the mRNA and protein levels are not a proxy for the importance of the role of the specific receptor in the disease. For the receptor to play a role, it simply needs to be shown to be present, preferably at both the mRNA and protein level, preferably in both non-PD TA cells and PD plaque-derived cells, which is true of ADORA1, ADORA2B and ERβ. These receptors were therefore taken forward to be tested using specific compound modulators in the α-SMA ICW assay.

The lack of tissue PCR data

The use of RNA extracted from tissue samples is preferable to the use of RNA extracted from cells derived from said tissues, as the natural molecular physiology of the tissues is preserved whether it is a healthy or diseased sample. However, the stability of RNA in a tissue sample is more vulnerable than in cells and in some tissues, it is extremely difficult to extract RNA as the disruption of tissue requires aggressive sample homogenisation.

Translational weakness of cellular assays

Even though the use of cell-based *in vitro* assays will provide a better understanding of the process under assessment and the effect of a compound in modulating said process, it is also a model of a process in a simplistic form to enable the adequate control of all variables. It is therefore, by its very nature, reductionist and cannot account for all the variables present in the human body. Furthermore, the use of the healthy and fibrotic tissue samples from the same patient would present a more accurate comparison; however, those samples were very difficult to obtain, due to ethical implications of removing penile tissue that would not otherwise be removed.

High concentrations of agonists/antagonists

In this study, the inhibitory effect of the adenosine receptor modulators and SERMs was assessed at relatively high concentrations that may not be physiologically relevant. For instance, tamoxifen was found to be effective in this report at inhibiting myofibroblast differentiation at approximately 18 µM (6.7 µg/ml). Obviously, such high concentrations would not be possible to reach when these compounds are administered systemically, as systemic oral application of tamoxifen at 20 mg/day in humans leads to serum concentrations of approximately 67 nM (25 ng/ml)[281]. However, as described in the Introduction, intralesional injection therapy of SERMs may be used in the treatment of PD, which greatly increases compound concentration at the effective site. It should be noted that in a recent animal study undertaken by our research group, systemic (intraperitoneal) daily administration of tamoxifen (5 mg/kg/day) has been shown to prevent fibrosis in an animal model of Peyronie's disease[275]. However, tissue concentrations of the drug were not measured at that study. Further *in vivo* animal studies will be needed to understand the tissue concentrations needed at the efficacious doses.

Effective medical treatments for PD are currently lacking and by understanding the myofibroblast differentiation process and the involvement of different receptors will shed light on potential novel therapeutic targets. Despite the limitations of this study, the data in this report support the hypothesis that

adenosine and/or estrogen receptors expression is involved in myofibroblast differentiation in PD and that these may be novel potential targets for anti-fibrotic therapies in this disease. In particular, agonism of ADORA2B and modulation of ERβ appear to be promising novel avenues for anti-fibrotic therapies in PD.

5 Conclusion

5.1 Establishment of primary cell cultures

Primary cell cultures were successfully established from non-PD TA tissue and PD plaque tissue, which were then characterised by investigating the expression and role of adenosine and estrogen receptors in myofibroblast differentiation in PD.

Both cell populations showed similar profiles in terms of the targets assessed and presented quantifiable protein and mRNA levels of ADORA1, ADORA2B and ERβ. TGF-β1 treatment had a variety of effects on these targets with no consistent effect on both mRNA and protein levels.

5.2 Modulation of adenosine and estrogen receptors

The ADORA2B agonist BAY 60-6583, as well as, the two SERMs tested, tamoxifen and raloxifene significantly inhibited TGF-β1-induced myofibroblast differentiation in a concentration-dependent manner in non-PD TA cells.

The data presented in this report has made original contributions to knowledge by demonstrating, for the first time, that:

- Human TA-derived cells express two of the four adenosine receptors (ADORA1 and ADORA2B), being a potential target for inhibition of myofibroblast differentiation in PD.
- An ADORA2B agonist inhibited TGF-β1-induced myofibroblast differentiation in a concentration-dependent manner.
- Human TA-derived cells express ERβ which also becomes a potential target for inhibition of myofibroblast differentiation in PD and possibly other fibrotic disorders.
- Two SERMs, tamoxifen and raloxifene, significantly inhibited TGF-β1-induced myofibroblast differentiation, with the results for raloxifene being novel.

- Translating to a clinical setting, the ADORA2B agonist and SERMs may be effective in the early, non-stable phase of PD as a non-surgical treatment option, particularly if applied in combination with other therapies.

5.3 General conclusion

In conclusion, this project achieved the stated aim and objectives by investigating adenosine and estrogen receptors expression in TA derived cells as well as the effect of modulating these receptors on TGF-β1-induced myofibroblast differentiation, leading to novel findings and potential novel therapeutic targets for Peyronie's disease.

These data, therefore, support the hypothesis that ADORA1, ADORA2B and ERβ expression is involved in myofibroblast differentiation in PD and may, therefore, be novel potential targets for anti-fibrotic therapies in this disease.

5.4 Further work

As future work, mRNA levels of the genes of interest from fresh tissues derived from normal TA and PD plaque should be assessed as this would yield physiologically relevant data on expression levels. A suggested method to perform this would be to snap freeze tissues using liquid nitrogen immediately after removing the tissue from the patient to avoid RNA degradation.

The function of the two adenosine receptors in TA cells should also be assessed by measuring the levels and changes in cAMP function, as well as, their ability to either inhibit or stimulate adenylate cyclase activity (the enzyme responsible for synthesising cAMP). This method could also be used to understand the effect of TGF-β1 and the source tissue on receptor function.

The screening of other adenosine receptor agonists or SERMs with improved structure-activity relationship (SAR) should also be investigated, which could provide new possibilities for the oral therapy of PD. In addition, it would also be interesting to measure the levels of other cytokines involved in the fibrotic process when cells are exposed to these receptor modulators.

As this thesis has described the methodology by which compounds can be assessed for their potential efficacy in inhibiting myofibroblast differentiation in the early, non-stable phase of PD, it would be interesting to test other oral compound treatments commonly used in PD that have not shown convincing evidence for their efficacy, such as vitamin E and potassium para-aminobenzoate.

Another interesting avenue of work would be to attempt to translate these data to other fibroproliferative diseases, particularly those that are poorly understood and show commonalities with PD, such as Dupuytren's contracture.

In the long term, data from this report could be used to design novel potential compounds with drug-like properties for the treatment of PD. This could be performed using a computational approach to develop SAR data on the active compounds and performing a hit expansion from there to find compounds with lower toxicity, higher activity and better drug-like characteristics.

To facilitate the above, the ICW assay could be further developed with the use of automation and miniaturization to 384-well plates. These improvements would facilitate the screening of increased numbers of compounds in the search for novel therapeutic compounds for PD.

Another interesting approach for the treatment of PD would be to test any future compounds that may show potential using the intralesional injection therapy, as this approach would minimise any side effects and higher concentrations of the compound would be injected directly into the penile plaque.

These compounds can then be taken down the drug discovery route through safety and pharmacology testing and into animal models, with the ultimate aim of developing a novel medical treatment for Peyronie's disease as well as other fibroproliferative disorders.

6 References

1. Wynn, T. A. & Ramalingam, T. R. Mechanisms of fibrosis: therapeutic translation for fibrotic disease. *Nat Med* **18,** 1028–1040 (2012).
2. Krenning, G., Zeisberg, E. M. & Kalluri, R. The origin of fibroblasts and mechanism of cardiac fibrosis. *J Cell Physiol* **225,** 631–637 (2010).
3. Hinz, B. Tissue stiffness, latent TGF-β1 activation, and mechanical signal transduction implications for the pathogenesis and treatment of fibrosis. *Curr Rheumatol Rep* **11,** 120–126 (2009).
4. Bollong, M. J. *et al.* Small molecule-mediated inhibition of myofibroblast transdifferentiation for the treatment of fibrosis. *Proc Natl Acad Sci* **114,** 4679–4684 (2017).
5. Kisseleva, T. & Brenner, D. A. Mechanisms of fibrogenesis. *Exp Biol Med* **233,** 109–122 (2008).
6. Shirol, P. D. & Shirol, D. D. Myofibroblasts in health and disease. *Int J Oral Maxillofac Pathol* **3,** 23–27 (2012).
7. Wynn, T. A. Common and unique mechanisms regulate fibrosis in various fibroproliferative diseases. *J Clin Invest* **117,** 524–529 (2007).
8. Lee, C. G. *et al.* Early growth response gene 1-mediated apoptosis is essential for transforming growth factor beta 1-induced pulmonary fibrosis. *J Exp Med* **200,** 377–389 (2004).
9. Malmström, J. *et al.* Transforming growth factor-beta 1 specifically induce proteins involved in the myofibroblast contractile apparatus. *Mol Cell Proteomics* **3,** 466–477 (2004).
10. Schwarz, F. *et al.* Soft tissue fibroblasts from well healing and chronic human wounds show different rates of myofibroblasts in vitro. *Mol Biol Rep* **40,** 1721–1733 (2013).
11. Vuillemenot, B. R., Rodriguez, J. F. & Hoyle, G. W. Lymphoid tissue and emphysema in the lungs of transgenic mice inducibly expressing tumor necrosis factor-alpha. *Am J Respir Cell Mol Biol* **30,** 438–448 (2004).
12. Yoshida, M. *et al.* A histological distinctive interstitial pneumonia induced by overexpression of the interleukin 6, transforming growth factor beta 1, or platelet-derived growth factor B gene. *Proc Natl Acad Sci* **92,** 9570–9574 (1995).
13. Kolb, M., Margetts, P. J., Anthony, D. C., Pitossi, F. & Gauldie, J. Transient expression of IL-1beta induces acute lung injury and chronic repair leading to pulmonary fibrosis. *J Clin Invest* **107,** 1529–1536 (2001).
14. Ask, K., Martin, G. E. M., Kolb, M. & Gauldie, J. Targeting genes for treatment in idiopathic pulmonary fibrosis: challenges and opportunities, promises and pitfalls. *Proc Am Thorac Soc* **3,** 389–393 (2006).
15. Lee, C. G. *et al.* Interleukin-13 induces tissue fibrosis by selectively stimulating and activating transforming growth factor β1. *J Exp Med* **194,** 809–821 (2001).

16. Bonniaud, P. *et al.* Adenoviral gene transfer of connective tissue growth factor in the lung induces transient fibrosis. *Am J Respir Crit Care Med* **168,** 770–778 (2003).

17. Ma, B., Kang, Q., Qin, L., Cui, L. & Pei, C. TGF-β2 induces transdifferentiation and fibrosis in human lens epithelial cells via regulating gremlin and CTGF. *Biochem Biophys Res Commun* **447,** 689–695 (2014).

18. Shi-Wen, X. *et al.* Endothelial-1 promotes myofibroblast induction through the ETA receptor via a rac/phosphoinositide 3-kinase/Akt-dependent pathway and is essential for the enhanced contractile phenotype of fibrotic fibroblasts. *Mol Biol Cell* **15,** 2707–2719 (2004).

19. Langdon, C., Kerr, C., Tong, L. & Richards, C. D. Oncostatin M regulates eotaxin expression in fibroblasts and eosinophilic inflammation in C57BL/6 mice. *J Immunol* **170,** 548–555 (2003).

20. Ramirez-Montagut, T. *et al.* FAP alpha, a surface peptidase expressed during wound healing, is a tumor suppressor. *Oncogene* **23,** 5435–5446 (2004).

21. Kalluri, R. & Zeisberg, M. Fibroblasts in cancer. *Nat Rev Cancer* **6,** 392–401 (2006).

22. Li, B. & Wang, J. Fibroblasts and myofibroblasts in wound healing: force generation and measurement. *J Tissue Viability* **20,** 108–120 (2011).

23. Duffield, J. S. Cellular and molecular mechanisms in kidney fibrosis. *J Clin Invest* **124,** 2299–2306 (2014).

24. Sampson, N., Berger, P. & Zenzmaier, C. Therapeutic targeting of redox signaling in myofibroblast differentiation and age-related fibrotic disease. *Oxid Med Cell Longev* **2012,** 1–15 (2012).

25. McAnulty, R. J. Fibroblasts and myofibroblasts: their source, function and role in disease. *Int J Biochem Cell Biol* **39,** 666–671 (2007).

26. Falke, L. L., Gholizadeh, S., Goldschmeding, R., Kok, R. J. & Nguyen, T. Q. Diverse origins of the myofibroblast - implications for kidney fibrosis. *Nat Rev Nephrol* **11,** 233–244 (2015).

27. Phan, S. H. Biology of fibroblasts and myofibroblasts. *Proc Am Thorac Soc* **5,** 334–337 (2008).

28. Hinz, B. *et al.* The myofibroblast: one function, multiple origins. *Am J Pathol* **170,** 1807–1816 (2007).

29. Micallef, L. *et al.* The myofibroblast, multiple origins for major roles in normal and pathological tissue repair. *Fibrogenesis Tissue Repair* **5,** 1–5 (2012).

30. Yang, X., Chen, B., Liu, T. & Chen, X. Reversal of myofibroblast differentiation: A review. *Eur J Pharmacol* **734,** 83–90 (2014).

31. Zavadil, J. & Böttinger, E. P. TGF-β and epithelial-to-mesenchymal transitions. *Oncogene* **24,** 5764–5774 (2005).

32. Duarte, S., Baber, J., Fujii, T. & Coito, A. J. Matrix metalloproteinases in

liver injury, repair and fibrosis. *Matrix Biol* **44,** 147–156 (2015).

33. Siani, A. & Tirelli, N. Myofibroblast differentiation: main features, biomedical relevance and the role of reactive oxygen species. *Antioxid Redox Signal* **21,** 768–785 (2014).
34. Giannandrea, M. & Parks, W. C. Diverse functions of matrix metalloproteinases during fibrosis. *Dis Model Mech* **7,** 193–203 (2014).
35. Iwanami, H., Ishizaki, M., Fukuda, Y. & Takahashi, H. Expression of matrix metalloproteinases (MMP)-12 by myofibroblasts during alkali-burned corneal wound healing. *Curr Eye Res* **34,** 207–214 (2009).
36. Howard, E. W. *et al.* MMP-2 expression by fibroblasts is suppressed by the myofibroblast phenotype. *Exp Cell Res* **318,** 1542–1553 (2012).
37. Elmore, S. Apoptosis: a review of programmed cell death. *Toxicol Pathol* **35,** 495–516 (2007).
38. Lawen, A. Apoptosis-an introduction. *BioEssays* **25,** 888–896 (2003).
39. Guicciardi, M. E. & Gores, G. J. Apoptosis: a mechanism of acute and chronic liver injury. *Gut* **54,** 1024–1033 (2005).
40. Thannickal, V. J. & Horowitz, J. C. Evolving concepts of apoptosis in idiopathic pulmonary fibrosis. *Proc Am Thorac Soc* **3,** 350–356 (2006).
41. Kulasekaran, P. *et al.* Endothelin-1 and transforming growth factor-β1 independently induce fibroblast resistance to apoptosis via AKT activation. *Am J Respir Cell Mol Biol* **41,** 484–493 (2009).
42. Zhang, H. Y. & Phan, S. H. Inhibition of myofibroblast apoptosis by transforming growth factor β1. *Am J Respir Cell Mol Biol* **21,** 658–665 (1999).
43. Jelaska, a & Korn, J. H. Role of apoptosis and transforming growth factor beta1 in fibroblast selection and activation in systemic sclerosis. *Arthritis Rheum* **43,** 2230–2239 (2000).
44. Huang, S. K. *et al.* Histone modifications are responsible for decreased Fas expression and apoptosis resistance in fibrotic lung fibroblasts. *Cell Death Dis* **4,** e621 (2013).
45. Frankel, S. K. *et al.* TNF-alpha sensitizes normal and fibrotic human lung fibroblasts to Fas-induced apoptosis. *Am J Respir Cell Mol Biol* **34,** 293–304 (2006).
46. Moodley, Y. P. *et al.* Comparison of the morphological and biochemical changes in normal human lung fibroblasts and fibroblasts derived from lungs of patients with idiopathic pulmonary fibrosis during FasL-induced apoptosis. *J Pathol* **202,** 486–495 (2004).
47. Bühling, F. *et al.* Altered expression of membrane-bound and soluble CD95/Fas contributes to the resistance of fibrotic lung fibroblasts to FasL induced apoptosis. *Respir Res* **6,** 1–9 (2005).
48. Moodley, Y. P. *et al.* Inverse effects of interleukin-6 on apoptosis of fibroblasts from pulmonary fibrosis and normal lungs. *Am J Respir Cell Mol*

Biol **29,** 490–498 (2003).

49. Loreto, C. *et al.* Tumor necrosis factor-related apoptosis-inducing ligand (TRAIL) and its death receptor (DR5) in Peyronie's disease. A biomolecular study of apoptosis activation. *J Sex Med* **8,** 109–115 (2011).
50. Loreto, C. *et al.* The Role of Intrinsic Pathway in Apoptosis Activation and Progression in Peyronie's Disease. *Biomed Res Int* **2014,** 1–10 (2014).
51. Zorba, O. U. *et al.* Comparison of apoptotic gene expression profiles between Peyronie's disease plaque and tunica albuginea. *Adv Clin Exp Med* **21,** 607–614 (2012).
52. Chan, E. S. L. *et al.* Adenosine A2A receptors in diffuse dermal fibrosis. *Arthritis Rheum* **54,** 2632–2642 (2006).
53. Cronstein, B. N. Adenosine receptors and fibrosis: a translational review. *F1000 Biol Rep* **3,** 1–6 (2011).
54. Chen, J.-F., Eltzschig, H. K. & Fredholm, B. B. Adenosine receptors as drug targets - what are the challenges? *Nat Rev Drug Discov* **12,** 265–286 (2013).
55. Karmouty-Quintana, H., Xia, Y. & Blackburn, M. R. Adenosine signaling during acute and chronic disease states. *J Mol Med* **91,** 173–181 (2013).
56. Grenz, A. *et al.* The reno-vascular A2B adenosine receptor protects the kidney from ischemia. *PLoS Med* **5,** 968–986 (2008).
57. Zhou, Y. *et al.* Distinct roles for the A2B adenosine receptor in acute and chronic stages of bleomycin-induced lung injury. *J Immunol* **186,** 1097–1106 (2011).
58. Schingnitz, U. *et al.* Signaling through the A2B adenosine receptor dampens endotoxin-induced acute lung injury. *J Immunol* **184,** 5271–5279 (2010).
59. Eckle, T. *et al.* Cardioprotection by Ecto-5'-Nucleotidase (CD73) and A2B adenosine receptors. *Circulation* **115,** 1581–1590 (2007).
60. Day, Y.-J. *et al.* Protection from ischemic liver injury by activation of A2A adenosine receptors during reperfusion: inhibition of chemokine induction. *Am J Physiol Gastrointest Liver Physiol* **286,** G285–G293 (2004).
61. Toldo, S. *et al.* GS-6201, a selective blocker of the A2B adenosine receptor, attenuates cardiac remodeling after acute myocardial infarction in the mouse. *J Pharmacol Exp Ther* **343,** 587–595 (2012).
62. Fernández, P. *et al.* Pharmacological blockade of A2A receptors prevents dermal fibrosis in a model of elevated tissue adenosine. *Am J Pathol* **172,** 1675–1682 (2008).
63. Chan, E. S. L. *et al.* Adenosine A(2A) receptors play a role in the pathogenesis of hepatic cirrhosis. *Br J Pharmacol* **148,** 1144–1155 (2006).
64. Sun, C.-X. *et al.* Role of A2B adenosine receptor signaling in adenosine-dependent pulmonary inflammation and injury. *J Clin Invest* **116,** 2173–2182 (2006).

65. Chunn, J. L. *et al.* Adenosine-dependent pulmonary fibrosis in adenosine deaminase-deficient mice. *J Immunol* **175,** 1937–1946 (2005).

66. Wen, J. *et al.* Increased adenosine contributes to penile fibrosis, a dangerous feature of priapism, via A2B adenosine receptor signaling. *FASEB J* **24,** 740–749 (2010).

67. Mi, T. *et al.* Excess adenosine in murine penile erectile tissues contributes to priapism via A2B adenosine receptor signaling. *J Clin Invest* **118,** 1491–1501 (2008).

68. Dai, Y. *et al.* A2B adenosine receptor-mediated induction of IL-6 promotes CKD. *J Am Soc Nephrol* **22,** 890–901 (2011).

69. Roberts, V. S., Cowan, P. J., Alexander, S. I., Robson, S. C. & Dwyer, K. M. The role of adenosine receptors A2A and A2B signaling in renal fibrosis. *Kidney Int* **86,** 685–692 (2014).

70. Wakeno, M. *et al.* Long-term stimulation of adenosine A2B receptors begun after myocardial infarction prevents cardiac remodeling in rats. *Circulation* **114,** 1923–1932 (2006).

71. Dubey, R. K., Gillespie, D. G. & Jackson, E. K. Adenosine Inhibits Collagen and Protein Synthesis in Cardiac Fibroblasts: Role of A2B Receptors. *Hypertension* **31,** 943–948 (1998).

72. Zhong, H., Belardinelli, L., Maa, T. & Zeng, D. Synergy between A2B adenosine receptors and hypoxia in activating human lung fibroblasts. *Am J Respir Cell Mol Biol* **32,** 2–8 (2005).

73. Sun, C.-X. *et al.* A protective role for the A1 adenosine receptor in adenosine-dependent pulmonary injury. *J Clin Invest* **115,** 35–43 (2005).

74. Sohail, M. *et al.* Adenosine induces loss of actin stress fibers and inhibits contraction in hepatic stellate cells via Rho inhibition. *Hepatology* **49,** 185–194 (2009).

75. Chan, E. & Cronstein, B. Adenosine in fibrosis. *Mod Rheumatol* **20,** 114–122 (2010).

76. Chen, Y. F. *et al.* Activation of A2aR attenuates bleomycin-induced pulmonary fibrosis via the SDF-1/CXCR4 axis-related pathway. *Am J Transl Res* **9,** 4125–4136 (2017).

77. Garcia, G. E., Truong, L. D., Chen, J., Johnson, R. J. & Feng, L. Adenosine A(2A) receptor activation prevents progressive kidney fibrosis in a model of immune-associated chronic inflammation. *Kidney Int* **80,** 378–388 (2011).

78. Vecchio, E. A., White, P. J. & May, L. T. Targeting adenosine receptors for the treatment of cardiac fibrosis. *Front Pharmacol* **8,** 1–7 (2017).

79. Perez-Aso, M., Fernandez, P., Mediero, A., Chan, E. S. & Cronstein, B. N. Adenosine 2A receptor promotes collagen production by human fibroblasts via pathways involving cyclic AMP and AKT but independent of Smad2/3. *FASEB J* **28,** 802–812 (2014).

80. Stevenson, S., Nelson, L. D., Sharpe, D. T. & Thornton, M. J. 17 β-estradiol

regulates the secretion of TGF-β by cultured human dermal fibroblasts. *J Biomater* **19,** 1097–1109 (2008).

81. Denger, S., Reid, G., Brand, H., Kos, M. & Gannon, F. Tissue-specific expression of human ERα and ERβ in the male. *Mol Cell Endocrinol* **178,** 155–160 (2001).

82. Reid, G., Denger, S., Kos, M. & Gannon, F. Human estrogen receptor-alpha: regulation by synthesis, modification and degradation. *Cell Mol Life Sci* **59,** 821–831 (2002).

83. Deroo, B. J. & Korach, K. S. Estrogen receptors and human disease. *J Clin Invest* **116,** 561–570 (2006).

84. Hall, G. & Phillips, T. J. Estrogen and skin: the effects of estrogen, menopause, and hormone replacement therapy on the skin. *J Am Acad Dermatol* **53,** 555–568 (2005).

85. Thornton, M. J. The biological actions of estrogens on skin. *Exp Dermatol* **11,** 487–502 (2002).

86. Martinkovich, S., Shah, D., Planey, S. L. & Arnott, J. A. Selective estrogen receptor modulators: tissue specificity and clinical utility. *Clin Interv Aging* **9,** 1437–52 (2014).

87. Heldring, N. *et al.* Estrogen receptors: how do they signal and what are their targets. *Physiol Rev* **87,** 905–931 (2007).

88. Lewis, J. S. & Jordan, V. C. Selective estrogen receptor modulators (SERMs): Mechanisms of anticarcinogenesis and drug resistance. *Mutat Res* **591,** 247–263 (2005).

89. Jordan, V. C. Chemoprevention of breast cancer with selective oestrogen-receptor modulators. *Nat Rev Cancer* **7,** 46–53 (2007).

90. Melamed, M. L. *et al.* Raloxifene, a selective estrogen receptor modulator, is renoprotective: a post-hoc analysis. *Kidney Int* **79,** 241–249 (2011).

91. Pedram, A., Razandi, M., O'Mahony, F., Lubahn, D. & Levin, E. R. Estrogen Receptor-β Prevents Cardiac Fibrosis. *Mol Endocrinol* **24,** 2152–2165 (2010).

92. Dixon, A. & Maric, C. 17β-Estradiol attenuates diabetic kidney disease by regulating extracellular matrix and transforming growth factor-beta protein expression and signaling. *Am J Physiol Renal Physiol* **293,** F1678–F1690 (2007).

93. Morani, A. *et al.* Lung dysfunction causes systemic hypoxia in estrogen receptor beta knockout (ERbeta-/-) mice. *PNAS* **103,** 7165–7169 (2006).

94. Smyk, D. S. *et al.* Sex differences associated with primary biliary cirrhosis. *Clin Dev Immunol* **2012,** 1–11 (2012).

95. Ashcroft, G. S., Greenwell-Wild, T., Horan, M. A., Wahl, S. M. & Ferguson, M. W. Topical estrogen accelerates cutaneous wound healing in aged humans associated with an altered inflammatory response. *Am J Pathol* **155,** 1137–1146 (1999).

96. Merlo, S., Frasca, G., Canonico, P. L. & Sortino, M. A. Differential involvement of estrogen receptor alpha and estrogen receptor beta in the healing promoting effect of estrogen in human keratinocytes. *J Endocrinol* **200,** 189–197 (2009).

97. Soldano, S. *et al.* Effects of estrogens on extracellular matrix synthesis in cultures of human normal and scleroderma skin fibroblasts. *Ann N Y Acad Sci* **1193,** 25–29 (2010).

98. Novotny, M. *et al.* ER-α agonist induces conversion of fibroblasts into myofibroblasts, while ER-β agonist increases ECM production and wound tensile strength of healing skin wounds in ovariectomised rats. *Exp Dermatol* **20,** 703–708 (2011).

99. Siqueira, O. H. *et al.* Tamoxifen decreases the myofibroblast count in the healing bile duct tissue of pigs. *Clinics* **68,** 101–106 (2013).

100. Delle, H. *et al.* Antifibrotic effect of tamoxifen in a model of progressive renal disease. *J Am Soc Nephrol* **23,** 37–48 (2012).

101. Greene, R. R., Burrill, M. W. & Ivy, A. C. Experimental Intersexuality: Modification of sexual development of the white rat with a synthetic estrogen. *Proc Soc Exp Biol Med* **41,** 169–170 (1939).

102. Stillman, R. J. In utero exposure to diethylstilbestrol: Adverse effects on the reproductive tract and reproductive performance in male and female offspring. *Am J Obs Gynecol* **142,** 905–921 (1982).

103. North, K. & Golding, J. A maternal vegetarian diet in pregnancy is associated with hypospadias. *BJU Int* **85,** 107–113 (2000).

104. Iguchi, T., Irisawa, S., Uesugi, Y., Kusunoki, S. & Takasugi, N. Abnormal development of the os penis in male mice treated neonatally with tamoxifen. *Acta Anat* **139,** 201–208 (1990).

105. Deveci, E., Onen, A., Tacar, O. & Yildirim, A. The effect of tamoxifen on the neonatal development of rat glans penis. *Clin Exp Obs Gynecol* **24,** 237–239 (1997).

106. Goyal, H. O. *et al.* Estrogen receptor-α mediates estrogen-inducible abnormalities in the developing penis. *Reproduction* **133,** 1057–1067 (2007).

107. Carreau, S., Genissel, C., Bilinska, B. & Levallet, J. Sources of oestrogen in the testis and reproductive tract of the male. *Int J Androl* **22,** 211–223 (1999).

108. Jesmin, S. *et al.* Evidence for a potential role of estrogen in the penis: detection of estrogen receptor-alpha and -beta messenger ribonucleic acid and protein. *Endocrinology* **143,** 4764–4774 (2002).

109. Dietrich, W., Haitel, a, Huber, J. C. & Reiter, W. J. Expression of estrogen receptors in human corpus cavernosum and male urethra. *J Histochem Cytochem* **52,** 355–360 (2004).

110. Voltz, J. W. *et al.* Male sex hormones exacerbate lung function impairment after bleomycin-induced pulmonary fibrosis. *Am J Respir Cell Mol Biol* **39,**

45–52 (2008).

111. Xu, J.-W. *et al.* Effects of estradiol on liver estrogen receptor-α and its mRNA expression in hepatic fibrosis in rats. *World J Gastroenterol* **10,** 250–254 (2004).

112. Zhou, Y. *et al.* Inhibitory effects of idoxifene on hepatic fibrosis in rats. *Acta Pharmacol Sin* **26,** 581–586 (2005).

113. Jiang, H. H.-S. *et al.* Estradiol attenuates the TGF-β1-induced conversion of primary TAFs into myofibroblasts and inhibits collagen production and myofibroblast contraction by modulating the Smad and Rho/ROCK signaling pathways. *Int J Mol Med* **36,** 801–807 (2015).

114. Datta, A., Scotton, C. J. & Chambers, R. C. Novel therapeutic approaches for pulmonary fibrosis. *Br J Pharmacol* **163,** 141–172 (2011).

115. Gu, L., Zhu, Y., Guo, Z., Xu, X. & Xu, W. Effect of IFN-gamma and dexamethasone on TGFb1-induced human fetal lung fibroblast-myofibroblast differentiation. *Acta Pharmacol Sin* **25,** 1479–1488 (2004).

116. Chua, F., Gauldie, J. & Laurent, G. J. Pulmonary fibrosis: searching for model answers. *Am J Respir Cell Mol Biol* **33,** 9–13 (2005).

117. Spagnolo, P., Wells, A. U. & Collard, H. R. Pharmacological treatment of idiopathic pulmonary fibrosis: an update. *Drug Discov Today* **20,** 514–524 (2015).

118. Spagnolo, P., Maher, T. M. & Richeldi, L. Idiopathic pulmonary fibrosis: Recent advances on pharmacological therapy. *Pharmacol Ther* **152,** 18–27 (2015).

119. Navaratnam, V. *et al.* The rising incidence of idiopathic pulmonary fibrosis in the UK. *Thorax* **66,** 462–467 (2011).

120. Raghu, G. *et al.* An Official ATS/ERS/JRS/ALAT Statement: Idiopathic pulmonary fibrosis: Evidence-based guidelines for diagnosis and management. *Am J Respir Crit Care Med* **183,** 788–824 (2011).

121. Della Latta, V., Cabiati, M., Rocchiccioli, S., Del Ry, S. & Morales, M.-A. The role of the adenosinergic system in lung fibrosis. *Pharmacol Res* **76,** 182–189 (2013).

122. Chunn, J. L. *et al.* Partially adenosine deaminase-deficient mice develop pulmonary fibrosis in association with adenosine elevations. *Am J Physiol Lung Cell Mol Physiol* **290,** L579–L587 (2006).

123. Zhou, Y., Murthy, J. N., Zeng, D., Belardinelli, L. & Blackburn, M. R. Alterations in adenosine metabolism and signaling in patients with chronic obstructive pulmonary disease and idiopathic pulmonary fibrosis. *PLoS One* **5,** e9224 (2010).

124. Volmer, J. B., Thompson, L. F. & Blackburn, M. R. Ecto-5'-Nucleotidase (CD73)-mediated adenosine production is tissue protective in a model of bleomycin-induced lung injury. *J Immunol* **176,** 4449–4458 (2006).

125. Montesinos, M. C. *et al.* Wound healing is accelerated by agonists of adenosine A2 (G-alpha-s-linked) receptors. *J Exp Med* **186,** 1615–1620

(1997).

126. Stabile, L. P. *et al.* Human non-small cell lung tumors and cells derived from normal lung express both estrogen receptor alpha and beta and show biological responses to estrogen. *Cancer Res* **62,** 2141–2150 (2002).

127. Mollerup, S., Jørgensen, K., Berge, G. & Haugen, A. Expression of estrogen receptors [alpha] and [beta] in human lung tissue and cell lines. *Lung Cancer* **37,** 153–159 (2002).

128. Card, J. W. & Zeldin, D. C. Hormonal influences on lung function and response to environmental agents: lessons from animal models of respiratory disease. *Proc Am Thorac Soc* **6,** 588–595 (2009).

129. Gharaee-kermani, M., Hatano, K., Nozaki, Y. & Phan, S. H. Gender-based differences in bleomycin-induced pulmonary fibrosis. *Am J Pathol* **166,** 1593–1606 (2005).

130. Koc, M., Polat, P. & Suma, S. Effects of tamoxifen on pulmonary fibrosis after cobalt-60 radiotherapy in breast cancer patients. *Radiother Oncol* **64,** 171–175 (2002).

131. Bese, N. S. *et al.* The effects of tamoxifen on radiation-induced pulmonary fibrosis in Wistar albino rats: Results of an experimental study. *The Breast* **15,** 455–459 (2006).

132. Nandhini, T. Molecular mechanism in renal fibrosis - a review. *J Pharm Sci Res* **6,** 334–337 (2014).

133. Cho, M. H. Renal fibrosis. *Korean J Pediatr* **53,** 735–740 (2010).

134. Meng, X.-M., Tang, P. M.-K., Li, J. & Lan, H. Y. TGF-β/Smad signaling in renal fibrosis. *Front Physiol* **6,** 1–8 (2015).

135. Hamer, R. A. The burden of chronic kidney disease. *BMJ* **332,** 563–564 (2006).

136. Kerr, M., Bray, B., Medcalf, J., O'Donoghue, D. J. & Matthews, B. Estimating the financial cost of chronic kidney disease to the NHS in England. *Nephrol Dial Transplant* **27,** 73–80 (2012).

137. Vallon, V., Mühlbauer, B. & Osswald, H. Adenosine and kidney function. *Physiol Rev* **86,** 901–940 (2006).

138. Vitzthum, H., Weiss, B., Bachleitner, W., Krämer, B. K. & Kurtz, A. Gene expression of adenosine receptors along the nephron. *Kidney Int* **65,** 1180–1190 (2004).

139. Zhang, W. *et al.* Elevated CD73-mediated increased renal adenosine signaling via A2B adenosine receptor contributes to chronic hypertension. *Circ Res* **112,** 1466–1478 (2013).

140. Xiao, H. *et al.* Adenosine A2A receptor: a target for regulating renal interstitial fibrosis in obstructive nephropathy. *PLoS One* **8,** e60173 (2013).

141. Potier, M. *et al.* Expression and regulation of estrogen receptors in mesangial cells: influence on matrix metalloproteinase-9. *J Am Soc Nephrol* **12,** 241–251 (2001).

142. Guyot, C. *et al.* Hepatic fibrosis and cirrhosis: The (myo)fibroblastic cell subpopulations involved. *Int J Biochem Cell Biol* **38,** 135–151 (2006).

143. Chen, R.-J., Wu, H.-H. & Wang, Y.-J. Strategies to prevent and reverse liver fibrosis in humans and laboratory animals. *Arch Toxicol* **89,** 1727–1750 (2015).

144. Martínez, S. M., Crespo, G., Navasa, M. & Forns, X. Noninvasive assessment of liver fibrosis. *Hepatology* **53,** 325–335 (2011).

145. Kumar, V. & Mahato, R. I. Delivery and targeting of miRNAs for treating liver fibrosis. *Pharm Res* **32,** 341–361 (2015).

146. Gressner, O. A., Weiskirchen, R. & Gressner, A. M. Evolving concepts of liver fibrogenesis provide new diagnostic and therapeutic options. *Comp Hepatol* **6,** 1–13 (2007).

147. Fallatah, H. I. Noninvasive biomarkers of liver fibrosis: an overview. *Adv Hepatol* **2014,** 1–15 (2014).

148. Hashmi, A. Z. *et al.* Adenosine inhibits cytosolic calcium signals and chemotaxis in hepatic stellate cells. *Am J Physiol Gastrointest Liver Physiol* **292,** G395–G401 (2007).

149. Peng, Z. *et al.* Ecto-5'-nucleotidase (CD73) -mediated extracellular adenosine production plays a critical role in hepatic fibrosis. *FASEB J* **22,** 2263–2272 (2008).

150. Feoktistov, I., Biaggioni, I. & Cronstein, B. N. Adenosine receptors in wound healing, fibrosis and angiogenesis. *Handb Exp Pharmacol* **193,** 383–397 (2009).

151. Zhou, Y. *et al.* Hepatic stellate cells contain the functional estrogen receptor β but not the estrogen receptor α in male and female rats. *Biochem Biophys Res Commun* **286,** 1059–1065 (2001).

152. Hellstrom, W. J. G. Medical management of Peyronie's disease. *J Androl* **30,** 397–405 (2009).

153. Langston, J. P. & Carson, C. C. Peyronie's disease: review and recent advances. *Maturitas* **78,** 341–343 (2014).

154. Garaffa, G., Trost, L. W., Serefoglu, E. C., Ralph, D. & Hellstrom, W. J. G. Understanding the course of Peyronie's disease. *Int J Clin Pract* **67,** 781–788 (2013).

155. Fitkin, J. & Ho, G. T. Peyronie's disease: current management. *Am Fam Physician* **60,** 549–552 (1999).

156. Lindsay, M. *et al.* The incidence of Peyronie's disease in Rochester, Minnesota, 1950 through 1984. *J Urol* **146,** 1007–1009 (1991).

157. Sommer, F. *et al.* Epidemiology of Peyronie's disease. *Int J Impot Res* **14,** 379–383 (2002).

158. Mulhall, J. *et al.* Subjective and objective analysis of the prevalence of peyronie's disease in a population of men presenting for prostate cancer screening. *J Urol* **171,** 2350–2353 (2004).

159. Arafa, M., Eid, H., El-Badry, A., Ezz-Eldine, K. & Shamloul, R. The prevalence of Peyronie's disease in diabetic patients with erectile dysfunction. *Int J Impot Res* **19,** 213–217 (2007).

160. Dibenedetti, D. B., Nguyen, D., Zografos, L., Ziemiecki, R. & Zhou, X. A population-based study of Peyronie's disease: prevalence and treatment patterns in the United States. *Adv Urol* **2011,** 1–9 (2011).

161. Hellstrom, W. J. G. History, epidemiology, and clinical presentation of Peyronie's disease. *Int J Impot Res* **15,** S91–S92 (2003).

162. Paulis, G., Romano, G. & Paulis, A. Prevalence, psychological impact, and risk factors of erectile dysfunction in patients with Peyronie's disease: a retrospective analysis of 309 cases. *Res Reports Urol* **8,** 95–103 (2016).

163. Kadioglu, A. *et al.* Factors affecting the degree of penile deformity in Peyronie disease: an analysis of 1001 patients. *J Androl* **32,** 502–508 (2011).

164. Gholami, S. S., Gonzalez-cadavid, N. F., Lin, C.-S., Rajfer, J. & Lue, T. F. Peyronie's disease: a review. *J Urol* **169,** 1234–1241 (2003).

165. Hsu, Y.-C. & Huang, S.-T. Peyronie's disease: etiology, diagnosis, and treatment. *JTUA* **19,** 5–11 (2008).

166. Lopez, J. & Jarow, J. Penile vascular evaluation of men with Peyronie's disease. *J Urol* **149,** 53–55 (1993).

167. Tefekli, A., Kandirali, E., Erol, B., Tunc, M. & Kadioglu, A. Peyronie's disease: a silent consequence of diabetes mellitus. *Asian J Androl* **8,** 75–79 (2006).

168. Mynderse, L. A. & Monga, M. Oral therapy for Peyronie's disease. *Int J Impot Res* **14,** 340–344 (2002).

169. Nugteren, H. M., Nijman, J. M., Jong, I. J. & van Driel, M. F. The association between Peyronie's and Dupuytren's disease. *Int J Impot Res* **23,** 142–145 (2011).

170. Lyles, K. W. *et al.* Peyronie's disease is associated with Paget's disease of bone. *J Bone Miner Res* **12,** 929–934 (1997).

171. Nachtsheim, D. A. & Rearden, A. Peyronie's Disease is associated with an HLA Class II antigen, HLA-DQ5, implying an autoimmune etiology. *J Urol* **156,** 1330–1334 (1996).

172. Qian, A., Meals, R. A., Rajfer, J. & Gonzalez-Cadavid, N. F. Comparison of gene expression profiles between Peyronie's disease and Dupuytren's contracture. *Urology* **64,** 399–404 (2004).

173. Singer, F. R. *et al.* Paget's disease of bone: an endrocrine society clinical practice guideline. *J Clin Endocrinol Metab* **99,** 4408–4422 (2014).

174. Schiavino, D. *et al.* Immunologic findings in Peyronie's disease: a controlled study. *Urology* **50,** 764–768 (1997).

175. Hellstrom, W. J. G. & Bivalacqua, T. J. Peyronie's disease: etiology, medical, and surgical therapy. *J Androl* **21,** 347–354 (2000).

176. Bivalacqua, T. J., Purohit, S. K. & Hellstrom, W. J. G. Peyronie's disease: advances in basic science and pathophysiology. *Curr Urol Rep* **1,** 297–301 (2000).

177. El-Sakka, A. I., Salabas, E., Dincer, M. & Kadioglu, A. The pathophysiology of Peyronie's disease. *Arab J Urol* **11,** 272–277 (2013).

178. Moreland, R. B. & Nehra, A. Pathophysiology of Peyronie's disease. *Int J Impot Res* **14,** 406–410 (2002).

179. Gonzalez-Cadavid, N. F. *et al.* Gene expression in Peyronie's disease. *Int J Impot Res* **14,** 361–374 (2002).

180. Jarow, J. P. & Lowe, F. C. Penile trauma: an etiologic factor in Peyronie's disease and erectile dysfunction. *J Urol* **158,** 1388–1390 (1997).

181. Smith, C. J., McMahon, C. & Shabsigh, R. Peyronie's disease: the epidemiology, aetiology and clinical evaluation of deformity. *BJU Int* **95,** 729–732 (2005).

182. Ghosh, A. K. & Vaughan, D. E. PAI-1 in tissue fibrosis. *J Cell Physiol* **277,** 493–507 (2012).

183. Somers, K. D. & Dawson, D. M. Fibrin deposition in Peyronie's disease plaque. *J Urol* **157,** 311–315 (1997).

184. El-Sakka, A., Hassoba, H., Pillarisetty, R., Dahiya, R. & Lue, T. Peyronie's disease is associated with an increase in transforming growth factor-beta protein expression. *J Urol* **158,** 1391–1394 (1997).

185. El-Sakka, A., Selph, C., Yen, T., Dahiya, R. & Lue, T. The effect of surgical trauma on rat tunica albuginea. *J Urol* **159,** 1700–1707 (1998).

186. El-Sakka, A. *et al.* An animal model of Peyronie's-like condition associated with an increase of transforming growth factor beta mRNA and protein expression. *J Urol* **158,** 2284–2290 (1997).

187. Domes, T. *et al.* Is there a role for proteomics in Peyronie's disease? *J Sex Med* **4,** 867–877 (2007).

188. Vernet, D. *et al.* Effect of nitric oxide on the differentiation of fibroblasts into myofibroblasts in the Peyronie's fibrotic plaque and in its rat model. *Nitric Oxide* **7,** 262–276 (2002).

189. Lin, C.-S., Lin, G., Wang, Z., Maddah, S. A. & Lue, T. F. Upregulation of monocyte chemoattractant protein 1 and effects of transforming growth factor-β1 in Peyronie's disease. *Biochem Biophys Res Commun* **295,** 1014–1019 (2002).

190. Davila, H. H., Magee, T. R., Zuniga, F. I., Rajfer, J. & Gonzalez-Cadavid, N. F. Peyronie's disease associated with increase in plasminogen activator inhibitor in fibrotic plaque. *Urology* **65,** 645–648 (2005).

191. Gentile, V. *et al.* Ultrastructural and immunohistochemical characterization of the tunica albuginea in Peyronie's disease and veno-occlusive dysfunction. *J Androl* **17,** 96–103 (1996).

192. Mulhall, J. P., Anderson, M. S., Lubrano, T. & Shankey, T. V. Peyronie's

disease cell culture models: phenotypic, genotypic and functional analyses. *Int J Impot Res* **14,** 397–405 (2002).

193. Cantini, L. P. *et al.* Profibrotic role of myostatin in Peyronie's disease. *J Sex Med* **5,** 1607–1622 (2008).
194. Jalkut, M., Gonzalez-cadavid, N. & Rajfer, J. Peyronie's disease: a review. *Rev Urol* **5,** 142–148 (2003).
195. Bilgutay, A. N. & Pastuszak, A. W. Peyronie's disease: a review of etiology, diagnosis, and management. *Curr Sex Heal Rep* **7,** 117–131 (2015).
196. Vardi, Y., Levine, L. A., Chen, J., Hatzimouratidis, K. & Sohn, M. Is there a place for conservative treatment in Peyronie's disease? *J Sex Med* **6,** 903–909 (2009).
197. Castro, R. M. P. *et al.* Combined treatment with vitamin E and colchicine in the early stages of Peyronie's disease. *BJU Int* **91,** 522–524 (2003).
198. Weidner, W., Hauck, E. W. & Schnitker, J. Potassium paraaminobenzoate (POTABA) in the treatment of Peyronie's disease: a prospective, placebo-controlled, randomized study. *Eur Urol* **47,** 530–536 (2005).
199. Biagiotti, G. & Cavallini, G. Acetyl- L-carnitine vs tamoxifen in the oral therapy of Peyronie's disease: a preliminary report. *BJU Int* **88,** 63–67 (2001).
200. Kim, J. *et al.* Progression of Peyronie's disease during tamoxifen treatment. *Korean J Androl* **30,** 52–56 (2012).
201. Safarinejad, M. R. Therapeutic effects of colchicine in the management of Peyronie's disease: a randomized double-blind, placebo-controlled study. *Int J Impot Res* **16,** 238–243 (2004).
202. Zenzmaier, C. *et al.* Phosphodiesterase type 5 inhibition reverts prostate fibroblast-to-myofibroblast trans-differentiation. *Endocrinology* **153,** 5546–5555 (2012).
203. Dickstein, R., Uberoi, J. & Munarriz, R. Severe, disabling, and/or chronic penile pain associated with Peyronie disease: management with subcutaneous steroid injection. *J Androl* **31,** 445–449 (2010).
204. Levine, L., Goldman, K. & Greenfield, J. Experience with intraplaque injection of verapamil for Peyronie's disease. *J Urol* **168,** 621–625 (2002).
205. Bennett, N. E., Guhring, P. & Mulhall, J. P. Intralesional verapamil prevents the progression of Peyronie's disease. *Urology* **69,** 1181–1184 (2007).
206. Judge, J. S. & Wisniewski, Z. S. Intralesional interferon in the treatment of Peyronie's disease: a pilot study. *Bristish J Urol* **79,** 40–42 (1997).
207. Hellstrom, W. J. G. *et al.* Single-blind, multicenter, placebo controlled, parallel study to assess the safety and efficacy of intralesional interferon α-2b for minimally invasive treatment for Peyronie's disease. *J Urol* **176,** 394–398 (2006).
208. Lipshultz, L. I. *et al.* Clinical efficacy of collagenase clostridium histolyticum in the treatment of Peyronie's disease by subgroups: results from two large,

double-blind, randomized, placebo-controlled, phase III studies. *BJU Int* **116,** 650–656 (2015).

209. Gelbard, M. *et al.* Phase 2b study of the clinical efficacy and safety of collagenase clostridium histolyticum in patients with peyronie disease. *J Urol* **187,** 2268–2274 (2012).
210. Valente, E. G. A. *et al.* L-arginine and phosphodiesterase (PDE) inhibitors counteract fibrosis in the Peyronie's fibrotic plaque and related fibroblast cultures. *Nitric Oxide* **9,** 229–244 (2003).
211. Ferrini, M. G., Kovanecz, I., Nolazco, G., Rajfer, J. & Gonzalez-cadavid, N. F. Effects of long-term vardenafil treatment on the development of fibrotic plaques in a rat model of Peyronie's disease. *BJU Int* **97,** 625–633 (2006).
212. Tan, R., Sangkum, P., Gregory, G. & Hellstrom, W. J. G. Update on medical management of Peyronie's disease. *Curr Urol Rep* **15,** 1–9 (2014).
213. Riedl, C., Plas, E., Engelhardt, P., Daha, K. & Pflüger, H. Iontophoresis for treatment of Peyronie's disease. *J Urol* **163,** 95–99 (2000).
214. Skolarikos, A., Alargof, E., Rigas, A., Deliveliotis, C. & Konstantinidis, E. Shockwave therapy as first-line treatment for Peyronie's disease: a prospective study. *J Endourol* **19,** 11–14 (2005).
215. Abern, M. R., Larsen, S. & Levine, L. A. Combination of penile traction, intralesional verapamil, and oral therapies for Peyronie's disease. *J Sex Med* **9,** 288–295 (2012).
216. Serefoglu, E. C. & Hellstrom, W. J. G. Treatment of Peyronie's disease: 2012 update. *Curr Urol Rep* **12,** 444–452 (2011).
217. Pryor, J. *et al.* Peyronie's disease. *J Sex Med* **1,** 110–115 (2004).
218. Vignozzi, L. *et al.* Oxytocin receptor is expressed in the penis and mediates an estrogen-dependent smooth muscle contractility. *Endocrinology* **145,** 1823–1834 (2004).
219. Crescioli, C. *et al.* Expression of functional estrogen receptors in human fetal male external genitalia. *J Clin Endocrinol Metab* **88,** 1815–1824 (2003).
220. Jiang, H. *et al.* Estradiol attenuates the TGF-β1-induced conversion of primary TAFs into myofibroblasts and inhibits collagen production and myofibroblast contraction by modulating the Smad and Rho/ROCK signaling pathways. *Int J Mol Med* **36,** 801–807 (2015).
221. Ralph, D. J., Brooks, M. D., Bottazzo, G. F. & Pryor, J. P. The treatment of Peyronie's disease with tamoxifen. *Br J Urol* **70,** 648–651 (1992).
222. Teloken, C. *et al.* Tamoxifen versus placebo in the treatment of Peyronie's disease. *J Urol* **162,** 2003–2005 (1999).
223. Stevenson, S., Sharpe, D. T. & Thornton, M. J. Effects of oestrogen agonists on human dermal fibroblasts in an in vitro wounding assay. *Exp Dermatol* **18,** 988–990 (2009).
224. Taylor, S., Wakem, M., Dijkman, G., Alsarraj, M. & Nguyen, M. A practical

approach to RT-qPCR - publishing data that conform to the MIQE guidelines. *Methods* **50,** S1–S5 (2010).

225. Fleige, S. & Pfaffl, M. W. RNA integrity and the effect on the real-time qRT-PCR performance. *Mol Aspects Med* **27,** 126–139 (2006).
226. Hecker, L. *et al.* NADPH oxidase-4 mediates myofibroblast activation and fibrogenic responses to lung injury. *Nat Med* **15,** 1077–1081 (2009).
227. Salas, S. *et al.* Ezrin and alpha-smooth muscle actin are immunohistochemical prognostic markers in conventional osteosarcomas. *Virchows Arch* **451,** 999–1007 (2007).
228. Livak, K. J. & Schmittgen, T. D. Analysis of relative gene expression data using real-time quantitative PCR and the 2(-Delta Delta C(T)) Method. *Methods* **25,** 402–408 (2001).
229. Brown, A. M. A step-by-step guide to non-linear regression analysis of experimental data using a Microsoft Excel spreadsheet. *Comput Methods Programs Biomed* **65,** 191–200 (2001).
230. Vladusic, E., Hornby, A., Guerra-Vladusic, F., Lakins, J. & Lupu, R. Expression and regulation of estrogen receptor β in human breast tumors and cell lines. *Oncol Rep* **7,** 157–167 (2000).
231. Bustin, S. A. *et al.* The MIQE guidelines: minimum information for publication of quantitative real-time PCR experiments. *Clin Chem* **55,** 611–622 (2009).
232. Derveaux, S., Vandesompele, J. & Hellemans, J. How to do successful gene expression analysis using real-time PCR. *Methods* **50,** 227–230 (2010).
233. D'haene, B. & Hellemans, J. The importance of quality control during qPCR data analysis. *Int Drug Discov* 18–24 (2010).
234. Vandesompele, J. *et al.* Accurate normalization of real-time quantitative RT-PCR data by geometric averaging of multiple internal control genes. *Genome Biol* **3,** 1–12 (2002).
235. Perez, R., Tupac-Yupanqui, I. & Dunner, S. Evaluation of suitable reference genes for gene expression studies in bovine muscular tissue. *BMC Mol Biol* **9,** 1–6 (2008).
236. Stebbeds, W. In vitro studies of Peyronie's disease-derived myofibroblasts: disease association and identification of novel therapeutic compounds. *Cranf Univ* **PhD Thesis,** 1–283 (2015).
237. Kottler, U. B. *et al.* Comparative effects of TGF-β1 and TGF-β2 on extracellular matrix production, proliferation, migration, and collagen contraction of human Tenon's capsule fibroblasts in pseudoexfoliation and primary open-angle glaucoma. *Exp Eye Res* **80,** 121–134 (2005).
238. Nakao, A. *et al.* TGF-β receptor-mediated signalling through Smad2, Smad3 and Smad4. *EMBO J* **16,** 5353–5362 (1997).
239. Biernacka, A., Dobaczewski, M. & Frangogiannis, N. G. TGF-β signaling in fibrosis. *Growth Factors* **29,** 196–202 (2011).

240. Sousa, A. M. *et al.* Smooth muscle alpha-actin expression and myofibroblast differentiation by TGF-β are dependent upon MK2. *J Cell Biochem* **100,** 1581–1592 (2007).

241. Desmoulière, A., Geinoz, A., Gabbiani, F. & Gabbiani, G. Transforming growth factor-β1 induces α-smooth muscle actin expression in granulation tissue myofibroblasts and in quiescent and growing cultured fibroblasts. *J Cell Biol* **122,** 103–111 (1993).

242. Magee, T. R. *et al.* Gene expression profiles in the Peyronie's disease plaque. *Urology* **59,** 451–457 (2002).

243. Haag, S. M. *et al.* Alterations in the transforming growth factor (TGF)-β pathway as a potential factor in the pathogenesis of Peyronie's disease. *Eur Urol* **51,** 255–261 (2007).

244. Zhang, J.-H., Chung, T. D. Y. & Oldenburg, K. R. A simple statistical parameter for use in evaluation and validation of high throughput screening assays. *J Biomol Screening1* **4,** 67–73 (1999).

245. Sui, Y. & Wu, Z. Alternative statistical parameter for high-throughput screening assay quality assessment. *J Biomol Screen* **12,** 229–234 (2007).

246. Xu, C.-L. *et al.* Effect of dimethyl sulfoxide on cell cycle synchronization of in vitro cultured monkey (Maccaca fascicularis) ear skin fibroblasts. *J Anim Vet Adv* **12,** 242–247 (2013).

247. Byfield, S. D., Major, C., Laping, N. J. & Roberts, A. B. SB-505124 is a selective inhibitor of transforming growth factor-beta type I receptors ALK4, ALK5, and ALK7. *Mol Pharmacol* **65,** 744–752 (2004).

248. Sapitro, J. *et al.* Suppression of transforming growth factor-β effects in rabbit subconjunctival fibroblasts by activin receptor-like kinase 5 inhibitor. *Mol Vis* **16,** 1880–1892 (2010).

249. Au, K. & Ehrlich, H. P. When the Smad signaling pathway is impaired, fibroblasts advance open wound contraction. *Exp Mol Pathol* **89,** 236–240 (2010).

250. Bordeaux, J. *et al.* Antibody validation. *Biotechniques* **48,** 197–209 (2010).

251. Stebbeds, W. *et al.* Development of a high-throughput, cell-based assay for the anti-myofibroblast activity in Peyronie's disease. *J Sex Med* **12,** 188–271 (2015).

252. Forbes, Stuart, J. *et al.* A significant proportion of myofibroblasts are of bone marrow origin in human liver fibrosis. *Gastroenterology* **126,** 955–963 (2004).

253. Hu, B. & Phan, S. H. Myofibroblasts. *Curr Opin Rheumatol* **25,** 71–77 (2013).

254. Viegas, M., Martins, T. C., Seco, F. & Do Carmo, A. An improved and cost-effective methodology for the reduction of autofluorescence in direct immunofluorescence studies on formalin-fixed paraffin-embedded tissues. *Eur J Histochem* **51,** 59–66 (2007).

255. Kalk, P. *et al.* The adenosine A1 receptor antagonist SLV320 reduces

myocardial fibrosis in rats with 5/6 nephrectomy without affecting blood pressure. *Br J Pharmacol* **151,** 1025–32 (2007).

256. Mustafa, S. J. *et al.* Effect of a specific and selective A2B adenosine receptor antagonist on adenosine agonist AMP and allergen-induced airway responsiveness and cellular influx in a mouse model of asthma. *J Pharmacol Exp Ther* **320,** 1246–1251 (2007).

257. Grden, M., Podgorska, M., Kocbuch, K., Szutowicz, A. & Pawelczyk, T. Expression of adenosine receptors in cardiac fibroblasts as a function of insulin and glucose level. *Arch Biochem Biophys* **455,** 10–17 (2006).

258. Tak, E. *et al.* CD73-dependent generation of adenosine and endothelial ADORA2B signaling attenuate diabetic nephropathy. *J Am Soc Nephrol* **25,** 547–563 (2014).

259. Sun, L. L. *et al.* Cyclopentyladenosine improves cell proliferation, wound healing, and hair growth. *J Surg Res* **87,** 14–24 (1999).

260. Wakeno, M. *et al.* Long-term stimulation of adenosine A2b receptors begun after myocardial infarction prevents cardiac remodeling in rats. *Circulation* **114,** 1923–1932 (2006).

261. Mueller, S. O. & Korach, K. S. in *The handbook of EnvironmentalChemistry* **3,** 1–25 (2001).

262. Schmidt, M. W., Houseman, A., Ivanov, A. R. & Wolf, D. A. Comparative proteomic and transcriptomic profiling of the fission yeast Schizosaccharomyces pombe. *Mol Syst Biol* **3,** 1–12 (2007).

263. Feetham, M. C. *et al.* Integrated genomic and proteomic analyses of gene expression in mammalian cells. *Mol Cell Proteomics* **3,** 960–969 (2004).

264. Schwanhäusser, B. *et al.* Global quantification of mammalian gene expression control. *Nature* **473,** 337–342 (2011).

265. Hattori, T., Stawski, L., Nakerakanti, S. S. & Trojanowska, M. Fli1 is a negative regulator of estrogen receptor α in dermal fibroblasts. *J Invest Dermatol* **131,** 1469–1476 (2011).

266. Haczynski, J. *et al.* Human cultured skin fibroblasts express estrogen receptor α and β. *Int J Mol Med* **10,** 149–153 (2002).

267. Palmieri, C. *et al.* The expression of oestrogen receptor (ER)-beta and its variants, but not ER alpha, in adult human mammary fibroblasts. *J Mol Endocrinol* **33,** 35–50 (2004).

268. Chau, D. *et al.* Tamoxifen downregulates TGF-β production in Keloid fibroblasts. *Ann Plast Surg* **40,** 490–493 (1998).

269. Mikulec, A. *et al.* Effect of tamoxifen on transforming growth factor β1 production by keloid and fetal fibroblasts. *Arch Facial Plast Surg* **3,** 111–114 (2001).

270. Kuhn, M. A., Wang, X., Payne, W. G., Ko, F. & Robson, M. C. Tamoxifen decreases fibroblast function and downregulates TGF(beta2) in dupuytren's affected palmar fascia. *J Surg Res* **103,** 146–152 (2002).

271. Ruffy, M., Kunnavatana, S. & Koch, R. Effects of tamoxifen on normal human dermal fibroblasts. *Arch Facial Plast Surg* **8,** 329–332 (2006).

272. Park, T. Y. *et al.* The Efficacy of medical treatment of Peyronie's disease: Potassium Para-Aminobenzoate monotherapy vs. combination therapy with Tamoxifen, L-Carnitine, and Phosphodiesterase Type 5 Inhibitor. *World J Mens Heal* **34,** 40–46 (2016).

273. Hatzimouratidis, K. *et al.* EAU guidelines on penile curvature. *Eur Urol* **62,** 543–552 (2012).

274. Nehra, A. *et al.* Peyronie's disease : AUA Guideline. *J Urol* **194,** 745–753 (2015).

275. Ilg, M. M. *et al.* Antifibrotic synergy between phosphodiesterase type 5 inhibitors and selective oestrogen receptor modulators in Peyronie's disease models. *Eur Urol* 1–12 (2018). doi:10.1016/j.eururo.2018.10.014

276. Muchmore, D. B. Raloxifene: A selective estrogen receptor modulator (SERM) with multiple target system effects. *Oncologist* **5,** 388–392 (2000).

277. Luo, F. *et al.* Raloxifene ameliorates liver fibrosis of nonalcoholic steatohepatitis induced by choline-deficient high-fat diet in ovariectomized mice. *Dig Dis Sci* **60,** 2730–2739 (2015).

278. Dixon, A., Wells, C. C., Singh, S., Babayan, R. & Maric, C. Renoprotective effects of a selective estrogen receptor modulator, raloxifene, in an animal model of diabetic nephropathy. *Am J Nephrol* **27,** 120–128 (2007).

279. Lee, J. H., Wen, Y., Polan, M. L. & Chen, B. The effect of raloxifene, a SERM, on extracellular matrix protein expression of pelvic fibroblasts. *Int Urogynecol J Pelvic Floor Dysfunct* **23,** 349–355 (2012).

280. Surazynski, A. *et al.* Differential effects of estradiol and raloxifene on collagen biosynthesis in cultured human skin fibroblasts. *Int J Mol Med* **12,** 803–809 (2003).

281. Furlanut, M. *et al.* Tamoxifen and its main metabolites serum and tissue concentrations in breast cancer women. *Ther Drug Monit* **29,** 349–352 (2007).

282. Schmittgen, T. D. & Livak, K. J. Analyzing real-time PCR data by the comparative Ct method. *Nat Protoc* **3,** 1101–1108 (2008).

283. Lin, X.-D. *et al.* Overexpression of thrombospondin-1 in stromal myofibroblasts is associated with tumor growth and nodal metastasis in gastric carcinoma. *J Surg Oncol* **106,** 94–100 (2012).

284. Bustin, S. A. Absolute quantification of mRNA using real-time reverse transcription polymerase chain reaction assays. *J Mol Endocrinol* **25,** 169–193 (2000).

285. Mackay, I. M., Arden, K. E. & Nitsche, A. Real-time PCR in virology. *Nucleic Acids Res* **30,** 1292–1305 (2002).

7 APPENDICES

Appendix I: Ethical information

A.1 Penile cancer patient information/consent form

Patient Information Sheet, version 2

Date: 23rd March 2012

Indication: Penile Cancer

Understanding how Peyronie's disease develops

You are being invited to take part in a research study. Before you decide it is important for you to understand why the research is being done and what it will involve. Please take time to read the following information carefully and discuss it with friends, relatives and your doctor if you wish. Ask us if there is anything that is not clear or if you would like more information. Take time to decide whether or not you wish to take part.

Thank you for reading this.

What is the purpose of the study?

We are carrying out a research project in collaboration with Cranfield University. The aim of this research project is to understand how Peyronie's disease develops. Peyronie's disease is caused by thickening of one side of the penis which causes curvature, deformation and erectile dysfunction. By understanding the disease better, we believe that we may be able to develop new and better treatment approaches for this disease.

We are taking tissue samples from patients with Peyronie's disease to study this disease. We need also penile tissue samples from patients who are not affected by this disease such as your penile tissue which will be removed during your surgery.

Why have I been chosen?

You are going to be operated for the treatment of penile tumour. During the surgery, the tumour will be removed. Much of this tissue will be examined by a pathologist, to gain a better understanding of your illness. The part of the tumour which will not be used by the pathologist is usually discarded. We are seeking your permission to use this tissue for the research project mentioned above. If you do not give your consent, this tissue will be discarded.

The tissue obtained from you with your permission will be transferred to the research laboratories at Cranfield University, Bedfordshire where the cellular structure and protein content will be analysed.

The tissue obtained from you will NOT be used for any genetic research that involves your DNA.

Do I have to take part?

It is up to you to decide whether or not to take part. If you do decide to take part you will be given this information sheet to keep and be asked to sign a consent form. If you decide to take part, you are free to withdraw at any time and without giving a reason. This will not affect the standard of care you receive.

What will happen to me if I take part?

You will undergo exactly the same surgery and receive exactly the same medical care as you would normally. No additional drugs or procedures will be used. This means that there are no additional risks, disadvantages or side effects.

What will happen to me if I do not take part?

Your decision of not taking part in this study will not affect the care you will receive. You will undergo exactly the same surgery and receive exactly the same medical care as you would normally.

What are the possible benefits of taking part?

You will not receive any direct benefit from participating in this study, but the results of this study may contribute towards better understanding of Peyronie's disease. You will not receive any payment for taking part in this study, now or in the future.

Will my taking part in this study be kept confidential?

All information which is collected about you during the course of this research project will be kept strictly confidential. Any information about you which leaves the hospital will have your name and address removed so that you cannot be recognised from it. To protect your privacy, your sample that is transferred to Cranfield University will be labelled only with a study subject number, not your name. We are not going to keep a link between the subject number and your hospital records meaning that the sample cannot be traced back to you. This total anonymisation process is to ensure that your private data is kept confidential at all times. Only your age, your diagnosis, stage of the disease, other diseases (if any) and your medication (if any) will be linked to the subject number.

What happens if I withdraw my consent after the operation?

You are free to withdraw your consent at any time, before or after the surgery. However, once the tissue is anonymised as explained above and transferred to the research laboratories, we will not be able to trace them back so it will not be possible to destroy the tissue.

What will happen to the results of the research study?

We hope to publish the results so that as many of our findings as possible will be made available to the medical and scientific community. You will not be personally identified in any publication. Because of the exploratory nature of the work, none of the results will be provided to you or to the physicians who are treating you or may treat you in the future. The timing of any publication will depend mostly on the speed with which we collect the data and cannot be predicted with certainty.

Who is organising and funding the research?

This is a joint programme of research collaboration between Dr David Ralph and his surgical team at University College London Hospitals and the research scientists headed by Dr Selim Cellek at Cranfield Health, Cranfield University. The doctors are not paid for including you in this study.

Who has reviewed the study?

This study has been reviewed and approved by the Cranfield University Health Research Ethics Committee and the Essex Research Ethics Proportionate Review Sub-Committee.

Contact details for further information:

Dr David Ralph,

Institute of Urology

2A Maple House

Rosenheim Wing

Ground Floor

25 Grafton Way

London

WC1E 6AU

Dr Selim Cellek

Cranfield Health

Cranfield University

Vincent Building

Bedfordshire

MK43 0AL

Comments or concerns during the study

If you have any comments or concerns you may discuss these with the investigator. If you wish to go further and complain about any aspect of the way you have been approached or treated during the course of the study, you should write or get in touch with the Complaints Manager, UCL hospitals. Please quote the UCLH project number at the top this consent form.

Version: 2

Date: February 2012

CONSENT FORM

Title of Project: Understanding how Peyronie's disease develops

Name of Researchers: Dr David Ralph, University College London Hospitals and Dr Selim Cellek, Cranfield University

Please initial box

1. I confirm that I have read and understand the information sheet dated January 2012 (version 1) for the above study and have had the opportunity to ask questions. ☐

2. I understand that my participation is voluntary and that I am free to withdraw at any time, without giving any reason. ☐

3. I understand that sections of any of my medical notes may be looked at by the surgical team with respect to age, sex, condition and treatment at admission. I have been assured that all data relating to my person will be treated with absolute confidentiality at all times and will not be made public. I give permission for these individuals to have access to my records. ☐

4. I understand that my tissue will be totally anonymised, meaning that there will be no link between my tissue and my medical records including my private data so that the tissue cannot be traced back to me.

5. I agree to take part in the above programme of work. ☐

_____ _____

Name of Patient Signature & Date

Name of Person obtaining consent Signature & Date

(if different from surgeon)

_____ _____

Surgeon Signature & Date

(1 for patient; 1 for researcher; 1 to be kept with hospital notes)

A.2 Peyronie's disease patient information/consent form

Patient Information Sheet, version 2

Date: 23rd March 2012

Indication: Peyronie's disase

Understanding how Peyronie's disease develops

You are being invited to take part in a research study. Before you decide it is important for you to understand why the research is being done and what it will involve. Please take time to read the following information carefully and discuss it with friends, relatives and your doctor if you wish. Ask us if there is anything that is not clear or if you would like more information. Take time to decide whether or not you wish to take part.

Thank you for reading this.

What is the purpose of the study?

We are carrying out a research project in collaboration with Cranfield University. The aim of this research project is to understand how Peyronie's disease develops. Peyronie's disease is caused by thickening of one side of the penis which causes curvature, deformation and erectile dysfunction. By understanding the disease better, we believe that we may be able to develop new and better treatment approaches for this disease.

Why have I been chosen?

You are going to be operated for the treatment of Peyronie's disease. During the surgery, the diseased tissue called "plaque" will be removed. Much of this tissue will be examined by a pathologist, to gain a better understanding of your illness. The part of the plaque which will not be used by the pathologist is usually discarded. We are seeking your permission to use this tissue for the research

project mentioned above. If you do not give your consent, this tissue will be discarded.

The tissue obtained from you with your permission will be transferred to the research laboratories at Cranfield University, Bedfordshire where the cellular structure and protein content will be analysed.

The tissue obtained from you will NOT be used for any genetic research that involves your DNA.

At the end of the research project, your tissue will be destroyed by incineration.

There is no other reason for choosing you to take part in this study. We intend to study material from a number of different patients, until we are able to draw proper conclusions.

Do I have to take part?

It is up to you to decide whether or not to take part. If you do decide to take part you will be given this information sheet to keep and be asked to sign a consent form. If you decide to take part, you are free to withdraw at any time and without giving a reason. This will not affect the standard of care you receive.

What will happen to me if I take part?

You will undergo exactly the same surgery and receive exactly the same medical care as you would normally. No additional drugs or procedures will be used. This means that there are no additional risks, disadvantages or side effects.

What will happen to me if I do not take part?

Your decision of not taking part in this study will not affect the care you will receive. You will undergo exactly the same surgery and receive exactly the same medical care as you would normally.

What are the possible benefits of taking part?

You will not receive any direct benefit from participating in this study, but the results of this study may contribute towards better understanding of Peyronie's disease. You will not receive any payment for taking part in this study, now or in the future.

Will my taking part in this study be kept confidential?

All information which is collected about you during the course of this research project will be kept strictly confidential. Any information about you which leaves the hospital will have your name and address removed so that you cannot be recognised from it. To protect your privacy, your sample that is transferred to Cranfield University will be labelled only with a study subject number, not your name. We are not going to keep a link between the subject number and your hospital records meaning that the sample cannot be traced back to you. This total anonymisation process is to ensure that your private data is kept confidential at all times. Only your age, your diagnosis, stage of the disease, other diseases (if any) and your medication (if any) will be linked to the subject number.

What happens if I withdraw my consent after the operation?

You are free to withdraw your consent at any time, before or after the surgery. However once the tissue is anonymised as explained above and transferred to the research laboratories, we will not be able to trace them back so it will not be possible to destroy the tissue.

What will happen to the results of the research study?

We hope to publish the results so that as many of our findings as possible will be made available to the medical and scientific community. You will not be personally identified in any publication. Because of the exploratory nature of the work, none of the results will be provided to you or to the physicians who are

treating you or may treat you in the future. The timing of any publication will depend mostly on the speed with which we collect the data and cannot be predicted with certainty.

Who is organising and funding the research?

This is a joint programme of research collaboration between Dr David Ralph and his surgical team at University College London Hospitals and the research scientists headed by Dr Selim Cellek at Cranfield Health, Cranfield University. The doctors are not paid for including you in this study.

Who has reviewed the study?

This study has been reviewed and approved by the Cranfield University Health Research Ethics Committee and the Essex Research Ethics Proportionate Review Sub-Committee.

Contact details for further information:

Dr David Ralph,

Institute of Urology

2A Maple House

Rosenheim Wing

Ground Floor

25 Grafton Way

London

WC1E 6AU

Dr Selim Cellek

Cranfield Health

Cranfield University

Vincent Building

Bedfordshire

MK43 0AL

Comments or concerns during the study

If you have any comments or concerns you may discuss these with the investigator. If you wish to go further and complain about any aspect of the way you have been approached or treated during the course of the study, you should write or get in touch with the Complaints Manager, UCL hospitals. Please quote the UCLH project number at the top this consent form.

Version: 2

Date: February 2012

CONSENT FORM

Title of Project: Understanding how Peyronie's disease develops

Name of Researchers: Dr David Ralph, University College London Hospitals and Dr Selim Cellek, Cranfield University

Please initial box

1. I confirm that I have read and understand the information sheet dated January 2012 (version 1) for the above study and have had the opportunity to ask questions. ☐

2. I understand that my participation is voluntary and that I am free to withdraw at any time, without giving any reason. ☐

3. I understand that sections of any of my medical notes may be looked at by the surgical team with respect to age, sex, condition and treatment at admission. I have been assured that all data relating to my person will be treated with absolute confidentiality at all times and will not be made public. I give permission for these individuals to have access to my records. ☐

4. I understand that my tissue will be totally anonymised, meaning that there will be no link between my tissue and my medical records including my private data so that the tissue cannot be traced back to me.

5. I agree to take part in the above programme of work. ☐

_____ _____

Name of Patient Signature & Date

Name of Person obtaining consent Signature & Date

(if different from surgeon)

_____ _____

Surgeon Signature & Date

(1 for patient; 1 for researcher; 1 to be kept with hospital notes)

Figure 7-1: Copy of approval letter from local ethics board (Cranfield University Health Research Ethics Committee; CUHREC)

Cranfield Health

Cranfield UNIVERSITY

Vincent Building
Cranfield University
Cranfield
Bedfordshire
MK43 0AL
England
T: +44 (0)1234 758300
F: +44 (0)1234 758380
www.cranfield.ac.uk/health

10th May 2012

Dear William

Project Reference No 01/12: Understanding how Peyronie's disease develops

Thank you for submitting the requested amendments to the above project, I can confirm that I am happy to take Chairman's Action approving the study be submitted to the NHS ethics committee.

Please note that subsequent to approval applicants are responsible for:

- reporting of any adverse incidents occurring during the course of the study to CUHREC, even if the incident is not directly related to the study (e.g. a complaint by a participant);
- notifying CUHREC of any major changes to the protocol and obtaining further ethical approval as appropriate;
- notifying CUHREC when the study has ended.

The committee may notify the NHS ethics committee if they become aware of any unethical or other improper practices during the execution of the research.

Yours sincerely

EJ Jones

pp

Professor Paul Harrison
Chairman
Cranfield University Health Research Ethics Committee

REGISTERED

The Queen's Anniversary Prizes
2011

Figure 7-2: Copy of approval letter from national ethics board (National Research Ethics Service; NRES)

NRES Committee East of England - Essex
East of England Rec Office 1
Victoria House
Capital Park
Fulbourn
Cambridge
CB21 5XB
Telephone: 01223 597693
Facsimile: 01223 597645

09 April 2012

Dr David Ralph
Senior Urological Consultant
University College London Hospitals,
The Institute of Urology
University College London,
252 Euston Rd, London
WC1E 6BT

Dear Dr Ralph

Study title: **Understanding how Peyronie's disease develops**
REC reference: **12/EE/0170**

The Proportionate Review Sub-committee of the NRES Committee East of England - Essex reviewed the above application on 05 April 2012.

Ethical opinion

On behalf of the Committee, the sub-committee gave a favourable ethical opinion of the above research on the basis described in the application form, protocol and supporting documentation, subject to the conditions specified below.

Ethical review of research sites

The favourable opinion applies to all NHS sites taking part in the study, subject to management permission being obtained from the NHS/HSC R&D office prior to the start of the study (see "Conditions of the favourable opinion" below).

Conditions of the favourable opinion

The favourable opinion is subject to the following conditions being met prior to the start of the study.

Management permission or approval must be obtained from each host organisation prior to the start of the study at the site concerned.

Management permission ("R&D approval") should be sought from all NHS organisations involved in the study in accordance with NHS research governance arrangements.

Guidance on applying for NHS permission for research is available in the Integrated Research Application System or at http://www.rdforum.nhs.uk.

Where a NHS organisation's role in the study is limited to identifying and referring potential participants to research sites ("participant identification centre"), guidance should be sought from the R&D office on the information it requires to give permission for this activity.

For non-NHS sites, site management permission should be obtained in accordance with the procedures of the relevant host organisation.

Sponsors are not required to notify the Committee of approvals from host organisations.

1. The Participant Information Sheet must tell participants that tissue samples will be destroyed at the end of the study. This must also be reflected by a specific point in the Consent Form.
2. The Participant Information Sheet must inform participants that this study will form part of an academic qualification i.e. a PhD.
3. The Participant Information Sheet must include details for an independent complaints commission e.g. PALS.

It is the responsibility of the sponsor to ensure that all the conditions are complied with before the start of the study or its initiation at a particular site (as applicable).

You should notify the REC in writing once all conditions have been met (except for site approvals from host organisations) and provide copies of any revised documentation with updated version numbers. Confirmation should also be provided to host organisations together with relevant documentation.

Approved documents

The documents reviewed and approved were:

Document	*Version*	*Date*
Investigator CV		
Other: C.V Supervisor Selim Cellek		
Other: C.V Student William Stebbeds		
Participant Consent Form: Consent Form Peyronie's Disease	2	01 February 2012
Participant Consent Form: Consent Form Penile Cancer	2	01 February 2012
Participant Information Sheet: Peyronie's Disease	2	23 March 2012
Participant Information Sheet: Penile Cancer	2	23 March 2012
Protocol	2	23 March 2012
REC application	3.4	05 April 2012

Membership of the Proportionate Review Sub-Committee

The members of the Sub-Committee who took part in the review are listed on the attached sheet.

Statement of compliance

The Committee is constituted in accordance with the Governance Arrangements for Research Ethics Committees and complies fully with the Standard Operating Procedures for Research Ethics Committees in the UK.

After ethical review

Reporting requirements

The attached document "After ethical review – guidance for researchers" gives detailed guidance on reporting requirements for studies with a favourable opinion, including:

- Notifying substantial amendments
- Adding new sites and investigators
- Notification of serious breaches of the protocol
- Progress and safety reports
- Notifying the end of the study

The NRES website also provides guidance on these topics, which is updated in the light of changes in reporting requirements or procedures.

Feedback

You are invited to give your view of the service that you have received from the National Research Ethics Service and the application procedure. If you wish to make your views known please use the feedback form available on the website.

Further information is available at National Research Ethics Service website > After Review

12/EE/0170	**Please quote this number on all correspondence**

With the Committee's best wishes for the success of this project

Yours sincerely

Dr Andy Stevens
Chair

Enclosures: List of names and professions of members who took part in the review

"After ethical review – guidance for researchers"

Copy to:

Dr Selim Cellek
Cranfield University
Cranfield Health
Vincent Building
Cranfield
MK43 0AL

Mr Philip Diamond,
University College London Hospitals
NHS Foundation Trust
1st Floor Maple House (Suite B)
149 Tottenham Court Road
London
W1T 7DN

Mr William Stebbeds
Cranfield Health
Cranfield University
Vincent Building
Cranfield
MK43 0AL

NRES Committee East of England - Essex

Attendance at PRS Sub-Committee of the REC meeting on 05 April 2012

Committee Members:

Name	*Profession*	*Present*	*Notes*
Ms Julie Lockhart	PPI Representative	Yes	
Dr Andy Stevens	Principal Lecturer/Media Consultant	Yes	
Mrs Caroline Ward	Head of Health & Wellbeing Children's Services	Yes	

Also In attendance:

Name	*Position (or reason for attending)*
Ms Suzanne Emerton	Administrator

Appendix II: Supplementary data to Material and Methods section

A.1 Real-time RT-PCR

A.1.1 Example of a detailed protocol used for RT-qPCR

The following protocols for RNA extraction, RNA quality, RT and qPCR (RT-qPCR) were performed as instructed by the manufacturers. These protocols were removed from each kit manual.

Seeding onto 6 well plates

Materials/Reagents:

- Cell line: TAN2A1 P4 & PD2A2 P4
- Complete media used: DMEM F-12 + Glutamax®: (Invitrogen Gibco, 31331093) supplemented with 10% FBS (Invitrogen Gibco, 10270106) 1% Penicillin-Streptomycin (Invitrogen Gibco, 15070063)
- Phosphate buffered saline (PBS; Fisher Scientific, 11510546)
- 0.25% Trypsin - EDTA (TE; Fisher Scientific, 11560626)
- Scepter™ + 60 µm sensors (Millipore)
- 6 well plate (NUNC, Fisher Scientific, 10469282)

Protocol:

1. Cells were grown under normal conditions in the T75 flask.
2. Cells detached and neutralised as previously described ("Basic Cell culture techniques", page 4, Book no. 1).
3. Perform cell counting using Scepter.
4. Dilute or concentrate cell suspension to the desired concentration.
5. Using a 6 well plate, add 2 ml of cell suspension to all wells at 1.0×10^5 cells/well.
6. On the next day, remove media from wells and add 2 ml of fresh media or 2 ml of media containing 5 ng/ml TGF-β1 to the plate.
7. Incubate plate at 37 °C, 5% CO_2 for 72 hours.

RNA extraction

Materials/Reagents:

- Cell line: TAN2A1 P4 & PD2A2 P4
- Medium: DMEM/F12 GlutaMAX™ supplemented with 10% FBS; 1% Pen-Strep
- Phosphate Buffered Saline (PBS; Fisher Scientific, 11510546)
- 0.25% Trypsin – EDTA (TE; Fisher Scientific, 11560626)
- Scepter™ + 60 µm sensors (Millipore)
- RNeasy Mini Kit (QIAGEN, 74104)
- RNase-free DNase Set (QIAGEN, 79254)
- QIAshredder (QIAGEN, 79654)
- β-mercaptoethanol (β-ME; Sigma- Aldrich, M6250-100)
- Ethanol (Fisher Scientific, 10437341)
- Nuclease-free water (Promega, P1195)
- DNAse/ RNAse free 0.5 mL microfuge tubes (Fisher Scientific, 11916955)

- DNAse/ RNAse free 1.5 mL microfuge tubes (Fisher Scientific, 11926955)

Protocol:

1. Prepare all the reagents and materials needed for RNA extraction:
    a. Prepare lysis buffer by adding 10 µl of β-ME per 1 ml of buffer RLT in a fume hood;
    b. Warm up TE, media and PBS at 37 °C;
    c. Prepare DNase I incubation mix by adding 10 µl of DNase I to a 70 µl of buffer RDD;
    d. Prepare lysis buffer and DNase I incubation mix according to the number of samples.
2. Remove media and wash cells with 1 ml of sterile and warm PBS.
3. Detach cells by adding 0.5 ml of TE and incubate for 2 min at 37 °C.
4. Neutralise TE by adding 0.75 ml of warm, fresh media and transfer the content to a DNAse/RNAse free eppendorf.
5. Perform cell count using scepter.
6. Centrifuge cell suspension at 300 g for 5 min.
7. Completely aspirate the supernatant and loosen the cell pellet thoroughly by flicking the tube.
8. Add 350 µl buffer RLT with β-ME and pipet to mix.
9. Homogenise the lysate by pipetting the lysate directly into a QIAshredder spin column placed in a 2 ml collection tube and centrifuge for 2 min at full speed.
10. Discard QIAshredder spin column and add 350 µl of 100 % ethanol to the homogenised lysate (inside the collection tube) and mix well by pipetting.
11. Transfer up to 700 µl of the sample to an RNeasy spin column placed in a 2 ml collection tube. Centrifuge at 11000 rpm for 15 sec. Discard collection tube.
12. Add 350 µl buffer RW1 to the spin column. Centrifuge at 11000 rpm for 15 sec. Discard collection tube.
13. Add 80 µl of DNase I incubation mix directly to the spin column membrane and place on the bench top (20 – 30 °C) for 15 min.
14. Add 350 µl buffer RW1 to the spin column. Centrifuge at 11000 rpm for 15 sec. Discard collection tube.
15. Add 500 µl buffer RPE to the spin column and centrifuge at 11000 rpm for 15 sec. Discard collection tube.
16. Add 500 µl buffer RPE to the spin column and centrifuge at 11000 rpm for 2 min. Discard collection tube.
17. Place the spin column in a new 2 ml collection tube and centrifuge at full speed for 1 min. Discard collection tube.
18. Place the spin column in a new 1.5 ml collection tube and add 50 µl of RNase-free water directly to the spin column membrane. Centrifuge at 11000 rpm for 1 min to elute RNA.
19. Make four 10 µl aliquots of RNA and two 3 µl aliquots for RNA integrity and for measuring RNA concentration and purity. Store RNA at -80 °C.

RNA concentration – NanoDrop

Materials/Reagents:

- RNA samples: TAN2A1 P4 & PD2A2 P4
- Distilled water
- Lens cleaning tissues 80mm x 100mm (Fisher Scientific, 11507362)
- NanoDrop 2000c (Thermo Scientific, UK)
- Filter-tips (P10; Fisher Scientific, 12639591)

Protocol:

1. Switch on NanoDrop 2000c and software – NanoDrop 2000.
2. Clean bottom pedestal by raising the sampling arm and pipetting 2 µl of distilled water. Lower the sampling arm and leave for two minutes.
3. Raise sampling arm and wipe the distilled water from the upper and lower pedestals using a dry, lint-free laboratory wipe.

4. Select Nucleic acid application from the main menu. If the wavelength verification window appears, ensure that the arm is down and click OK.
5. Select the type of sample to be measured from the Type drop-down list (RNA will appear in purple).
6. Choose the concentration units (ng/µl) from the drop-down list adjacent to the colour coded concentration box.
7. Perform a blank by pipetting 1 µl of distilled water into the bottom pedestal, lower the arm and click the Blank button.
8. Wipe out the water from both upper and lower pedestals.
9. Enter a sample ID in the appropriate field and then pipette 1 µl of RNA sample into the bottom pedestal. Press measure.
10. Between each sample, wipe both pedestals and load distilled water to prevent sample carryover. Wipe again using a lens cleaning tissue.
11. After measuring all samples, pipette 2 µl of distilled water into the bottom pedestal and leave it for 10 seconds. Wipe the upper and lower pedestals using a lens cleaning tissue.
12. Switch off software and NanoDrop.

RNA quality control using Agilent Bioanalyzer

Materials/Reagents:

- RNA samples: TAN2A1 P4 & PD2A2 P4
- Agilent 2100 Bioanalyzer (Agilent Technologies, UK)
- Agilent RNA 6000 Nano Kit (Agilent Technologies, 5067-1511)
- Nuclease-free water (Promega, P1195)
- RNaseZAP (Fisher Scientific, 10708345)
- Heating block
- DNAse/ RNAse free 1.5 mL microfuge tubes (Fisher Scientific, 11926955)
- DNAse/ RNAse free 0.5 mL microfuge tubes (Fisher Scientific, 11916955)

Protocol:

1. Preparing the RNA ladder after arrival:
    a. After reagent kit arrival, pipette the ladder in RNase-free vial;
    b. Heat denature it for 2 min at 70 °C in a hot block;
    c. Immediately cool down the vial on ice for at least 5 minutes;
    d. Prepare aliquots in RNase-free vials with the required amount for a typical daily use;
    e. Store aliquots at -80 °C;
    f. Before use, thaw ladder aliquots and keep them on ice (avoid extensive warming upon thawing process).
2. Before beginning the chip preparation protocol, ensure that the chip priming station and the bioanalyzer are set up and ready to use:
    a. Replace the syringe at the chip priming station with each new kit:
        i. Unscrew the old syringe from the lid of the chip priming station;
        ii. Release the old syringe from the clip. Discard the old syringe;
        iii. Remove the plastic cap of the new syringe and insert it into the clip;
        iv. Slide it into the hole of the luer lock adapter and screw it tightly to the chip priming station.
    b. Adjust the base plate of the chip priming station:
        i. Open the chip priming station by pulling the latch;
        ii. Using the screwdriver, open the screw on the underside of the base plate;
        iii. Lift the base plate and insert it again in position. Retighten the screw.
    c. Adjust the syringe clip at the chip priming station:
        i. Release the level of the clip and slide it up to the top position.
    d. Adjust the bioanalyzer's chip selector:

i. Open the lid of the bioanalyzer and make sure that the electrode cartridge is inserted in the instrument. If not, open the latch, remove the pressure cartridge and insert the electrode cartridge;
ii. Remove any remaining chip and adjust the chip selector to the position.

e. Set up the vortex mixer by adjusting the speed knob to 2400 rpm;
f. Start the software (2100 Expert) before the chip is loaded.

3. Decontaminating the electrodes:
    a. Slowly fill one of the wells of an electrode cleaner with 350 µl RNaseZAP;
    b. Open the lid and place electrode cleaner in the Agilent 2100 bioanalyzer;
    c. Close the lid and leave it closed for about 1 minute;
    d. Open the lid and remove the electrode cleaner. Label the electrode cleaner and keep it for future use. You can reuse the electrode cleaner for all 25 chips in the kit;
    e. Slowly fill one of the wells of another electrode cleaner with 350 µl RNase-free water;
    f. Place electrode cleaner in the Agilent 2100 bioanalyzer;
    g. Close the lid and leave it closed for about 10 seconds;
    h. Open the lid and remove the electrode cleaner. Label it and keep it for further use;
    i. Wait another 10 seconds for the water on the electrodes to evaporate before closing the lid.
4. Preparing the gel:
    a. Allow the reagents to equilibrate to room temperature for 30 minutes before use;
    b. Place 550 µl of Agilent RNA 6000 Nano gel matrix into the top receptacle of a spin filter;
    c. Place the spin filter in a microcentrifuge and spin for 10 minutes at 1500 g ± 20% at room temperature (for eppendorf microcentrifuge, this corresponds to 4000 rpm);
    d. Aliquot 65 µl filtered gel into 0.5 ml RNase-free microfuge tubes that are included in the kit. Store the aliquots at 4 °C and use them within one month of preparation.
5. Preparing the Gel-Dye Mix:
    a. Vortex RNA 6000 Nano dye concentrate for 10 seconds and spin down;
    b. Add 1 µl of RNA 6000 Nano dye concentrate to a 65 µl aliquot of filtered gel;
    c. Cap the tube, vortex thoroughly and visually inspect proper mixing of the gel and dye;
    d. Store the dye concentrate at 4 °C in the dark again;
    e. Spin tube for 10 minutes at room temperature at 13000 g (for eppendorf microcentrifuge corresponds to 14000 rpm). Use prepared gel-dye mix within one day.
6. Loading the Gel-Dye Mix:
    a. Before loading the gel-dye mix, make sure that the base plate of the chip priming station is in position (C) and the adjustable chip is set to the top position;
    b. Take a new RNA Nano chip out of its sealed bag;
    c. Place the chip on the chip priming station;
    d. Pipette 9 µl of the gel-dye mix at the bottom of the well-marked “G” and dispense the gel-dye mix;
    e. Set the timer to 30 seconds, make sure that the plunger is positioned at 1 ml and then close the chip priming station. The lock of the latch will click when the priming station is closed correctly;
    f. Press the plunger of the syringe down until it is held by the clip;
    g. Wait for exactly 30 seconds and then release the plunger with the clip release mechanism;
    h. Visually inspect that the plunger moves back at least to the 0.3 ml mark;
    i. Wait for 5 seconds, then slowly pull back the plunger to the 1 ml position;
    j. Open the chip priming station;
    k. Pipette 9 µl of the gel-dye mix in each of the wells marked “G”.
7. Loading the RNA 6000 Nano marker:
    a. Pipette 5 µl of the RNA 6000 Nano marker into the well-marker with the ladder symbol and each of the 12 samples wells.
8. Loading the ladder and samples:
    a. Before use, thaw ladder aliquots and keep them on ice (avoid extensive warming upon thawing process);
    b. To minimise secondary structure, heat denature (70 °C for 2 minutes) the samples before loading on the chip in a hot block;

c. Pipette 1 µl of each sample into each of the 12 samples wells;
d. Pipette 1 µl of the RNA ladder into the well marked with the ladder symbol;
e. Set the timer for 60 seconds;
f. Place the chip horizontally in the adapter of the IKA vortex mixer and make sure not to damage the buldge that fixes the chip during vortexing. If there is liquid spill at the top of the chip, carefully remove it with a tissue;
g. Vortex for 60 seconds at 2400 rpm (place between 2000 rpm and 2400 rpm).

9. Inserting a chip in the Agilent 2100 bioanalyzer:
    a. Open the lid of the Agilent 2100 bioanalyzer;
    b. Check that the electrodes cartridge is inserted properly and the chip selector is in position (1);
    c. Place the chip carefully into the receptacle. The chip fits only one way;
    d. Carefully close the lid. The electrodes in the cartridge fit into the wells of the chip;
    e. The 2100 expert software screen shows that the chip is inserted. Close the lid by displaying the chip icon at the top left of the *Instrument* context. Make sure that the run starts within 5 minutes.
10. Starting the chip run:
    a. Make sure that the Bioanalyzer is connected to line power and connected to the PC;
    b. Turn on the line switch at the rear of the instrument. The status LED at the front of the bioanalyzer should light up;
    c. To start the 2100 expert software on the connected PC, go to desktop and click the 2100 expert icon;
    d. Make sure that the Bioanalyzer has been detected before continuing;
    e. In the *Instrument* context, select the appropriate assay from the *Assay* menu (Eukaryote RNA Nano Series II for the use of RNA 6000 Nano Chips);
    f. The chip should be detected if this is not the case open lid and repeat;
    g. When the chip is detected, the image on the instrument tab changes to a chip;
    h. Accept the current *File Prefix* or modify it;
    i. Click the *Start* button in the upper right of the window to start the chip run.
11. After the chip run is finished, remove the chip from the receptacle of the bioanalyzer and dispose of it according to good laboratory practices. Save run and export the data.
12. Cleaning up after an RNA 6000 Nano Chip run:
    a. Slowly fill one of the wells of the electrode cleaner with 350 µl RNase-free water;
    b. Open the lid and place the electrode cleaner in the Agilent 2100 bioanalyzer;
    c. Close the lid and leave it closed for about 10 seconds;
    d. Open the lid and remove the electrode cleaner;
    e. Wait another 10 seconds to allow the water on the electrode to evaporate before closing the lid.

cDNA synthesis

Materials/Reagents:

- RNA template: TAN2A1 P4 & PD2A2 P4
- High Capacity cDNA Reverse Transcription Kit (Applied Biosystems, 4368814)
- Thermal cycler: G-STORM
- Low-Profile 0.2 ml 8-Tube Strips without Caps (Bio-Rad, TLS-0801)
- RNaseZAP (Fisher Scientific, 10708345)
- Optical Flat 8-Cap Strips (Bio-Rad, TCS-0803)
- Nuclease-free water (Promega, P1195)
- DNAse/ RNAse free 0.5 mL microfuge tubes (Fisher Scientific, 11916955)
- DNAse/ RNAse free 1.5 mL microfuge tubes (Fisher Scientific, 11926955)

Protocol:

1. Clean hood with 70% IPA followed by RNaseZAP and place all the reagents/material necessary for the procedure inside the hood.
2. Leave for 30 minutes under UV light.
3. Allow kit components and RNA samples to thaw on ice.
4. Prepare the RNA samples according to the following table.
    a. TAN2A1 P4

Sample no.	Sample	Concentration (ng/µl)	No. tubes used	No. reactions	Volume of RNA (µl)	Volume of water (µl)
2	- TGF-β1	58.7	1	1	8.5	1.5
3	- TGF-β1	66.5	1	1	7.5	2.5
4	+ TGF-β1	83.9	1	1	6.0	4.0
5	+ TGF-β1	93.1	1	1	5.4	4.6

    b. PD2A2 P4

Sample no.	Sample	Concentration (ng/µl)	No. tubes used	No. reactions	Volume of RNA (µl)	Volume of water (µl)
1	- TGF-β1	79.6	1	1	6.3	3.7
3	- TGF-β1	69.8	1	1	7.2	2.8
4	+ TGF-β1	93.0	1	1	5.4	4.6
5	+ TGF-β1	113.6	1	2	4.4	5.6

5. Prepare RT master mix on ice.

Components	Volume (µl)	
	Per reaction	Samples (9 reactions + 2 extra)
10X RT buffer	2.0	22.0
25X dNTP Mix (100 mM)	0.8	8.8
10X RT random primers	2.0	22.0
MultiScribe™ Reverse Transcriptase	1.0	11.0
Nuclease-free H_2O	4.2	46.2
TOTAL	10.0	110.0

6. Prepare the cDNA RT reactions by pipetting 10 µl 2X RT master mix into individual PCR tubes and by pipetting 10 µl of RNA samples (at 50 ng/µl) into each tube and mix gently. Add 30 µl of RNase-free water to all tubes to make a total volume of 50 µl.
7. Briefly, centrifuge the tubes to spin down the contents and to eliminate any air bubbles.
8. Place the tubes on ice until you are ready to load the thermal cycler.
9. Open the program named as “cDNA AB Marta” in the thermal cycler and confirm that the conditions are the same as described in the following table.

	Step 1	Step 2	Step 3	Step 4
Temperature (°C)	25	37	85	4
Time (min)	10	120	5	∞

10. Load the reactions into the thermal cycler.
11. Start the reverse transcription run.
12. After the run, the cDNA can be stored at 4 °C for short-term storage (up to 24 hours) or at -20 °C for long-term storage (in 25 µl aliquots).

Real-time PCR

Materials/Reagents:

- cDNA samples: TAN2A1 P4 & PD2A2 P4 & MCF-7 P5
- Nuclease-free water (Promega, P1195)
- DNAse/ RNAse free 0.5 mL microfuge tubes (Fisher Scientific, 11916955)
- DNAse/ RNAse free 1.5 mL microfuge tubes (Fisher Scientific, 11926955)
- QuantiTect® SYBR® Green PCR Kit (QIAGEN, 204143)
- DNA Away (Fisher Scientific, 10223471)
- QuantiTect® Primer Assay for human ESR1 (ER-α; QIAGEN, QT00044492)
- QuantiTect® Primer Assay for EIF4A2 (QIAGEN, QT00079226)
- QuantiTect® Primer Assay for TOP1 (QIAGEN, QT00068915)
- CFX Connect Real-time PCR detection system (Bio-Rad, UK)
- Hard-Shell® Low-Profile Thin-Wall 96-Well Skirted PCR Plates (Bio-Rad, HSP9645)
- Optically Clear Heat Seal (Bio-Rad, 1814030)
- PX1™ PCR Plate Sealer (Bio-Rad, UK)

Protocol:

1. Clean hood with 70 % IPA followed by DNA Away and place all the reagents/materials necessary for the procedure inside the hood. Leave for 30 minutes under UV light.
2. Thaw 2X QuantiTect SYBR Green PCR master mix, 10X QuantiTect Primer Assay, cDNA template and RNase-free water on ice. Mix the individual solutions.
3. Prepare reaction mix for each gene (ERα, EIF4A2 and TOP1) and place it on the ice.

Component	Volume (µl)		Final Concentration
	Per reaction	30 reactions + 5 extras	
2X QuantiTect SYBR Green PCR master mix	2.5	87.5	1X
Primer Mix	0.5	17.5	1X
cDNA template	0.6	-	≤ 500 ng/reaction
RNase-free water	1.4	49.0	-
TOTAL	5.0	154.0	-

4. Prepare four standard dilutions (from neat to 1/1000), by adding 10 µl of nuclease-free water to each tube (except on neat sample). Add 1 µl of neat sample to 1/10 dilution, homogenise and spin down. Perform the same step for the other dilutions.
    a. Prepare the standard dilutions for the ERα by using the cDNA from MCF7 cells, as described above.
5. Add 15 µl of reaction mix and 2.25 µl of cDNA sample/standard dilution to each labelled tube. Briefly, mix each sample and spin down.
6. Add 5 µl of reaction mix with the sample to the 96 well plate.
7. Seal PCR plate using the PX1™ PCR Plate Sealer (180 °C) for 3 seconds.
8. Spin down 96-well plate for 2 min at 2000 rpm.
9. Program the CFX Connect real-timer cycler and start qPCR run.
10. Perform a melting curve analysis of the PCR products (from 60 °C to 95 °C).

Step	Time	Temperature
Enzyme activation	15 min	95 °C
Denaturation	15 s	94 °C
Annealing	30 s	55 °C
Extension	30 s	72 °C
Number of cycles	40	

Representative 96-well plate layout:

Plate Layout used for qPCR: Estrogen receptor												
	1	2	3	4	5	6	7	8	9	10	11	12
A	Std neat	Std 1/100	TA +	NTC	Std neat	Std 1/100	TA +	NTC	Std neat	Std 1/100	TA +	NTC
B	Std neat	Std 1/1000	TA +	NTC	Std neat	Std 1/1000	TA +	NTC	Std neat	Std 1/1000	TA +	NTC
C	Std neat	Std 1/1000	PD -	NTC	Std neat	Std 1/1000	PD -	NTC	Std neat	Std 1/1000	PD -	NTC
D	Std 1/10	Std 1/1000	PD -	- RT	Std 1/10	Std 1/1000	PD -	- RT	Std 1/10	Std 1/1000	PD -	- RT
E	Std 1/10	TA -	PD -	-RT	Std 1/10	TA -	PD -	-RT	Std 1/10	TA -	PD -	-RT
F	Std 1/10	TA -	PD +	-RT	Std 1/10	TA -	PD +	-RT	Std 1/10	TA -	PD +	-RT
G	Std 1/100	TA -	PD +		Std 1/100	TA -	PD +		Std 1/100	TA -	PD +	
H	Std 1/100	TA +	PD +		Std 1/100	TA +	PD +		Std 1/100	TA +	PD +	
	ERα				EIF4A2				TOP1			

A.2 Immunocytochemistry

A.2.1 Example of a detailed protocol used for ICC

Seeding into 6 well plates

Materials/Reagents:

- Cell line: TAN2A1 P5 & PD3B1 P4
- Complete media used: DMEM F-12 + Glutamax®: (Invitrogen Gibco, 31331093) supplemented with 10% FBS (Invitrogen Gibco, 10270106) 1% Penicillin-Streptomycin (Invitrogen Gibco, 15070063)
- Phosphate buffered saline (PBS; Fisher Scientific, 11510546)
- 0.25% Trypsin - EDTA (TE; Fisher Scientific, 11560626)
- Transforming growth factor-β1 human (TGF-β1; Sigma-Aldrich, T7039-2UG) – 5 ng/ml
- Scepter™ + 60 µm sensors (Millipore)
- 2 x 6 well plate (NUNC, Fisher Scientific, 10469282)
- Ethanol (Fisher Scientific, 10437341)
- Coverslips (Fisher Scientific, 12312128)
- Forceps (Fisher Scientific, 12740926)

Protocol:

1. In a sterile 6 well plate, add 2 ml of 100% ethanol and place coverslips inside the well that contains 100% ethanol for 1 min.
2. Transfer the sterile coverslips to the empty wells and place them vertically and left to dry (10-15 min).
3. Once dried, transfer the coverslip to the new 6 well plate and add 2 ml of media to each well. Make sure there is no remain ethanol.
4. Remove bubbles present on the underside of the coverslip by pushing the coverslip with a pipette into the surface.
5. Incubate plates at 37 °C for 2 hours.
6. Cells were grown under normal conditions in the T75 flask.
7. Cells detached and neutralised as previously described (“Basic Cell culture techniques”, page 4, Book no. 1).
8. Perform cell counting using Scepter.
9. Dilute or concentrate cell suspension to the desired concentration.
10. Remove plates from the incubator and remove bubbles underneath the coverslip with a pipette.
11. Remove media from wells and gently add 2 ml of cell suspension at 2.5 x 10^4 cells/well.
12. Incubate plates at 37 °C, 5% CO_2 overnight.
13. On the next day, remove media from wells and add 2 ml of fresh media or 2 ml of media containing 5 ng/ml TGF-β1 to both plates, as indicated in the plate layout below.
14. Incubate plate at 37 °C, 5% CO_2 for 72 hours.

		1	2	3
Control	A	2.5 x 10^4	2.5 x 10^4	2.5 x 10^4
TGF-β1 (5 ng/ml)	B	2.5 x 10^4	2.5 x 10^4	2.5 x 10^4

ICC: α-SMA staining

Materials/Reagents:

- Phosphate buffered saline (PBS; Fisher Scientific, 11510546)
- Methanol (at -25 °C; Fisher Scientific, 10284580)
- Hydrophobic pen (Invitrogen, 008877)
- Primary antibody: Monoclonal anti-ASMA produced in mouse - diluted to 1:1,000 in PBS (Sigma-Aldrich, A5228)
- Secondary antibody: Donkey anti-mouse IgG Ab, FITC conjugate – Diluted to 1:250 in PBS (Millipore, AP192F)
- Mounting medium containing PI (Vectorlabs, VECTASHIELD, H-1200)
- Glass slides (Fisher Scientific, 12352108)
- Blocking solution: 10% donkey serum (Millipore, S30-100ML) in PBS
- Zeiss LSM 510 confocal microscope
- Humidified chamber
- Forceps (Fisher Scientific, 12740926)

Protocol:

1. Wash coverslip removed from the well in a beaker containing PBS.
2. Fix cells on 6 well plate containing ice-cold methanol (-25 °C) for 10 seconds.
3. Wash coverslip in a beaker containing PBS and repeat this step again in a second beaker containing PBS. Remove excess of PBS with an absorbent paper.
4. Place coverslip in a glass slide facing (side containing cells) up and left to dry.
5. Make a contour with a hydrophobic pen around each coverslip.
6. Add 50 µl of blocking solution by spreading evenly over the coverslip and incubate 60 min at room temperature in a humidified chamber.
7. Add 50 µl of primary antibody (1:1,000 diluted in PBS) by spreading evenly over the coverslip and incubate 2 hours at room temperature in a humidified chamber.
8. Wash coverslip three times with PBS by adding 1 ml over on one of the corners of the coverslip.
9. Add 50 µl of secondary antibody (1:250 diluted in PBS) by spreading evenly over the coverslip and incubate 2 hours at room temperature in a humidified chamber in the dark.
10. Wash coverslip three times with PBS by adding 1 ml over on one of the corners of the coverslip.
11. Add a small drop of mounting medium with PI in a new glass slide and place the coverslip facing (side containing cells) down.
12. Observed glass slides under the confocal microscope in the dark. Take images of three random areas in each coverslip.
13. Keep glass slides at 4 °C wrapped in foil.

A.3 Immunohistochemistry

A.3.1 Example of a detailed protocol used for IHC

Materials:

- Samples (dehydrated and stored at -80 ˚C)
    - 2 slides (serial sectioning) from:
        - PD10/PD5/PD7
        - TAC3a
- OCT Compound (tissue freezing medium; VWR, 361603E)
- Superfrost Plus Gold slides (Fisher Scientific, 11847732)
- Scalpel (Fisher Scientific, 12397999)
- Specimen freezing moulds (Fisher Scientific, 6401015)
- Marigold Insulator KTI Gloves (Buck & Hickman, 321804)
- C35 cryostat blades (VWR, FEAT207500003)
- Cutting heads, blade holder, brushes
- Cover slips (Fisher Scientific, MNJ-350-070P)
- Hydrophobic pen (Invitrogen, 008877)
- Phosphate buffered saline (PBS; Fisher Scientific, 11510546)
- Wash Buffer – PBS
- Blocking Buffer – 10% donkey serum (Millipore, S30-100ML) in PBS + 0.1% Triton X 100
- Anti-adenosine A2B receptor antibody rabbit polyclonal (Abcam, ab188796) – **1:100**
- Anti-adenosine A1 receptor antibody rabbit monoclonal (Abcam, ab124780) – **1:100**
- Donkey anti-rabbit IgG Ab, FITC conjugate (Millipore, UK; AP182F) - **1:250**
- Mounting medium containing PI (Vectorlabs, VECTASHIELD, H-1200)
- Humidified incubation chamber
- Zeiss LSM 510 confocal Microscope
- Cryostat (Bright, Model OTF)

Protocol:

- **Sectioning:**

1. Turn on cryostat [on ; off ; off ; off ; on].
2. Turn demist and light on, until end of the protocol.
3. Place blade holder centrally in chamber and blade within the holder, lock in place. Allow cooling.
4. Turn thickness adjuster to 15-20 µm.
5. Turn outside dial to the lowest point and retract sectioning arm by turning the dial clockwise.
6. Place sample in the chamber (minimising time exposed to RT). Push sample out.
7. Place OCT compound in the middle of cutting head, stick sample on top, allow to freeze.
8. Place OCT compound on side of the sample to ensure firm attachment of sample to mould.
9. Allow freezing.
10. Place cutting head on arm and tighten, ensuring the sample is square to blade (also ensure bottom side of the frozen block has at least some OCT between edge and sample).
11. Adjust cutting bed towards the sample, ensuring they do not come into contact.
12. Turn outside dial clockwise until the first full flat cut.
13. Adjust anti-roll guide plate so that it is square to the blade, with both sides of the plate in contact with the blade and the edge of the plate, when viewed from above, is on or just before blade end (use blue lines as guides).
14. Start cutting procedure.
15. Use a smooth and moderate circular motion when cutting, when a section is cut which is deemed satisfactory, roll over anti-roll plate onto the blade.
16. Test whether the section is attached to plate, if not, heat plate with a finger and turn plate back.
17. Place glass slide, face down onto tissue, hovering over until attached.

18. Repeat until glass slide is full, brushing away residual sample and OCT from the blade, sample and anti-roll plate.
19. During cutting, if cutting is not functioning properly, the most common problems are:
    a. Dull blade – move blade along or, if necessary, replace with new blade;
    b. Anti-roll plate is misaligned – realign;
    c. Chamber or specifics are not cool – wait 2-3 minutes;
    d. Chamber arm requires retracting – retract as detailed previously.
20. When finished, remove the blade, unscrew and remove blade holder.
21. With a scalpel, carefully cut off OCT attaching the sample to cutting head.
22. Put sample back in the mould, ensuring the sample is not heated and store at -80 °C.
23. Place cutting heads on top of the left shelf.
24. Turn of demist and light.
25. Leave samples to dry, protected from dust deposition, for 3 hours.

- **Staining:**

1. Once dried, mark the border of the slide with hydrophobic pen and add 200 µl of blocking buffer (10% donkey serum in 0.1% Triton X 100 in PBS), ensuring entire slide is covered and tissues are not dislodged. Incubate for 90 minutes at RT in a humidified chamber.
2. Make primary antibody dilutions as described in the materials section in PBS and add 150 µl to each slide ensuring entire slide is covered and tissues are not dislodged. Incubate overnight at 4 °C.
3. Remove antibody solution and wash slides 3 times with PBS by adding 600 µl of PBS to slide and discarding – tip-off solution from slides onto paper towels and dry edges of slides, ensuring entire slide is covered and tissues are not dislodged.
4. Make secondary antibody dilution at 1:250 in PBS and add 150 µl to each slide ensuring entire slide is covered and tissues are not dislodged. N.B. – Ensure correct type of antibody (mouse or rabbit) is used. Incubate for 2 hours at RT in the dark.
5. Remove antibody solution and wash slides 3 times with PBS by adding 600 µl of PBS to slide and discarding, ensuring entire slide is covered and tissues are not dislodged.
6. Add one drop of mounting media with PI and place coverslips on carefully.
7. Slides can be stored in the dark at 4°C or viewed immediately.

- **Confocal microscopy:**

1. Uncover microscope and switch remote on and lamp power on, turn on pc if necessary.
2. Open LSM510 – Scan new images/start expert mode.
3. Open menus laser, micro, configuration and scan and switch lasers on.
4. Set scan control mode to 2048/1024, 12 bit and fw/rw.
5. Select Vis to manually select an area to capture. Once selected, turn off reflected light and start Fast XY and adjust channel settings for the best image.
6. Select Z-stack in the Scan control menu and select Mark First/last.
7. Adjust image focus to the point where target fluorescence is beginning to decrease and select mark first.
8. Then focus the image (reverse) all the way through the optimum image until the fluorescence is beginning to decrease and mark last.
9. Ensure the number of stacks to be taken is not exaggerated as this will not massively improve the quality of the image and will take longer. Ensure transparency is at maximum and X:Y:Z is set to 1:1:1.
10. View image by selecting 3D projection and save file(s) as required with scale overlay.
11. Shut down microscope by performing start-up procedure in reverse.

A.4 In-Cell Western

A.4.1 Example of a detailed protocol used for ICW

Materials:

- Cell line used: TAN2A2 P4 – SD = $5x10^4$ cells/ml
- Nunc® 96 well optical flat bottom black microplates (Fisher Scientific, 10281092)
- Complete media used: DMEM F-12 + Glutamax®: (Invitrogen Gibco, 31331093) supplemented with 10% FBS (Invitrogen Gibco, 10270106) 1% Penicillin-Streptomycin (Invitrogen Gibco, 15070063)
- 0.25% Trypsin - EDTA (TE; Fisher Scientific, 11560626)
- DRAQ5 (Biostatus, DR50200) – 1:1,000
- Anti-ASMA antibody raised in mouse (Sigma-Aldrich, A5228) –1:3,000
- 800nm IRdye donkey anti-mouse (Li-COR, 926-32212) –1:500
- Transforming growth factor-β1 human (TGF-β1; Sigma-Aldrich, T7039-2UG) – 5 ng/ml
- Fixing media – 4% paraformaldehyde in PB
- PBS (Fisher Scientific, 11510546)
- Permeabilisation buffer – 0.1% Triton X 100 (Sigma-Aldrich, T8787-100ml) in PBS
- Blocking buffer – 5% donkey serum (Millipore, S30-100ML) in permeabilisation buffer
- Wash buffer – 0.1% tween 20 (Sigma-Aldrich, P1379-250ML) in PBS

Protocol:

1. Cells were grown under normal conditions in T75 Flasks.
2. Cells detached and neutralised as previously described (“Basic Cell culture techniques”, Book 1 pp 1-4).
3. Perform cell counting using Scepter® and dilute to a concentration of $5x10^4$ cells/ml.
4. Add 200 µl of sterile 1X PBS to indicated wells and 100 µl of cell suspension to the indicated wells.
5. Incubate plates at 37°C, 5% CO_2 overnight.
6. Remove media and replace with 200 µl complete media or 200 µl complete media with TGF-β1 at 5 ng/ml and incubate plates at 37°C, 5% CO_2 for 72 hours.
7. Remove media and add 150 µl of fixing solution and incubate for 20 minutes at room temperature.
8. Remove fixing solution and wash three times with 0.1% Triton X 100 in PBS by adding 150 µl to each well and incubating at room temperature for 5 minutes on a plate shaker per wash.
9. Remove wash buffer and 150 µl of blocking buffer and incubate for 90 minutes at RT.
10. Remove blocking buffer, add 50 µl of 1:3,000 primary antibody solution, diluted in PBS to indicated wells and incubate for 2 hours at RT.
11. Wash three times with 0.1% tween 20 in PBS, adding 150 µl to each well and incubating at room temperature for 5 minutes per wash.
12. Add 50 µl secondary antibody solution to all wells at 1:500 with 1:1,000 DRAQ5 in PBS.
13. Incubate for 60 minutes at RT, protect plate from light.
14. Wash three times with 0.1% tween 20 in PBS and once with PBS, as previously described and remove wash solution completely from wells, turn the plate upside down and tap on paper towels.
15. Clean underside of plate and scanner with paper and scan immediately at both the 700 and 800nm channels; Settings: Resolution = 169 µm; Quality = medium; Focus offset = 3 mm; Intensity = 5.
16. Analysis, including z-factor calculation, was performed using Microsoft® Excel® 2013.

Representative 96-well plate layout:

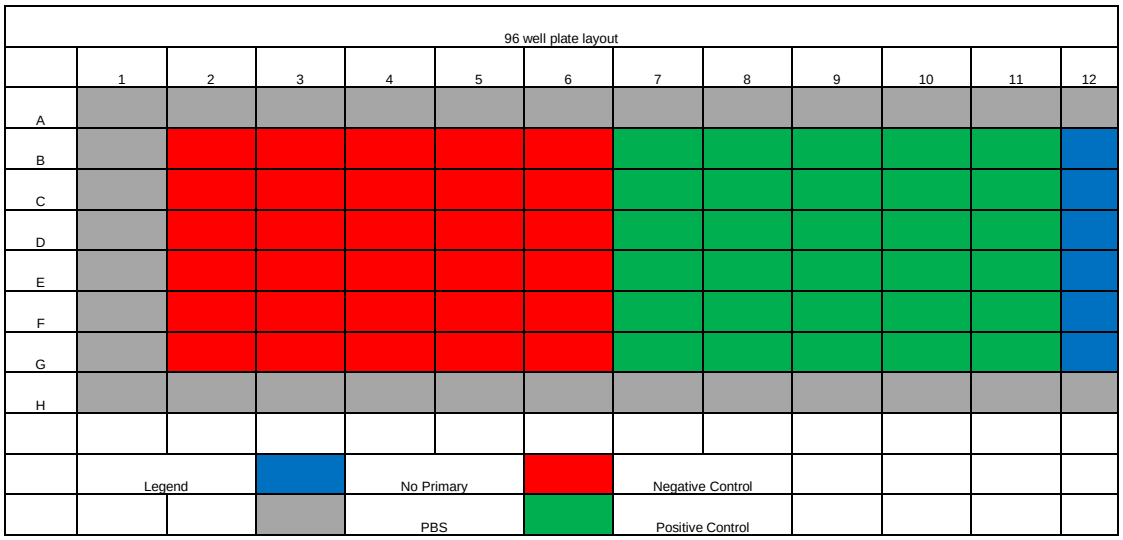

A.4.2 Buffer recipes used in ICW

Table 7-1: Recipe for fixing solution (4% paraformaldehyde).

Chemical	Location	Volume/Mass
8% Paraformaldehyde	Chemical cupboard	100 ml
0.2M Phosphate buffer	Chemical cupboard	100 ml

Table 7-2: Recipe for permeabilisation buffer (0.1% Triton X-100 in PBS).

Chemical	Supplier & Catalogue number	Location	Final concentration	Volume/Mass
1X PBS	Fisher Scientific, 11510546	Chemical cupboard	1X	2 tablets
Triton X-100	Sigma-Aldrich; T8787-100ML	Chemical cupboard	0.1%	1 ml
Distilled water	-	Prep room	-	1L

Table 7-3: Recipe for blocking buffer (5% donkey serum in permeabilisation buffer).

Chemical	Supplier & Catalogue number	Location	Final concentration	Volume/Mass
Permeabilisation buffer (0.1% Triton X-100 in PBS)	See Table 7-2	See Table 7-2	See Table 7-2	19 ml
Donkey serum	Millipore, S30-100ML	Freezer FZ-01	5%	1 ml

Table 7-4: Recipe for wash buffer.

Chemical	Supplier & Catalogue number	Location	Final concentration	Volume/Mass
1X PBS	Fisher Scientific, 11510546	Chemical cupboard	1X	2 tablets
Tween 20	Sigma-Aldrich; P1379-250ML	Chemical cupboard	0.1%	1 ml
Distilled water	-	Prep room	-	1L

A.4.3 Preparation of Phosphate Buffer and Paraformaldehyde

Materials/Reagents:

- For 8% paraformaldehyde:
  - Open neck 3-5L container
  - Heater/Mixer base
  - Filter
  - 2M Sodium hydroxide (NaOH; Sigma-Aldrich, S5881-500G)
  - Paraformaldehyde (VWR; 28794.295)
  - Distilled water
- For phosphate buffer (PB):
  - Open neck 3-5L containers
  - Potentiometer
  - Sodium phosphate monobasic monohydrate ($NaH_2PO_4H_2O$; Fisher Scientific, 10754534)
  - Di-sodium hydrogen orthophosphate dodecahydrate ($Na_2HPO_4.12H_2O$; Fisher Scientific, 10656462)
  - Distilled water

Protocol:

1. **For 8% paraformaldehyde:**
   a. Measure 2L in a suitable (3-5L) container and mark level with a pen.
   b. Remove approximately 500 ml into a sterile bottle.
   c. Warm remainder of water to 70 ˚C, stirring with a magnet, within a fume hood.
   d. Add 160 g of paraformaldehyde, ensuring no spillage and minimise the risk of inhalation, wear a mask.
   e. Slowly add sodium hydroxide with a Pasteur pipette until solution clarifies.
   f. Add water to the marker.
   g. Pour into bottles using paper filters and funnels.
2. **For phosphate buffer (PB):**
   a. <u>Solution A – Mosodium phosphate</u>
      i. Measure 1L in 1L bottle and mark level with a pen;
      ii. Remove approximately 200 ml into another bottle;
      iii. Add 27.58 g of monosodium phosphate ($NaH_2PO_4H_2O$) into initial bottle and add water to marked line, mix well;
      iv. If required, make 2L.
   b. <u>Solution B – Disodium phosphate</u>
      i. Measure 2L in suitable container and mark level with a pen;
      ii. Remove approximately 500 ml into another bottle;
      iii. Add 143.26 g of disodium phosphate ($Na_2HPO_4.12H_2O$) into the initial bottle and add water to the marked line, mix well.
   c. <u>Mix solutions</u>
      i. Calibrate potentiometer to pH 7;
      ii. Place container with solution B on mixer with magnet, and place electrode in solution;
      iii. Add Solution A slowly to pH 7.4;
      iv. Pour into 1L bottles and label 0.2M PB with the date.

A.5 Western blot

A.5.1 Example of a detailed protocol used for Western blot

Seeding onto 6 well plates

Materials/Reagents:

- Cell line: TAN1B1 P5, PD1B2 P4
- Complete media used: DMEM F-12 + Glutamax®: (Invitrogen Gibco, 31331093) supplemented with 10% FBS (Invitrogen Gibco, 10270106) 1% Penicillin-Streptomycin (Invitrogen Gibco, 15070063)
- Phosphate buffered saline (PBS; Fisher Scientific, 11510546)
- 0.25% Trypsin - EDTA (TE; Fisher Scientific, 11560626)
- Scepter^{TM} + 60 µm sensors (Millipore, UK)
- 4 x 6 well plate (NUNC, Fisher Scientific, 10469282)
- Transforming growth factor-β1 human (TGF-β1; Sigma-Aldrich, T7039-2UG) – 5 ng/ml

Protocol:

1. Cells were grown under normal conditions in the T75 flask.
2. Cells detached and neutralised as previously described ("Basic Cell culture techniques", page 4, Book no. 1).
3. Perform cell counting using Scepter.
4. Dilute or concentrate cell suspension to the desired concentration.
5. Using a 6 well plate, add 2 ml of cell suspension to all wells at 1.0 x 10^5 cells/well.
6. Incubate plates at 37 °C, 5% CO_2 overnight.
7. On the next day, remove media from wells and add 2 ml of fresh media to indicated wells or 2 ml of media with TGF-β1 at 5 ng/ml, as indicated in the plate layout below.
8. Incubate plate at 37 °C, 5% CO_2 for 72 hours.

TA and PD cells		1	2	3
Control	**A**	1.0 x 10^5	1.0 x 10^5	1.0 x 10^5
TGF-β1 at 5 ng/ml	**B**	1.0 x 10^5	1.0 x 10^5	1.0 x 10^5

Preparation of lysate from cell culture

Materials:

- Tris base (Fisher Scientific, 10376743)
- Glycerol (Fisher Scientific, 10579570)
- Sodium dodecyl sulfate (SDS; Fisher Scientific, 10552785)
- Sodium deoxycholate (Sigma-Aldrich, D6750-10G)
- NP-40 Surfact-Amps detergent solution (Fisher Scientific, 13434269)
- EDTA (Fisher Scientific, 10335460)
- Sodium fluoride (NaF; Fisher Scientific, 10742222)
- Sodium pyrophosphate tetrabasic ($Na_4P_2O_7$; Sigma-Aldrich, P8010-500G)
- Sodium orthovanadate (Na_3VO_4; Sigma-Aldrich, S6508-10G)
- Ethylene glycol-bis(2-aminoethylether)-N, N, N', N'-tetraacetic acid (EGTA; Sigma-Aldrich, E4378-10G)
- Sodium chloride (NaCl; Fisher Scientific, 10428420)
- DC Protein Assay kit II (Bio-Rad, 500-0112)
- Triton X-100 (Sigma-Aldrich, T8787-100ML)
- Phosphate buffered saline (Fisher Scientific, 11510546)

- Distilled water
- iMark™ Microplate Absorbance Reader (Bio-Rad, UK)
- Nunclon 0.2mL flat bottom 96 well microplates (Fisher, 10212811)
- Cell scraper (Fisher Scientific, 11597692)
- Aprotinin (Fisher Scientific, 11854101)
- PMSF (Fisher Scientific, 10485015)
- Leupeptin (Fisher Scientific, 10736392)
- Pepstatin A (Fisher Scientific, 10786834)

Protocol:

1. Keep PBS chilled on ice before starting the protocol.
2. Prepare 10 ml of lysis buffer and keep on ice until use.
   a. RIPA buffer

Chemical	Location	Final concentration	Volume/Mass
10% NP-40	Chemical cupboard	1%	1 ml
1 M Tris-HCl, pH 7.4	Fridge FR-01	10 mM	100 µl
1 M NaCl	Chemical cupboard	0.15 M	1.5 ml
0.1 M EGTA	Fridge FR-01	1 mM	100 µl
100 mM EDTA	Fridge FR-01	10 mM	1 ml
100 mM PMSF	Freezer FZ-01	1 mM	100 µl
1 mg/ml Aprotinin	Freezer FZ-01	2 µg/ml	20 µl
10 mg/ml Leupeptin	Freezer FZ-01	2 µg/ml	2 µl
10 mg/ml Pepstatin A	Freezer FZ-01	2 µg/ml	2 µl
0.5 M NaF	Freezer FZ-01	50 mM	1 ml
0.1 M $Na_4P_2O_7$	Freezer FZ-01	20 mM	2 ml
100 mM Na_3VO_4	Freezer FZ-01	100 µM	10 µl
Distilled water	Prep room	-	Adjust to 10 ml

*After 12 hours these reagents become inactive.

b. Tris-Triton buffer

Chemical	Location	Final concentration	Volume/Mass
1 M Tris, pH 7.4	Fridge FR-01	10 mM	100 µl
1 M NaCl	Chemical cupboard	100 mM	1 ml
100 mM EGTA	Fridge FR-01	1 mM	100 µl
Triton X-100	Chemical cupboard	1%	100 µl
Glycerol	Chemical cupboard	10%	1 ml
10% SDS	Chemical cupboard	0.1%	100 µl
10% Sodium deoxycholate	Chemical cupboard	0.5%	500 µl
100 mM EDTA	Fridge FR-01	10 mM	1 ml
100 mM PMSF	Freezer FZ-01	1 mM	100 µl
1 mg/ml Aprotinin	Freezer FZ-01	2 µg/ml	20 µl
10 mg/ml Leupeptin	Freezer FZ-01	2 µg/ml	2 µl
10 mg/ml Pepstatin A	Freezer FZ-01	2 µg/ml	2 µl
0.5M NaF	Freezer FZ-01	1 mM	20 µl
0.1 M $Na_4P_2O_7$	Freezer FZ-01	20 mM	2 ml
100 mM Na_3VO_4	Freezer FZ-01	2 mM	200 µl
Distilled water	Prep room	-	Adjust to 10 ml

*After 12 hours these reagents become inactive.

3. Preparation of lysate from the cell culture:
   a. Switch on the refrigerated centrifuge. Make sure that the centrifuge is at 4 °C.
   b. Inspect cells under the light microscope before starting the protocol.
   c. During cell lysis, work quickly and keep the cells/cell lysates on ice.
   d. Remove medium from wells and wash cells with 1 ml of cold PBS. Keep 6 well- plate on ice throughout.
   e. Scrape cells from the bottom of the well with a plastic cell scraper.
   f. Transfer the cell suspension (from wells exposed to the same conditions) to an eppendorf.
   g. Spin down at 3,000 rpm for 5 minutes at 4 °C to pellet the cells. Discard the supernatant.
   h. Add 300 µl of ice-cold lysis buffer with protease inhibitor cocktail to the cell pellet and leave on ice for 30 minutes. Every 10 minutes briefly vortex samples.
   i. Centrifuge cells at 3,000 rpm for 5 minutes at 4 °C.
   j. Transfer supernatant to a fresh ice-cold eppendorf.
   k. Remove 5 µl of protein for assay. Place the tube on ice.
   l. Aliquot cell lysates (50-100 µl) to avoid repeat freeze/thaw cycles. Store cell lysate at -80 °C.
   m. Store lysis buffer at 4 °C and if reused (after 12 hours) make sure that the four reagents* are added again.
4. Determination of protein concentration:
   a. Prepare working reagent by adding 20 µl of reagent S to each ml of reagent A that will be needed for the run. This working reagent (S + A) is stable for one week even though a precipitate will form after 1 day. If precipitate forms, warm the solution and vortex. Do not pipet the undissolved precipitate, as this will likely plug the tip of the pipet, thereby altering the volume of reagent that is

added to the sample. If samples do not contain detergent, this step can be omitted and simply use reagent A as supplied.

b. Prepare 5 dilutions of a protein standard containing from 1.5 mg/ml to 0.09 mg/ml (1.5 – 0.75 – 0.375 – 0.18 – 0.09 mg/ml). Prepare a standard curve each time the assay is performed. Prepare the standards in the same buffer as the sample. Store the rehydrated protein solution at -20 °C for 6 months in aliquots.
c. Pipet 5 µl of standards and samples (diluted 1 in 3) in duplicate into a clean, dry 96 well plate.
d. Add 25 µl of reagent A (with reagent S) into each well.
e. Add 200 µl reagent B into each well. Gently agitate the plate to mix the reagents. If bubbles form, pop them with a clean, dry pipette tip. Be careful to avoid cross-contamination of sample wells.
f. After 15 minutes, read absorbance at 750 nm using the plate reader. The absorbance will be stable for about 1 hour.
    i. Switch on the microplate reader and switch on software (MPM 6 – desktop).
    ii. Enter the password 00000 to enter the main menu on the screen of the plate reader.
    iii. Open the reading chamber door and insert 96-well plate without a lid. Close the chamber door.
    iv. If using the microplate reader press: MAIN – MEMORY RECALL – PROTOCOL – ENTER – END POINT – FILTER 03-490 nm – FILTER 05-655 nm – ENTER – START. The read-out will be sent to and automatically printed out.
    v. If using the software, make sure that iMark is selected by pressing the button with a green arrow (the third one from the left).
    vi. To prepare the protocol, select the button with a green arrow (the first button from the left). Select endpoint and if two wavelengths are needed select dual and write down the wavelength. If only one wavelength is needed, select single and add the appropriate wavelength.
    vii. Press start read and export data to an excel file.
    viii. Turn off microplate reader (by pressing on/off button for a few seconds) and switch off software.

g. Calculate on excel sheet protein concentrations.
h. If protein concentration is not high enough at the end, it is advised to repeat the procedure with a higher proportion of protease inhibitor cocktail.

Mini gel preparation, SDS-PAGE & Western Blotting

Materials:

- Distilled water
- DL-Dithiothreitol solution (DTT; Sigma-Aldrich, 43816-50ML)
- Electrode with MultiPhor paper (Fisher Scientific, 10586555)
- Any kD™ Mini-PROTEAN® TGX™ Precast Protein Gels (Bio-Rad, 456-9034)
- Heating block
- Hoefer Mini VE Vertical Electrophoresis System
- Lysis buffer inactive: Tris-Triton and RIPA buffer
- Marvel dried skimmed milk powder (Tesco)
- Membrane filter Immobilon-FL transfer membranes 0.45 µm pore size (Fisher Scientific, 10452792)
- Methanol (Fisher Scientific, 10675112)
- Precision Plus Protein™ Dual Color Standards (Bio-Rad, 161-0374)
- Tris-buffered saline, 10X (TBS; Fisher Scientific, BP2471-1)
- 2X laemmli sample buffer (Bio-Rad, 161-0737)
- Primary antibodies
- 10X Running buffer: Tris-Glycine-SDS buffer (Bio-Rad, 161-0732)
- Secondary antibodies
- Sodium dodecyl sulfate (SDS; Fisher Scientific, 10552785)
- 10X Transfer buffer: Tris-Glycine buffer (Bio-Rad, 161-0734)
- Tris base (Fisher Scientific, 10376743)
- Tween 20 (Sigma-Aldrich, P1379-250ML)

- Plastic Bio-Rad trays, plastic tweezers
- Odyssey CLx (Li-COR, UK)

Protocol:

1. Set up the electrophoresis system. Make sure that all items are clean as this interfere with the electrophoresis.
2. Make 2 L of 1X running buffer from the 10X stock, by adding 200 ml of running buffer 10X to 1800 ml of distilled water.
3. Remove gel from the fridge and washed it with distilled water.
4. Remove green comb carefully to avoid breaking the legs of the wells. Remove green tape at the bottom of the gel.
5. Place gel in the modules and lower each module into the tank, seating it in the locating slots.
6. Fill the tank with 1X running buffer. Make sure the buffer covers the gel completely and that the wells are also filled. Rinse wells with running buffer.
7. Defrost tubes containing cell lysate on ice.
8. Using the chilled protein sample derived from lysed cells, make the appropriate dilutions in lysis buffer (inactive). Make sure all cell lysates have the same concentration before adding to the gel. Add the same amount (20 µl) of 2X sample buffer with DTT to each sample.
9. Boil (95 °C) 40 µl prepared samples for 10 minutes.
10. Load 5 µl of the protein ladder and 20 µl of each sample into the gel wells slowly.
11. Connect the leads to the electrophoresis power supply EPS 3501 XL (do not forget to add the adapters) and turn on. Choose the correct program and press Set Enter.
12. Run gels at 120V for 10 minutes and subsequently at 200V for 50 minutes.
13. Stop the run when the dye from reaches the bottom of the glass plates (check on both sides if running 2 gels).
14. Turn off the power supply and disconnect the leads.
15. Make 1L of 1X transfer buffer (20% methanol) from the 10X stock solution. Make a fresh solution each time.
16. Refill tank with transfer buffer.
17. Fill one plastic Bio-Rad tray with methanol (Tray 1) and three with transfer buffer (Trays 2-4).
18. Cut the Immobilon-FL Transfer Membrane to a size that overlaps the SDS-PAGE gel (handle with care).
19. Carefully remove the membrane from the blue paper and soak in methanol (Tray 1) for 2 minutes, handling with plastic tweezers.
20. Wash the membrane in transfer buffer (Tray 2).
21. Cut the filter paper to overlap the membrane and soak in transfer buffer (Tray 3) – 1 piece of filter paper per side.
22. Remove the gel from the tank. Gently loosen and then slide away both spacers. Slip an extra spacer into the bottom edge to prevent breaking the “ears” of the notched plates and separate the plates. Cut away and discard the stacking gel.
23. Transfer the gel into transfer buffer (Tray 4) using the gel spacer.
24. Add more transfer buffer into the blotting apparatus then place the filter paper in.
25. Use tweezers to place the membrane on the filter paper. Cut the membrane in the opposite bottom corner of the protein marker. Make sure that the membrane is always wet.
26. Lay the gel on top of the membrane then add more transfer buffer before placing the second piece of soaked filter paper on top of the gel.
27. Use a cropped serological pipette to roll out bubbles by applying medium pressure whilst holding down one side and rolling away in the opposite direction.
28. Apply the lid followed by a weight then plug in and turn on.
29. Run at 50V for 1 hour.
30. Turn off the power supply and disassemble the sandwich. Rinse the cathode and anode with distilled water and leave to dry.
31. Make 10% and 5% (w/v) Marvel in 0.1% TBST solution.
32. Block the membrane in 10% (w/v) Marvel in 0.1% TBST solution for 1 hour at room temperature.
33. Make 1L of TBS with 0.1% tween 20 (0.1% TBST), by adding 100 ml 10X TBS to 900 ml of distilled water. Add 1 ml of tween 20.

34. Add primary antibody solution diluted in blocking buffer (5% Marvel in 0.1% TBST) overnight at 4°C.
35. On the next day, wash membrane four times with 0.1% TBST for 5 minutes each, rocking.
36. Add secondary antibody solution in a 1:5,000 diluted in blocking buffer (5% Marvel in 0.1% TBST) and incubate for 1 hour at room temperature.
37. Wash membrane four times with 0.1% TBST for 5 minutes each, rocking.
38. Scan membrane using the Odyssey CLx at both 700 and 800 nm channels.
39. Analyse data using the Image Studio™ software.

A.5.2 Sample preparation

Table 7-5: Ingredients of RIPA (Radioimmunoprecipitation assay) lysis buffer used to extract protein from cultured cells. Lysis buffer can be stored at 4 °C for several weeks. Protease inhibitors were added fresh to the lysis buffer.

Chemical	Supplier & Catalogue number	Location	Final concentration	Volume/Mass
10% NP-40	Fisher Scientific; 13434269	Chemical cupboard	1%	1 ml
1 M Tris-HCl, pH 7.4	Fisher Scientific; 10376743	Fridge FR-01	10 mM	100 µl
1 M NaCl	Fisher Scientific; 10428420	Chemical cupboard	0.15 M	1.5 ml
0.1 M EGTA	Sigma-Aldrich; E4378-10G	Fridge FR-01	1 mM	100 µl
100 mM EDTA	Fisher Scientific; 10335460	Fridge FR-01	10 mM	1 ml
100 mM PMSF	Fisher Scientific; 10485015	Freezer FZ-01	1 mM	100 µl
1 mg/ml Aprotinin	Fisher Scientific; 11854101	Freezer FZ-01	2 µg/ml	20 µl
10 mg/ml Leupeptin	Fisher Scientific; 10736392	Freezer FZ-01	2 µg/ml	2 µl
10 mg/ml Pepstatin A	Fisher Scientific; 10786834	Freezer FZ-01	2 µg/ml	2 µl
0.5 M NaF	Fisher Scientific; 10742222	Freezer FZ-01	50 mM	1 ml
0.1 M $Na_4P_2O_7$	Sigma-Aldrich; P8010-500G	Freezer FZ-01	20 mM	2 ml
100 mM Na_3VO_4	Sigma-Aldrich; S6508-10G	Freezer FZ-01	100 µM	10 µl
Distilled water	-	Prep room	-	Adjust to 10 ml

Table 7-6: Ingredients of Tris-Triton lysis buffer used to extract proteins from cultured cells. Lysis buffer can be stored at 4 °C for several weeks. Protease inhibitors were added fresh to the lysis buffer.

Chemical	Supplier & Catalogue number	Location	Final concentration	Volume/Mass
1 M Tris, pH 7.4	Fisher Scientific; 10376743	Fridge FR-01	10 mM	100 µl
1 M NaCl	Fisher Scientific; 10428420	Chemical cupboard	100 mM	1 ml
100 mM EGTA	Sigma-Aldrich; E4378-10G	Fridge FR-01	1 mM	100 µl
Triton X-100	Sigma-Aldrich; T8787-100ML	Chemical cupboard	1%	100 µl
Glycerol	Fisher Scientific; 10579570	Chemical cupboard	10%	1 ml
10% SDS	Fisher Scientific; 10552785	Chemical cupboard	0.1%	100 µl
10% Sodium deoxycholate	Sigma-Aldrich; D6750-10G	Chemical cupboard	0.5%	500 µl
100 mM EDTA	Fisher Scientific; 10335460	Fridge FR-01	10 mM	1 ml
100 mM PMSF	Fisher Scientific; 10485015	Freezer FZ-01	1 mM	100 µl
1 mg/ml Aprotinin	Fisher Scientific; 11854101	Freezer FZ-01	2 µg/ml	20 µl
10 mg/ml Leupeptin	Fisher Scientific; 10736392	Freezer FZ-01	2 µg/ml	2 µl
10 mg/ml Pepstatin A	Fisher Scientific; 10786834	Freezer FZ-01	2 µg/ml	2 µl
0.5M NaF	Fisher Scientific; 10742222	Freezer FZ-01	1 mM	20 µl
0.1 M $Na_4P_2O_7$	Sigma-Aldrich; P8010-500G	Freezer FZ-01	20 mM	2 ml
100 mM Na_3VO_4	Sigma-Aldrich; S6508-10G	Freezer FZ-01	2 mM	200 µl
Distilled water	-	Prep room	-	Adjust to 10 ml

A.5.3 SDS-PAGE

Table 7-7: Recipe for 10X running buffer (pH 8.3) used for SDS-PAGE.

Chemical	Supplier & Catalogue number	Location	Volume
Tris Base	Fisher Scientific; 10376743	Chemical cupboard	30.3 g
Glycine	Fisher Scientific; 10070150	Chemical cupboard	144 g
10% SDS	Fisher Scientific; 10552785	Chemical cupboard	10 ml
Distilled water	-	Prep room	Make up to 1L

A.5.4 Western blotting

Table 7-8: Recipe for 10X transfer buffer used for Western blotting.

Chemical	Supplier & Catalogue number	Location	Volume/Mass
Tris Base	Fisher Scientific; 10376743	Chemical cupboard	30.3 g
Glycine	Fisher Scientific; 10070150	Chemical cupboard	144 g
Distilled water	-	Prep room	Make up to 1L

Table 7-9: Recipe for 0.1% Tween 20 in 1X TBS (0.1% TBST).

Chemical	Supplier & Catalogue number	Location	Final concentration	Volume/Mass
10X TBS	Fisher Scientific, BP2471-1	Chemical cupboard	1X	100 ml
Tween 20	Sigma-Aldrich; P1379-250ML	Chemical cupboard	0.1%	1 ml
Distilled water	-	Prep room	-	Make up to 1L

Appendix III: RT-qPCR method development rationale

A.1 Development of real-time RT-PCR method

The amplicons can be detected using DNA-binding dyes (such as SYBR Green) or fluorescently labelled sequence-specific probes (such as TaqMan). In this project, SYBR Green was chosen as the detection method due to its capability of testing numerous genes quickly without designing multiple probes, simple and easy assay design, ability to perform a melting curve analysis to check the specificity of the amplification reaction and the greater cost-effectiveness.

However, one of the main disadvantages of SYBR Green is the lack of specificity, as this dye binds non-specifically to any double-stranded DNA (dsDNA), such as non-specific products or primer-dimers, which can contribute to the overall fluorescence and affect the accuracy of the PCR. Hence, it is essential to perform a melting curve analysis in each qPCR run to check the specificity of PCR products.

There are two different methods to report data from real-time PCR: absolute and relative quantification. Absolute quantification determines the amount of target (expressed as concentration or copy number) and should be used in situations where the absolute transcript copy number is necessary, whereas relative quantification determines the ratio between the amount of target and the amount of reference gene and it is normally used to compare changes in gene expression of different samples[282]. Therefore, to investigate the gene expression of genes of interest in different samples with different treatments, relative quantification was sufficed.

Numerous methods have been developed to report relative gene expression, such as sigmoidal curve fitting method, efficiency correction method and $2^{-\Delta\Delta Cq}$ method. The latter was used, as it is capable of reporting qPCR data as “fold-change” in expression, its ease of use and it is one of the most used methods in the literature to analyse and report relative gene expression data.

A.2 RNA Quality Control

The RNA extraction and purification must fulfil the following criteria[225]:

- Free of nucleases during storage;
- Free of protein;
- Free of genomic DNA (gDNA);
- High quality;
- Free of enzymatic inhibitors for downstream applications.

The quantification of RNA is essential as similar amounts of RNA should be used when comparing different samples. There are several methods to quantify RNA, including spectrophotometry, capillary gel electrophoresis, microfluidic analysis and fluorescence dye detection[231]. However, different results are obtained with these methods, which makes it unwise to try to compare data; therefore, only one single method (spectrophotometry) was used to report this information.

A typical example of the concentration, purity and quality of the extracted RNA from cultured cells is shown in the table below.

Table 7-10: Quality control of RNA extracted from cells derived from non-PD TA tissue and PD plaque tissue. Data correspond to the average of three replicates ± SEM.

Samples		Concentration (ng/µl)	Purity (A_{260}/A_{280} ratio)	Quality (RIN)	rRNA ratio (28S:18S)
TAN2A1	**-TGF-β1**	111.8 ± 5.68	2.25 ± 0.02	10.0 ± 0.00	1.83 ± 0.06
	+TGF-β1	109.8 ± 5.94	2.25 ± 0.02	9.9 ± 0.05	1.68 ± 0.04
TAC1B1	**-TGF-β1**	92.9 ± 6.19	2.17 ± 0.04	9.9 ± 0.04	1.88 ± 0.03
	+TGF-β1	113.3 ± 3.82	2.26 ± 0.02	9.9 ± 0.05	1.87 ± 0.01
TAC4A2	**-TGF-β1**	115.6 ± 11.43	2.27 ± 0.01	9.9 ± 0±.00	1.69 ± 0.02
	+TGF-β1	141.1 ± 4.99	2.29 ± 0.02	9.8 ± 0.07	1.79 ± 0.05
TAC4B2	**-TGF-β1**	96.8 ± 1.54	2.04 ± 0.02	9.7 ± 0.02	2.00 ± 0.04
	+TGF-β1	95.7 ± 5.12	2.01 ± 0.01	10.0 ± 0.00	1.83 ± 0.02
PD1B1	**-TGF-β1**	62.3 ± 1.57	2.27 ± 0.01	10.0 ± 0.00	1.87 ± 0.03
	+TGF-β1	67.2 ± 1.32	2.18 ± 0.01	9.8 ± 0.10	1.70 ± 0.01
PD2A2	**-TGF-β1**	104.7 ± 4.60	2.24 ± 0.04	10.0 ± 0.00	1.87 ± 0.00
	+TGF-β1	115.4 ± 5.02	2.18 ± 0.02	9.8 ± 0.07	1.87 ± 0.02
PD3A1	**-TGF-β1**	114.8 ± 6.64	2.16 ± 0.01	9.9 ± 0.07	1.90 ± 0.06
	+TGF-β1	94.6 ± 7.12	2.16 ± 0.04	9.7 ± 0.03	1.80 ± 0.03
PD3A2	**-TGF-β1**	52.5 ± 2.88	2.06 ± 0.01	9.9 ± 0.02	1.97 ± 0.06
	+TGF-β1	67.3 ± 1.89	2.03 ± 0.00	10.0 ± 0.00	1.93 ± 0.06

The figures below show a representative electropherogram of the RNA ladder (Figure 7-3) and of an RNA sample (Figure 7-4) obtained using the Bioanalyzer.

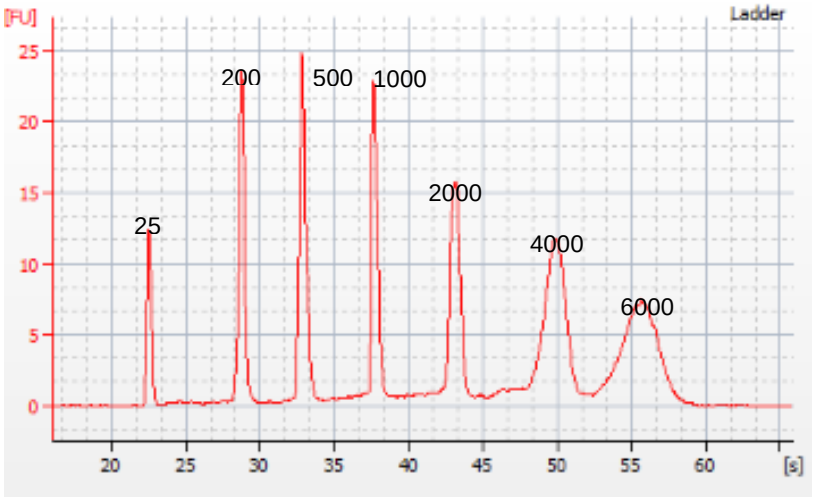

Figure 7-3: Electropherogram data of the RNA ladder. At the end of a run, the software shows an electropherogram of the RNA ladder, displaying seven peaks generated by the separation of the RNA ladder. The first peak corresponds to the lower alignment marker (25 nucleotides), which is a component of the loading buffer and the ladder, and it should always appear in the ladder and in the samples electropherogram. If the separation is successful, six more RNA peaks (6000 nt to 200 nt) in the ladder well will appear which should be well resolved. In the x-axis is shown the time in seconds and in the y-axis is represented the fluorescence.

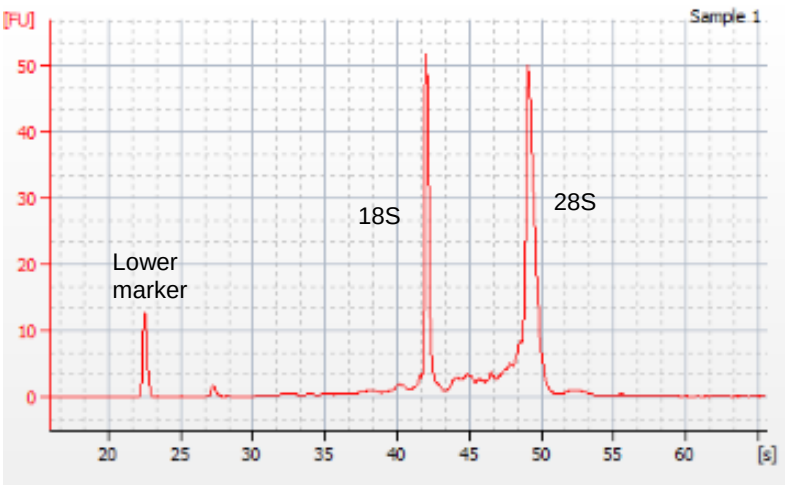

Figure 7-4: Representative electropherogram of an RNA sample. When RNA is separated, it will display two peaks corresponding to the 18S rRNA and 28S rRNA. The first peak corresponds to the lower alignment marker. Both 18S and 28S should exhibit sharp and narrow peaks, which indicates that the RNA is not degraded. In the x-axis is shown the time in seconds and in the y-axis is represented the fluorescence.

RNA extraction from tissue samples

RNA extraction was also attempted in human non-PD TA tissue and PD plaque tissue. Several optimisations were performed in the protocol; however, RNA was

not obtained from these tissues (Table 7-11). Initially, RNA was extracted from tissues used to establish cell lines and subsequently frozen. These tissues were rubbed into the surface of a 6 well plate and incubated at 37°C for at least 5 days, during cell line establishment, leading to the degradation of RNA. The RNA in harvested tissue is not protected until the tissue is entirely submerged in a solution to stabilise the RNA. Therefore, fresh tissue was placed inside RNA*later* straight after being removed from the patient to protect the RNA and avoid changes in the gene expression pattern. Other alterations to the protocol were also performed, including the use of liquid nitrogen to freeze the tissue prior to potential disruptions (which can lead to the degradation of RNA); however, RNA was still not obtained. It was evident that the degradation of RNA happened straight after removal of the tissue from the patient; thus, to ensure extraction of RNA, the tissue should be placed in liquid nitrogen straight after being removed to avoid degradation of RNA. In the author's opinion, this is the best way to guarantee extraction of RNA from tissue samples as reported by several authors[51,283]. As the tissue samples were collected from UCLH and transported to the university laboratories, freezing in liquid nitrogen was not carried out due to health and safety issues during transportation.

The table below shows the different optimisations performed and the concentration and purity obtained.

Table 7-11: RNA extraction from tissues of patients with and without PD.

Optimisations	Tissue samples	Concentration (ng/µl)	Purity (A_{260}/A_{280} ratio)
Use of frozen tissue at -80 °C (used to establish cell lines)	TAP3A1	-1.1	0.99
	PD8B1	1.8	-18.88
Ceramic vs glass beads for homogenisation step	TAP4B1	-6.4	2.06
	PD3B2	0.6	1.66
Use of RNA*later* RNA Stabilisation Reagent	TAC3a	0.2	0.23
Use of liquid nitrogen	TAC4	1.0	1.04
Use of fresh tissue	TAP14	-0.1	1.00
Use of a different homogenisation program (6000 rpm, 2 x 30 seconds)	TAC3b	0.1	-0.31

A.3 cDNA synthesis by reverse transcription

Several methods are available to convert RNA into stable cDNA by performing RT reactions: one-step RT (RT and real-time PCR are carried out in the same tube) or a two-step RT (RT and real-time PCR are performed in separate tubes). In this study, two-step RT method was chosen as enables long-term storage of cDNA, multiple PCR reactions can be carried out from a single RT reaction and it is flexible with the RT primer choice. For the RT reaction, random primers were chosen over oligo(dT) primers and gene-specific primers, as several different transcripts can be analysed from a single RT reaction and it also enables RT reactions from the entire RNA population.

A.4 Real-time PCR

The amplification curve is a plot of cycle number versus fluorescence signal which correlates with the start amount of target nucleic acid during the exponential

phase. The figures below show representative amplification plot in log scale and linear scale (Figure 7-5A and 7-5B).

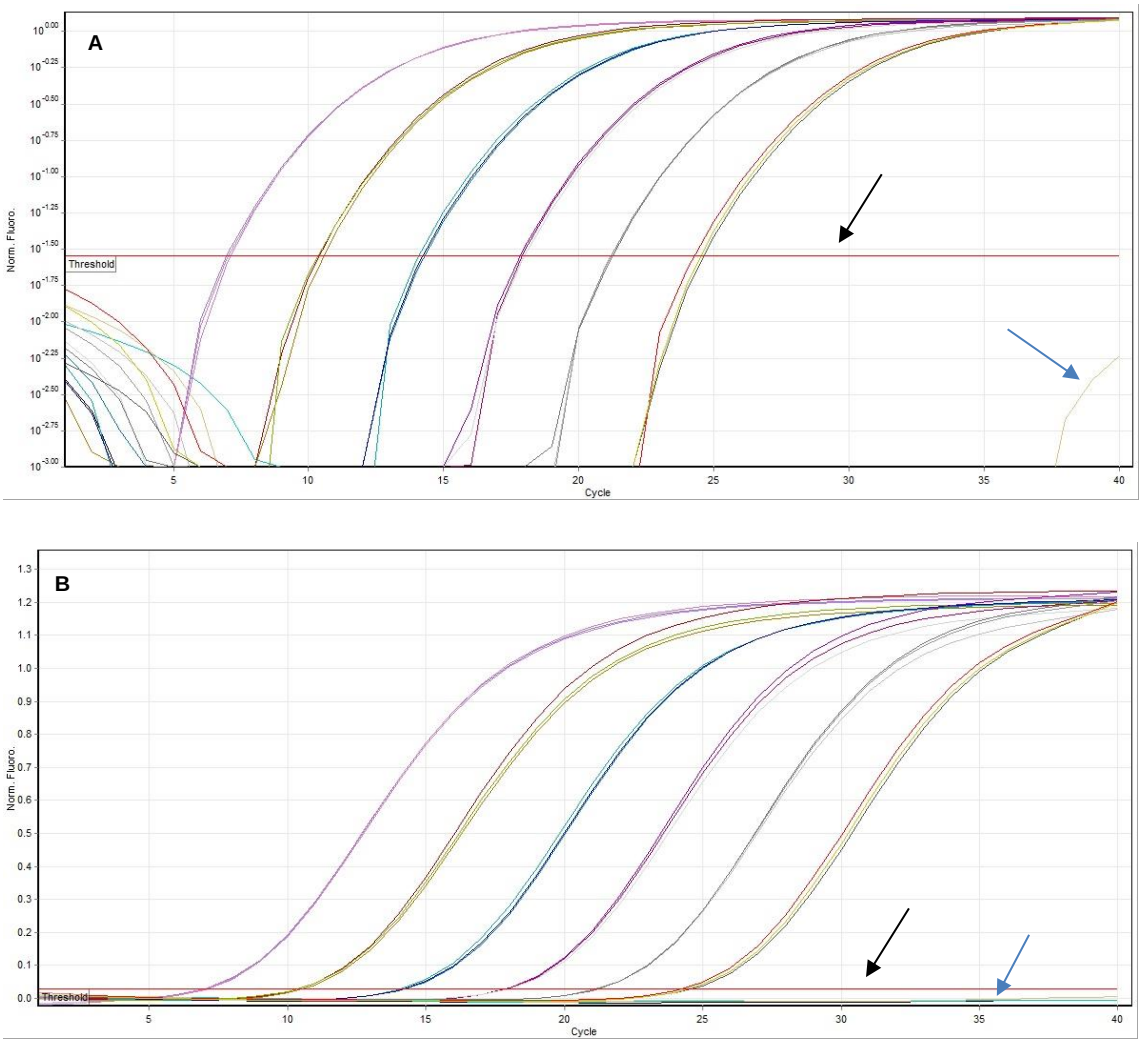

Figure 7-5: Representative amplification plots of 18S gene. (A) In log scale. (B) In linear scale. A real-time PCR was performed on 10-fold serial dilutions of the cDNA template in triplicate and the Cq values were determined for each dilution. The red bar (black arrows) corresponds to the threshold, which is used to determine the Cq values. Samples with higher concentrations (10-2) cross the threshold at lower cycle number and, therefore are positioned towards the left of the plot, whereas diluted samples (10-7) cross the threshold at higher cycle number (situated towards the right of the graph). In the x-axis is shown the number of cycles and in the y-axis is represented the normalised fluorescence (SYBR Green intensity divided by the intensity of ROX, a passive reference dye incorporated in the SYBR Green master mix). Blue arrow represents negative controls included in the real-time PCR run.

From this plot, the quantification cycle, which corresponds to the cycle number at which the fluorescence generated within a reaction crosses the threshold can be determined. By plotting the Cq value acquired during amplification of each dilution

against the log starting amount of template, it was possible to generate standard curves for the target and reference genes.

A qPCR run was carried out using the cDNA obtained from an untreated cell line derived from non-PD TA tissue (calibrator sample), after which, standard curves were generated for α-SMA, β-actin and 18S before any optimisations (Figure 7-6) and after optimisations for α-SMA, EIF4A2 and TOP1 (Figure 7-7).

A

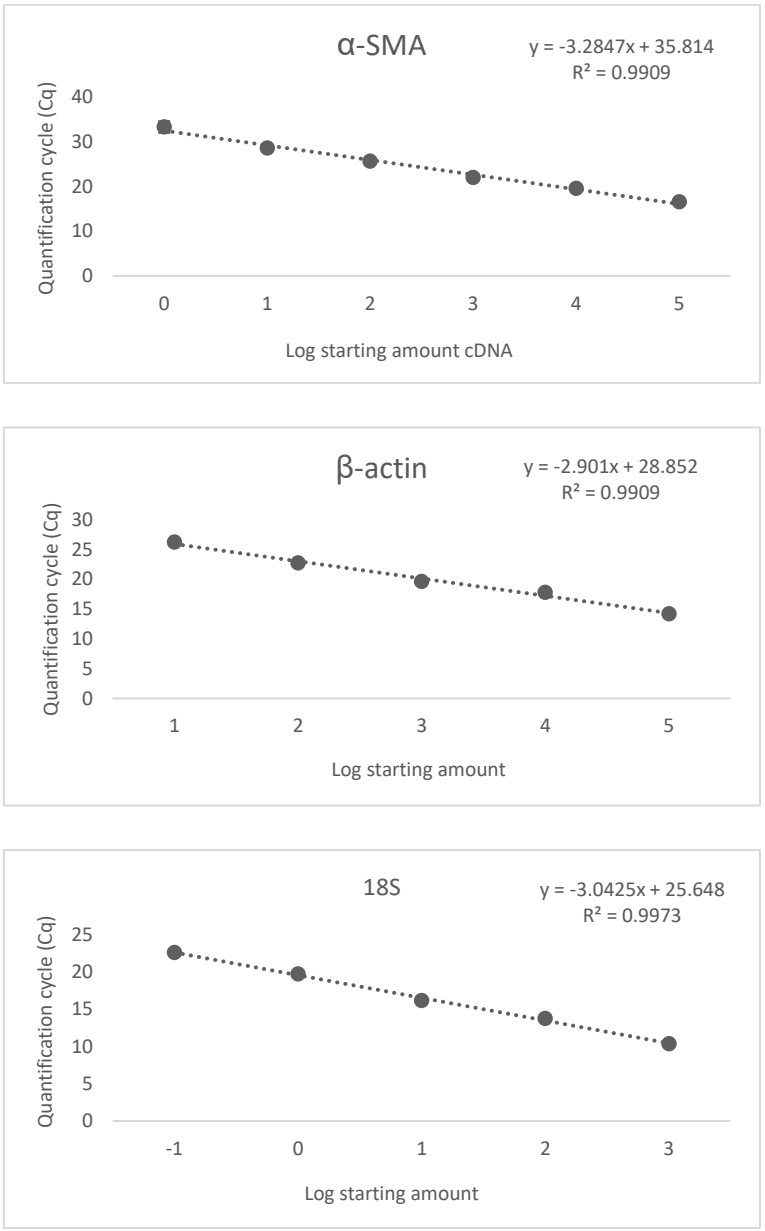

Figure 7-6: Representative standard curves for α-SMA, β-actin and 18S before optimisations. Six dilutions of TAC4A2 cDNA (calibrator sample) for α-SMA and β-actin were used: neat; 10^{-1}; 10^{-2}; 10^{-3}; 10^{-4} and 10^{-5}, whereas for 18S five dilutions were prepared: 10^{-2}; 10^{-3}; 10^{-4}; 10^{-5} and 10^{-6}. To construct standard curves, the Cq value and the log starting amount of template were used. Through the slope of each standard curve, it was possible to calculate the amplification efficiency of each gene. Data points were plotted as mean ± SEM.

A

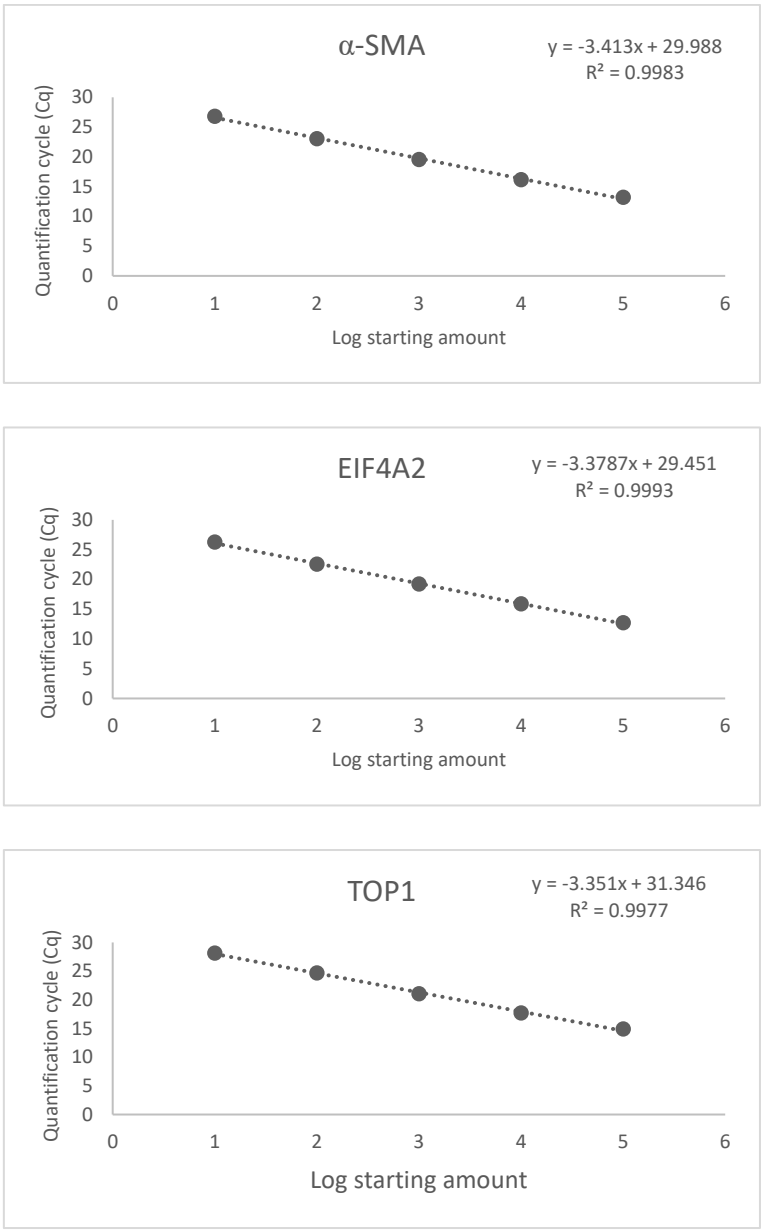

Figure 7-7: Representative standard curves for α-SMA, EIF4A2 and TOP1 after optimisations. Dilutions ranging from neat to 10^{-4} were used to generate standard curves for all three genes by using the Cq value and the log starting amount of template. Through the slope of each standard curve, it was possible to determine the amplification efficiency of each gene. Data points were plotted as mean ± SEM.

Melting curve corresponds to the denaturation of each double-stranded species present in the sample, which results in an increment in fluorescence as these double-stranded species dissociate, displaying one single sharp peak. A specific peak at the PCR product melting temperature (the temperature at which 50% of the base pairs of dsDNA are separated) can discriminate the amplicons from non-specific products, which melt at different temperatures[284,285]. The melting

temperatures are determined by several factors including nucleotide composition, the length of the molecule and salt concentration[284]. Primer-dimers, non-specific products generally have a lower melting temperature than the amplicons, which can also be analysed by performing a post-PCR analysis by running, at least, one sample per primer pair on an agarose gel.

The figure below shows representative melting curve of all target and reference genes used.

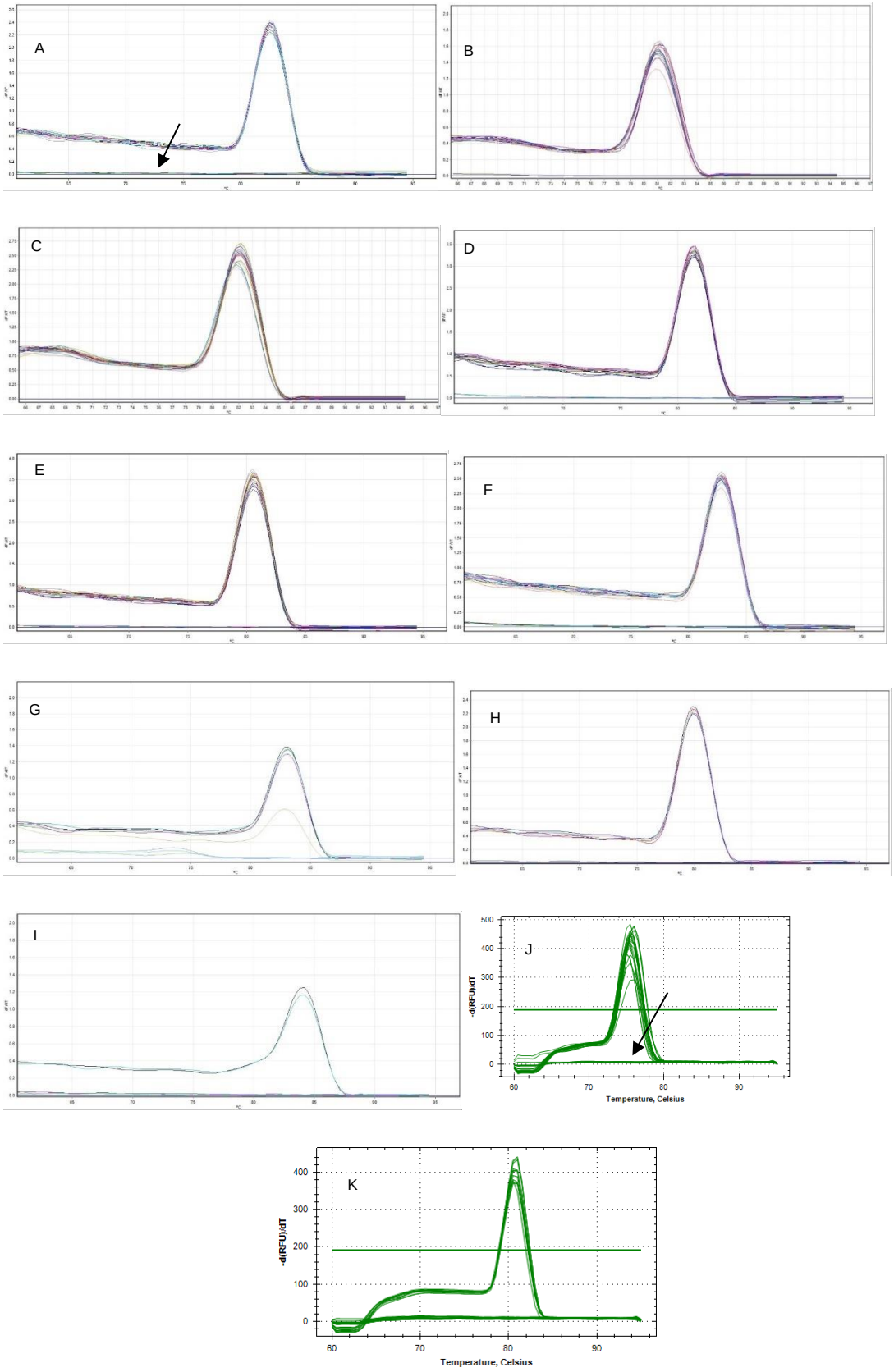

Figure 7-8: Representative melting curve of all target and reference genes used. (A) α-SMA, (B) β-actin, (C) 18S, (D) EIF4A2, (E) TOP1, (F) ADORA1, (G) ADORA2A,

(H) ADORA2B, (I) ADORA3, (J) ERα and (K) ERβ. Only one peak per sample was observed in the melting curve plot, corresponding to the denaturation of the PCR products obtained by the real-time PCR. Black arrow corresponds to the negative controls (NTC and NRT) included in the run, where no amplification was detected.

Appendix IV: Antibody validation

A.1 Alpha-smooth muscle actin (α-SMA) antibody

The α-SMA antibody was purchased from Sigma-Aldrich, UK (catalogue number A5228). This antibody has been validated by the manufacturer showing a single band at the known molecular weight. Furthermore, this antibody was also validated by its use in 206 published peer-reviewed papers.

- Elliott CG *et al.* Periostin modulates myofibroblast differentiation during full-thickness cutaneous wound repair. *J Cell Sci*. **125**, 121-132 (2012).
- Didangelos A *et al*. Extracellular matrix composition and remodeling in human abdominal aortic aneurysms: a proteomics approach. *Mol Cell Proteomics* **10(8)**:M111 (2011).

This antibody was also extensively validated within our research team: Stebbeds, W. *In vitro* studies of Peyronie's disease-derived myofibroblasts: disease association and identification of novel therapeutic compounds. Cranfield University PhD Thesis, 1–283 (2015).

A.2 Adenosine receptor A1 (ADORA1) antibody

The anti-adenosine A1 receptor antibody was purchased from Abcam, UK (catalogue number ab124780). This antibody has been validated by the manufacturer showing a single band at the correct molecular weight in different cell lysates (Saos 2 cell lysate, SH SY5Y cell lysate, Caco 2 cell lysate, A549 cell lysate and 293T cell lysate).

A.3 Adenosine receptor A2B (ADORA2B) antibody

The anti-adenosine A2B receptor antibody was purchased from Abcam, UK (catalogue number ab135865). This antibody has been validated by the manufacturer showing a single band at the correct molecular weight in HT29 cells (colon epithelial cells). The ADORA2B antibody was also used to confirm ADORA2B expression in the following peer-reviewed paper:

- Corciulo C *et al.* Endogenous adenosine maintains cartilage homeostasis and exogenous adenosine inhibits osteoarthritis progression. *Nat Commun* **8**:15019 (2017).

A.4 Estrogen receptor α (ERα) antibody

The anti-estrogen receptor alpha antibody was purchased from Abcam, UK (catalogue number ab32063). This antibody has been validated by the manufacturer showing a single band at the correct molecular weight in MCF-7 cells and in tissue lysate from human ovary cancer. In addition, it was also validated by its use in 37 published peer-reviewed papers.

- Guo L *et al.* 17ß-estradiol regulates the malignancy of cancer stem-like cells derived from the MCF7 cell line partially through Sox2. *Oncol Lett* **15**:3790-3795 (2018).
- Zhang W *et al.* The correlation between DNMT1 and ERα expression and the methylation status of ERα, and its clinical significance in breast cancer. *Oncol Lett* **11**:1995-2000 (2016).

A.5 Estrogen receptor β (ERβ) antibody

The anti-estrogen receptor beta antibody was purchased from Abcam, UK (catalogue number ab3576). This antibody has been validated by the manufacturer and it was also validated by its use in 28 published peer-reviewed papers.

- Li P *et al.* 17beta-estradiol Attenuates TNF-a-Induced Premature Senescence of Nucleus Pulposus Cells through Regulating the ROS/NF-κB Pathway. *Int J Biol Sci* **13**,145-156 (2017).
- Ma Y *et al.* Estrogen replacement therapy-induced neuroprotection against brain ischemia-reperfusion injury involves the activation of astrocytes via estrogen receptor ß. *Sci Rep* **6**:21467 (2016).

The use of these antibodies in published, peer-reviewed journals combined with the use of proper negative controls enabled their validation in the ICW technique.

Appendix V: List of publications

During this research project, several national and international conferences were attended where some of the results reported herein were presented. A complete list of publications is shown below.

- Mateus, M., Stebbeds, W., Raheem, A., Muneer, A., Christopher, N., Ralph, D.J. & Cellek, S. Investigation of the role of myofibroblast differentiation in Peyronie's disease. *BAUS Abstracts. Br J Surg* **101**, 56–68 (2014).
- Mateus, M., Stebbeds, W., Raheem, A., Muneer, A., Christopher, N., Ralph, D.J. & Cellek, S. Investigation of the role of myofibroblast differentiation in Peyronie's disease. *J Sex Med* **11(S1)**, 1–108 (2014).
- Mateus, M., Stebbeds, W., Raheem, A., Spilotros, M., Garaffa, G., Muneer, A., Christopher, N., Cellek, S., & Ralph, D.J. The expression of adenosine receptors in Peyronie's disease. *J Sex Med* **12(S3)**, 187–271 (2015).
- Mateus, M., Stebbeds, W., Bright, A., Raheem, A., Spilotros, M., Garaffa, G., Muneer, A., Christopher, N., Cellek, S., & Ralph, D.J. Development of a high-throughput, cell-based assay for anti-myofibroblast activity in Peyronie's disease. *J Sex Med* **13(S1)**, S8 (2016).
- Mateus, M., Stebbeds, W., Bright, A., Raheem, A., Spilotros, M., Garaffa, G., Muneer, A., Christopher, N., Cellek, S., & Ralph, D.J. First results from a novel cell-based assay for anti-myofibroblast activity in Peyronie's disease. *J Sex Med* **13(S2)**, S89 (2016).
- Mateus, M., Ilg, MM., Stebbeds, WJ., Christopher, N., Muneer, A., Ralph, D.J. & Cellek, S. Understanding the role of adenosine receptors in the myofibroblast transformation in Peyronie's disease. *J Sex Med* **15(7)**, 947-957 (2018).
- Ilg, MM., Mateus, M., Stebbeds, WJ., Milenkovic, U., Christopher, N., Muneer, A., Albersen, M., Ralph, D.J. & Cellek, S. Antifibrotic Synergy Between Phosphodiesterase Type 5 Inhibitors and Selective Oestrogen Receptor Modulators in Peyronie's Disease Models. *European Urology* (2018).